



THE UNIVERSITY *of* EDINBURGH

This thesis has been submitted in fulfilment of the requirements for a postgraduate degree (e.g. PhD, MPhil, DClinPsychol) at the University of Edinburgh. Please note the following terms and conditions of use:

This work is protected by copyright and other intellectual property rights, which are retained by the thesis author, unless otherwise stated.

A copy can be downloaded for personal non-commercial research or study, without prior permission or charge.

This thesis cannot be reproduced or quoted extensively from without first obtaining permission in writing from the author.

The content must not be changed in any way or sold commercially in any format or medium without the formal permission of the author.

When referring to this work, full bibliographic details including the author, title, awarding institution and date of the thesis must be given.

The regulatory role of Pax6 on Cell Division Cycle Associated
7 and cortical progenitor cell proliferation

Yu-Ting Huang, BSc, MSc

Thesis submitted for the degree of Doctor of Philosophy at
the University of Edinburgh

March 2017

Table of Contents

Disclaimer	xi
Acknowledgements	xii
Abstract	xiii
Lay summary.....	xvii
Abbreviations	xvii
Chapter 1 : General Introduction	1
<i>1.1 Early development of the brain in mammals</i>	1
1.1.1 Development of forebrain in mouse.....	1
1.1.2 Gradients of signalling molecules in the cortex affect cerebral cortical development	6
1.1.3 Cell cycle control in mouse development	9
1.1.4 Differentiation and proliferation of cortical progenitors.....	13
<i>1.2 Pax6 and its role in cortical development</i>	22
1.2.1 Discovery of PAX6/Pax6 and its related human disease	22
1.2.2 Disruption of the pallial-subpallial boundary (PSPB) in <i>Pax6</i> mutants	22
1.2.3 Cortical lamination and migration of post-mitotic neurons regulated by Pax6	25
1.2.4 Downstream targets of Pax6 involved in corticogenesis	27
1.2.5 The regulatory role of Pax6 in the cell cycle progression and cell fate decision	29
<i>1.3 Current understanding of the novel protein Cdca7</i>	30
<i>1.4 Aims of this thesis</i>	36
Chapter 2 : Materials and Methods	37

2.1	<i>Animals</i>	37
2.2	<i>Histology</i>	37
2.2.1	Embryo collection and fixation.....	37
2.2.2	Wax sectioning.....	38
2.2.3	Cryostat sectioning.....	38
2.2.4	<i>In Situ</i> Hybridisation (ISH)	38
2.2.5	Immunofluorescence staining (IF staining)	40
2.3	<i>Generation of RNA probe for in situ hybridisation</i>	42
2.4	<i>Cloning of DNA constructs</i>	43
2.4.1	<i>Cdca7</i> promoter region construct for luciferase assay.....	43
2.4.2	<i>Cdca7</i> expression construct for <i>in utero</i> electroporation.....	44
2.5	<i>Cell culture and Luciferase assays</i>	45
2.6	<i>Western Blotting</i>	46
2.7	<i>Quantitative Chromatin Immuo</i> precipitation (<i>qChIP</i>).....	46
2.8	<i>In Utero Electroporation (IUE)</i>	48
2.9	<i>Microscope and imaging software</i>	48
2.10	<i>Statistical analysis</i>	49
Chapter 3	: Expression patterns of <i>Pax6</i> and <i>Cdca7</i> in the developing cortex.	50
3.1	<i>Introduction</i>	50
3.2	<i>Results</i>	51
3.2.1	Embryonic stage E12.5	51
3.2.2	Embryonic stage E13.5	61
3.2.3	Embryonic stage E14.5	68
3.2.4	Embryonic stage E15.5	75

3.2.5	Comparing the overall expression level between developmental stages, genotypes and positions	82
3.2.6	Cluster analysis	95
3.2.7	The relative gene expression of <i>Pax6</i> and <i>Cdca7</i>	100
3.3	<i>Discussion</i>	103
3.3.1	The spatial and temporal expression dynamics of <i>Pax6</i> and <i>Cdca7</i> ..	103
3.3.2	The expression territory of the <i>Cdca7</i> mRNA throughout the developmental stages	103
3.3.3	More accurate methods needed to assess the relationship of <i>Pax6</i> and <i>Cdca7</i>	104
3.3.4	Effects of overexpression of human PAX6 on the expression of <i>Cdca7</i>	106
Chapter 4	: Identification of Pax6 binding sites in the <i>Cdca7</i> locus.....	108
4.1	<i>Introduction</i>	108
4.1.1	Importance of regulation through direct binding and binding site prediction.....	108
4.1.2	How may Pax6 affect <i>Cdca7</i> expression?.....	109
4.2	<i>Results</i>	110
4.2.1	Identification of putative Pax6 binding sites in the regulatory elements of <i>Cdca7</i>	110
4.2.2	Functional characterisation of Pax6 binding regions in the regulatory element of <i>Cdca7</i>	115
4.2.3	Does Pax6 bind the <i>Cdca7</i> regulatory region in vivo?	123
4.3	<i>Discussion</i>	126
4.3.1	The regulatory function of Pax6 on <i>Cdca7</i> expression.....	126
4.3.2	Current ChIP procedures and possible experimental errors.....	128

4.3.3	Re-exploring potential Pax6 target sites in the <i>Cdca7</i> genomic region	130
.....		
Chapter 5	: Understanding functions of <i>Cdca7</i> in cortical progenitor cells....	142
5.1	<i>Introduction</i>	142
5.1.1	Pax6 regulates the proliferation and differentiation of neural progenitors	142
5.1.2	Cell cycle kinetics change during neural differentiation.....	143
5.2	<i>Results</i>	145
5.2.1	Overexpression of <i>Cdca7 in vitro</i>	145
5.2.2	Overexpression of <i>Cdca7 in vivo</i>	149
5.2.3	Understanding biological functions of <i>Cdca7</i> in the developing cortex	
.....		152
5.3	<i>Discussion</i>	166
5.3.1	Tag fusion protein: pros and cons	166
5.3.2	Comparison of progenitor behaviours in <i>Pax6^{Sey/Sey}</i> and <i>wild-type</i> with <i>Cdca7</i> overexpression	167
5.3.3	Effects of <i>Cdca7</i> overexpression in the mid-neurogenesis.....	168
Chapter 6	: General Discussion.....	170
6.1	<i>Summary</i>	170
6.2	<i>The role of Cdca7 in relation to proliferation and differentiation of progenitors remains unclear</i>	174
6.3	<i>The relationship between Pax6 expression levels and neurogenesis</i>	178
References	181
Appendix 1	Quantitative Chromatin Immunoprecipitation (qChIP)	200
Reagents	200
Protocol	202

Appendix 2 The physical interactions between Pax6 and other proteins..... 205

Publications

List of Figures

Figure 1.1 The forebrain compartments and the thalamocortical tracts.....	Error!
Bookmark not defined.	
Figure 1.2 The signalling centres and gradients in the embryonic brain.	7
Figure 1.3 Structure, regulation and checkpoints of a cell cycle.	11
Figure 1.4 Interkinetic nuclear migration of radial glia cells and neurogenesis in developing mouse cortex.....	14
Figure 1.5 The link between the cleavage plane and the mode of division in radial glia cells.	18
Figure 1.6 The link between G1 length and the mode of division in cortical progenitors.	21
Figure 1.7 The expression pattern of Pax6 at E12.5 in mice.	23
Figure 1.8 Schematic representation of human and mouse CDCA7/Cdca7.	32
Figure 3.1 Expression of <i>Pax6</i> and <i>Cdca7</i> mRNA at various positions in E12.5 <i>wild-</i> <i>type</i> coronal sections	53
Figure 3.2 Expression of <i>Pax6</i> and <i>Cdca7</i> at various positions in E12.5 <i>Pax6</i> ^{<i>Sey/Sey</i>} coronal sections.....	55
Figure 3.3 Expression of <i>Pax6</i> and <i>Cdca7</i> at various positions in E12.5 <i>PAX77</i> coronal sections.....	57
Figure 3.4 Expression of <i>Pax6</i> and <i>Cdca7</i> on E12.5 <i>wild-type</i> and <i>Pax6</i> ^{<i>Sey/Sey</i>} sagittal sections.....	59
Figure 3.5 Expression of <i>Pax6</i> and <i>Cdca7</i> at various positions in E13.5 <i>wild-type</i> coronal sections.....	62
Figure 3.6 Expression of <i>Pax6</i> and <i>Cdca7</i> at various positions in E13.5 <i>Pax6</i> ^{<i>Sey/Sey</i>} coronal sections.....	64

Figure 3.7 Expressions of <i>Pax6</i> and <i>Cdca7</i> at different positions in E13.5 <i>PAX77</i> coronal sections.....	66
Figure 3.8 Expression of <i>Pax6</i> and <i>Cdca7</i> at various positions in E14.5 <i>wild-type</i> coronal sections.....	69
Figure 3.9 Expression of <i>Pax6</i> and <i>Cdca7</i> at various positions in E14.5 <i>Pax6^{Sey/Sey}</i> coronal sections.....	71
Figure 3.10 Expression of <i>Pax6</i> and <i>Cdca7</i> at various positions in E14.5 <i>PAX77</i> coronal sections.....	73
Figure 3.11 Expression of <i>Pax6</i> and <i>Cdca7</i> at various positions in E15.5 <i>wild-type</i> coronal sections.....	76
Figure 3.12 Expressions of <i>Pax6</i> and <i>Cdca7</i> at different positions in E15.5 <i>Pax6^{Sey/Sey}</i> coronal sections.....	78
Figure 3.13 Expression of <i>Pax6</i> and <i>Cdca7</i> at various positions in E15.5 <i>PAX77</i> coronal sections.....	80
Figure 3.14 Pixel intensity analysis of the mRNA expression	83
Figure 3.15 The slope values of mRNA expression gradient over time in <i>wild-type</i> , <i>Pax6^{Sey/Sey}</i> and <i>PAX77</i> samples in the dorsal and ventral telencephalon.	86
Figure 3.16 A general trend of <i>Pax6</i> and <i>Cdca7</i> mRNA expression gradient at different developmental stages.....	89
Figure 3.17 The mRNA expression gradients of different ages	91
Figure 3.18 The mRNA expression gradients of <i>Pax6</i> and <i>Cdca7</i> in different ages from <i>WT</i> and <i>PAX77</i> samples	94
Figure 3.19 The comparison of mRNA expression slopes across time from <i>WT</i> , <i>Pax6^{Sey/Sey}</i> and <i>PAX77</i> samples.	96
Figure 3.20 The comparison of mRNA expression slope across time from <i>wild-type</i> , <i>Pax6^{Sey/Sey}</i> and <i>PAX77</i> samples in the dorsal area.....	98
Figure 3.21 The comparison of mRNA expression slopes across time from <i>wild-type</i> , <i>Pax6^{Sey/Sey}</i> and <i>PAX77</i> samples in the ventral area.....	99

Figure 3.22 The comparison of <i>Cdca7</i> mRNA expression from <i>PAX77</i> , <i>wild-type</i> and <i>Pax6^{Sey/Sey}</i>	101
Figure 3.23 Expression patterns of Pax6 and <i>Cdca7</i> protein in the <i>wild-type</i> at E12.5 Cortex.....	102
Figure 4.1 <i>Cdca7</i> genomic region and computationally predicted Pax6 binding sites relative to its TSS.....	112
Figure 4.2 Optimal Pax6 binding motifs for <i>in silico</i> predictions.....	113
Figure 4.3 Schematic representation of the firefly luciferase construct and Pax6 mediated regulation via 2.6 kb upstream region.	117
Figure 4.4 Schematic representation of the firefly luciferase construct and Pax6 mediated regulation via 4.4 kb upstream region.	120
Figure 4.5 Overexpression of Pax6 protein in HEK293 cells.....	122
Figure 4.6 Validation of direct <i>in vivo</i> Pax6 binding to the <i>Cdca7</i> upstream regulatory elements by quantitative chromatin precipitation (qChIP).	125
Figure 4.7 Optimal Pax6 binding motifs for <i>in silico</i> predictions.....	122
Figure 4.8 The topological associated domain and Pax6 binding sites near the <i>Cdca7</i> genomic region.....	122
Figure 4.9 Epigenetic marks in the TAD covering the <i>Cdca7</i> genomic region	122
Figure 4.10 Evolutionary conservation test on one of the predicted binding sites .	122
Figure 4.11 Epigenetic marks found within and close to the <i>Cdca7</i> genomic region	122
Figure 5.1 <i>Cdca7</i> expression clones for <i>in utero</i> electroporation.	146
Figure 5.2 <i>In vitro</i> expression of <i>Cdca7</i> and <i>in utero</i> electroporation paradigm.	148
Figure 5.3 Validation of <i>in utero</i> expression of <i>Cdca7</i> after electroporation.	150
Figure 5.4 Overexpression of <i>Cdca7</i> at E12.5 prevents the production of intermediate progenitor cells.....	153

Figure 5.5 Overexpression of <i>Cdca7</i> at E14.5 does not alter the production of intermediate progenitor cells.....	155
Figure 5.6 Overexpression of <i>Cdca7</i> at E12.5 prevents the production of post-mitotic neurons.	158
Figure 5.7 Overexpression of <i>Cdca7</i> at E14.5 does not affect the production of post-mitotic neurons.....	160
Figure 5.8 Overexpression of <i>Cdca7</i> at E12.5 does not affect the cell division rate in the cortex.....	162
Figure 5.9 Overexpression of <i>Cdca7</i> at E14.5 does not affect the cell division rate in the cortex.....	164
Figure 6.1 The function of <i>Cdca7</i> in the Pax6-mediated regulation of cell cycle progression.	172
Figure 6.2 Current understanding of <i>Cdca7</i> during the differentiation process from progenitors to neurons.....	172

List of tables

Table 1.1 Evolutionary conservation of CDCA7 protein.....	33
Table 2.1 List of primary antibodies and usage conditions	42
Table 2.2 List of probes details	43
Table 2.3 List of primers for q-PCR	47
Table 4.1 The sequences were predicted by multiple Pax6 binding motifs within <i>Cdca7</i> genomic region	114

Table 4.2 In silico prediction of Pax6 binding sites near and within the Cdca7 genomic region.....	131
Table 4.3 Summary of predicted binding sites.....	141

Disclaimer

I, Yu-Ting Huang, performed all of the experiments presented in this thesis unless otherwise clearly stated. In particular I would like to acknowledge Asimina Pantazi and Katrin Ruisu for carrying out some of the *in situ* hybridisation work in chapter 3 and Katrin Ruisu for her assistance with the vector construction in chapter 4 and 5. No part of this work has been or is being submitted for any other degree or qualification.

Signed:

Date:

Acknowledgements

I would like to thank Prof David Price and Dr John Mason for their continuous supervision and patience throughout my PhD period as well as Dr Tom Pratt as the chair of my committee meeting to give valuable guidance. I would also like to thank Dr Da Mi for his teaching in most of my experiments as well as Mr Michael Molinek for *in situ* hybridisation and laboratory maintenance. For *in vivo* studies, I would like to thank Dr Malgorzata Borkowska and Dr Thomas Theil for their help to set up the experiments as well as whole BRR, Hugh Robson Building team for taking care of animals. For computational works I would like to thank Dr Ian Simpson and Mr Zrinko Kozic for their teaching and sharing the results. Thanks to Dr Andrew Jarman and Dr Lynn Powell for their help in the luciferase promoter assay. Thanks to Katrin Ruisu and Asimina Pantazi for their helps in mRNA and cloning works, Dr Martine Manuel for valuable discussions and maintaining the mice colonies, Ms Vivian Allison and Ms Louise Dunn for running the histology laboratory. Thanks to all Developmental Biology Group members for all suggestions, ideas and challenges.

I would like to thank my examiner Dr Nicoletta Kessarar, Prof Martin Collinson and Prof Robert Hill for giving many comments to improve thesis to a better state.

I would like to give thanks to my whole family, my baby girl and especially my husband Dr Thomas Tan, who unconditionally support me throughout whole PhD and be the proof-reader for this thesis. And I would also like to thank all my friends who have encouraged me throughout all my PhD life and Taiwan government which supported my PhD study.

Finally thanks be to God my lord.

Abstract

Forebrain development is controlled by a set of transcription factors which are expressed in dynamic spatiotemporal patterns in the embryonic forebrain and are known to regulate complex gene networks. Pax6 is a transcription factor that regulates corticogenesis and mutations affecting Pax6 protein levels cause neurodevelopmental defects in the eyes and forebrain in both humans and mice. In previous studies, it was shown that the graded expression pattern of Pax6 protein, which is high rostro-laterally to low caudo-medially in the cerebral cortex, is critical for its control of cell cycle progression and proliferation of cortical progenitors. However the underlying mechanisms are still unclear.

Based on a microarray analysis carried out in our laboratory, a number of cell cycle-related candidate genes that may be affected by Pax6 have been identified. One such gene, *Cell division cycle associated 7 (Cdca7)* is expressed in a counter-gradient against that of Pax6. In my current study, I found that *Cdca7* mRNA expression in the telencephalon is upregulated in *Pax6* null (*Small eye*) mutants and downregulated in mice that overexpress PAX6 (*PAX77*) across developing time points from E12.5 to E15.5. There are several potential Pax6 binding motifs located in the genomic locus upstream of *Cdca7*. However, by chromatin immunoprecipitation, it is showed that none of the predicted binding sites are physically bound by Pax6. Promoter luciferase assays using fragments combining five suspected binding motifs show that Pax6 is functionally critical.

Cdca7 is also identified as a Myc and E2F1 direct target and is upregulated in some tumours but its biological role is not fully understood. Current work using *in utero*

electroporation to overexpress *Cdca7* around the lateral telencephalon, where *Cdca7* expression levels are normally low, tested the effects on the proliferation and differentiation of cortical progenitor cells in this region. In E12.5 mice embryos, overexpression of *Cdca7* protein causes fewer intermediate progenitor cells and post-mitotic neurons to be produced but these effects were not found in E14.5 embryos. This result implies that *Cdca7* may affect cell fate decision during cortical development.

Lay summary

Our brain is responsible for many functions such as sensory and motion control, consciousness and cognition. In order to execute those functions correctly, brain needs to develop correctly. This is achieved by the co-ordination of a set of protein called transcription factors. Transcription factors regulate the mRNA expression of their target genes, this regulation is tightly controlled both in time and space. Pax6 is one of these transcription factors, its functions have been found important in the development of forebrain, which consists of neocortex, hypothalamus, hippocampus and thalamus. Insufficient PAX6 protein in human causes aniridia, or absence of iris. Patients having this disease suffer from impaired or loss eyesight. Scientists adopt mice carrying the same mutation in human PAX6-insufficient patients as a disease model. In mouse cortex, the expression pattern of Pax6 protein is high rostro-laterally and low caudo-medially. Previous study showed that Pax6 was able to affect progression of cell cycle in radial glia cells only from the region where Pax6 protein levels were high and moderate. However the underlying mechanisms remain elusive. Also in the cortex, a gene called *Cell division cycle associated 7 (Cdca7)* was identified as a potential downstream target of Pax6 regulation. In my current study, the expression of *Cdca7* showed a counter-gradient against that of Pax6 at mouse embryonic stage E12.5 to E15.5. Furthermore the expression of *Cdca7* was upregulated in mice lacking functional Pax6 protein, indicating that Pax6 may negatively control the expression of *Cdca7*. Mechanistically Pax6 as a transcription factor must be able to interact with the promoter or enhancer regions of its target genes. However in this study, no physical Pax6 binding sites were found near or

within the *Cdca7* genomic regions, suggesting that Pax6 does not directly control the expression of *Cdca7*.

The function of *Cdca7* in cortical development has not been previously investigated. Using a technique called *in utero* electroporation, *Cdca7* were overexpressed around the embryonic lateral cortex, where its expression levels are normally low, to investigate the effect of this protein on the proliferation and differentiation of cortical progenitor cells in this region. In E12.5 mice embryos, overexpression of *Cdca7* protein caused decreased production of intermediate progenitor cells, one of the two main progenitors in the cortex. In addition, production of neurons was also reduced by the overexpression of *Cdca7* at E12.5. These effects were not observed in E14.5 embryos. Taken together, *Cdca7* may affect differentiation of radial glia cells into neurons during cortical development.

Abbreviations

AF	anterior forebrain
AGM	aorta-gonad-mesonephros
ANOVA	analysis of variance
AP	anteroposterior
APs	apical progenitors
BMP	bone morphogenetic proteins
BPs	basal progenitors
BrdU	5-bromo-2'-deoxyuridine
Cad6	Cadherin-6
Cdca7	Cell division cycle associated 7
C-Cdca7	C-HA-Cdca7_IRES-NLS-GFP_pCAGGS
N-Cdca7	N-HA-Cdca7_IRES-NLS-GFP_pCAGGS
Cdh4	R-cadherin
CDK	cyclin-dependent kinase
ChIP	chromatin immunoprecipitation
CML	chronic myelogenous leukaemia
CP	cortical plate
CR	Cajal-retzius
CSB	cortico-striatal boundary
Di	diencephalon
Dll1	Delta-like 1
DTB	diencephalon-telencephalon boundary
DV	dorsoventral

ESCs	embryonic stem cells
FACS	Fluorescence-activated cell sorting
FBS	foetal bovine serum
FGFR	FGF receptor
FGFs	fibroblast growth factors
Fucci	fluorescent ubiquitylation-based cell-cycle indicator
GE	ganglionic emnence
HA	human influenza hemagglutinin
HD	homeodomain domain
Hip	hippocampus
HRP	horseradish peroxidase
Hy	hypothalamus
IC	internal capsule
ICF	Immunodeficiency, Centromeric Instability and Facial Anomalies
INM	interkinetic nuclear migration
IPCs	intermediate progenitor cells
ISH	in situ hybridisation
IZ	intermediate zone
Kif1b	Kinesin Family Member 1B
KO	knockout
LGE	lateral ganglionic emnence
Mb	Mindbomb
MGE	medial ganglionic emnence
MZ	marginal zone

NBR	non-binding control region
NCs	neuroepithelial cells
ncx	neocortex
Ngn1	Neurogenin 1
Ngn2	Neurogenin 2
NLS	nuclear localization sequence
NSCs	neural stem cells
OB	olfactory bulb
ORF	open reading frame
PD	paired domain
PI	protease inhibitors
POC	preoptic area
PP	pre-plate
PSPB	pallial-subpallial boundary
PTh	prethalamus
PWM	position weight matrix
qPCR	quantitative PCR
RA	retinoic acid
Rb	retinoblastoma
RGCs	radial glia cells
RT	room temperature
SD	Standard deviation
Shh	Sonic hedgehog
SVZ	subventricular zone

TCAs	thalamocortical tracts
Tel	telencephalon
dTel	dorsal telencephalon
vTel	ventral telencephalon
TF	transcription factor
Th	thalamus
dTh	dorsal thalamus
PTh	pre-thalamus
vTh	ventral thalamus
TSS	transcriptional start site
VZ	ventricular zone
Wnts	wingless/ints
WT	wild-type
Zli	zona limitans intrathalamica
ZNF	zinc finger

Chapter 1 : General Introduction

1.1 Early development of the brain in mammals

1.1.1 Development of forebrain in mouse

Mechanisms behind the formation of a complex brain which contains several compartments controlling movements, sensations and cognition has been one of the most intriguing topics in neuroscience field. During gastrulation, ectodermal cells default to neural fate, with fibroblast growth factors (FGFs) signalling playing a role in the induction of neural tissues. Bone morphogenetic proteins (BMPs) act against FGFs, and are expressed in the ectodermal tissues surrounding the future neuroectoderm to trigger epidermal fate (Beccari et al., 2013; Kudoh et al., 2004; Muñoz-Sanjuán and Brivanlou, 2002; Wilson and Edlund, 2001). Neural induction starts from a group of ectodermal cells transforming into neuroepithelial cells, which proceeds to form a flat sheet termed the neural plate. The neural plate elongates as development progresses and finally its edges fuse to become the neural tube (Colas and Schoenwolf, 2001; Schoenwolf and Smith, 1990; Smith, 1997; Vieira et al., 2010). The most rostral part of neural plate called anterior neural plate, requires coordination of several signalling molecules acting in a highly patterned and graded fashion to develop into different forebrain compartments, as well as to set up dorso-ventral, antero-posterior, and proximo-distal axes which shape the structure of the growing organ. These signalling molecules include BMP, Wnts (wingless/ints), FGFs and retinoic acid (RA) (Wilson and Houart, 2004).

The forebrain derives from the anterior vesicle of the neural tube, and resides in the most anterior part of the neural tube along the rostro-caudal axis followed by midbrain, hindbrain and spinal cord (Lumsden and Krumlauf, 1996; Wurst and Bally-Cuif, 2001). The telencephalon is located at the dorsal side of the forebrain. It consists of dorsal and ventral telencephalon, which later become the cerebral cortex and the basal ganglia, respectively, as well as the eyes. In addition to the telencephalon, the forebrain also contains the diencephalon, which is located caudally to the telencephalon. Diencephalon is further divided into prethalamus

The regulatory role of Pax6 on Cell Division Cycle Associated 7 and cortical progenitor cell proliferation (pTh), thalamus (Th) and pretectum (PT) from rostral to caudal direction (Figure 1.1A) (Lim and Golden, 2007; Martinez-Ferre and Martinez, 2012).

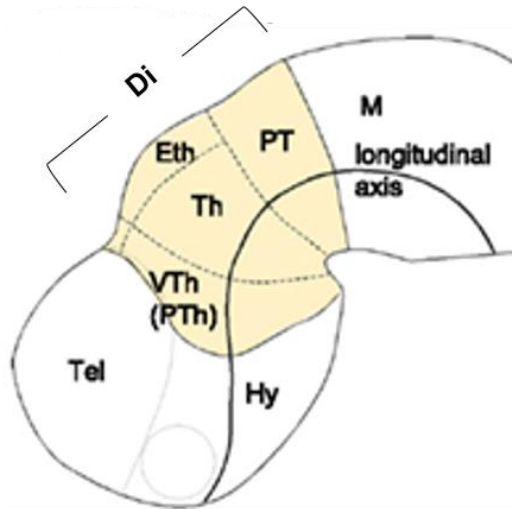


Figure 1.1 The forebrain compartments and the thalamocortical tracts.

Schematic diagram showing the neural tube of an E10.5 mouse embryo. The telencephalon (Tel) is located at the dorsal side of the forebrain. The diencephalon (Di) shown in yellow colour is located caudally to the telencephalon and is further divided into ventral thalamus or prethalamus (vTh or pTh), thalamus (Th), and pretectum (PT) from rostral to caudal direction. Hypothalamus (Hy) is located ventrally to the diencephalon. Eth:epithalamus

Drawings originate from (Lokmane and Garel, 2011; Martinez-Ferre and Martinez, 2012)

The regulatory role of Pax6 on Cell Division Cycle Associated 7 and cortical progenitor cell proliferation FGFs are secreted by the gastrula organiser, or node in mammals, as well as endodermal cells beneath the future neuroectoderm. These molecules are able to trigger neural fate by induction of pre-neural markers. Neural induction is further proceeded by release of BMP antagonist by the neural tissue, which progresses to separate from the epidermis (Kudoh et al., 2004; Muñoz-Sanjuán and Brivanlou, 2002; Wilson and Edlund, 2001; Wilson and Houart, 2004). The function of Wnts is finely controlled temporally. Wnts at first cooperate with FGFs to induce neural fate but a later stage they promote non-neural ectoderm together with BMPs signals (Baker et al., 1999; Erter et al., 2001; Gaulden and Reiter, 2008; Heeg-Truesdell and LaBonne, 2006). FGFs are also important in determining the antero-posterior axis in the neural tube. In the anterior end of the neural tube, FGFs are highly expressed together with Wnt antagonists such as Sfrp family members, which localise in a anterior^{high} to posterior^{low} gradient, counteracting the Wnts gradient which exists in the opposite pattern (Beccari et al., 2013). Gain-of-function experiment found Fgf8-soaked beads placed in the anterior neural plate can induce the production of Foxg1b, a transcription factor required for telencephalic and optic regionalisation (Shimamura and Rubenstein, 1997). Anterior overexpression of FGF8 in mice resulted in reduction of Wnt signalling in the cortical hem and hippocampus shrinkage (Shimogori et al., 2004).

Fgf molecules also locate along the dorso-ventral axis, where their gradients are high dorsally and low ventrally, opposite to the gradient of Sonic hedgehog (Shh). Opposing gradients of the two genes act co-ordinately to develop telencephalon in the dorsal, and hypothalamus in the ventral region (Wilson and Maden, 2005). High level of Shh signalling secreted from the ventral regions activates Gli1/2 and represses Gli3 function, which further induce several ventral markers such as Foxa2, Nkx2.2, Olig2 and Dbx1/2. Shh also inhibits Pax6 and Irx3 (Briscoe et al., 2000). Overexpression of Shh induced ventral interneuron and motor neurons while mice lacking Shh failed to develop floor plate and various types of ventral interneurons (Chiang et al., 1996; Echelard et al., 1993; Krauss et al., 1993; Roelink et al., 1994). Together, the gradient of Shh determines the localisation of various transcription factors, which patterns the dorso-ventral axis in the telencephalon.

The regulatory role of Pax6 on Cell Division Cycle Associated 7 and cortical progenitor cell proliferation Shh can also be secreted from a small group of cells in an organizer region called the zona limitans intrathalamica (Zli). The Zli locates between thalamus and prethalamus and separates the telencephalon from diencephalon. High level of Shh secreted from the Zli regionalises surrounding areas (Kiecker and Lumsden, 2004; Zeltser, 2005). The Zli region is flanked by an area expressing Lunatic fringe (*Lfng*). Overexpression of *Lfng* prevents the formation of Zli. In *Pax6*^{-/-} mice, Zli regions expand along the dorso-ventral axis in the diencephalon, possibly mediated by the transcription factor *Barhl2*. Together these data suggest formation of Zli is dependent on the combinatorial signalling between Shh, Pax6 and *Lfng*. (Caballero et al., 2014; Kiecker and Lumsden, 2004; Larsen et al., 2001; Parish et al., 2016).

Wnts are secreted glycoproteins which function to establish posterior identity along the antero-posterior axis of the neural tube by antagonising FGF signalling (Wilson and Houart, 2004). Later in the development, Wnts are secreted from the dorso-medial border of cortex, named the cortical hem, where BMPs molecules are also produced (Furuta et al., 1997; Grove et al., 1998; Shimogori et al., 2004). Signalling from the cortical hem is essential for the development of adjacent tissues such as hippocampus and choroid plexus. Choroid plexus was abnormally formed in *Wnt-3a*-deficient mice. Hippocampus and dentate gyrus failed to form in this mutant mice. (Lee et al., 2000). In *Gli3* mutant mice, the cortical hem was absent, causing significant reduction of cortical hem-derived Wnts and BMPs (Grove et al., 1998).

The function of retinoic acid (RA) in forebrain development is less studied. RA is derived from vitamin A, it is synthesised by family members of retinaldehyde dehydrogenase and catabolized by the CYP26 class of P450 enzymes in the cytoplasm (Chithalen et al., 2002). The function of RA involves establishment of antero-posterior and dorso-ventral axis in a gradient-dependent manner (Maden, 2007). Combined anterior expression of CYP26 in the forebrain and midbrain, and posterior expression of retinaldehyde dehydrogenase in the spinal cord specified the hindbrain compartments (Glover et al., 2006; Reijntjes et al., 2004). Defective expression of *Fgf8* and Shh were seen in chick forebrain treated with RA receptors antagonist (Schneider et al., 2001). Moreover, retinaldehyde dehydrogenase 2-null mice also displayed downregulations of *Fgf8* and Shh signalling, concurrent with

The regulatory role of Pax6 on Cell Division Cycle Associated 7 and cortical progenitor cell proliferation malformation of the telencephalon, optic vesicle and ventral diencephalon (Rhinn and Dollé, 2012; Ribes et al., 2005).

In the next section, gradients of signalling molecules in the cortex will be further discussed in details.

1.1.2 Gradients of signalling molecules in the cortex affect cerebral cortical development

Multiple signalling pathways act in concord to regulate self-proliferation and differentiation of neural stem cells, as well as neuronal subtype specification and arealisation in the telencephalon. Signalling molecules and transcription factors are expressed in the signalling organisers or in restricted areas, and sometimes the expression occurs in a graded fashion to exert regional influences during cortical development (Figure 1.2A) (Montiel and Aboitiz, 2015; Sansom and Livesey, 2009).

Secreted molecules such as fibroblast growth factors (FGFs) are some of the best characterised morphogens involved in the forebrain development. Early expression of Fgf3, 8, 15, 17 and 18 are observed from E9.5 in mouse embryos in the rostral midline regions forming a secreting centre of Fgf molecules which function in a concentration-dependent manner (purple region, Figure 1.2A) (Bachler and Neubüser, 2001; Maruoka et al., 1998; McWhirter et al., 1997). Fgf8 is expressed in a high rostrally to low caudally pattern in the forebrain (Figure 1.2B). Gain or loss-of function studies have demonstrated that Fgf8 is essential for rostral neocortex identity (Fukuchi-Shimogori and Grove, 2001; Okada et al., 2008; Sahara et al., 2007; Storm et al., 2006). Motor cortex, somatosensory cortex and primary visual cortex are located from rostral to caudal in the neocortex. Ectopically expressed Fgf8 by *in utero* electroporation in the rostral end of the neocortex results in an expansion and caudal shift of the motor cortex and shrinkage of somatosensory and primary visual areas (Fukuchi-Shimogori and Grove, 2001). In contrast, the rostral regions reduce when the area is injected with soluble Fgf receptor (sFgfr3) which competes with cell surface receptors for Fgf8, thereby inhibiting signals to the cells (Fukuchi-Shimogori and Grove, 2003, 2001). Moreover, ectopic introduction of Fgf8 in the caudal area of the cortex promotes the formation of an extra somatosensory cortex in the region (Fukuchi-Shimogori and Grove, 2001). The function of Fgf signalling was further demonstrated using a mouse model deficient in Fgf receptor (Fgfr)1 specifically in the forebrain. *Fgfr1-deficient* embryos possess normal rostro-caudal axis patterning indicated by the regional markers Pax6 and Emx2, but the olfactory bulb (OB), which is located at the rostral tip of the forebrain, fails to form (Hébert et al., 2003).

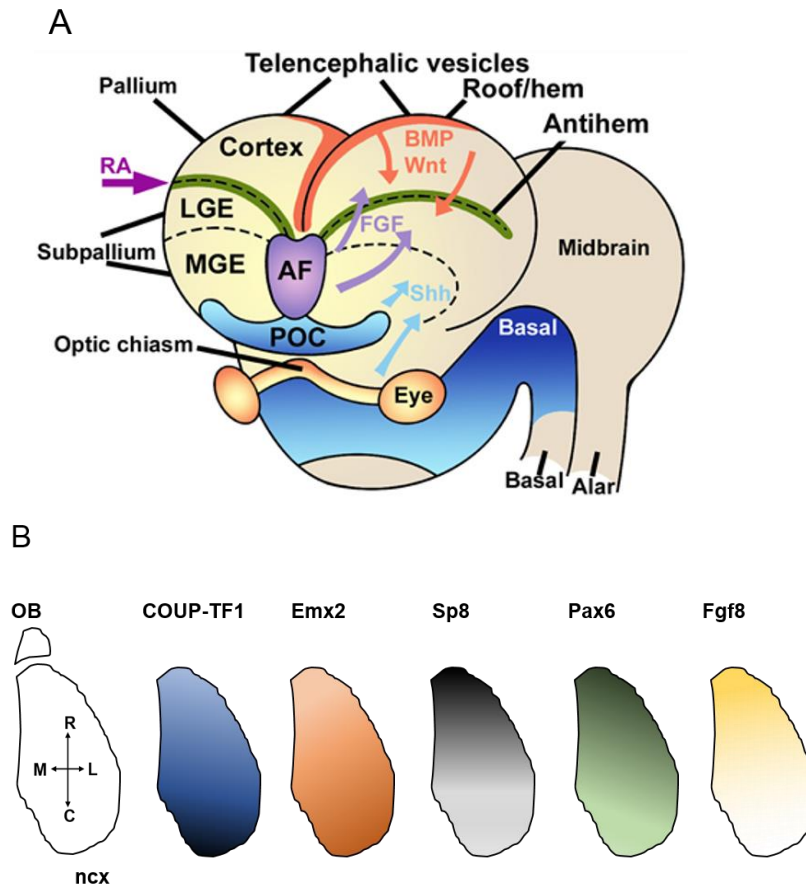


Figure 1.2 The signalling centres and gradients in the embryonic brain.

(A) There are four distinct signalling centres which account for the regional patterning in the forebrain. A rostral signalling centre or the anterior forebrain (AF, violet) secretes fibroblast growth factors (Fgfs) and the cortical hem (orange) on the caudodorsal side of the forebrain secretes Wnts (wingless/ints) and bone morphogenetic proteins (BMPs). A rostroventral centre close to commissural preoptic area (blue, POC) secretes sonic hedgehog (Shh) and the Antihem located at the interface of the cortex and the lateral ganglionic eminence (green, LGE) secretes retinoic acid (RA). (B) The graded expression of four transcription factors and one signalling molecule (Fgf8) in a mouse neocortex (ncx). The expression patterns of COUP-TF and Emx2 are caudal^{high} to rostral^{low} while those of Sp8, Pax6 and Fgf8 are high rostrally and low caudally. OB: olfactory bulb; R:rostral; C: caudal; M:medial; L: lateral

Diagrams originate from (Montiel and Aboitiz, 2015; Sansom and Livesey, 2009)

The regulatory role of Pax6 on Cell Division Cycle Associated 7 and cortical progenitor cell proliferation Sp8 is a zinc finger transcription factor which is essential for rostral identity in neocortex (Figure 1.2B). Loss of Sp8 results in expansion of the caudal area in developing cortex (Zembrzycki et al., 2007). Moreover, conditional inactivation of Sp8 in embryonic ventral telencephalon causes downregulation of interneurons in the OB (Waclaw et al., 2006). Sp8 and Fgf8 mutually induce each other's expression and Sp8 protein physically binds to *Emx2* regulatory elements, repressing the expression of Fgf8, implying a sophisticated interactive regulatory network controlling region identity in developing cortex (Zembrzycki et al., 2007).

Another transcription factor COUP-TF1 is expressed high caudomedially and low rostromedially in developing cortex (Figure 1.2B)(Liu et al., 2000; Zhou et al., 2001). This gradient is similar to that of *Emx2* but is opposite to those of Fgfs, Sp8 and Pax6. COUP-TF1 has been shown to be responsible for the caudal identity of neocortex. Mice with cortex-specific deletion of COUP-TF1 exhibit phenotypes similar to those seen in the Fgf8 overexpression model in the rostral part of neocortex, with massive expansion of the rostral area or motor cortex at the expense of the caudal regions, and shrinkage of somatosensory and primary visual cortex (Armentano et al., 2007; Faedo et al., 2008). Being a transcriptional repressor, COUP-TF1 is also thought to inhibit rostral fate in the caudal area in a gradient-dependent manner. Further studies have shown that the activity of Fgf signalling and COUP-TF1 are mutually repressive during area specification in the cortex (Borello et al., 2014). Upregulation of Fgfs expression in the rostral cortex results in contraction of the COUP-TF1 gradient, while downregulation of Fgfs leads to expansion (Fukuchi-Shimogori and Grove, 2003; Garel, 2003). Molecular studies have revealed that COUP-TF1 is repressed by Sp8, a downstream factor of Fgf8 signalling. Overexpression of Sp8 during early corticogenesis causes a reduction in COUP-TF1 expression, while reduction in Sp8 expression leads to increased COUP-TF1. Additionally, COUP-TF1 overexpression results in downregulation of Sp8 (Borello et al., 2014). Taken together these two transcription factors, COUP-TF1 and Sp8 act in a mutually repressive manner.

Studies using models with various expression levels of *Emx2* have shown that caudal identity is determined by *Emx2* dosage (Figure 1.2B) (Hamasaki et al., 2004). Elevated *Emx2* expression under the control of the Nestin promoter results in an

The regulatory role of Pax6 on Cell Division Cycle Associated 7 and cortical progenitor cell proliferation expansion of the caudal area in neocortex, while in *Emx2*-null mutants, reduction in the caudomedial area and later the primary visual cortex have been observed (Bishop et al., 2002; Hamasaki et al., 2004; Muzio et al., 2002a, 2002b). The phenotypes of the *Emx2*-null mutant are similar to those of the *COUP-TF1* mutant. However the expression level of COUP-TF1 is not altered in *Emx2*-null cortex, suggesting that COUP-TF1 may function upstream to *Emx2* (Cecchi, 2002; Sansom and Livesey, 2009; Zhou et al., 1999).

1.1.3 Cell cycle control in mouse development

Building a functioning cortex requires precise control of the number and type of neurons in the region, as well as correct formation of neural circuits. Neural progenitors undergo one to several rounds of cell cycles before committing to neurogenic division (Edlund and Jessell, 1999; Galderisi et al., 2003). The rate of cell cycle progression and the balance between cell cycle re-entry and exit have been demonstrated to correlate with the number of neurons in individual layers of the cerebral cortex (Polleux et al., 1997). Modulation of cell cycle kinetics can also alter neuron production. Early mathematical models show that acceleration of proliferative division in progenitors results in an excess amount of neurons (Dehay and Kennedy, 2007; Pilaz et al., 2009; Polleux et al., 1997). In contrast, acceleration of differentiative division in progenitors leads to a transient increase in neurons but eventually the number reduces due to exhaustion of the progenitor pool (Caviness et al., 2003; Polleux et al., 1997). Here, I will first focus on the general control of cell cycle progression and the outcomes of its misregulation during mouse cortical development.

A complete cell cycle consists of four phases including G1, S, G2 and M (Figure 1.3). During S phase DNA synthesis occurs and chromosomes are replicated, and in M phase (mitosis) the cell divides into two daughter cells. The two gap phases, G1 and G2 both possess checkpoint roles which can halt the cell cycle to ensure that the cell is fully prepared for the coming DNA synthesis or cell division, respectively. There is an extra phase, known as G0, in post-mitotic and terminally differentiated cells which have become quiescent. Various protein complexes have been found to promote or restrict the progression of the cell cycle. Different combinations of

The regulatory role of Pax6 on Cell Division Cycle Associated 7 and cortical progenitor cell proliferation
Cyclin-CDKs (cyclin-dependent kinases) tightly regulate cell cycle progression. During early G1 phase, Cyclin D/CDK4, 6 complex senses both intrinsic and environmental growth signals to promote cell cycle progression while in late G1 phase, Cyclin E/CDK2 is required for transition to S phase. Expression of Cyclin A/CDK2, Cyclin A/CDK1, 2 and Cyclin B/CDK1 are required in S, G2 and M phases, respectively (Ciemerych and Sicinski, 2005).

The restriction point in G1 is the time when cells become committed to cell cycle progression even without extracellular growth factors. After passing this point, cells become growth factor-independent (Foster et al., 2010; Pardee, 1989). Various cell cycle inhibitors are produced by the cell to modulate passage through phases. The CIP/KIP inhibitor family contains p21, p27 and p57 and inhibits a broad range of cyclins and CDKs throughout the cell cycle, especially at the G1/S and G2/M checkpoints. The CIP/KIP family proteins act downstream of the tumour suppressor p53 which halts the progression of cell cycle in response to DNA damage, hypoxia stress and cell injury (Brugarolas et al., 1995; El-Deiry, 1993). The other inhibitor family INK4 consists of p15, p16, p18 and p19. INK4 family members modulate the G1/S checkpoints by competing with CDK4 and CDK6 in binding to Cyclin D, thereby interfering the formation of the Cyclin D/CDK4, 6 complex (Pavletich, 1999; Tvrđík et al., 2002). The cyclin D/CDK4, 6 complex can phosphorylate retinoblastoma protein (Rb) (Dyer and Cepko, 2001; Massagué, 2004; Pavletich, 1999). Rb when hypophosphorylated physically binds to E2f family transcription factors E2f1, 2, and 3. Phosphorylated Rb is released from this interaction, allowing E2fs to enter the nucleus and trigger the expression of their downstream target genes which include regulators of cell cycle progression (Blais and Dynlacht, 2007; Helin et al., 1993; Lees et al., 1993).

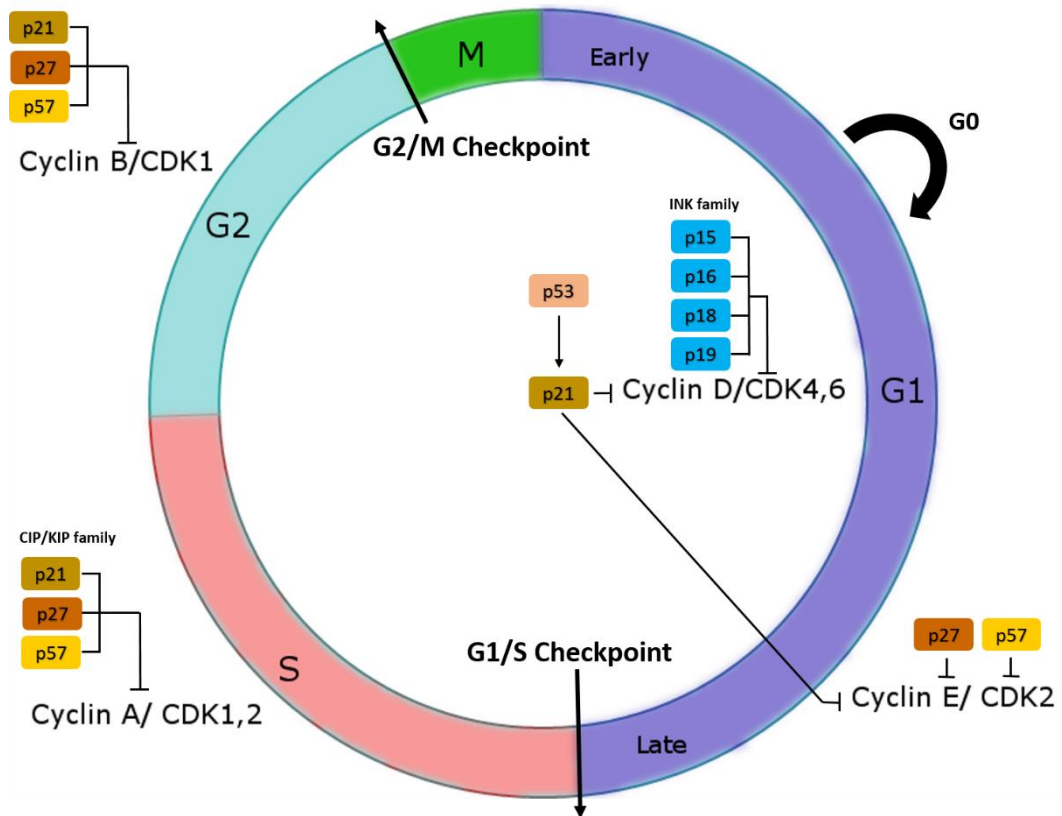


Figure 1.3 Structure, regulation and checkpoints of a cell cycle.

A full cycle comprises four consecutive phases including S phase for DNA synthesis, M phase for cell division, and the two gap phases G1 and G2 for the cell to pause and become ready for the coming cellular events. There is an extra stage called G0. Cells in G0 phase exit the cell cycle and become quiescent or terminally differentiated. Protein complexes consisting of different combination of cyclins and CDKs tightly control cell cycle progression. The complexes are also monitored by groups of inhibitors including the INK family and CIP/KIP proteins. Adapted from (Dehay and Kennedy, 2007; www.pathophys.org)

Previous studies have adopted loss-of-function approaches to reveal the importance of cyclin/CDK complexes as well as the inhibitory protein families. Some mutants display relatively normal and viable phenotypes while some are embryonic lethal (Berthet and Kaldis, 2007; Sherr and Roberts, 2004). Mice lacking Cyclin D1, D2 and D3 (three members of the D-type cyclins) or Cyclin D2 and D3 die at E16.5 and E17.5-18.5, respectively, with megaloblastic anaemic phenotypes (Ciemerych et al., 2002; Kozar et al., 2004). *Cdk4*^{-/-} and *Cdk6*^{-/-} double mutant mice also die embryonically between E14.5-E18.5 of severe anaemia and haematopoiesis-related deficits (Malumbres et al., 2004). Mice lacking individual INK family members are relatively normal during embryonic development but possess an increased risk of tumour occurrence in adulthood (Franklin et al., 2000, 1998; Latres et al., 2000; Serrano et al., 1996); however *p27*^{-/-};*p57*^{-/-} double mutants are embryonic lethal at E12-E16.5 with abnormal proliferation in lens, limbs and intestine (Ciemerych and Sicinski, 2005; Zhang et al., 1998).

The developmental functions of the pRb-E2f pathway have also been elucidated. Mice deficient in individual E2f family members, *E2f1-6*, except *E2f4*, are viable but suffer from developmental defects in multiple organs (Swiss and Casaccia, 2010). Mice with combined null mutations in *E2f2* and *E2f3* or *E2f1* and *E2f3* are embryonic lethal (Wu et al., 2001). *pRb* knockout embryos die between E12-E15 with severe defects in erythroid, neural and lens development (Clarke et al., 1992; Jacks et al., 1992; Lee et al., 1992; Swiss and Casaccia, 2010).

Regulation of cell cycle progression is critical in mouse embryo development. In developing cortex, control of the progression rate both temporally and spatially determines the number of neurons and circuit connections in the region. In the next section I will summarise the decision making between proliferative or differentiative division in cortical progenitors, and the cell cycle kinetic mechanisms involved in this regulation.

1.1.4 Differentiation and proliferation of cortical progenitors

In the dorsal telencephalon (dTel), a single layer of neuroepithelial cells which reside in the area closest to the ventricle become a type of neural progenitor cells called radial glia cells (RGCs). The shape of RGCs is elongated with their processes attached to the ventricle (inside) and the pial surface (outside), therefore RGCs are also called the apical progenitors (APs) (Barry et al., 2014; Kriegstein and Götz, 2003; Malatesta et al., 2003). During neurogenesis, the nuclei of RGCs move within the ventricular zone (VZ) at different phases of the cell cycle. This movement is termed interkinetic nuclear migration (INM) (Hayes and Nowakowski, 2000; Miyata et al., 2001; Noctor et al., 2001), and results in nuclei undergoing S-phase at the outer edge of the VZ and mitosis at the ventricular surface. RGCs are thought to give rise to most of the glutamatergic neurons via direct neurogenesis or indirectly via another type of progenitor cell called the intermediate progenitor cells (IPCs) (Figure 1.4). At the beginning of neurogenesis, around E11 to E12 in mouse, RGCs mainly undergo symmetrical divisions, doubling their population in order to expand the progenitor pool; a minority of RGCs divide asymmetrically, producing one RGC and one IPC or one neuron which exits the cell cycle and migrates to the preplate near the pial surface (Huttner and Kosodo, 2005; Noctor et al., 2004). At later stages of neurogenesis, from E13, the proportion of RGCs undergoing asymmetric division increases, thereby accelerating the production of IPCs and neurons. IPCs reside in the subventricular zone (SVZ) and their cellular processes are not attached to the apical nor basal surfaces of the dTel. In mice they are committed to the neuronal lineage and divide symmetrically to generate two neurons which exit the cell cycle and migrate further outside to occupy the cortical plate (Haubensak et al., 2004; Noctor et al., 2004; Pontious et al., 2008). IPCs are the major type of transient-amplifying progenitors, which in mouse only divide once to produce two daughter neurons, in contrast to these cells in human which are also capable of self-renewal (Hansen et al., 2010).

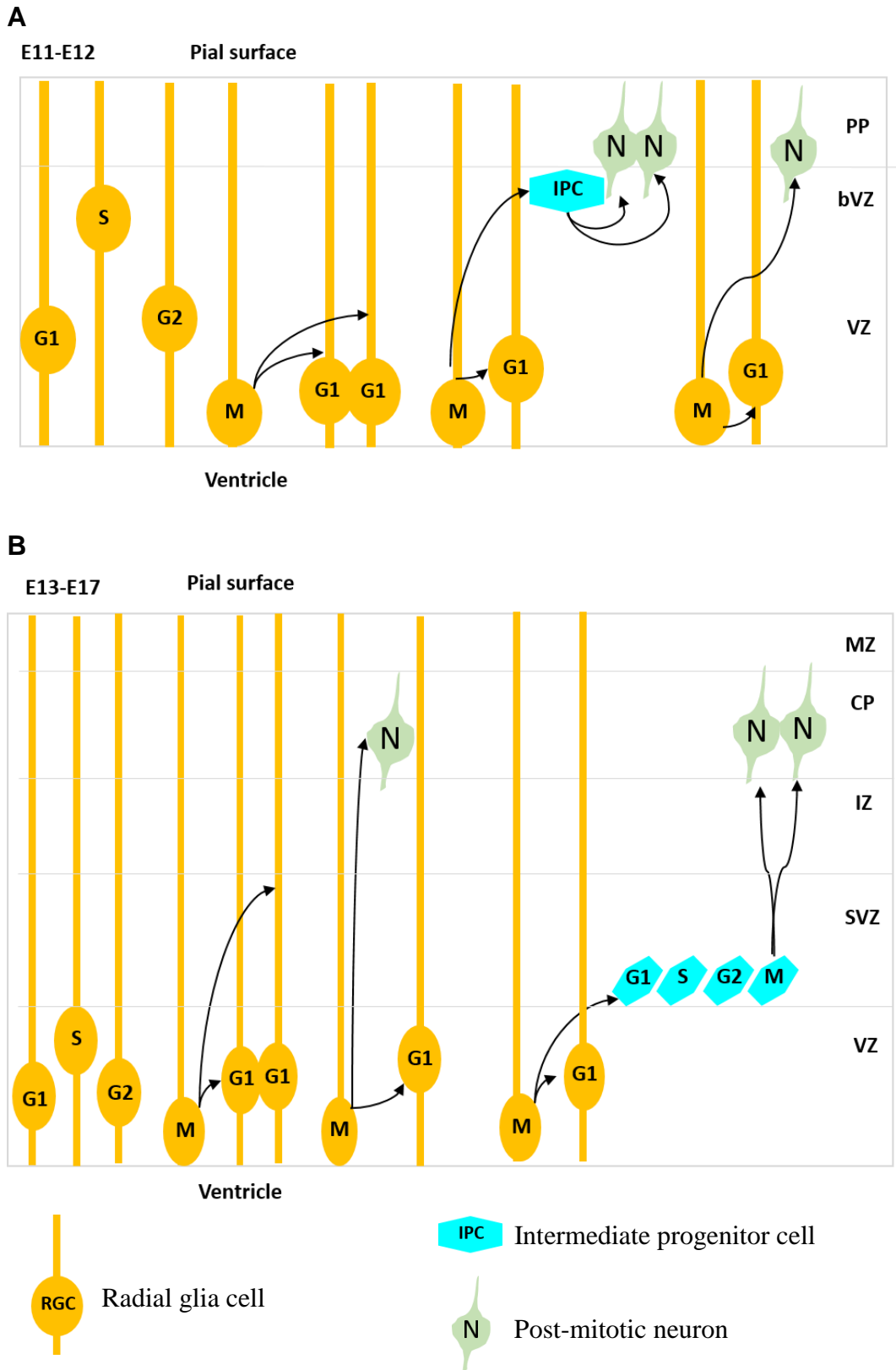


Figure 1.4 Interkinetic nuclear migration of radial glia cells and neurogenesis in developing mouse cortex.

Figure 1.4 Interkinetic nuclear migration of radial glia cells and neurogenesis in developing mouse cortex.

(A) During early neurogenesis (E11-12), radial glia cells (RGCs) mainly undergo symmetrical division to generate two RGCs. Interkinetic nuclear migration (INM) is a specific feature of RGCs. The migration involves movement of the nucleus within the ventricular zone (VZ) during the cell cycle. The cell divides when the nucleus is at the ventricular surface, the nucleus then moves upward to the basal side of the VZ (bVZ) for DNA synthesis in S phase. During G2 phase, the nucleus moves apically for the next round of division. A small population of RGCs divide asymmetrically to either produce one RGC and one intermediate progenitor cells (IPCs, indirect neurogenesis) or one RGC and one post-mitotic neuron (direct neurogenesis). (B) During mid-neurogenesis, RGCs still undergo symmetrical and asymmetrical divisions, however the proportion of asymmetrical division increases. IPCs do not exhibit INM feature and they divide in the subventricular zone (SVZ). IPCs are the main source of post-mitotic neurons that migrate to the cortical plate (CP). PP: pre-plate; IZ: intermediate zone; MZ: marginal zone. Adapted from (Guillemot, 2005)

The regulatory role of Pax6 on Cell Division Cycle Associated 7 and cortical progenitor cell proliferation. The mechanisms regulating the transition of RGCs from self-renewing to neurogenic or differentiative division are not fully understood. Two extracellular signalling pathways, retinoic acid (RA) and FGF signalling, have been found to be responsible for the transition, although the detailed biochemical events remain elusive (Diez del Corral and Storey, 2004; Kang et al., 2009). Meningeal derived retinoic acid may be the cause of the defects seen in *Foxc1* mutants, which include a significant reduction of IPCs and neurons and abnormal meningeal development. *In utero* replacement of RA in *Foxc1* mutants is able to rescue the deficit (Siegenthaler et al., 2009). *Fgfr 1-3* triple mutant mice show an early depletion of Pax6⁺ RGC cells which are committed to the IPC fate, causing reduced neuron production and ultimately a thinner cortex (Kang et al., 2009). Further evidence shows that transient expression of Fgf10 by the neuroepithelial cells (NCs) regulates the transition of NCs to RGCs. Loss of Fgf10 signalling leads to delayed RGC production and fewer RGCs and IPCs in early neurogenesis, but eventually the production of progenitors and neurons becomes excessive, resulting in a larger cortex (Sahara and O'Leary, 2009).

Notch signalling is known to maintain the proliferative capacity of RGCs. RGCs express Notch receptor while their daughter cells, both IPCs and post-mitotic neurons, and surrounding cells express Notch ligands such as Delta-like 1 (Dll1). Engagement of Notch receptor with the ligand is required for RGCs to stay proliferative and prevents the cells from entering differentiation (Kageyama et al., 2008; Shimojo et al., 2011, 2008).

It has been hypothesised that unequal distribution of cell fate determinants promotes asymmetrical division of stem cells and highly polarised RGCs provide an ideal model to study these factors. The cleavage plane for RGC division is variable; in mouse cortical RGCs, which divide at the ventricular surface during M phase, the mitotic spindles align at certain angles (either parallel or perpendicular, or any angles in between) to the ventricular surface. The arrangement of mitotic spindles also determines the position of the cleavage plane. Based on previous studies as well as advanced time-lapse imaging techniques, it was found that the cleavage plane vertical or between 60-120 degrees to the ventricular surface leads to proliferative RGC (Figure 1.5A) while the cleavage plane parallel or between ± 30 degrees to the ventricular surface results in neurogenic division (Figure 1.5B). It is therefore

The regulatory role of Pax6 on Cell Division Cycle Associated 7 and cortical progenitor cell proliferation possible that the cleavage plane may control or be controlled by the distribution of cell fate determinants. Although there is no correlation between unequal inheritance of the apical membrane to the two daughter cells and fate decision (Shitamukai et al., 2011), it is known that only one daughter cell will receive the basal process which attaches to the pial surface during neurogenic division of RGCs (Miyata et al., 2001; Noctor et al., 2001; Shitamukai et al., 2011).

A number of studies have suggested several fate determinants which when unequally distributed will eventually influence the destiny of daughter cells. Numb and Mindbomb (Mb) are two candidates for such factors (Knoblich, 2008; LeBorgne and Schweisguth, 2003; Roegiers and Jan, 2004; Shen et al., 2002). Numb and its homolog Numb-like are regulators of membrane trafficking involved in the internalisation of Notch receptor, causing down-regulation of Notch signalling and triggers differentiation (Bhalerao et al., 2005; McGill and McGlade, 2003). Numb is also involved in the unequal distribution of Par3 which is associated with mitotic spindle alignment; cells that inherit more Par3 will stay in self-renewal mode with a reduction in Numb activity (Bultje et al., 2009). Asymmetrical inheritance of Mb in daughter cells also correlates with Notch signalling. A study has shown that cells receiving more Mb are associated with higher Delta activity, which eventually drives differentiation (Dong et al., 2012).

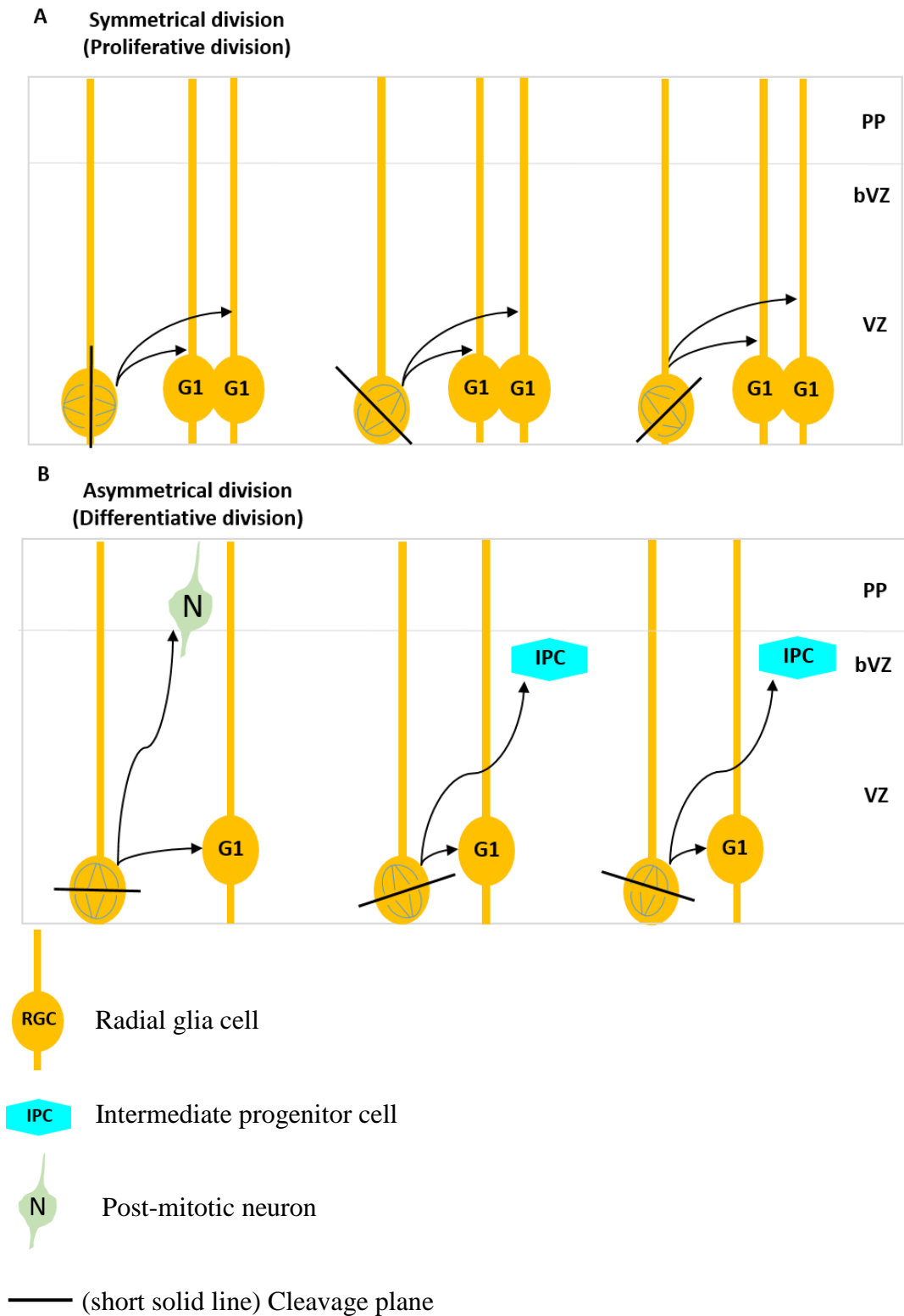


Figure 1.5 The link between the cleavage plane and the mode of division in radial glia cells.

Figure 1.5 The link between the cleavage plane and the mode of division in radial glia cells.

The cleavage planes (solid black lines) are believed to associate with the mode of division.

(A) In M phase, mitotic spindles are aligned in the middle of the cell. When the cleavage line is perpendicular to the ventricular surface or the angle is between 60-120 degrees, the RGC undergoes proliferative division, producing two RGCs. (B) Mitotic spindles tilt during asymmetrical division. When the cleavage plane is parallel or within ± 30 degrees to the ventricular surface, the RGC undergoes differentiative division, producing one RGC plus one IPC or one neuron. Correlation between the decision for IPC or neuron production and the cleavage plane is unclear. Adapted from (Guillemot, 2005)

The regulatory role of Pax6 on Cell Division Cycle Associated 7 and cortical progenitor cell proliferation. It has been observed that during differentiation of stem cells to post-mitotic neurons, the duration of the cell cycle, especially the G1 phase, is extended (Roccio et al., 2013). In addition, it is also hypothesised that two daughter cells which inherit unequal level of fate determinants will progress to different destinies, proliferation or differentiation, according to the length of their G1 phase (Figure 1.6). Cells that possess different amounts of determinants would act in the same manner under most circumstances. However upon reaching the threshold of G1 length, cells that possess more neurogenic-promoting molecules will be able to receive greater influences from both intrinsic and environmental stimuli to trigger differentiation. This theory is supported by studies manipulating the length of G1 by targeting CDKs and cyclins in cortical neural progenitors, which have shown that lengthened G1 triggers differentiation and inhibits proliferation (Calegari andHuttner, 2003; Glickstein et al., 2009; Lange et al., 2009; Pilaz et al., 2009). However, whether prolonged G1 is the cause or the consequence of neural differentiation remains elusive.

In summary, development of the dTel is tightly regulated both temporally and spatially by multiple signalling pathways and transcription factors. Later in this chapter I will discuss two key molecules, Pax6 and Cell division cycle associated 7 (Cdca7) and how they may affect cortical development.

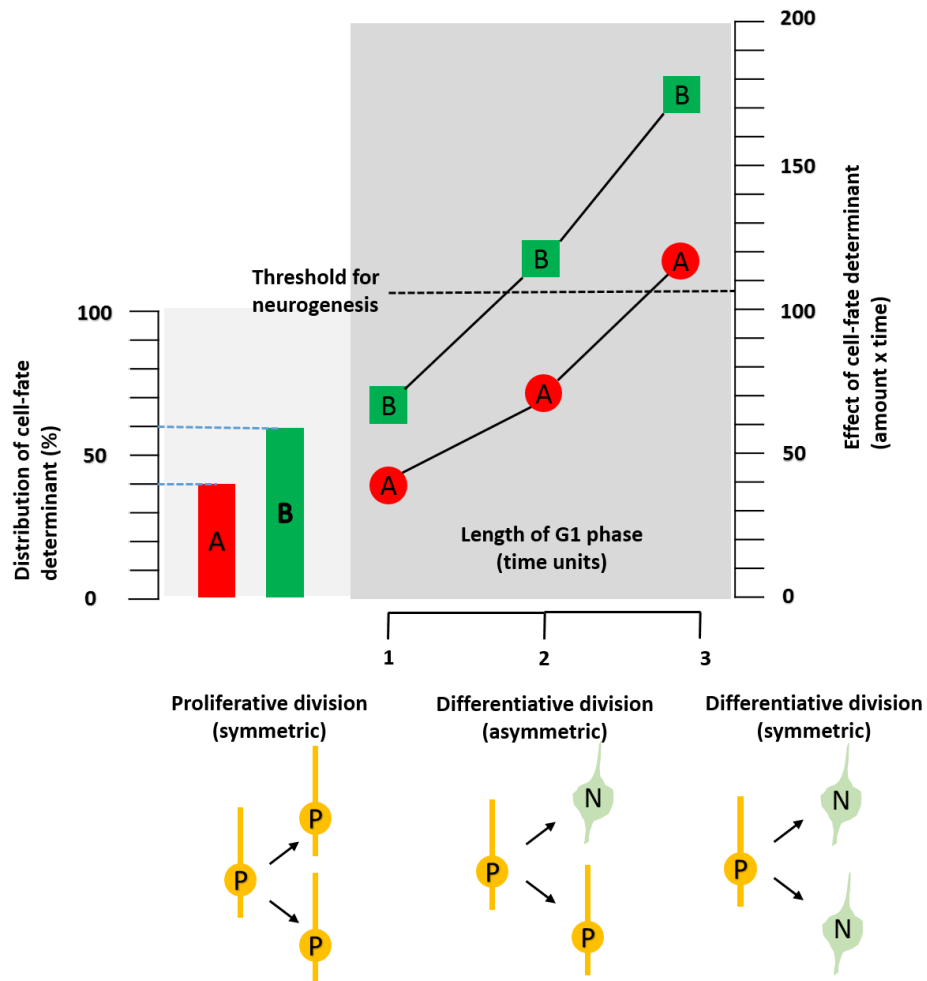


Figure 1.6 The link between G1 length and the mode of division in cortical progenitors.

It is hypothesised that the duration of a cell cycle, especially the G1 phase is important for the progenitor cell to choose whether it should undergo proliferative or differentiative division. For instance, cell A and cell B contain unequal amounts of cell-fate determinants (40% and 60%, respectively). When the G1 phase is short (time unit = 1), both cell A and B undergo proliferative divisions to produce two daughter progenitors. When the G1 phase is long (time unit = 3), both cells perform differentiative division to generate two neurons. When the G1 phase is intermediate at the threshold (time unit = 2), intrinsic and environmental neurogenic signals cause cell B to exceed the neurogenesis threshold and enter asymmetrical division while leaving cell A in proliferative division. Adapted from (Calegari and Huttner, 2003; Dehay and Kennedy, 2007; Götz and Huttner, 2005)

1.2 Pax6 and its role in cortical development

1.2.1 Discovery of PAX6/Pax6 and its related human disease

Pax6 is an evolutionarily conserved paired-box family transcription factor (Glaser et al., 1992). PAX6/Pax6 contains two DNA binding domains, a paired domain (PD) and a homeodomain (HD), each of which can individually or co-operatively interact with DNA (Czerny et al., 1993; J. A. Epstein et al., 1994; Jun and Desplan, 1996). The expression of Pax6 can be observed from embryonic day 8 (E8) (Walther and Gruss, 1991) in the neural epithelium of forebrain, including the telencephalon, diencephalon, and hindbrain. Throughout the development of a mouse embryo, Pax6 expression is maintained in the cortex and thalamus as well as in the olfactory bulb, developing eyes, spinal cord and pancreatic islet cells (Grindley et al., 1995; Stoykova and Gruss, 1994; Walther and Gruss, 1991). PAX6 mutations have been identified as the cause of the human disease Aniridia (Glaser et al., 1992; Jordan et al., 1992). Haploinsufficient PAX6 protein production leads to development of aniridia and patients carrying this disease suffer from iris hypoplasia, malformation of lens, cornea and retina and impaired vision (Guercio and Martyn, 2007). *Small eye* (*Sey*) mice carrying a mutation in *Pax6* have become a great model for studying aniridia. Heterozygous mutant mice (*Pax6^{Sey/+}*) suffer from similar symptoms as seen in human patients while *Pax6^{Sey/Sey}* mice possess severe phenotypes including loss of eyes and nasal cavity, smaller brain size and die soon after birth (Hill et al., 1991; van der Meer-de Jong et al., 1990).

1.2.2 Disruption of the pallial-subpallial boundary (PSPB) in Pax6 mutants

Pax6 protein is expressed in a gradient fashion in the dTel as well as in the diencephalon (Figure 1.7) (Bishop et al., 2000; Georgala et al., 2011a; Mi et al., 2013a; Sansom et al., 2009; Walther and Gruss, 1991). The telencephalon is subdivided into dorsal and ventral telencephalon or pallium and subpallium, respectively. Establishment of the anatomical boundary between the dTel and vTel requires the presence of Pax6 (Stoykova et al., 2000; Stoykova and Gruss, 1994; Yun et al., 2001).

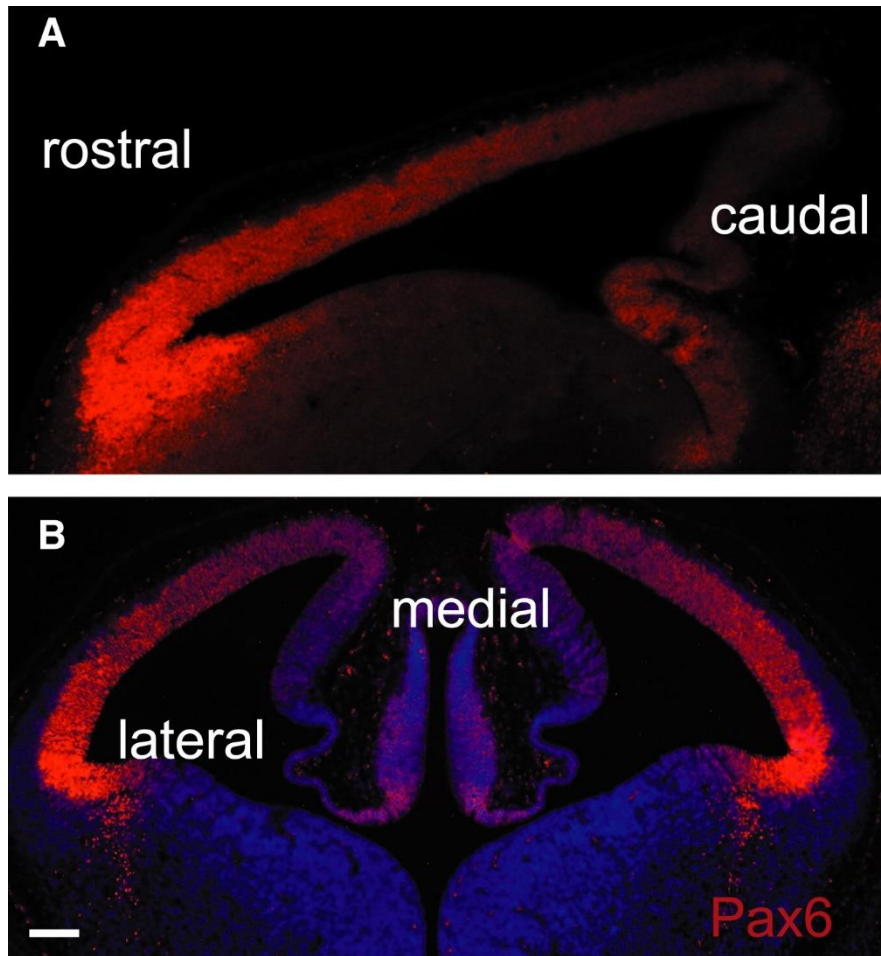


Figure 1.7 The expression pattern of Pax6 at E12.5 in mice.

Representative immunofluorescent images showing the gradient expression pattern of Pax6 protein in the telencephalon. The gradient is rostralateral^{high} to caudomedial^{low} at E12.5. (A) Sagittal section showing the expression of Pax6 which reaches the highest level at the rostral tip of the dorsal telencephalon (dTel) (B) Coronal section showing the expression of Pax6 which reaches the highest level at the most lateral part of dTel. Both pictures demonstrate that the expression of Pax6 is fairly weak in the ventral telencephalon (vTel). Scale bar: 100 μ m. Picture originally from (Mi et al., 2013a)

Pax6 is highly expressed in the VZ of dTel together with other proteins including Neurogenin 2 (Ngn2 or Neurog2) and Dbx (Fode et al., 2000; Lu et al., 1994, 1992). The expression of Pax6 in the subpallium is much reduced and instead Ascl1, Gsx2 and Nkx2.1 are highly expressed (Georgala et al., 2011a; Toresson et al., 2000). Disruption of the PSPB can be observed in the *Pax6^{Sey/Sey}* mutant and multiple mechanisms contribute to this defect. First, cells from the dorsal or the ventral side of PSPB express different cell adhesion molecules, such as R-cadherin (cdh4) in the dorsal and cadherin-6 (cad6) in the ventral region (Georgala et al., 2011a). Cells isolated from *wild-type* (WT) cortex and striatum tend to segregate *in vitro* while the segregation is defective in cells from the *Pax6^{Sey/Sey}* mutant, indicating that the cell identities are regulated by Pax6 in a cell-autonomous manner (Tyas, 2003). Second, Pax6 is also involved in regulating the expression of some pallial and subpallial markers. As mentioned before, regional specific markers are expressed on either side of the PSPB from E9.5 in *wild-type*. A dorsal shift of ventral markers including Ascl1, Gsx2 and Oligo2 has been found to coincide with a down-regulation of dorsal markers such as Ngn2 and Tbr2 in *Pax6*-null embryos (Quinn et al., 2007; Stoykova et al., 1996; Toresson et al., 2000; Yun et al., 2001). In contrast, *Gsx2^{-/-}* embryos possess opposite phenotypes to those seen in *Pax6^{Sey/Sey}* embryos at E10.5, with ectopic expression of pallial markers Pax6, Ngn1, Ngn2 and Tbr2 in the subpallium and reduced expression of Ascl1 and Dlx1. However this mis-arealisation disappears later at E14.5 partially due to the upregulation and consequentially the compensation effects of Gsx1 (Toresson et al., 2000; Yun et al., 2001).

1.2.3 Cortical lamination and migration of post-mitotic neurons regulated by Pax6

Neocortex consists of a six-layered structure with different cell types, cell density and inputs/outputs from/to other regions of mammalian brain and body, this area is responsible for sensory and motor control, as well as consciousness. (ref). Cortical neurons are classified into two groups: excitatory or glutamatergic neurons, and inhibitory or GABAergic interneurons. Excitatory neurons mainly originate from the VZ of the cortex, while inhibitory interneurons migrate from the vTel to the cortex after being produced in the medial and caudal ganglionic eminences. A small proportion of the inhibitory interneuron population is produced in the lateral ganglionic eminences and septal area (Nadarajah, 2003; Nadarajah and Parnavelas, 2002; Wonders and Anderson, 2006). Both types of neurons co-operatively form the layers of a mature cortex. Early in neurogenesis, around E12-13 in mouse, radial glia cells divide asymmetrically to produce excitatory neurons. Newborn neurons move out of the VZ via the radial glia cell scaffold, reaching cortical plate, or layer 6, at the end. As neurogenesis proceeds, more neurons are generated to populate deeper layers, layer 5 and 6. Neurons that are destined to upper layers (layer 2-4) are produced a later stage, and migrate through deeper layers. In summary, generation of cortical layers proceeds in an inside-first, outside-late fashion (Kwan et al., 2012).

Excitatory neurons in different layers are responsible for processing information from/to different regions. Neurons in layer 1 and 2 send axons to other cortical layers. Layers 2/3, 4 and 5 neurons send axons across corpus callosum to cortex or striatum in the other hemisphere. Projection neurons located in layer 6 (and small numbers in layer 5) send projections to thalamus and to spinal cord (Thomson and Bannister, 2003). Inputs from other regions are also specified, as thalamic signals are mainly transported to layer 4, and signals from other cortical areas are conducted in upper layers, layer 1-4 (Purves et al., 2001; Thomson and Bannister, 2003).

Production and migration of inhibitory interneurons is less known. It has been shown that inhibitory neurons generated in the vTel tangentially migrate into neocortex and further via radial movement to reach their destination in the cortical layers (Ang et al., 2003; Kwan et al., 2012; Nadarajah and Parnavelas, 2002; Yokota et al., 2007).

The regulatory role of Pax6 on Cell Division Cycle Associated 7 and cortical progenitor cell proliferation
Tangential migration of interneurons has been demonstrated to be regulated by some chemokine signalling involving C-X-C motif ligand 12 (CXCL12) and its receptors CXCR4 and CXCR7 (Sánchez-Alcañiz et al., 2011; Sessa et al., 2010; Wang et al., 2011).

Many molecules have been found to affect cortical lamination. Transcription factor Sox5 is expressed in the deep-layer projection neurons, but not in the progenitors in the VZ and SVZ. Mice lacking *Sox5* are defective in neural migration in the deep-layer (Kwan et al., 2008; Lai et al., 2008). *Tbr1* is mainly expressed in deep-layer neurons (layer 5 and 6) in the embryonic stage. Lamination defects was also found in *Tbr1*-deficient mice, with deep-layer neurons scattered in the cortical plate and upper-layer neurons failed to migrate across the subplate (Han et al., 2011; Hevner et al., 2001).

Pax6 also controls the migration of neurons during corticogenesis (Chapouton et al., 1999; Marín and Rubenstein, 2003; Talamillo et al., 2003). During mid-late corticogenesis, the overall cortical thickness is decreased in *Pax6*^{Sey/Sey} compared to *WT* embryos (Caric et al., 1997; Schmahl et al., 1993; Tuoc et al., 2009). This reduction may be due to a proliferation defect which will be discussed later in section 1.2.5, although impairment in neuron migration may also contribute to the thinner cortex. Loss of Pax6 affects both radial migration of glutamatergic neurons in the cortex and tangential migration of interneurons from the vTel. At late stage of corticogenesis, accumulations of cells which have acquired neural identity, defined by the expression of markers such as Tuj1 and MAP2, can be observed in the border between SVZ and IZ in the *Pax6*-null mutant (Caric et al., 1997; Talamillo et al., 2003). Further studies have also demonstrated that in *Pax6*^{Sey/Sey} embryos, late-born neurons which form the cortical plate and superficial layers of cerebral cortex fail to migrate into their destined positions while early-born neurons which form the deeper layers of the cerebral cortex are not affected (Caric et al., 1997; Fukuda et al., 2000; Georgala et al., 2011b). Transplantation of cortical cells from *Pax6*^{Sey/Sey} embryos into a *WT* context environment has proved that the migration defect is not cell-autonomous and is caused by an abnormal morphology of RGCs in which late-born neurons are mainly utilised as scaffolds for migration (Caric et al., 1997; Götz et al., 1998; Heins et al., 2002).

The regulatory role of Pax6 on Cell Division Cycle Associated 7 and cortical progenitor cell proliferation *Pax6*-null mice as a lamination model has limited practicality due to their perinatal death. Conditional knockout model allows *Pax6* to be deleted at specific time and locations. A hGFAP-cre line was used by Tuoc et. al to delete *Pax6* at E14-E16, with this approach it was found that the specification and number of neurons in superficial layers were not affected by *Pax6* deletion. Cortex-specific deletion of *Pax6* resulted in premature cell cycle exit of radial glia cells, leading to a significant reduction of upper-layer neurons. These data suggest that superficial layer defect in the cortex is likely to result from early exhaustion of progenitors for late-born neurons (Tuoc et al., 2009).

Pax6-null mice possess an increased number of interneurons migrated from vTel in the subpial and paraventricular area of the cortex and this increase may due to a disruption of the PSPB (Chapouton et al., 1999; Kroll and O'Leary, 2005). This migration defect is not cell-autonomous since it can be rescued by transplanting *Pax6*-null cells into the *WT* environment (Gopal and Golden, 2008). A misspecification of guidance molecules such as SFRP-2, which are normally expressed in the PSPB region and provide inhibitory signals for cell migration, is lost in *Pax6*^{Sey/Sey} (Kim et al., 2001; Roth et al., 2000). Disorganisation of thalamocortical and corticofugal axon tracts seen in *Pax6*^{Sey/Sey} embryos (Hevner et al., 2002; Jones et al., 2002; Mastick et al., 1997; Pratt et al., 2002) may also contribute to the non-autonomous defect since disassociated migrating interneurons and axon tracts were observed in the mutant (Gopal and Golden, 2008).

1.2.4 Downstream targets of Pax6 involved in corticogenesis

Pax6 as a transcription factor has been demonstrated to modulate the expression of numerous genes related to neural proliferation, differentiation, progression of cell cycle, cell-cell signalling, cell fate identity and lens and forebrain development (Mi et al., 2013a; Sansom and Livesey, 2009; Xie et al., 2013). Proneural transcription factor *Ngn2* is a notable direct target of *Pax6* and is transiently expressed in the cortical progenitors differentiated from *Pax6*⁺ to *Tbr2*⁺ cells (Englund et al., 2005; Hevner, 2006; Hodge et al., 2008). Previous research using the *Pax6*^{Sey/Sey} rat has shown that loss of *Pax6* results in absence of *Ngn2* and *Olig2* in the hindbrain (Mizuguchi et al., 2001). A later study further demonstrated that *Pax6* is able to up-

The regulatory role of Pax6 on Cell Division Cycle Associated 7 and cortical progenitor cell proliferation regulate Ngn2 expression by binding to its E1 enhancer element and this effect is dosage dependent in the lateral telencephalon, where Pax6 is most highly expressed (Scardigli et al., 2003). Activation of Ngn2 is known to suppress the expression of several genes at G1 and S phase such as *Ccnd1* and *Ccne1/2*, causing delays in cell cycle progression and promoting cell cycle exit (Lacomme et al., 2012).

Kinesin Family Member 1B (Kif1b) is another identified direct target of Pax6 in developing forebrain and lens (Sansom and Livesey, 2009; Wolf et al., 2009; Xie et al., 2013). Kif1b interacts with the tumour suppressor DLC2 and co-operatively maintains spindle positioning and the plane of division during mitosis as well as cell junction integrity (Vitiello et al., 2014). Although little is known about the function of Kif1b in developing cortex, the general function of Kif1b in regulating division plane via control over microtubules and actin may also affect the division of cortical progenitor cells.

Eomes/Tbr2, regarded as a marker of basal progenitors (BPs) or IPCs in the cortex (Englund et al., 2005; Hevner et al., 2006), is also positively regulated by Pax6. A chimera experiment in which cells from *Pax6*^{-/-} host were grafted to *Pax6*^{+/+} tissues produced a reduced number of neurons and a population of immaturely derived IPCs which fails to express the Tbr2 marker (Quinn et al., 2007; Sansom and Livesey, 2009).

Other Pax6 target genes such as *Cux1*, *Tle1*, *Sox4* and *Btg2* are effective during neurogenesis (Sansom and Livesey, 2009; Tuoc et al., 2013). *Cux1* is a homeobox transcription factor which is expressed in the VZ and SVZ of the vTel and interneurons in the upper layers of cerebral cortex (Nieto et al., 2004; Zimmer et al., 2004). The number of *Cux1*⁺ neurons in *Pax6*^{-/-} mutant embryos is greatly reduced, resulting in a much thinner cortical plate and a defect in late-born neuron specification as previously mentioned (Caric et al., 1997; Nieto et al., 2004).

Another large set of Pax6 targets involve in the cell cycle progression and progenitor fate decision, these are discussed in the next section.

1.2.5 The regulatory role of Pax6 in the cell cycle progression and cell fate decision

As discussed before, the duration of a cell cycle extends from 8.1 hours at E11 to 18.4 hours at E16 in mouse embryos (Estivill-Torrus et al., 2002; Takahashi et al., 1995, 1993) mainly due to G1 phase elongation. Loss of Pax6 results in shortened cell cycle as well as an increased proliferation rate and asymmetrical division of RGCs (Estivill-Torrus et al., 2002; Mi et al., 2013a; Warren, 1999; Warren and Price, 1997) at E12.5 but a decreased production of neurons and elongated cell cycling time compared to WT and overall reduced size of cortex during mid-corticogenesis at E15.5 (Estivill-Torrus et al., 2002). Furthermore, elevated levels of Pax6 *in vivo* also trigger expression of neural and basal progenitor genes such as *Ngn2* and *Tbr2* at E12.5, indicating premature neuron production as well as early depletion of the progenitor pool (Sansom and Livesey, 2009). A transgenic mouse model *PAX77*, in which human PAX6 protein is expressed at twice the physiological level in the region that resembles its physiological location, has been used for gain-of-function experiments (Manuel et al., 2007). Previous studies found that overexpression of PAX6/Pax6 protein affects the late-born or superficial layer neurons especially in the region where the highest level of Pax6 is present (Georgala et al., 2011b; Manuel et al., 2007). These results indicate that regulation of neurogenesis by Pax6 is both dosage and location dependent.

In the dTel, the gradient of Pax6 expression is rostralateral^{high} to caudomedial^{low} (Figure 1.7) (Bishop et al., 2000; Georgala et al., 2011a; Sansom and Livesey, 2009; Walther and Gruss, 1991). This gradient has been proven important for its regional specific role in modulating cell cycle progression in RGCs (Mi et al., 2013a; Talamillo et al., 2003).

The graded expression of Pax6 in the dTel has been found to affect the cell cycle progression of neural progenitors. Acceleration of cell cycle in *Pax6*^{Sey/Sey} mutant at E12.5 is only observed in the region where Pax6 expression is either strong or moderate in *wild-type*. Further research into the mechanism shows that Pax6 negatively regulates its downstream target, Cdk6 to modulate the checkpoint control during G1/S transition. The phosphorylation of Rb protein is elevated in the

The regulatory role of Pax6 on Cell Division Cycle Associated 7 and cortical progenitor cell proliferation *Pax6*^{Sey/Sey} mutant, concomitant with enhanced checkpoint transition and shorter cell cycle progression time in this model (Mi et al., 2013a).

During the preneurogenic to neurogenic transition in chick retinal progenitors, the level of Pax6 is dynamic, implying a regulatory role during retinogenesis (Hsieh and Yang, 2009). During retinogenesis, the expression level of Pax6 is down-regulated from G1 to S phase of the proliferation cycle and is either up-regulated or down-regulated during G2/M phase. Up-regulated Pax6 expression favours the production of retinal ganglion cells or amacrine interneurons while downregulation of Pax6 promotes the production of cone photoreceptors. This finding indicates that Pax6 protein level is essential for fate determination, and specific levels of the protein give rise to specific cell types during neurogenesis in retina (Hsieh and Yang, 2009).

Previous studies show that a novel Myc and E2F1 target, *Cdca7*, is up-regulated in *Pax6*-null embryos and in cortex-specific conditional *Pax6* knockout mice (Mi et al., 2013; Martine Manuel unpublished), suggesting that *Cdca7* may be a direct target, and may function downstream of Pax6 to modulate forebrain development through mechanisms that are poorly understood. In the next section I will briefly introduce our current understanding of the gene.

1.3 Current understanding of the novel protein *Cdca7*

Cell division cycle associated 7 (CDCA7) or *JPO1* was first discovered as a c-MYC-responsive gene (Lewis et al., 1997) and was further identified as a c-Myc direct target (Haggerty et al., 2003; Prescott et al., 2001). *CDCA7/Cdca7* is a nuclear protein which contains 371 amino acid in human and 382 amino acids in mouse. Figure 1.8 shows the schematic structure of *CDCA7/Cdca7*, which contains a zinc-finger domain of monoamine-oxidase A repressor R1 (zf-4CXXC_R1) in the C-terminus in both human and mouse. Extra motifs have been identified in human *CDCA7*, including a leucine zipper region, a c-Myc/14-3-3 interaction domain and a cysteine-rich region. Both the leucine zipper and cysteine-rich regions are suggested to be important for protein-protein and protein-DNA interaction (Branschädel et al.,

The regulatory role of Pax6 on Cell Division Cycle Associated 7 and cortical progenitor cell proliferation 2010; Landschulz et al., 1988; Lüscher and Larsson, 1999; Voutsina et al., 2001). The expression of *CDCA7* mRNA is detected in the thymus, small intestine, and colon and is relatively low in the foetal and adult brain.

Multi-species alignment of protein sequence was performed, the pairwise multiple alignment scores are shown in Table 1.1. The alignment was carried out using the HomoloGene function on NCBI website (Edgar, 2004)

(<https://www.ncbi.nlm.nih.gov/homologene>) The result shows that the mouse *Cdca7* gene is 79.5% identical to the human homolog, and the *Cdca7* protein in mouse is 81.1% identical to human *CDCA7*. The alignment also shows that both protein and DNA sequences are highly similar between mouse (*M.musculus*) and rat (*R.norvegicus*) and much less similar between mouse and zebrafish (*D.rerio*), in agreement with the evolution distance between these species.

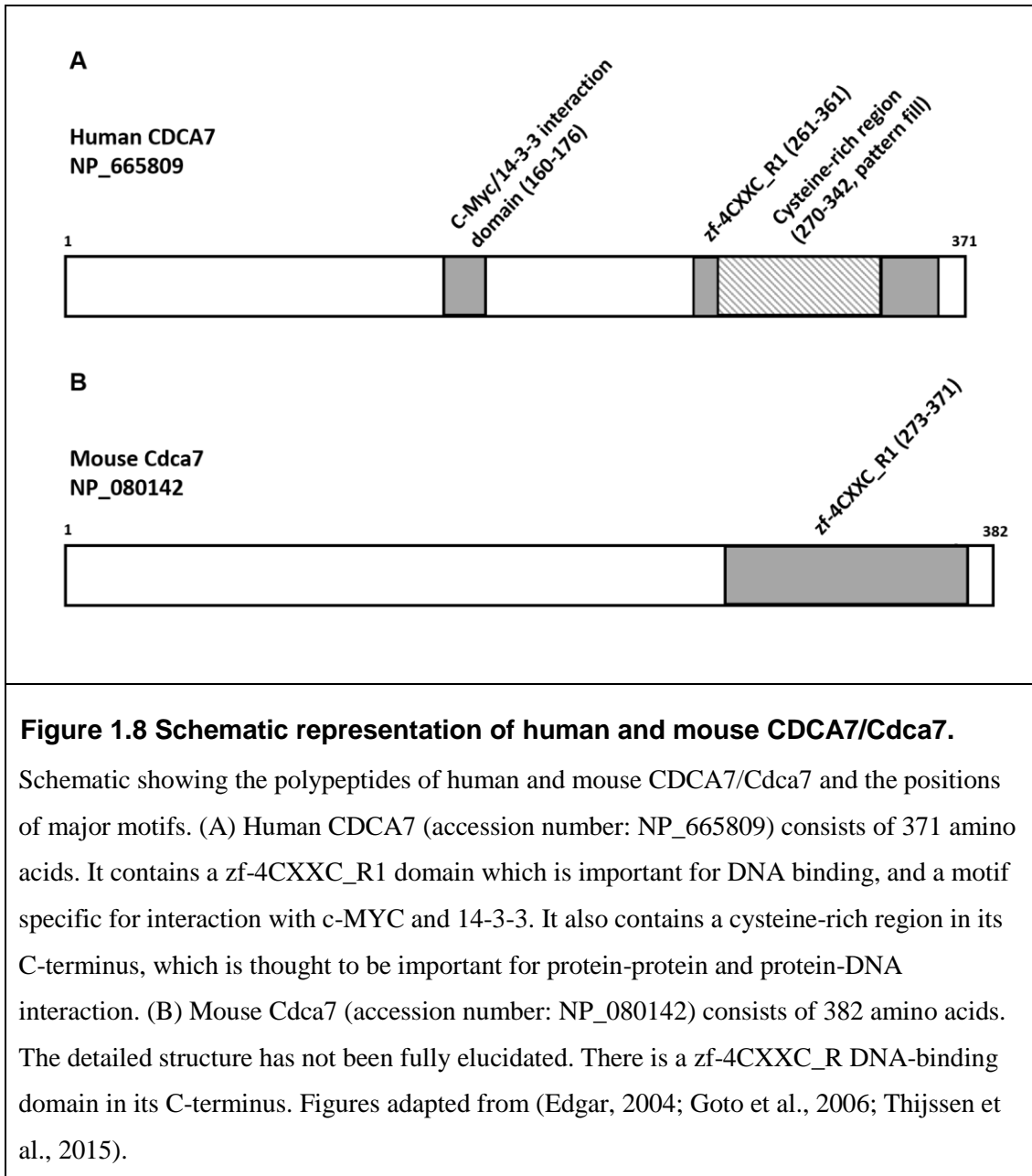







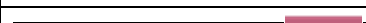
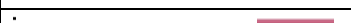
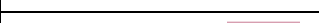


Table 1.1 Evolutionary conservation of CDCA7 protein

		Identity (%)		Protein structure
Species	Symbol	Protein	DNA	
<i>M.musculus</i>	Cdca7			
vs. <i>H.sapiens</i>	CDCA7	81.1	79.5	
vs. <i>P.troglodytes</i>	CDCA7	81.6	79	
vs. <i>M.mulatta</i>	CDCA7	82.1	79.9	
vs. <i>C.lupus</i>	CDCA7	81.4	77.6	
vs. <i>B.taurus</i>	CDCA7	84.5	81.1	
vs. <i>R.norvegicus</i>	Cdca7	94.2	91.8	
vs. <i>G.gallus</i>	CDCA7	63.2	65	
vs. <i>X.tropicalis</i>	cdca7	64.9	63.5	
vs. <i>D.rerio</i>	cdca7a	58.3	58.8	

Pink bar marked in the protein structure is the Zinc-finger domain of monoamine-oxidase A repressor R1 (zf-4CXXC_R1).

A conserved DNA binding domain zf-4CXXC_R1 is present in Cdca7 protein sequences across the species (Chen et al., 2005) (Table 1.1). This DNA binding domain is also present in the transcription repressor R1 that inhibits the expression of monoamine oxidase A. The domain structure contains four-CXXC zinc finger motifs located at the C-terminal end of R1(Chen et al., 2005). The zf-4CXXC_R1 domain is also located at the C-terminal of CDCA7 protein in all species analysed here. CDCA7 is overexpressed in some human solid tumours such as colon, ovary and lung cancers. CDCA7 is also frequently upregulated in patients during the blast crisis phase of chronic myelogenous leukaemia (CML), in which overexpression of Myc is also observed (Osthus et al., 2005). Induction of c-MYC expression *in vitro* leads to upregulation of CDCA7 (Prescott et al., 2001). Previous study focusing on the tumourigenicity of CDCA7 has demonstrated that it promotes anchorage-independent growth and enhances the transforming ability of MYC *in vitro* (Prescott et al., 2001). An increased incidence of tumours including various lymphomas as

The regulatory role of Pax6 on Cell Division Cycle Associated 7 and cortical progenitor cell proliferation well as intestinal adenocarcinoma and carcinoma has also been observed in a CDCA7-transgenic mouse model (Osthus et al., 2005).

How CDCA7 facilitates MYC-dependent apoptosis and transformation has been elucidated (Gill et al., 2013). The MYC and 14-3-3 binding motifs of CDCA7 overlap and this region contains a threonine residue (T163) which is a target of phosphorylation by AKT. Phosphorylation of T163 triggers the relocation of CDCA7 from nucleus to cytoplasm, promotes the interaction with 14-3-3 and reduces its binding affinity with MYC. CDCA7 also sensitises the cell to MYC-induced apoptosis upon serum withdrawal/starvation in the culture system. Moreover, interaction of CDCA7 with MYC largely promotes MYC-mediated transformation, as overexpression or knockdown of CDCA7 can affect the transformation ability of MYC (Gill et al., 2013).

CDCA7 was also found to be a direct target of E2F1. E2F is a family of transcription factors involving in cell cycle progression, DNA replication as well as DNA damage response (Biswas and Johnson, 2012). Inactive E2F forms a complex with hypophosphorylated RB and becomes active following phosphorylation of RB. Hyperphosphorylated RB disassociates from E2F, allowing E2F to translocate into nucleus and subsequently activates its downstream targets which promote G1 to S phase progression (Blais and Dynlacht, 2007; Helin et al., 1993; Lees et al., 1993). Overexpression of E2F1 correlates with upregulation of CDCA7 in HeLa cells. Moreover, E2F1 increases the activities of both human and mouse *CDCA7/Cdca7* promoter (Goto et al., 2006).

It is known that both MYC and E2F1 can regulate the cell cycle, especially progression through the G1/S checkpoint (McMahon et al., 1998; Meyer and Penn, 2008). Both MYC and E2F1 can activate CDC25A, which is required for G1/S transition. MYC further activates cyclin D1, cyclin D2 and CDK4 which are all essential for G1/S checkpoint control (Ciemerych and Sicinski, 2005). Together these suggest that CDCA7, a common target of MYC and E2F1, may facilitate cell cycle progression (Iwanaga et al., 2006).

Cdca7 is expressed in the embryonic telencephalon in mouse (Castro et al. 2011; www.genepaint.org). A genome-wide search for Mash1/Ascl1 targets in E12.5 basal

The regulatory role of Pax6 on Cell Division Cycle Associated 7 and cortical progenitor cell proliferation ganglia has found that targets of *Ascl1* include not only pro-neural genes such as *Foxm1* and *Gadd45g*, but also proliferative genes such as *E2f1*, *Cdk1*, *Cdk2* and *Cdca7* (Castro et al., 2011). Furthermore, *Cdca7* is down-regulated in the ventral telencephalon in *Ascl1*^{-/-} mice, but whether the function of *Cdca7* is proliferative or neurogenic remains elusive.

Cdca7 is also involved in Notch signalling and is required during the haematopoietic process (Guiu et al., 2014). Notch signalling is activated by cell to cell contact and is required for T cell differentiation in adulthood. In addition, Notch is also essential for the generation of haematopoietic stem cells (HSCs) during embryonic development and its downstream targets have recently been identified (Bigas and Espinosa, 2012; Guiu et al., 2014). Based on a ChIP-on-chip experiment with E11.5 aorta-gonad-mesonephros (AGM) tissues, *Cdca7* was found to be a direct target of Notch and the *Cdca7* promoter was further shown to be activated by Notch signalling. Furthermore, down-regulation of *Cdca7* using shRNA *in vitro* strongly promotes haematopoietic stem cell differentiation, while knockdown of the gene by morpholino oligos in zebrafish causes a reduced number of HSCs. Taken together, *Cdca7* is one of the down-stream targets of Notch and is involved in haematopoiesis in a Notch-dependent manner (Guiu et al., 2014).

A recent report has found that the function of *Cdca7* is closely related to Immunodeficiency, Centromeric Instability and Facial Anomalies (ICF) syndrome. ICF is an autosomal recessive genetic disorder causing low levels of B cells in blood and distinct facial anomalies in patients (Hagleitner et al., 2008; Thijssen et al., 2015; Weemaes et al., 2013). A CpG hypomethylation in the juxtacentromeric satellite is a characteristic feature of ICF and mutations in *DNA methyltransferase 3B (DNMT3B)* and *zinc-finger and BTB domain containing 24 (ZBTB24)* are responsible for approximately 80% of the disease incidence (deGreef et al., 2011; Weemaes et al., 2013). Using whole-exome sequencing with ICF patients free of *DNMT3B* and *ZBTB24* mutations in comparison with healthy family members, it has been found that individuals carrying missense mutations in the zinc finger domain of *Cdca7* also develop ICF syndrome (Thijssen et al., 2015).

The regulatory role of Pax6 on Cell Division Cycle Associated 7 and cortical progenitor cell proliferation. In summary, *CDCA7/Cdca7* was originally discovered as a MYC target involving in MYC-dependent oncogenic process. The gene was further identified as a direct target of E2F1 and a putative target of Ascl1, suggesting its putative function in cell cycle progression in embryonic telencephalon. *Cdca7* is up-regulated in embryonic telencephalon in the *Pax6^{Sev/Sev}* mutant, and its mRNA expression pattern is complementary to that of *Pax6* in *WT* dTel at E12.5 (Mi et al., 2013a). Recent evidence has identified a function of *Cdca7* in the emergence of HSCs and provided insights into its role in fate determination in progenitor cells (Guiu et al., 2014).

1.4 Aims of this thesis

Based on previous knowledge, in this thesis I would like to study the functions of *Cdca7* in neural progenitor cell proliferation as well as its relationship to Pax6. In Chapter 3 I aim to compare the mRNA expression patterns of *Pax6* and *Cdca7* at different developmental stages in embryonic brain sections from three genetic backgrounds of mice with altered Pax6 expression levels, I aim to reveal details of how Pax6 may regulate the expression of *Cdca7*. In Chapter 4 I would like to confirm whether *Cdca7* is a direct target of Pax6 using chromatin immunoprecipitation (ChIP) and luciferase-based promoter assay. Finally in Chapter 5 experiments have been conducted to verify if *Cdca7* is involved in the decision between proliferation and differentiation of neural progenitor cells in mouse embryonic telencephalon.

Chapter 2 : Materials and Methods

2.1 Animals

Pax6-null embryos, designated *Pax6*^{Sev/Sev} or *Pax6*^{-/-} were obtained from crossing *Pax6*^{Sev/+} heterozygote mice (Hill et al., 1991). *PAX77* homozygous mice carry 10-14 copies of human *PAX6* transgene and phenotypically overexpress both Pax6/PAX6 mRNA and protein (Schedl et al., 1996). *PAX6* transgene was detected by genomic PCR that specifically amplified human *PAX6*. All mice were maintained on an albino CD1 background and bred in accordance to UK Home Office Animals (Scientific Procedures) Act 1986 regulations. The morning of vaginal plug appeared was designated E0.5.

Human *PAX6* primer for genotyping:

Forward: 5'- CCGTGTGCCTCAACCGTA

Reverse: 5'- CACGGTTTACTGGGTCTGG

Annealing Temp: 55°C

2.2 Histology

2.2.1 Embryo collection and fixation

All mice embryos used in the experiments were terminated under Schedule 1 to the animals (Scientific Procedures) Act 1986 according to Home Office, UK publication. Embryonic heads were fixed in 4% para-formaldehyde/PBS (PFA/PBS) solution overnight and then transferred into 70% ethanol for paraffin wax embedding or 30% sucrose/PBS for cryo-protection overnight. Embryos after sucrose protection were embedded in the 50% sucrose/OCT solution and stored in the -20°C freezer.

2.2.2 Wax sectioning

Embryos were dehydrated through ethanol gradients and embedded in paraffin wax. Microtome (Leica RM2245) was set to cut 10 μ m-thickness sections, which were then mounted on Superfrost Plus glass slides (Thermo). Sections on slides were firstly air-dried in the room temperature (RT) and moved to a 37°C oven overnight. Sections were kept in the RT for short-term or fridge for long-term storage.

2.2.3 Cryostat sectioning

Tissues blocks kept in the 50% sucrose/OCT solution were used for cryo-section. Cryostat machine (Leica CM3050S) was normally set at -23°C to -25°C and cut for 10 μ m-thickness. Sections were also mounted on the Superfrost Plus glass slides (Thermo) and once the sections were air-dried, they were stored in the -20°C freezer.

2.2.4 *In Situ* Hybridisation (ISH)

In situ hybridisation (ISH) was performed on the cryo-sections.

Pre-hybridisation (first day)

Cryo-sections were removed to RT at least 30 minutes before prehybridisation. Antisense RNA probes (200 μ L/slide) were pre-heated at 90°C for 10 minutes before applying to cryo-sections. Sections with RNA probes were placed in a hybridization box with pre-hybridisation buffer in a 70°C oven overnight.

10X Salt solution

Reagents	Weight or Volume	Final concentration
NaCl	11.4 g	2M
Tris-HCl	1.404g	90mM
Tris	0.34g	10mM
NaH ₂ PO ₄ ·2H ₂ O	0.78g	50mM
Na ₂ HPO ₄	0.71g	50mM

0.5M EDTA	10 mL	50mM
ddH ₂ O (RNase free)	To 100 mL	

Pre-hybridisation buffer

Reagents	Final concentration
10X Salt	10.5X (dilute with ddH ₂ O)
Formamide	50%

Post-hybridisation (second day)

Sections were washed in 2xSSC/50% Formamide/0.1% Tween-20 buffer for 30 minute in the 70°C oven and then washed in MABT buffer for 1 hours at RT.

Sections were blocked in 2% blocking reagent (Roche Cat no.11096176001) (w/v) /20% sheep serum/MABT for 1 hour at RT and incubated with anti-DIG antibody (1:1500 dilution, Roche Cat no. 11093274910) overnight.

20X SSC (pH=7.0)

Reagents	Final concentration
NaCl	3M
Tri-sodium citrate	0.3M

2xSSC/50% Formamide/0.1% Tween-20 buffer

Reagents	Weight or Volume	Final concentration
20X SSC	15 mL	2X
Formamide	150 mL	50%
Tween-30	0.3 mL	0.1%

ddH₂O To 300 mL

MABT (pH=7.5)

Reagents	Final concentration
Maleic Acid	0.1M
NaCl	0.15M

Post-antibody and colour development (third day)

Sections were washed in MABT buffer for 1 hour at RT and further incubated in the staining buffer for 30 minutes for equilibrium purpose. Sections then were finally under a colour development reaction in 1.8 %NBT-BCIP (Roche Cat no.11681451001)/staining buffer at RT avoiding exposing to light and the incubation times were purely dependent on the individual probe and signal/background condition.

2.2.5 Immunofluorescence staining (IF staining)

Staining buffer

Reagents	Final concentration
NaCl	100mM
Tris-HCl	100mM
MgCl ₂	50mM
Tween-20	0.1%
ddH ₂ O	To 300 mL

Samples for IF are either from wax or cryostat sectioning. Wax sections were needed to pre-treated with xylene, 15 minutes twice to remove paraffin and subsequently rehydration was performed by immersing slides in alcohol solutions with grading concentrations (from 100% to 70%), 5 minutes in each concentration. Cryostat

The regulatory role of Pax6 on Cell Division Cycle Associated 7 and cortical progenitor cell proliferation sections removing from freezer were placed at RT for 30 minutes before using. After above procedures, sections from both preparations were treated in the same manner.

Slides were firstly washed in 1x PBS for 5 minutes and then in antigen retrieval buffer (10mM citric acid buffer, pH=6.0) for 10 minutes. Slides underwent antigen retrieval treatment by microwaving at 800W for 5 minutes, 4 times. After microwaving, slides were allowed to cool to RT followed by washing in 1x PBS-0.1% Triton-X 100 solution. Subsequent blocking step was performed in blocking solution (20% donkey serum/1x PBS-0.1% Triton-X 100) for 1 hour at RT. Primary antibodies were diluted in blocking solution according to its own conditions and left overnight at 4°C.

Antigen retrieval buffer, 10 mM citrate acid

Reagents	Weight or Volume
Tri-sodium citrate·dihydrate (Mw= 294)	2.94g
ddH ₂ O	To 1000 mL
	Adjust pH value to 6.0

On the next day, slides were washed in 1x PBS-0.1% Triton-X 100 solution for 5 mins x 6 times and then incubated with secondary antibodies according to the primary antibody for 1 hour at RT in the dark. All secondary antibodies were diluted in blocking solution. After incubation, slides were washed in 1x PBS-0.1% Triton-X 100 solution for 5 mins x 6 times. Final nuclear counter staining were either in DAPI or Topro-3 solution, 1:1000 in ddH₂O for 5 minutes at RT. Slides were then washed in 1x PBS for 5 minutes and mounted in Vectorshield HardSet antifade solution. Slides were stored in the fridge avoiding to light.

List of primary antibody and usage conditions.

Table 2.1 List of primary antibodies and usage conditions

Antibody name	Company	Catalogue no.	Application	Dilution
Pax6	Covance	PRB-278P	Immunofluorescence	1:200
Cdca7	ProteinTech	15249-1-AP	Immunofluorescence	1:100
GFP	Abcam	Ab6673	Immunofluorescence	1:200
DAPI	Invitrogen	D3571	Immunofluorescence	1:1000
Tbr2	Abcam	Ab23345	Immunofluorescence	1:100
Tbr1	Abcam	ab31940	Immunofluorescence	1:100
BrdU	Abcam	ab6326	Immunofluorescence	1:200
Pax6	Covance	PRB-278P	Western blotting	1:2000
GAPDH	Ambion	AM4300	Western blotting	1:5000
HA	Sigma	H6533	Western blotting	1:1000

2.3 Generation of RNA probe for *in situ* hybridisation

Pax6 anti-sense probe generated by Dr Catherine Carr can recognise full-length *Pax6* mRNA (Mi et al., 2013b). This full-length *Pax6* probe is able to detect mRNA in wild-type and *Pax6*^{Sey/Sey} mutants as there is a single nucleotide nonsense mutation in *Pax6*^{Sey/Sey}, which does not affect the recognition of the probe. Pax6 probe also detects overexpressed *PAX6* mRNA in PAX77. The protein sequence of human and mouse PAX6/Pax6 is 99% identical. Pairwise alignment of their coding DNA sequence showed a 94% identity. Full length *Cdca7* cDNA was obtained from reverse transcription of E14.5 cortex tissues mRNA extraction followed by PCR step using specific primer sets. The *Cdca7* probe fragment was cloned into pGEMT-easy vector. SacII restriction enzyme was used for linearization and SP6 RNA polymerase was used for antisense probe generation.

Table 2.2 List of probes details

Probe	Plasmid	Linearised enzyme antisense	RNA polymerase antisense	Probe size
Pax6	pCR-Blunt II-TOPO	BamHI	T7	1.8 kb
Cdca7	pGEMT-easy	SacII	SP6	745 bps

Cdca7 probe primer:

Forward: 5'-TCTGAGAGCTCTGCAAACGA

Reverse: 5'-AGCTGCAGTTGCAAATTCCT

Annealing Temp: 50°C

2.4 Cloning of DNA constructs

2.4.1 Cdca7 promoter region construct for luciferase assay

To predict Pax6 binding sites in the *Cdca7* genomic region, three Pax6 conserved binding motifs Pax6CON (J.Epstein et al., 1994), M00979, (Duncan et al., 1998; Zhou et al., 2000; Transfac) and PC0010 (Coutinho et al., 2011) were utilised to generate a custom track by Dr Ian Simpson for prediction (See Figure 4.2 for details). In addition, Transfac, which utilises a well-established transcription factor PWM database, was also adopted to collectively predict putative sites. In the Transfac programme, the match and matrix score was set at 0.8 to reduce false positive hits. Taken together, there are six putative sites located in the 5 kb region upstream of the transcriptional start site (TSS) of *Cdca7* and five of them are located within 2.6 kb to the TSS site.

To obtain the 4.4 kb and 2.6 kb DNA fragments upstream to the transcriptional start site (TSS) of *Cdca7*, a BAC clone (RPCI-121B8) was used as template to amplify the genomic fragment. For PCR reaction, Platinum® Taq DNA Polymerase High Fidelity (Cat no. 11304-011) was used according to the manual. Two *Cdca7* genomic

The regulatory role of Pax6 on Cell Division Cycle Associated 7 and cortical progenitor cell proliferation fragments both flanked by restriction enzyme SalI were cloned into pGEMT-easy vector and then subcloned into pGL4.10 promoter-less firefly luciferase vector through XhoI restriction site (Promega).

Primers:

4.4 kb Forward: 5'-ACGCAGGTCGACCAGTATCAAGTTTCAAACAAGAAGC

2.6 kb Forward: 5'-ACGCAGGTCGACCGGTGGGGGTCTGGGAG

Shared Reverse primer: 5'-ACGCAGGTCGACCGTTGGCGGCGGGTAC

(GTCGAC: SalI recognition sequence)

2.4.2 *Cdca7* expression construct for *in utero* electroporation

Cdca7 cDNA open reading frame (ORF) clone (NM_025866) was obtained from Origene. ORF fragments were PCR amplified with attached either the N-terminus or the C-terminus influenza hemagglutinin (HA) tag sequence for detection. Extra NheI restriction enzyme flanking both ends were also added to the ORF fragments for cloning into the final expression vector IRES-NLS-GFP_pCAGGS plasmid.

Primers:

N-HA-Cdca7-IRES-NLS-GFP_pCAGGS

Forward: 5'-cata GCTAGC ATG TACCCATACGATGTTCCAGATTACGCT
GAGGCTCGCCGCGC

Reverse: 5'-cata GCTAGC CTACGCTTGC ATTTCAAATT CCTG

C-HA-Cdca7-IRES-NLS-GFP_pCAGGS

Forward: 5'-cata GCTAGC ATG GAGGCTCGCCGC

Reverse: 5'-cata GCTAGC AGCGTAATCTGGAACATCGTATGGGTA CG
CTTGCATTTC AAATTCCTG

GCTAGC: NheI recognition sequence

TACCCATACGATGTTCCAGATTACGCT: HA tag sequence

2.5 Cell culture and Luciferase assays

HEK293 cells were maintained in T75 flasks (Corning) containing DMEM growth medium supplemented with 10% foetal bovine serum (FBS). Cells were incubated at 37°C with 5% CO₂ level.

One day before transfection, cells were split to 24-well plates at a density of 1x10⁵ cells per well. Next day (16~18 hours after splitting), cells reached 80-90% confluency in monolayer. Transfection was carried by using Lipofectamin 2000 (Invitrogen) according to the manual. DNAs used in the transfection include firefly luciferase construct with or without *Cdca7* genomic locus, Renilla luciferase construct (pRL SV40, Promega) for internal transfection efficiency control and *Pax6* expression construct or empty expression construct alone control. Full length *Pax6* cDNA was cloned into pCMV-Script by Dr Da Mi and expression of *Pax6* was driven by CMV promoter (Mi et al., 2013a). There is also a GFP expression indicator in the *Pax6* expression construct, which can be used for visualisation of transfection. DNA was mixed in 50µL of OPTI-MEM (Invitrogen) and Lipofectamin was diluted in equal volume of OPTI-MEM. Added DNA solution to Lipofectamin and allowed the mixture to stand for 20 minutes at RT before adding to cells. 4 hours later, fresh DMEM-10% FBS medium was applied to cell to remove the old medium and transfection reagents. 24 hours later, transfection was monitored by fluorescence microscopy. 48 hours post transfection, cells were harvested and lysed in Passive Lysis Buffer (Promega) according to the manufacturer's instructions.

Cell lysates collected by the Passive Lysis Buffer were used for determining the expression levels of Pax6 by western blotting and for luciferase detection. Luciferase assays were carried by Dual Luciferase Reporter Assay system (Promega) according to the instructions. Firefly and renilla luciferase activities were detected by Promega Glomax Luminometer. For each sample, the activities of firefly and renilla luciferase were represented by Relative Light Unit.

2.6 Western Blotting

Cell lysates were collected after Passive Lysis Buffer treatment during luciferase assays. All samples were mixed with 4x sample loading buffer (Li-Cor) to a final concentration of 1x and sent for boiling at 90°C for 5 minutes. 4%-12% Bis-Tris mini Nu-Page gels (Thermo) were used to resolve the samples in a condition of 200V for 50 minutes in 1x MOPS buffer (Thermo). After gel running, proteins on the gel were transferred onto nitrocellulose membrane under 190 mA for 2 hours. After protein transfer step, nitrocellulose membrane was blocked with Odyssey Blocking Buffer (Li-cor) for 1 hour at RT and incubated with primary antibodies (see antibody list for concentrations) diluted in Odyssey blocking Buffer overnight at 4°C. On the next day, membrane was washed with 1x PBS-0.1% Tween-20 buffer, 3 times and 10 minutes each time followed by incubation with secondary antibodies (IRDye 1:5000, Li-cor) for 1 hour at RT and washed again with 1x PBS-0.1% Tween-20 buffer, 3 times and 10 minutes each time. Finally membrane was washed with 1x PBS for 5 minutes and ready for detection by Li-cor scanning system.

2.7 Quantitative Chromatin Immunoprecipitation (qChIP)

Chromatin was collected from 20-25 E12.5 embryonic cortices from *Pax6*^{+/+} and *Pax6*^{Sey/Sey}. Chromatin complex was cross-linked by formaldehyde and fragmented by sonication to approximately 500 bp long. DNA-protein complexes from *wild-type* and *Pax6-null* samples were precipitated by anti-Pax6 antibody (Millipore Cat no. AB2237) on the rotation platform overnight at 4°C. After precipitation and purification of the genomic DNA, the DNA was analysed by quantitative PCR using Quantitect SYBR Green PCR Kit (Qiagen). The enrichment of each binding site that amplified by its specific primer set was first calculated by dividing the q-PCR outputs from *Pax6 wildtype* by the outputs from *Pax6-null* (formula A). The ratio for each binding region from formula A was then further divided by the ratio of the *Syt8* negative control (formula B) to calculate the final enrichment for each binding region. More experimental details are described in Appendix 1.

The regulatory role of Pax6 on Cell Division Cycle Associated 7 and cortical progenitor cell proliferation
q-PCR output for each primer from *Pax6*^{+/+}

$$\frac{\text{q-PCR output for each primer from } Pax6^{+/+}}{\text{q-PCR output for each primer from } Pax6^{-/-}} = X \text{ ----- (Formula A)}$$

$$\frac{X \text{ for each primer set}}{X \text{ for Syt8 negative control}} = \text{fold enrichment ----- (Formula B)}$$

Table 2.3 List of primers for q-PCR

Binding Site 1 (BS1)	Forward	5'-AATTCTTGGTGCAGGGTGAC
	Reverse	5'-TTTCCTAAGCCTGGTGGATG
BS2	Forward	5'-GAAGAATTCATCCCGAGCAC
	Reverse	5'-CTTGTGCTTCTGTTCCGTCA
BS3	Forward	5'-GGGACTCTTGGCTGCTTCAT
	Reverse	5'-CAGCCAGAAATCTGAGTGGTC
BS4	Forward	5'-GGCCTGGAATAAATGCAGAG
	Reverse	5'-GGTCAGAAAGGAAGCGACAG
BS5	Forward	5'-GTTTCCGAGGACACTCAAGG
	Reverse	5'-GGTCCTGCCAGCTAAGATGA
BS6	Forward	5'-GGTCATCTTAGCTGGCAGGA
	Reverse	5'-CACTCAGAGCCCGAACAAC
Non-binding control region	Forward	5'-CAAACGGGGTTTATGGTGTC
	Reverse	5'-AGGAGGAGGAGGCATCGTAT
Pou3f4	Forward	5'-GAGAGAGGGAGAGGCAGAGGGAAT

	Reverse	5'-GGGGAGAAAACCTTGCATCTG
Syt8	Forward	5'-CAGCCTAGCACTGTGGTCC
	Reverse	5'-GTGCTCTGAAGTTGGCATGG

2.8 *In Utero Electroporation (IUE)*

Wild-type CD1 pregnant females were used for *in utero* electroporation. Purified plasmid DNA (N-HA-Cdca7-IRES-NLS-GFP_pCAGGS, C-HA-Cdca7-IRES-NLS-GFP_pCAGGS or IRES-NLS-GFP_pCAGGS control) was adjusted to 2µg/µl. On the electroporation day, animals were given one dose of analgesia agent Vetergesic (Buprenorphine) subcutaneously and anaesthetic inhalation agent Isoflurane using an anaesthetic rig throughout whole operation process. Plasmids (approximate 2µg) were injected into the first ventricle of embryos at aged E12.5 or E14.5. Plasmids then were forced to enter the lateral telencephalon by electrical shock provided by CUY21-Sonidel Limited ®, 32 volt for E12.5 and 35 volt for E14.5 embryos in 50ms duration and 950 ms interval. All procedures were included in the Home Office Project License (60/4545; personal license: 60/13925), followed the on-site BRR regulations and approved by the veterinary physicians. 15.5 hours post electroporation, a single dose of bromodeoxyuridine (BrdU, Sigma) was intraperitoneally administrated into pregnant females at 70µg/g of body weight. 30 minutes after injection, pregnant females were terminated and embryos were sent for cryo-fixed and immunofluorescent staining.

2.9 *Microscope and imaging software*

For *in situ* hybridisation, light microscope Leica LB30T microscope and LAS version 3.6 software were used for taking images. For immunofluorescent staining, fluorescent microscope Leica DM5500 B and LAS fluorescent 2.6.3 software were used for acquiring low magnified images (5-20 folds). 40x magnification images

The regulatory role of Pax6 on Cell Division Cycle Associated 7 and cortical progenitor cell proliferation were acquired by Nikon A1R confocal microscope and NIS Elements software. All image analysis was performed using Fiji software.

2.10 Statistical analysis

One-way and two-way Analysis of variance (ANOVA), Tukey and the TwoStep cluster analysis were carried out by SPSS package (IBM Corporation) version 20. Student's t-test was performed by Microsoft Excel software. The significance level was set at $P < 0.05$.

Chapter 3 : Expression patterns of *Pax6* and *Cdca7* in the developing cortex

3.1 Introduction

Correct formation of the complex brain structure requires all progenitors to sense both intracellular and environmental signals which mediate neural development. Many signalling molecules and transcription factors (TFs) are involved in this developmental process to establish subdivisions along the dorsoventral (DV) and the anteroposterior (AP) axis (Puelles and Rubenstein, 1993; Tucker et al., 2008). These molecules and TFs set up overlapping gradients in developing cortex to exert their functions in building the correct cytoarchitectural map. A previous study from human embryonic cortical tissues between 8-12.5 PCW has shown that there are several differentially expressed genes along the AP axis. For example, ROBO1 and CTIP2 are enhanced anteriorly while FGF receptor 3, COUP-TF1 and EMX2 are upregulated posteriorly (Ip et al., 2010). Further studies of gene expression gradients have been done in rodents (Muzio et al., 2002; O'Leary et al., 2007; Rakic et al., 2009). One notable example is Fgf signalling, which regulates the regionalisation of neocortex. An Fgf secreting signalling centre is located at the rostral midline of the neocortex and one of the Fgf molecules (Bachler and Neubüser, 2001), Fgf8, has been demonstrated to regulate rostral area specification of motor cortex (Fukuchi-Shimogori and Grove, 2001). It is also known that COUP-TF1 and EMX2 are repressed by FGF8 signal (Fukuchi-Shimogori and Grove, 2003; Garel, 2003). Both factors exhibit a high caudo-medial to low rostro-lateral expression pattern in the cerebral cortex. Loss of function mutations of the two factors cause a mis-arealisation in neocortex which results in significant enlargement of motor cortex (Sansom and Livesey, 2009). The anatomical changes caused by abnormal expression of Fgf8 and their receptors as well as TFs have been documented in previous studies listed above, however the underlying cellular mechanisms are not widely understood.

In a previous study, my colleagues have dissected the regulatory role of Pax6 in cortical progenitor proliferation via direct repression of *Cdk6* production and hypophosphorylation of pRb (Mi et al., 2013). Expression of *Pax6* mRNA and

The regulatory role of Pax6 on Cell Division Cycle Associated 7 and cortical progenitor cell proliferation protein follows a gradient pattern which is high rostral-laterally and low caudo-medially in the cerebral cortex during early corticogenesis (Bishop et al., 2000; Georgala et al., 2011; Sansom and Livesey, 2009; Walther and Gruss, 1991). Cdk6 was identified as a direct downstream target of Pax6 by ChIP and promoter assay and Cdk6 is negatively regulated by Pax6. Furthermore, the study also showed that a shortened cell cycle in neural progenitors in *Pax6^{Sey/Sey}* compared to *wild-type (WT)* embryos is only observed in regions with high or moderate Pax6 expression (Mi et al., 2013). It is known that Cdk6 can phosphorylate its downstream target, Rb, and thereby to free E2f factors to enter the nucleus and trigger G1/S transition (Blais and Dynlacht, 2007; Helin et al., 1993; Lees et al., 1993). It has also been proven that the total duration of cell cycle is shorter in neural progenitor cells than that in post-mitotic cells (Roccio et al., 2013). Taken together, it is suggested that Pax6 can influence the length of cell cycle in neural progenitor cells and further affect decision between proliferation or differentiation in neural progenitor cells

A previous microarray-based study has identified *Cdca7* as a potential target of Pax6, and subsequent RT-qPCR validation has found that the expression of *Cdca7* mRNA is upregulated in *Pax6^{Sey/Sey}* and in *Pax6* conditional knockout embryos (Mi et al., 2013; Martin Manuel unpublished). In addition, the mRNA expression patterns of *Pax6* and *Cdca7* at E12.5 suggested that they may be expressed in counter-gradients in developing cortex (Mi et al., 2013). The exact relationship between Pax6 and *Cdca7* and the temporal and spatial expression of *Cdca7* are still unknown.

In this chapter I have done a series of gene expression pattern analyses from E12.5 to E15.5 in mice with different Pax6 expression levels to investigate the potential relationships between *Pax6* and *Cdca7* and to study the function of *Cdca7* given its graded expression pattern during brain development.

3.2 Results

3.2.1 Embryonic stage E12.5

ISH was performed to reveal the mRNA expression patterns of *Pax6* and *Cdca7* in *WT* (n=4), *Pax6^{Sey/Sey}* (n=4) and *PAX77* (n=3) embryos at E12.5 (Figure 3.1-3.3). In *WT* embryos, *Pax6* mRNA is expressed in a high-lateral to low-medial gradient in

The regulatory role of Pax6 on Cell Division Cycle Associated 7 and cortical progenitor cell proliferation the dTel with the highest level near the pallial-subpallial boundary (PSPB) region. The expression level gradually increases from medial to lateral direction in the dTel and disappears rapidly after the PSPB (Figure 3.1). *Cdca7* mRNA is not expressed in an obvious gradient, but its level is exceptionally weak around the PSPB, indicating that the two genes are expressed at opposing levels in this specific region of the brain.

In addition to the telencephalon, *Cdca7* mRNA is also present in the thalamus, prethalamus and hippocampus but is absent in the zona limitans intrathalamica (ZLI).

In *Pax6^{Sey/Sey}* embryos where no functional Pax6 protein is present, the pattern of *Pax6* mRNA expression in the dorsal telencephalon (dTel) is similar to that in *WT* samples (Figure 3.2), but the graded expression of *Cdca7* mRNA seems less clear across the dorsal to ventral parts of the telencephalon. In one noticeable area, the PSPB region, where the expression of *Cdca7* mRNA is very low in *WT*, no such reduction was observed in *Pax6^{Sey/Sey}* embryos, suggesting that Pax6 may act as a potential negative regulator of *Cdca7*.

In *PAX77* embryos where the human form of PAX6 protein is overexpressed, the patterns of *Pax6* and *Cdca7* mRNA expression in the dorsal region are very similar to those seen in *WT* samples (Figure 3.3). However in the ventral telencephalon (vTel), *Pax6* mRNA is noticeably lower compared to the *WT* and the difference between the two genotypes seems to maximise at this embryonic stage (see also Figure 4.17B). In contrast, *Cdca7* mRNA exhibits a similar expression pattern to that seen in the *WT* at this stage (Figure 3.3).

Figure 3.4 shows the expression patterns of *Pax6* and *Cdca7* mRNA in *WT* and *Pax6^{Sey/Sey}* embryos in a sagittal orientation. *Pax6* mRNA appears high rostrally and low caudally while *Cdca7* mRNA was found in an opposite graded direction in the *WT*. The highest level of *Pax6* mRNA was observed around the PSPB, where the lowest level *Cdca7* mRNA was seen. No apparent graded expression of *Pax6* or *Cdca7* was detected in the dTel in *Pax6^{Sey/Sey}* embryos; although the mRNA level of *Pax6* also peaks around the PSPB, no reduction of *Cdca7* mRNA was seen in this region in *Pax6^{Sey/Sey}* embryos.

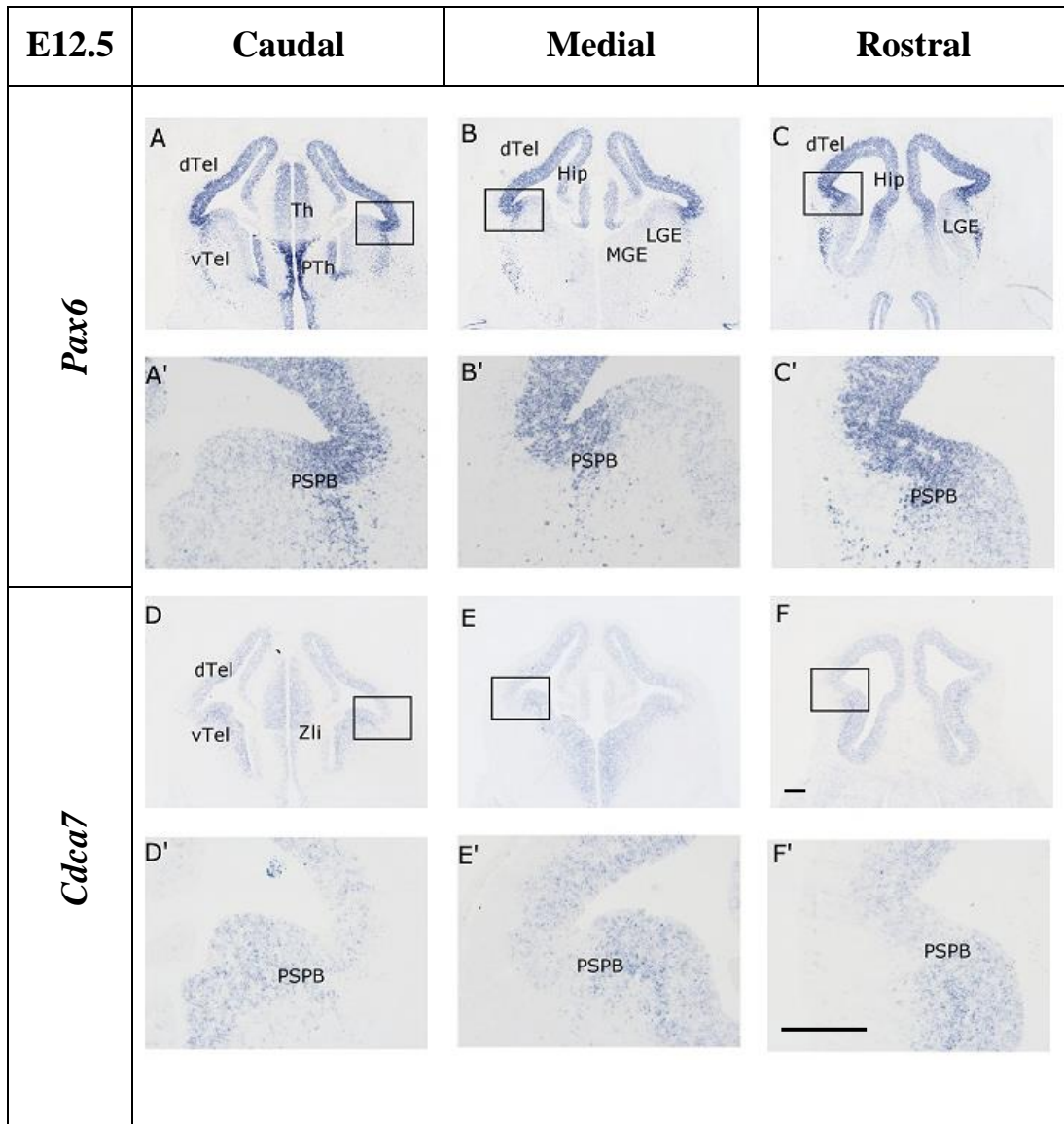


Figure 3.1 Expression of *Pax6* and *Cdca7* mRNA at various positions in E12.5 *wild-type* coronal sections

Figure 3.1 Expression of *Pax6* and *Cdca7* mRNA at various positions in E12.5 *wild-type* coronal sections

The graded expression pattern of *Pax6* from caudal to rostral forebrain. (A-C) Representative ISH results produced from caudal, medial, and rostral sections, respectively, showing that *Pax6* mRNA is expressed in a low-medial to high-lateral gradient in the dorsal telencephalon (dTel). The expression is sharply reduced in the ventral telencephalon (vTel) ventral to the PSPB. (A'-C') High magnification images enlarged from the rectangle areas in Panel A-C, respectively. *Pax6* mRNA reaches its highest expression level near the PSPB region and declines rapidly after passing the highest point. (D-F) The mRNA expression pattern of *Cdca7* possesses a counter gradient compared to the *Pax6* pattern, with its lowest level at the PSPB region. (D'-F') High magnification views enlarged from the rectangles in Panel D-F, respectively. *Cdca7* mRNA is low around the PSPB and increases greatly after the PSPB. Panel A and D, B and E, C and F are anatomically similar (adjacent sections), therefore the regional labels shown in A-C are also shared in D-F. MGE: medial ganglionic eminences; LGE: lateral ganglionic eminence; Hip: Hippocampus; Zli: zona limitans intrathalamica; Th: Thalamus; PTh: Pre-thalamus; PSPB: pallial-subpallial boundary. Scale bars: 200 μm .

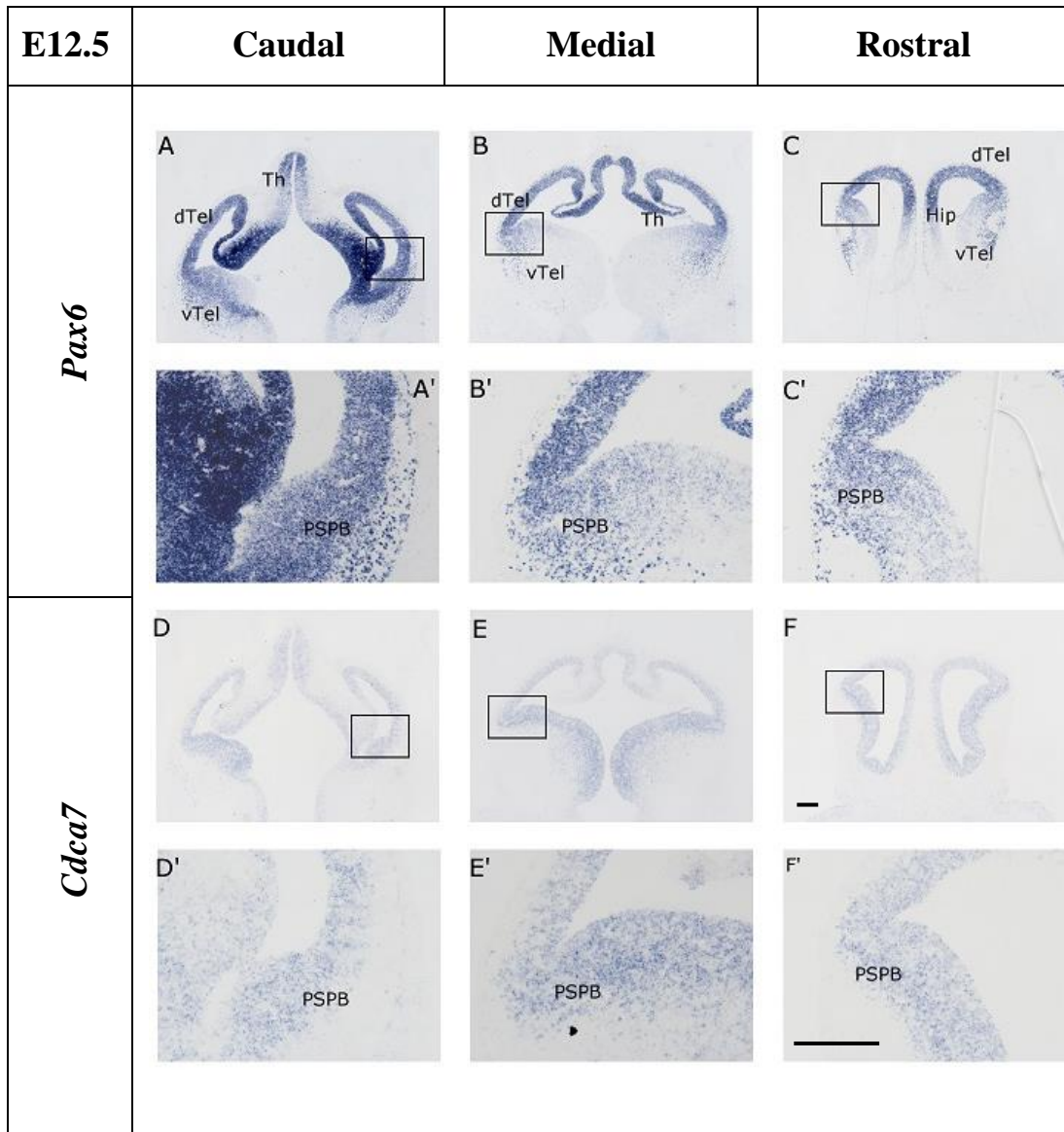


Figure 3.2 Expression of *Pax6* and *Cdca7* at various positions in E12.5 *Pax6*^{Sey/Sey} coronal sections

Figure 3.2 Expression of Pax6 and Cdca7 at various positions in E12.5

***Pax6*^{Sey/Sey} coronal sections**

(A-C) Representative ISH images produced from caudal, medial, and rostral sections, respectively, showing that *Pax6* mRNA is expressed evenly in the dTel. (A'-C') High magnification images enlarged from the rectangle areas in Panel A-C, respectively. In the caudal section, *Pax6* mRNA remains highly expressed in the vTel, while in the medial and rostral sections, the mRNA expression reduces in this region. (D-F) Representative ISH images showing *Cdca7* mRNA has an even expression pattern from the dTel to the vTel. (D'-F') High magnification views of the rectangle areas in Panel D-F, respectively. These results indicate no obvious changes in the expression intensity of *Cdca7* dorsal or ventral to the PSPB. Panel A and D, B and E, C and F are anatomically similar (adjacent sections), therefore the regional labels shown in A-C are also shared in D-F. Scale bars: 200 μ m.

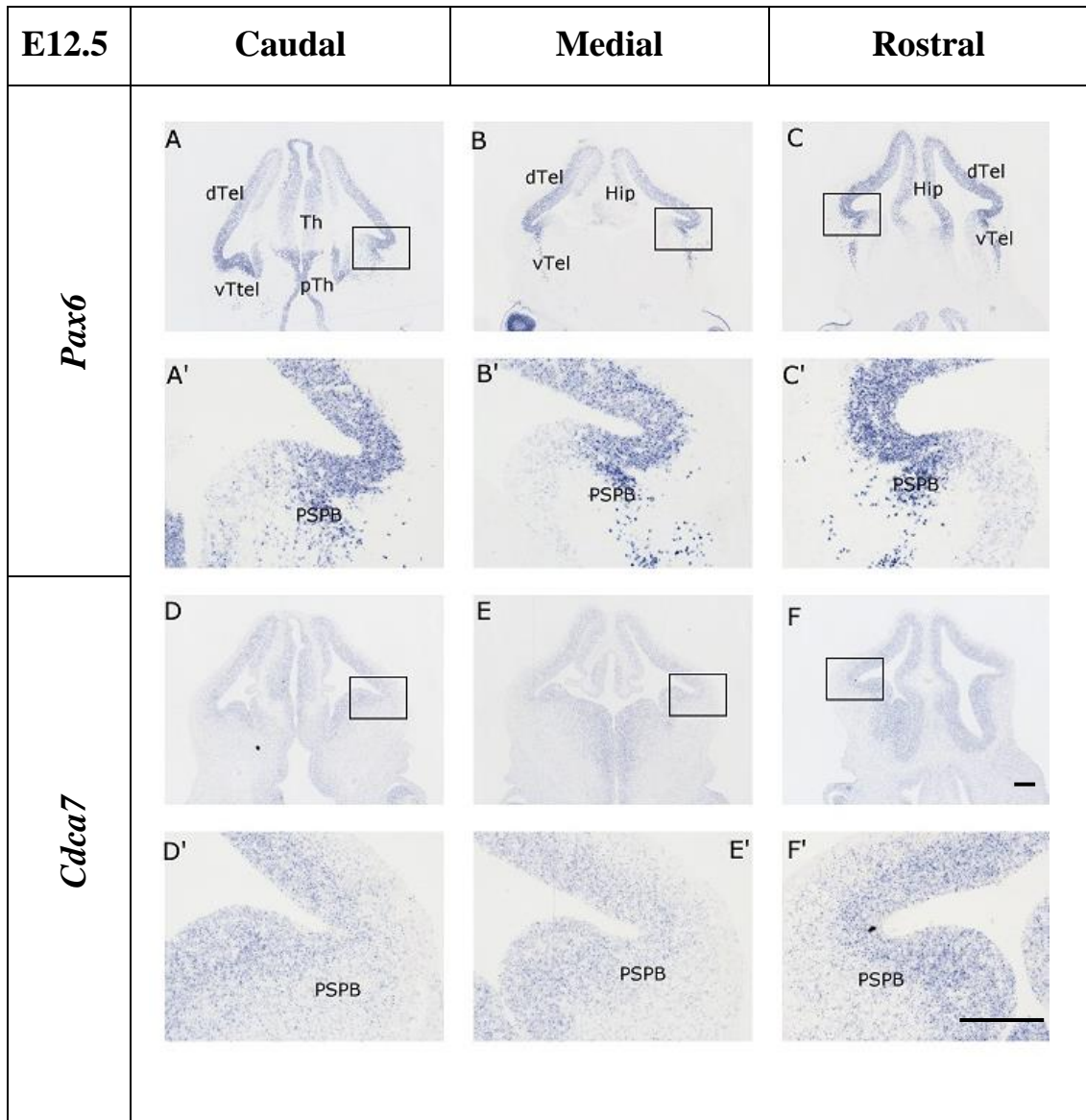


Figure 3.3 Expression of *Pax6* and *Cdca7* at various positions in E12.5 *PAX77* coronal sections

Figure 3.3 Expression of *Pax6* and *Cdca7* at various positions in E12.5 PAX77 coronal sections

(A-C) Representative ISH images produced from caudal, medial, and rostral sections, respectively, showing that *Pax6* mRNA is expressed in a low-medial to high-lateral gradient in the dTel, and is sharply reduced in the vTel after crossing the PSPB region, similar to the pattern seen in *WT* embryos. (A'-C') High magnification images enlarged from the rectangle areas in Panel A-C, respectively. The *Pax6* mRNA reaches its highest point near the PSPB region and decreases immediately after crossing this region into the vTel. (D-F) Representative ISH images of *Cdca7* mRNA expression, showing a counter gradient compared to the *Pax6* pattern. The expression reaches its lowest level at the PSPB region. (D'-F') High magnification views of the rectangles in Panel D-F, respectively. *Cdca7* mRNA level is low around the PSPB and the level increases after crossing the PSPB into the vTel. Panel A and D, B and E, C and F are anatomically similar (adjacent sections), therefore the regional labels shown in A-C are also shared in D-F. Scale bars: 200 μ m.

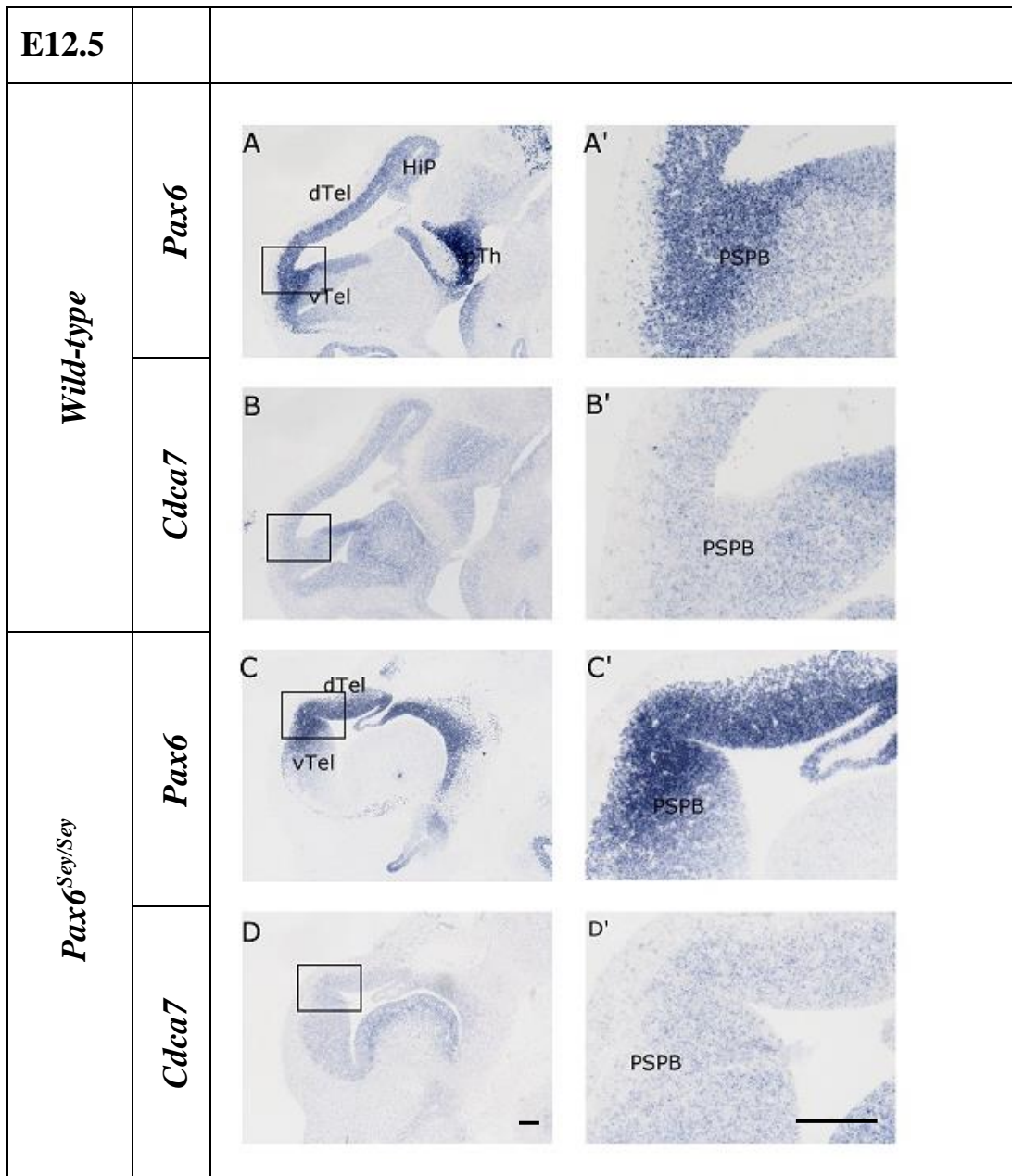


Figure 3.4 Expression of *Pax6* and *Cdca7* on E12.5 *wild-type* and *Pax6^{Sey/Sey}* sagittal sections

Figure 3.4 Expression of *Pax6* and *Cdca7* on E12.5 *wild-type* and *Pax6*^{Sey/Sey} sagittal sections

(A-A') A representative ISH image produced from a sagittal section, showing *Pax6* mRNA expression in *WT* forebrain. Panel A' contains a high magnification view of the area inside the rectangle in Panel A. *Pax6* is expressed in a low-caudal to high-rostral gradient, reaching its highest level near the PSPB. (B-B') *Cdca7* mRNA is expressed in an opposite pattern compared to the *Pax6* mRNA in the dTel. The expression level is low at the PSPB and increases sharply in the adjacent vTel. (C- C', D-D') No obvious graded expression patterns of *Pax6* and *Cdca7* are seen in the dTel in *Pax6*^{Sey/Sey}. Although *Pax6* mRNA still reaches its highest level near the PSPB, no reduction of *Cdca7* mRNA is seen at this region. Scale bars: 200 μ m.

3.2.2 Embryonic stage E13.5

At E13.5, the mRNA expression pattern of *Pax6* is indistinguishable between *WT* (n=3) and *PAX77* (n=2) embryos. The pattern also appears less graded in the dTel at this stage compared to E12.5 (Figure 3.5-7). *Pax6* mRNA is expressed throughout the whole dTel up to the PSPB region, where the expression level peaks, the expression rapidly decreases after crossing the PSPB into the vTel and very low level is present in the remaining part of the vTel. In *Pax6^{Sey/Sey}* embryos (n=3), *Pax6* mRNA is expressed in a high-medial to low-lateral gradient in the dTel, in agreement with the pattern seen in the same genotype at E12.5 but in contrast to the opposite patterns seen in *WT* and *PAX77* samples at this stage. In the vTel, *Pax6* mRNA expression is similar between *WT* and *PAX77* tissues at E13.5, with a gradient less obvious compared to samples at E12.5. In *Pax6^{Sey/Sey}* the expression decreases continuously from the dorsal-medial telencephalon to the vTel, indicating that the strongest level is located at the dorsal-medial telencephalon instead of the PSPB.

Cdca7 mRNA expression in *WT* and *PAX77* embryos at E13.5 possess similar patterns to those seen in samples at E12.5, in which a weak gradient was observed in the dTel (Figure 3.5-7). In the vTel, no significant difference between E12.5 and E13.5 samples were seen. Overall the expression level is very low in the lateral telencephalon and the weakest area is seen around the PSPB in *WT* and *PAX77* embryos. In *Pax6^{Sey/Sey}* mutants, the level of *Cdca7* mRNA appears in a gradient which gradually increases from the dorsal-medial telencephalon to the vTel. *Cdca7* expression also appears higher in the subventricular zone (SVZ) in the lateral telencephalon as well as in the vTel (Figure 3.6, arrows). The change in the expression territory from the VZ to the SVZ is very clear in *Pax6^{Sey/Sey}* mutants from E13.5 onwards but is not seen in *WT* and *PAX77*. Whether this change indicates behavioural alteration of progenitors is still unknown.

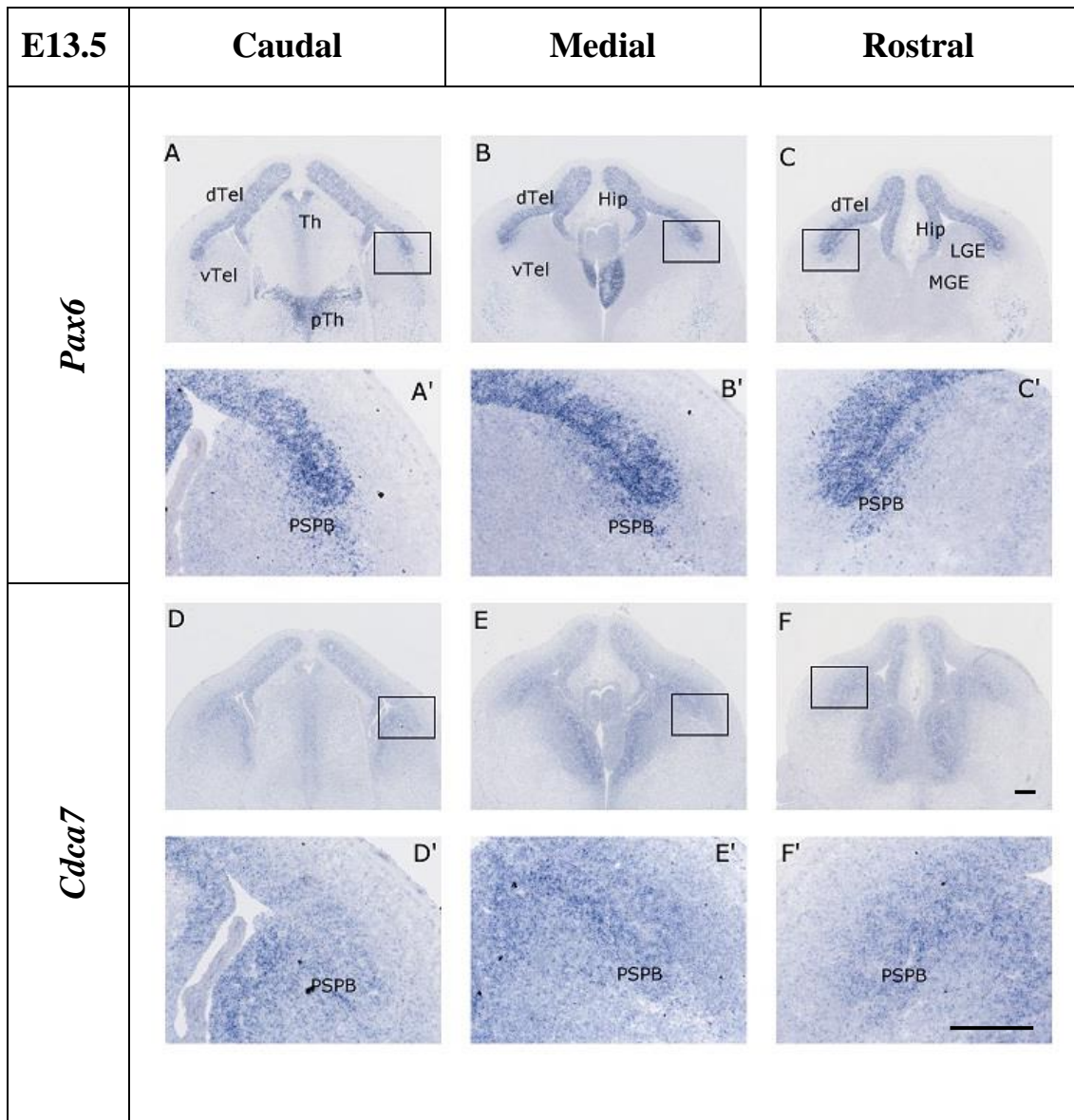


Figure 3.5 Expression of *Pax6* and *Cdca7* at various positions in E13.5 *wild-type* coronal sections

Figure 3.5 Expression of Pax6 and Cdca7 at various positions in E13.5 wild-type coronal sections

(A-C) Representative ISH images produced from caudal, medial, and rostral sections, respectively, showing *Pax6* mRNA expression in the dTel and around the PSPB region. (A'-C') High magnification views of the areas inside the rectangles in Panel A-C, respectively. The level of *Pax6* mRNA expression is higher near the PSPB region compared to the dTel, and declines rapidly after crossing the PSPB into the vTel. (D-F) Representative ISH images showing the mRNA expression of *Cdca7* which possesses an even pattern across the dTel. (D'-F') High magnification views of the areas inside the rectangles in Panel D-F, respectively. It can be seen that the expression level of *Cdca7* mRNA is slightly lower at the PSPB region compared to the adjacent ventricular and subventricular zones of the vTel. Panel A and D, B and E, C and F are anatomically similar (adjacent sections), therefore the regional labels shown in A-C are also shared in D-F. Scale bars: 200 μ m.

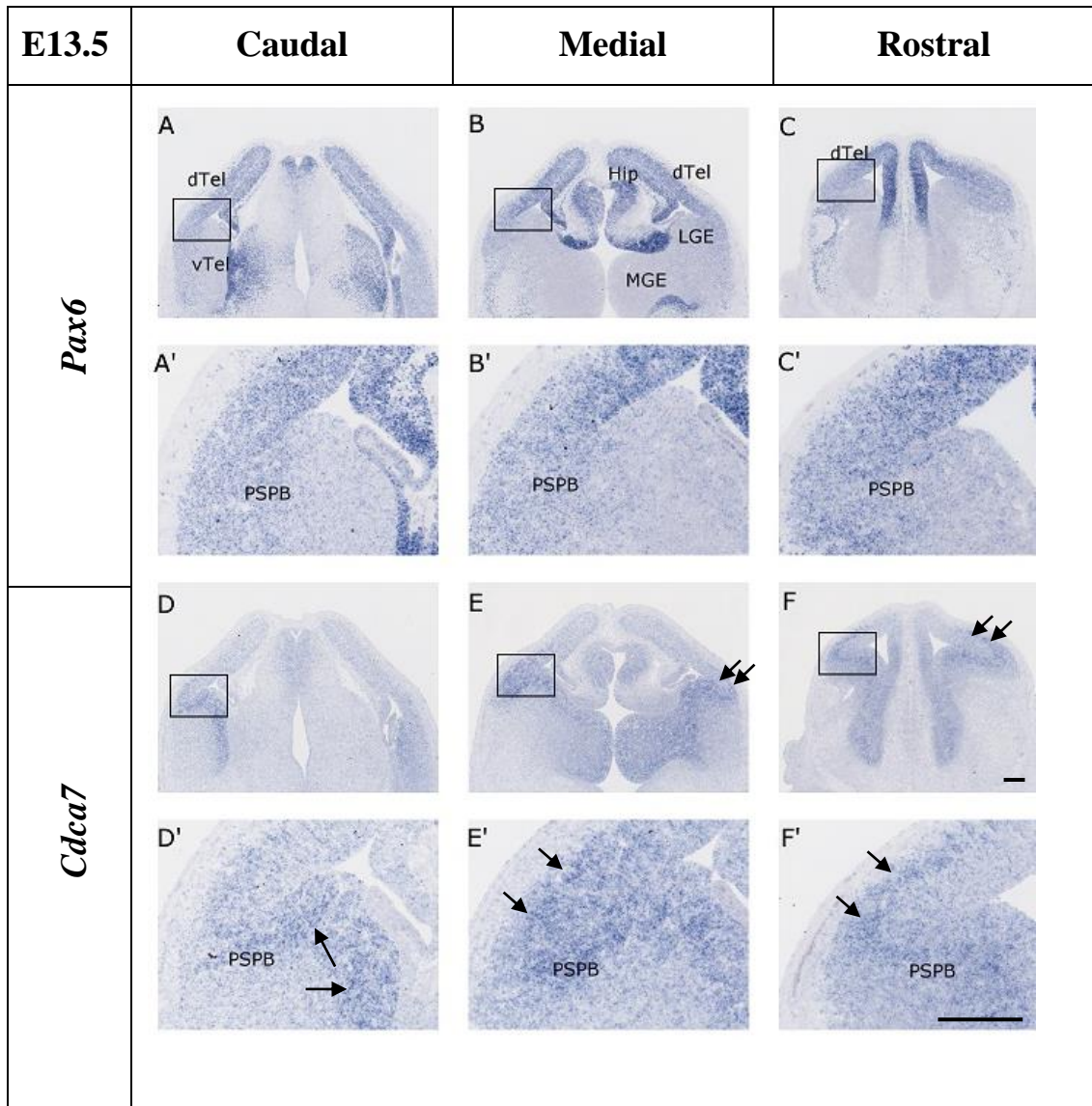


Figure 3.6 Expression of *Pax6* and *Cdca7* at various positions in E13.5 *Pax6*^{Sey/Sey} coronal sections.

Figure 3.6 Expression of *Pax6* and *Cdca7* at various positions in E13.5 *Pax6*^{Sey/Sey} coronal sections.

(A-C) Representative ISH images produced from caudal, medial, and rostral sections, respectively, showing the expression pattern of *Pax6* mRNA which possesses a high-medial to low-lateral gradient in the dTel. Unlike the pattern in *WT*, the expression does not peak at the PSPB region. (A'-C') High magnification images enlarged from the rectangle areas in Panel A-C, respectively. *Pax6* mRNA is lowly expressed in the lateral telencephalon and continuously declines in the vTel. (D-F) Representative ISH images of *Cdca7* mRNA showing an opposite gradient compared to the *Pax6* mRNA in the dTel towards the PSPB region. (D'-F') High magnification views of the regions inside the rectangle areas in Panel D-F, respectively. No obvious change in the expression intensity can be seen between the PSPB and the vTel. Generally, *Cdca7* mRNA is highly expressed in the subventricular zone (SVZ) of the lateral and ventral telencephalon (arrows). Panel A and D, B and E, C and F are anatomically similar (adjacent sections), therefore the regional labels shown in A-C are also shared in D-F. Scale bars: 200 μm .

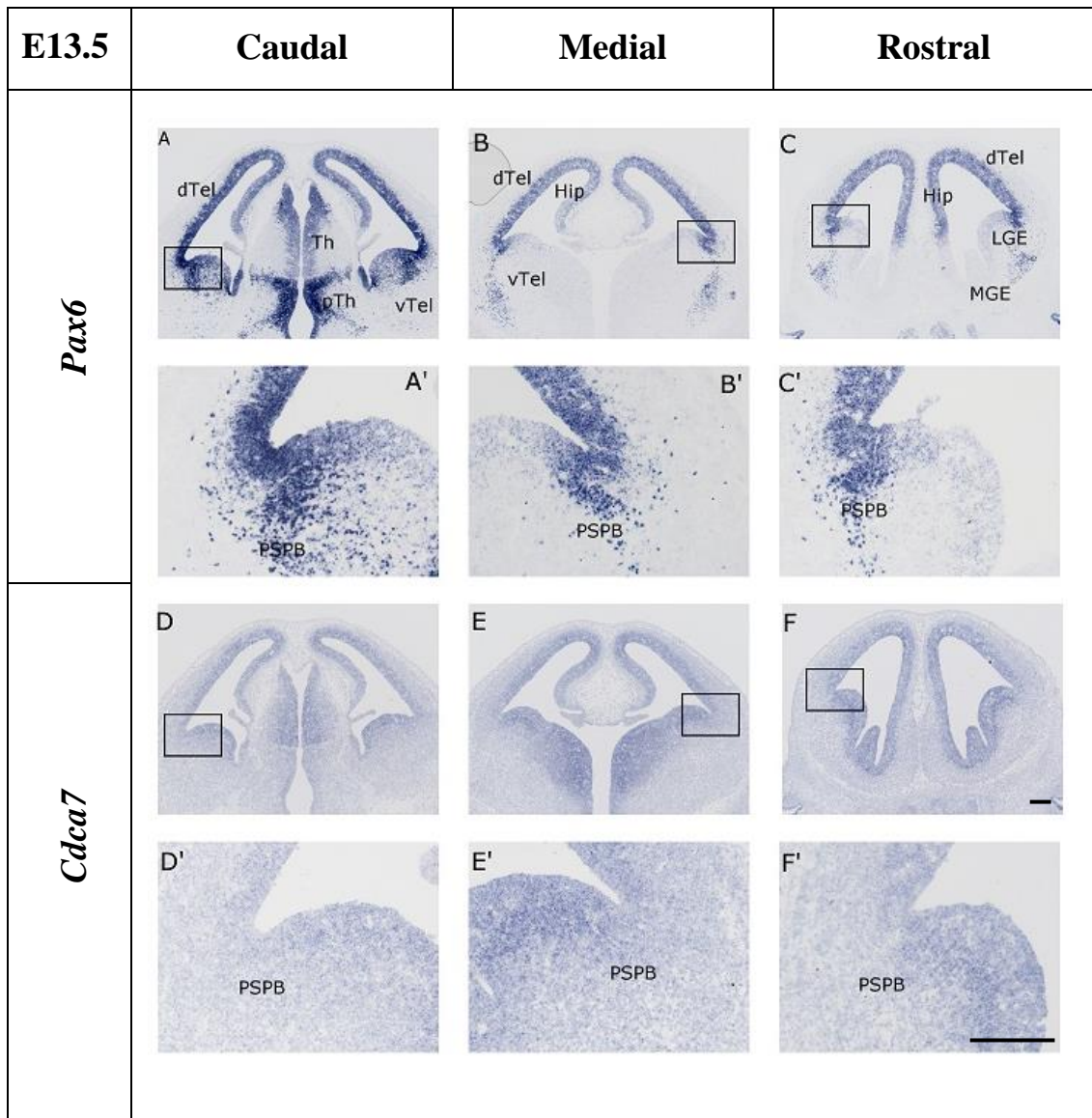


Figure 3.7 Expression of *Pax6* and *Cdca7* at various positions in E13.5 *PAX77* coronal sections

Figure 3.7 Expression of Pax6 and Cdca7 at various positions in E13.5 PAX77 coronal sections

(A-C) Representative ISH images produced from caudal, medial, and rostral sections, respectively, showing the expression of *Pax6* mRNA which has a low-medial to high-lateral gradient in the dTel. The gradient is less obvious compared to E12.5. (A'-C') High magnification images of the areas inside the rectangles in Panel A-C, respectively. The mRNA expression of *Pax6* reaches its highest level near the PSPB region, and decreases immediately after crossing this region into the vTel. (D-F) *Cdca7* mRNA is expressed in an opposite gradient compared to the pattern of *Pax6* mRNA, with its lowest level at the PSPB region. (D'-F') High magnification views of the rectangle areas in Panel D-F, respectively. The expression of *Cdca7* mRNA is lowest around the PSPB and the level increases after crossing the PSPB into the vTel. Panel A and D, B and E, C and F are anatomically similar (adjacent sections), therefore the regional labels shown in A-C are also shared in D-F. Scale bars: 200 μm .

3.2.3 Embryonic stage E14.5

At E14.5, *Pax6* and *Cdca7* mRNA expression patterns seem identical between *WT* (n=4) and *PAX77* (n=3) samples and no obvious change can be seen in the dTel between E13.5 and E14.5 (Figure 3.8 and 3.10). The expression of *Pax6* mRNA can be seen evenly in the dTel, turning slightly stronger at the PSPB and disappears immediately after crossing the PSPB into the vTel. In *WT* and *PAX77* embryos, *Cdca7* mRNA is also evenly expressed in most areas of the dTel, the level is very low at the PSPB, where the highest level of *Pax6* mRNA expression is present. In consistence with the finding in E13.5 samples, the expression of *Cdca7* mRNA becomes stronger after crossing the PSPB into the vTel in both *WT* and *PAX77* embryos.

In *Pax6^{Sey/Sey}* samples (n=4), compared to samples at E13.5, the medial^{high} to lateral^{low} expression gradient of *Pax6* seems stronger at E14.5 in the dTel, indicating a greater reduction in expression from the medial to the lateral telencephalon (Figure 3.9). In the vTel, *Pax6* mRNA expression reduces continuously in a lateral to medial direction but does not disappear abruptly after the PSPB. *Cdca7* expression is strong from the lateral to the ventral telencephalon. In contrast to *WT* and *PAX77* samples, *Cdca7* mRNA is not downregulated at the PSPB region in *Pax6^{Sey/Sey}* embryos, suggesting the loss of functional Pax6 protein has affected the expression of *Cdca7* mRNA. It was also found that *Cdca7* mRNA is highly expressed in the SVZ in the lateral and the ventral telencephalon in *Pax6^{Sey/Sey}* samples (Figure 3.9 D-F, indicated by arrows).

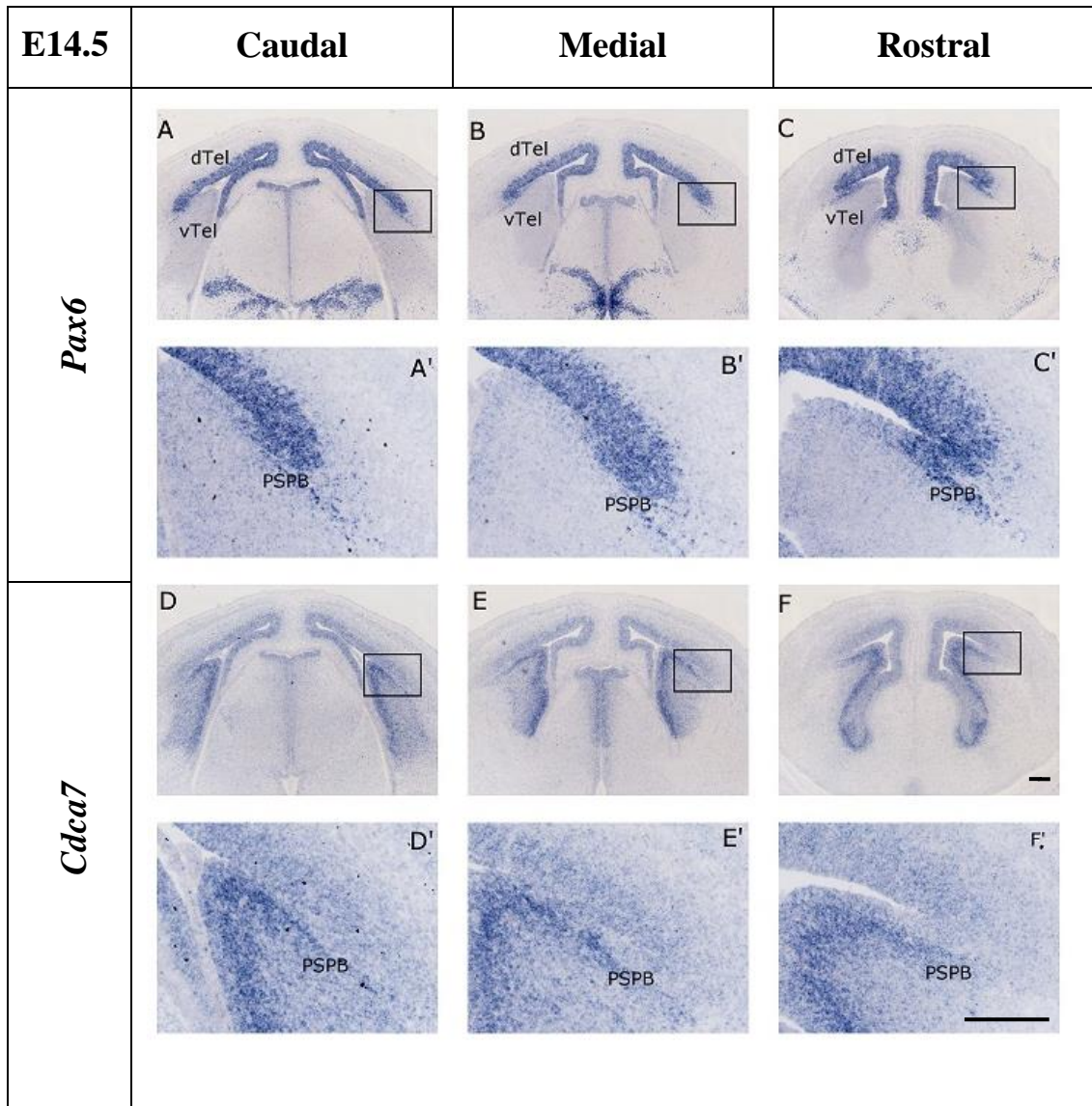


Figure 3.8 Expression of *Pax6* and *Cdca7* at various positions in E14.5 *wild-type* coronal sections

Figure 3.8 Expression of *Pax6* and *Cdca7* at various positions in E14.5 *wild-type* coronal sections

(A-C) Representative ISH images produced from caudal, medial, and rostral sections, respectively, showing the expression of *Pax6* mRNA in forebrain. (A'-C') High magnification images enlarged from the rectangle areas in Panel A-C, respectively. *Pax6* mRNA is highly expressed near the PSPB compared to the dTel, and declines rapidly after crossing this region into the vTel. (D-F) *Cdca7* mRNA is expressed in a high-medial to low-lateral gradient across the dTel. (D'-F') High magnification views of the areas inside the rectangles in Panel D-F, respectively. The expression level of *Cdca7* mRNA is lowest at the PSPB region and increases immediately after crossing the PSPB into the vTel. Additionally the level is higher in the SVZ than in the VZ in the vTel. Panel A and D, B and E, C and F are anatomically similar (adjacent sections), therefore the regional labels shown in A-C are also shared in D-F. Scale bars: 200 μm .

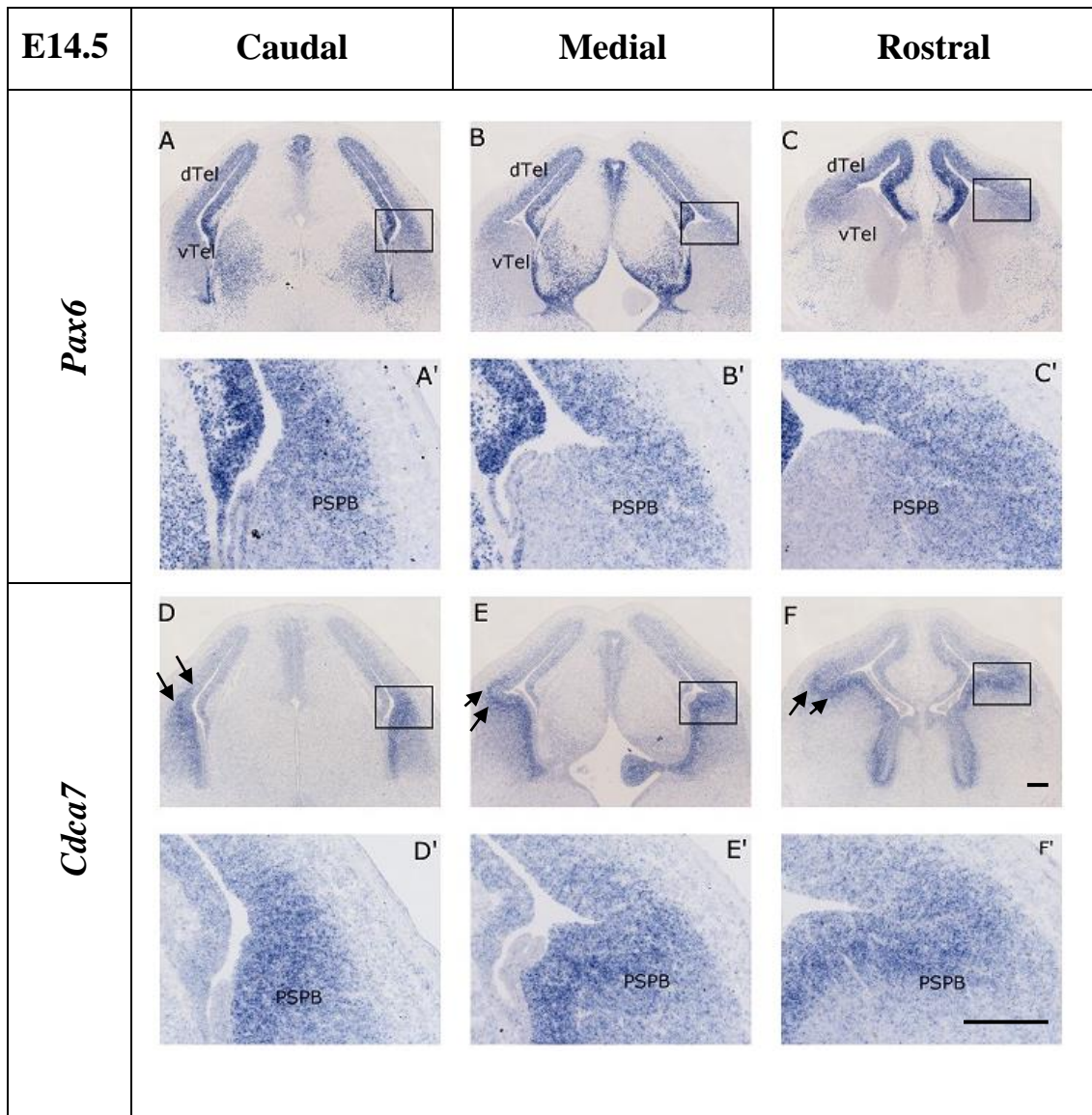


Figure 3.9 Expression of *Pax6* and *Cdca7* at various positions in E14.5 *Pax6^{Sey/Sey}* coronal sections

Figure 3.9 Expression of *Pax6* and *Cdca7* at various positions in E14.5

***Pax6*^{Sey/Sey} coronal sections**

(A-C) Representative ISH images produced from caudal, medial, and rostral sections, respectively, showing that *Pax6* mRNA is expressed in a high-medial to low-lateral gradient in the dTel, the level decreases even further in the vTel. (A'-C') High magnification images enlarged from the rectangle areas in Panel A-C, respectively. *Pax6* mRNA is lowly expressed in the lateral telencephalon and the level declines continuously in the vTel. (D-F) *Cdca7* mRNA is expressed in an opposite gradient compared to the pattern of *Pax6* mRNA in the dTel and the PSPB, and is highly expressed in the lateral telencephalon. (D'-F') High magnification views of the areas inside the rectangles in Panel D-F, respectively. *Cdca7* mRNA is highly expressed in the SVZ of the lateral and the ventral telencephalon (arrows in D-F). In contrast to the pattern seen in *WT* and *PAX77*, no obvious difference in the *Cdca7* expression intensity can be seen dorsal and ventral to the PSPB in *Pax6*^{Sey/Sey} mutants. Panel A and D, B and E, C and F are anatomically similar (adjacent sections), therefore the regional labels shown in A-C are also shared in D-F. Scale bars: 200 μ m.

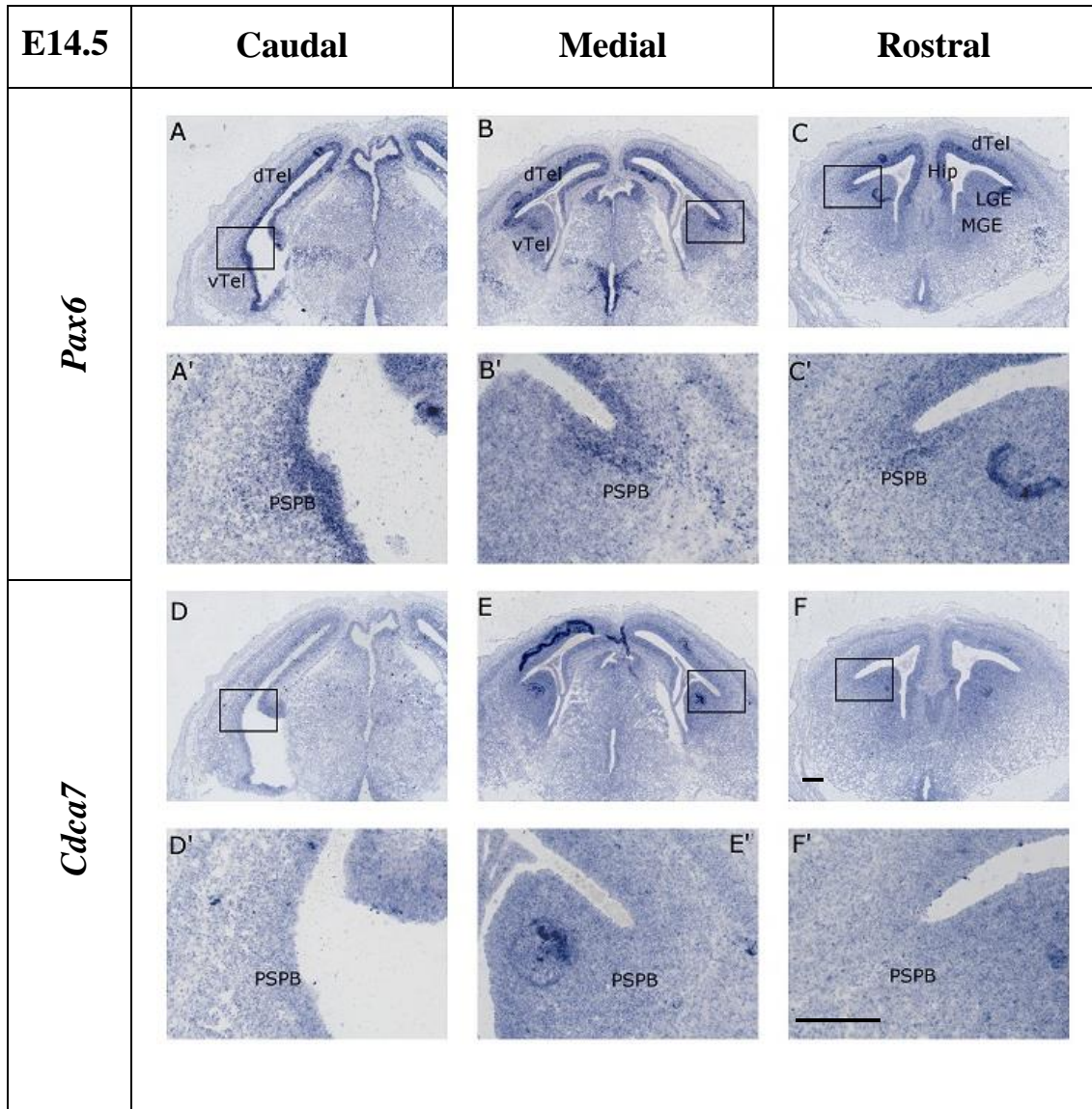


Figure 3.10 Expression of *Pax6* and *Cdca7* at various positions in E14.5 *PAX77* coronal sections

Figure 3.10 Expression of *Pax6* and *Cdca7* at various positions in E14.5 PAX77 coronal sections

(A-C) Representative ISH images produced from caudal, medial, and rostral sections, respectively, showing that *Pax6* mRNA is evenly expressed in the dTel. (A'-C') High magnification images enlarged from the rectangle areas in Panel A-C, respectively. The expression level of *Pax6* mRNA is high in the vTel in the caudal section, and decreases slightly in the medial and rostral sections. (D-F) The expression of *Cdca7* mRNA does not alter from the dTel to the vTel. (D'-F') High magnification images of the areas inside the rectangles in Panel D-F, respectively. No clear change in *Cdca7* expression level can be seen around the PSPB in the caudal and medial sections, while in the rostral section the level is lower dorsal to the PSPB. Panel A and D, B and E, C and F are anatomically similar (adjacent sections), therefore the regional labels shown in A-C are also shared in D-F. Scale bars: 200 μ m.

3.2.4 Embryonic stage E15.5

At E15.5, *Pax6* mRNA is expressed evenly across the dTel with no obvious upregulation at the PSPB region in *WT* (n=4) and *PAX77* (n=4) tissues (Figure 3.11, 3.13). Consistent with previous time points, *Pax6* mRNA is not detected after crossing the PSPB into the vTel. In *Pax6^{Sey/Sey}* mutants (n=4) (Figure 3.12), *Pax6* mRNA is expressed in a strong gradient which is high in the dorsal-medial telencephalon and low in the vTel, similar to the finding at earlier developmental stages in this genotype. *Cdca7* mRNA is also expressed evenly across most of the telencephalon in *WT* and *PAX77* samples, with an exception around the PSPB where the mRNA level is reduced. The overall expression intensity of *Cdca7* mRNA is lower in *PAX77* compared to *Pax6^{Sey/Sey}* samples, in which the expression is also evenly distributed across the dorsal and the ventral telencephalon.

In addition, although it is difficult to define the absolute expression level of mRNAs using ISH, it is clear, especially at later developmental stages, that *Pax6* mRNA is more abundant in the *Pax6^{Sey/Sey}* mutant and in *PAX77* compared to *WT*, while *Cdca7* expression is slightly higher in *Pax6^{Sey/Sey}* and lower in *PAX77* and *WT* embryos.

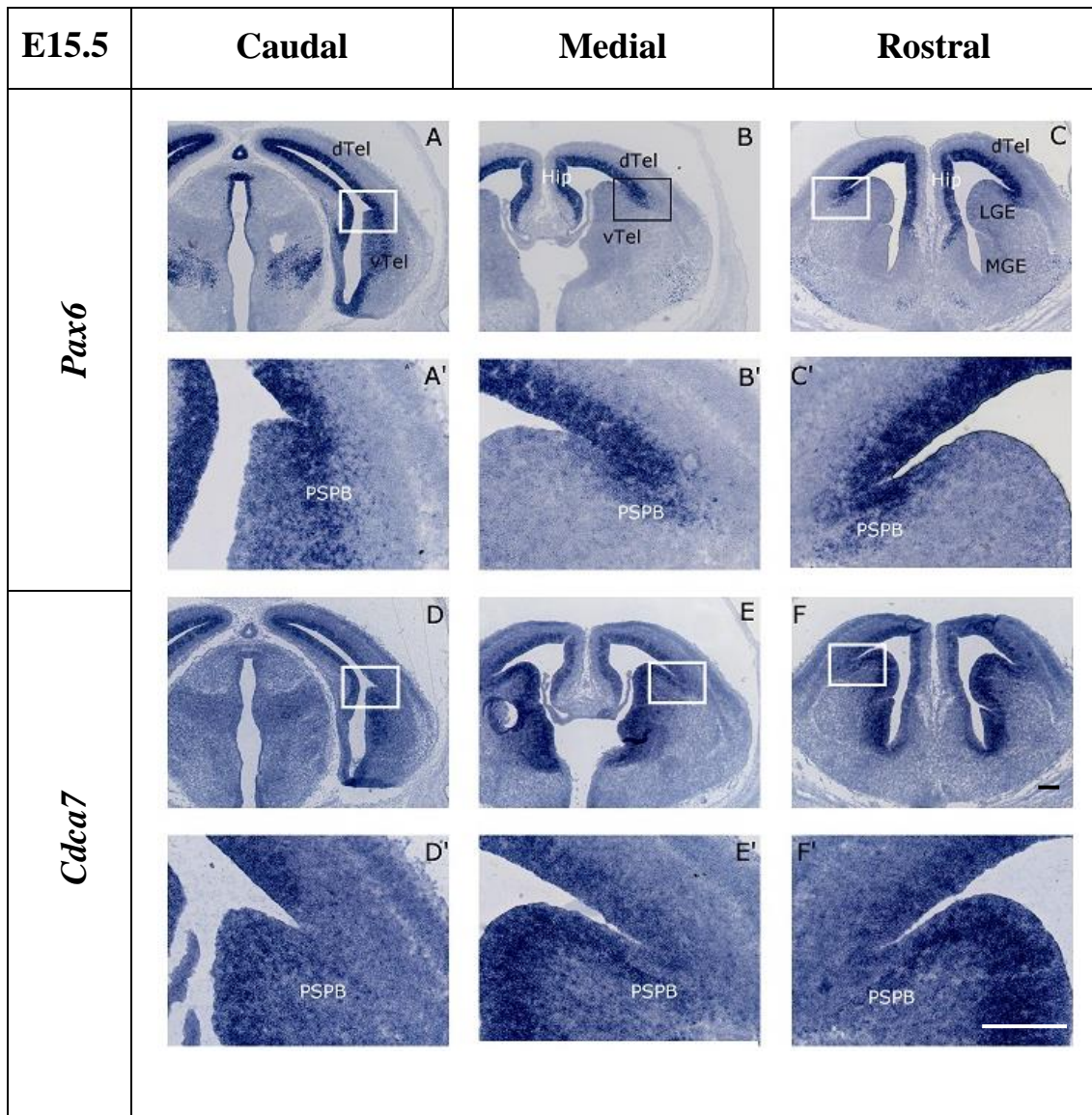


Figure 3.11 Expression of *Pax6* and *Cdca7* at various positions in E15.5 *wild-type* coronal sections

Figure 3.11 Expression of *Pax6* and *Cdca7* at various positions in E15.5 *wild-type* coronal sections

(A-C) Representative ISH images produced from caudal, medial, and rostral sections, respectively, showing that *Pax6* mRNA is expressed evenly in the dTel until the PSPB. (A'-C') High magnification images enlarged from the rectangle areas in Panel A-C, respectively. *Pax6* mRNA is highly expressed near the PSPB compared to the dTel, and declines rapidly ventral to the PSPB in the medial and rostral sections. (D-F) The expression of *Cdca7* mRNA appears even in most parts of the dTel but declines in the lateral telencephalon. (D'-F') High magnification views of the rectangle areas in Panel D-F, respectively. The expression level of *Cdca7* mRNA is lowest at the PSPB region and increases immediately after crossing the PSPB into the vTel, where the level is higher in the SVZ than in the VZ. Panel A and D, B and E, C and F are anatomically similar (adjacent sections), therefore the regional labels shown in A-C are also shared in D-F. Scale bars: 200 μm .

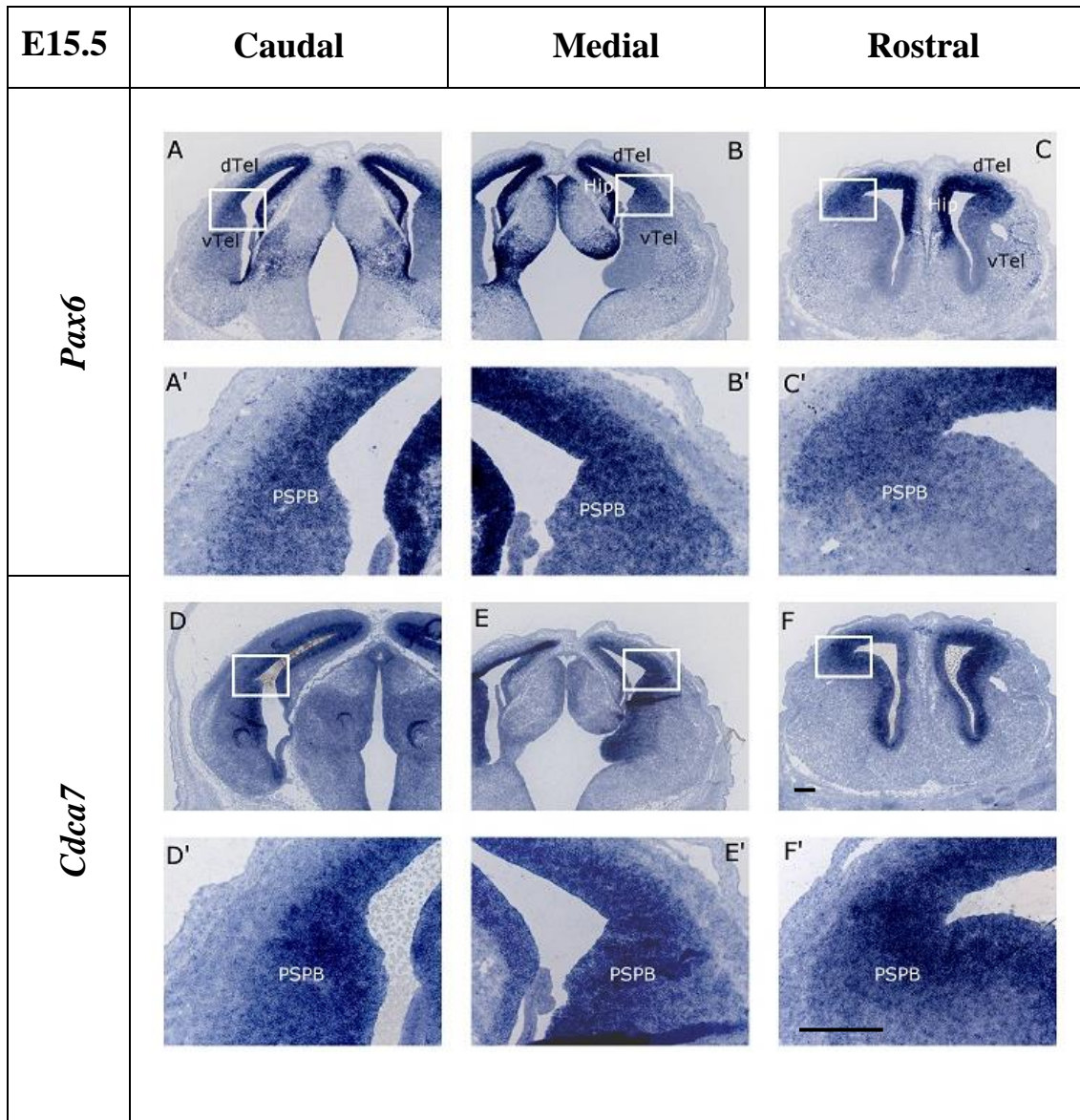


Figure 3.12 Expressions of *Pax6* and *Cdca7* at different positions in E15.5 *Pax6*^{Sey/Sey} coronal sections

Figure 3.12 Expressions of *Pax6* and *Cdca7* at different positions in E15.5 *Pax6*^{Sey/Sey} coronal sections

(A-C) Representative ISH images produced from caudal, medial, and rostral sections, respectively, showing that *Pax6* mRNA is expressed in a high-medial to low-lateral gradient in the dTel. (A'-C') High magnification images enlarged from the rectangle areas in Panel A-C, respectively. *Pax6* mRNA is lowly expressed in the lateral telencephalon and the level decreases further in the vTel. (D-F) *Cdca7* mRNA is expressed in an opposite gradient compared to the pattern of *Pax6* mRNA in the dTel up to the PSPB, and is highly expressed in the lateral telencephalon. (D'-F') High magnification views of the areas inside the rectangles in Panel D-F, respectively. *Cdca7* mRNA is highly expressed in the SVZ of the lateral and the ventral telencephalon (arrows in D-F). In contrast to the pattern seen in *WT* and *PAX77*, no obvious difference in the *Cdca7* expression intensity can be seen dorsal and ventral to the PSPB in *Pax6*^{Sey/Sey} mutants. Panel A and D, B and E, C and F are anatomically similar (adjacent sections), therefore the regional labels shown in A-C are also shared in D-F. Scale bars: 200 μ m.

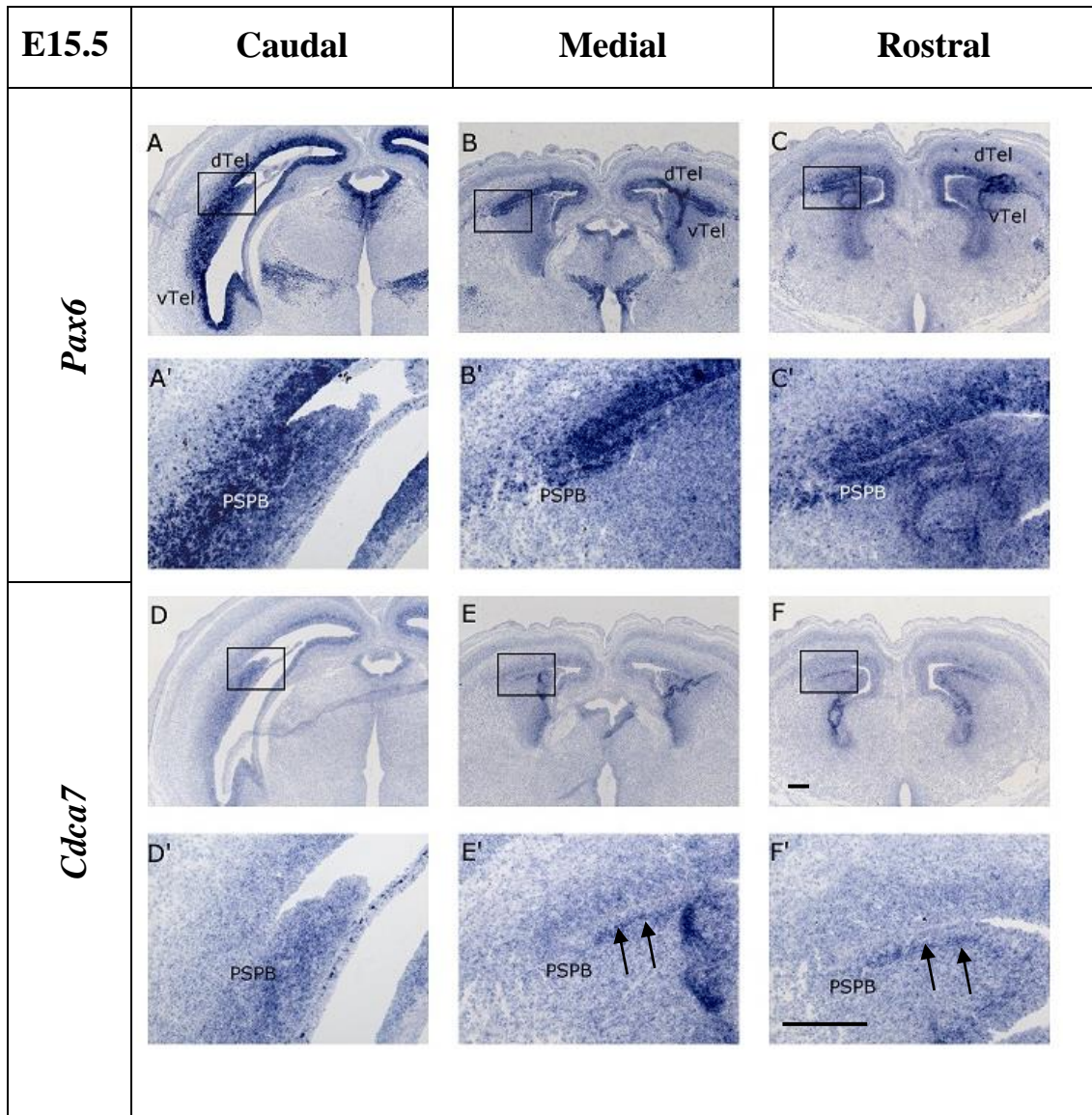


Figure 3.13 Expression of *Pax6* and *Cdca7* at various positions in E15.5 *PAX77* coronal sections

Figure 3.13 Expression of *Pax6* and *Cdca7* at various positions in E15.5 PAX77 coronal sections

(A-C) Representative ISH images produced from caudal, medial, and rostral sections, respectively, showing that *Pax6* mRNA is expressed evenly in the dTel until the PSPB. (A'-C') High magnification images enlarged from the rectangle areas in Panel A-C, respectively. The expression level of *Pax6* mRNA remains high in the vTel in the caudal section, and decreases slightly in the medial and rostral sections. (D-F) No noticeable change in the expression level of *Cdca7* mRNA can be seen in the dTel except in the caudal section, where the intensity decreases in the lateral telencephalon. (D'-F') High magnification views of the rectangle areas in Panel D-F, respectively. A slight reduction in *Cdca7* mRNA level can be seen dorsal to the PSPB in the caudal section, and the level is high in the SVZ in the vTel in both the medial and the rostral sections (arrows in E' and F'). Panel A and D, B and E, C and F are anatomically similar (adjacent sections), therefore the regional labels shown in A-C are also shared in D-F. Scale bars: 200 μ m.

3.2.5 Comparing the overall expression level between developmental stages, genotypes and positions

In order to understand how the mRNA levels of *Pax6* and *Cdca7* differ between genotypes during neurogenesis, in-depth quantitative image analysis was conducted as follows:

WT, *Pax6*^{*Sev/Sev*} and *PAX77* embryos were gathered at embryonic stage E12.5 to E15.5. *WT* and *Pax6*^{*Sev/Sev*} samples collected from the same litter were arrayed on the same slide to minimise experimental batch effects. Full heads were cryo-sectioned in coronal or sagittal orientation and 10µm-thick sections were collected in series. Colorimetric ISH for *Pax6* and *Cdca7* mRNA was carried out on adjacent slides for further analysis.

ISH images were taken on a Leica LB30T microscope with LAS software version 3.6 and were further analysed by Fiji software. For each image, it was first converted to an 8-bit image (0-255) and either the left or the right hemisphere was selected for pixel intensity analysis. A ribbon with the width corresponding to the gene expression area was drawn from the medial to lateral dTel and further to the lateral ganglionic eminences (LGE) (Figure 3.14A). Pixel intensity was calculated and average taken approximately every 10 µm (bin size=10). The data was then further divided into two parts according to the expression intensity of *Pax6* mRNA and the anatomical position, which is near the PSPB. A region where neither *Pax6* nor *Cdca7* are expressed was selected as the background area and the pixel intensity value of the background was used as a baseline from which other areas of the same section subtract to correct the data. Finally, background corrected data were multiplied by -1 and were plotted on a scatter graph (Figure 3.14B). Since the pixel intensity reading ranges from 0 to 255 (8-bit figure), where 0 indicates the weakest and 255 indicates the strongest expression. Background corrected data multiplied by -1 provides a much intuitive representation of the change in expression level when readings from various points along a certain axis on the section are plotted, where a trend line with a positive slope corresponds to increasing expression level and one with a negative slope illustrates diminishing expression along the axis. For example, positive slope values seen in the dorsal area represent gene expression is medial^{low} to lateral^{high}.

The regulatory role of Pax6 on Cell Division Cycle Associated 7 and cortical progenitor cell proliferation

When the slope of the trend line is close to zero, it represents an even expression across the region. In order to understand whether the expression of *Pax6* and *Cdca7* is correlated, the slopes of the trend lines of the two genes across the medial dTel-lateral dTel-PSPB-vTel axis were calculated in all three genotypes between E12.5-E15.5.

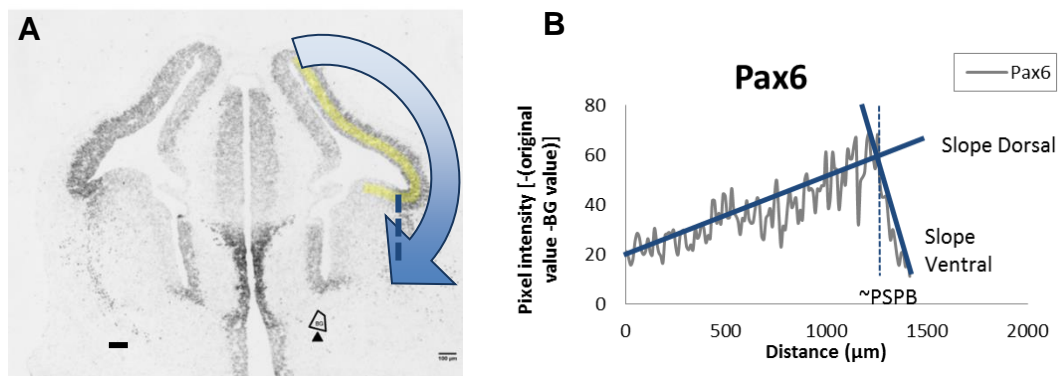


Figure 3.14 Pixel intensity analysis of the mRNA expression

(A) A yellow ribbon from medial dTel to the vTel was drawn and a background area was selected (quadrangle, arrowhead). Pixel intensity values were then calculated by Fiji. The dashed line represents the PSPB region and corresponds to the dashed line in Panel B. The blue arrow indicates the expression gradient which is low in the medial and high in the lateral dTel. (B) Pixel intensity values along the yellow ribbon in (A) were recorded in the direction from medial cortex to the vTel (blue arrow in (A).) Background signal was measured in a region where neither *Pax6* or *Cdca7* was expressed. Pixel intensity values collected from yellow ribbon area were corrected by subtracting the values with the background expression intensity. Background corrected data were further multiplied by -1 to create intuitive representation of the change in expression level (see text for explanation). Finally, processed data were plotted and separated into dorsal and ventral parts divided by the dashed line. The slopes of the trend lines for both dorsal and ventral pixel intensities were then calculated. Scale bar: 100 μm .

Because both *Pax6* and *Cdca7* possess different expression patterns before and after the PSPB across the axis, after collecting all data, the first step I performed was to separate the data into dorsal to ventral parts based on previous definitions and then plot the values of the slopes in a line chart along the developmental stages (Figure 3.15). The slope values of *Pax6* and *Cdca7* in the dTel region from *WT*, *Pax6^{Sey/Sey}* and *PAX77* embryos, respectively are shown in Figure 3.15A-C. *Pax6* values were similar in *WT* and *PAX77*, which were strongly positive at E12.5 and decreased with time. The slopes of *Cdca7* were also similar in *WT* and *PAX77*, with negative values in most timepoints. Figure 3.15A and 3.15C indicate the expression gradient of *Pax6* and *Cdca7* was negatively correlated in the dTel. In *WT* and *PAX77*, *Pax6* had a positive slope at E12.5 and the values decreased over time to zero, suggesting the medial^{low} to lateral^{high} expression gradient faded as development progressed. The slope value of *Cdca7* was negative at E12.5 and increased to close to zero at E14.5 in *WT* and *PAX77*, indicating the lateral^{low} to medial^{high} gradient of *Cdca7* diminished at this later stage. The expression slope values of *Cdca7* in *Pax6^{Sey/Sey}* mutants (Figure 3.15B), which lacks functional Pax6 protein, were close to zero at E12.5 and gradually increased over time until E14.5, indicating a medial^{low} to lateral^{high} gradient was formed. This pattern is distinctive from those in *WT* and *PAX77* samples. In summary, *Pax6* and *Cdca7* were expressed in counter-gradient in *PAX77* and *WT*, while this dynamic was disrupted in *Pax6^{Sey/Sey}*. Overlay of the slope patterns in all three genotypes (Figure 3.15D-E) further illustrates that *Pax6* and *Cdca7* were expressed in a similar manner between *WT* and *PAX77*, while the pattern was altered in *Pax6^{Sey/Sey}*. The difference between *Pax6* and *Cdca7* over time was significant both in *WT* and *Pax6^{Sey/Sey}* ($P < 0.05$, two-way ANOVA). *PAX77* samples were not included in the statistical analysis as values for E13.5 were taken from only two embryos. Data from the vTel is shown in Figure 3.15F-J. In contrast with the dTel, positive slope value in this region correspond to a lateral^{low} to medial^{high} expression gradient. The slope values of *Pax6* mRNA were negative at all stages in both *WT* and *PAX77*, with *PAX77* having stronger negative values than *WT*, indicating a more robust decrease in *Pax6* transcript level in *PAX77* in the vTel. Conversely the slopes of *Cdca7* mRNA in *WT* and *PAX77* were positive in most cases and did not fluctuate

The regulatory role of Pax6 on Cell Division Cycle Associated 7 and cortical progenitor cell proliferation over time in *PAX77*, indicating the expression gradients were lateral^{low} to medial^{high} (Figure 3.15F and H). Similar to the data from the dTel, the patterns of *Pax6* and *Cdca7* expression in the vTel in *Pax6*^{Sev/Sev} mutants were distinctive from those in *WT*, with negative slope values decreasing over time for both genes. Overlay of *Pax6* expression gradients showed unique patterns between genotypes at E12.5, the difference faded over time and the slopes gradually moved towards zero (Figure 5.15I). In comparison, *Cdca7* was expressed in a low-lateral to high-medial fashion in *WT* and *PAX77* (Figure 3.15J), while the expression slopes in *Pax6*^{Sev/Sev} mutant fluctuated from near zero at E12.5 to -0.07 at E15.5, indicating a reduction of mRNA expression from lateral to medial area in the vTel at later stage of development.

Taken together, the mRNA expression level of *Pax6* and *Cdca7* were negatively correlated in *WT* and *PAX77* embryos, both in the dorsal and the ventral telencephalon from E12.5 to E14.5. These counter-gradients seemed abolished or altered in direction in the *Pax6*^{Sev/Sev} mutant, where no functional Pax6 protein was present. At E15.5, the expression gradients of the two genes became less apparent in all three genotypes in the dorsal area, except for *Pax6* mRNA in the *Pax6*^{Sev/Sev} mutant which is not expected to form functional protein. The opposite gradients of the two genes were still visible in the ventral part in *WT* and *PAX77* at E15.5, while in the *Pax6*^{Sev/Sev} mutants, this negative correlation was lost, suggesting this mutually-exclusive expression pattern required functional *Pax6* protein.

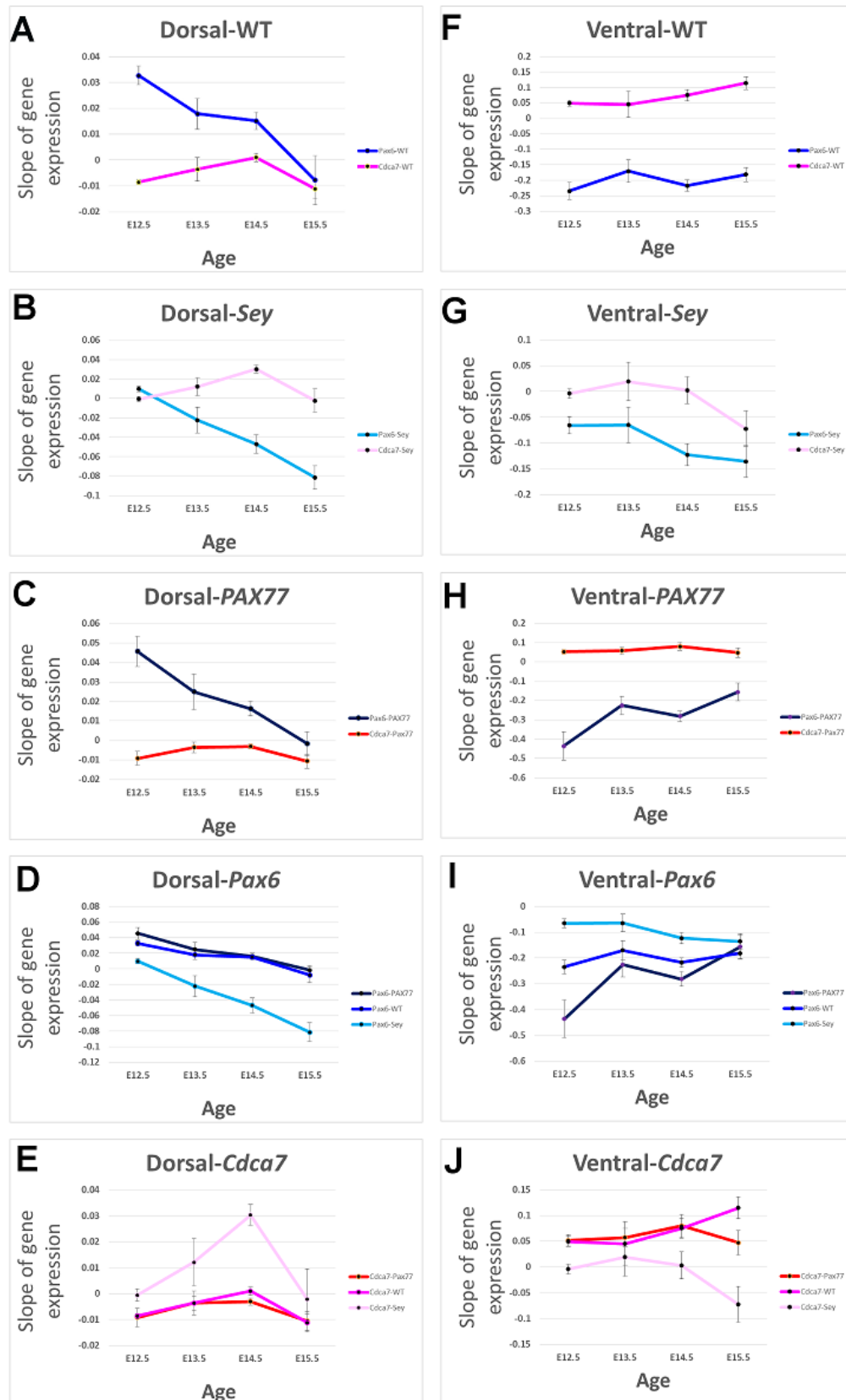


Figure 3.15 The slope values of mRNA expression gradient over time in *wild-type*, *Pax6^{Sey/Sey}* and *PAX77* samples in the dorsal and ventral telencephalon.

Figure 3.15 The slope values of mRNA expression gradient over time in *wild-type*, *Pax6*^{Sey/Sey} and *PAX77* samples in the dorsal and ventral telencephalon.

(A-E) Expression slope data measured from the dorsal telencephalon samples between E12.5 and E15.5. (A-C) The slope values of *Pax6* and *Cdca7* transcript gradient were plotted to illustrate the relative pattern between the two genes in each of the three genotypes. (D-E) The slope values of *Pax6* and *Cdca7* mRNA expression, respectively, in all three genotypes were overlaid. (F-J) Expression slope data measured from the ventral telencephalon samples between E12.5 and E15.5. (F-H) The slope values of *Pax6* and *Cdca7* transcript gradient were plotted to illustrate the relative pattern between the two genes in each of the three genotypes. (I-J) The slope values of *Pax6* and *Cdca7* mRNA expression, respectively, in all three genotypes were overlaid. Three to four embryos were measured in each genotype at each developmental stage, except for *PAX77* at E13.5, where only two embryos were measured. Difference between *Pax6* and *Cdca7* over time was significant both in *WT* and *Pax6*^{Sey/Sey} from the dorsal region (A, C) and the significance was not observed in the ventral area, neither in *WT* and *Pax6*^{Sey/Sey} ($P < 0.05$, Two-way ANOVA). Data set generated from *PAX77* was not used for statistical analysis due to low n number.

In Figure 3.16, data obtained from the dorsal and the ventral regions were analysed separately. Each point represents the average value of data obtained from all the three genotypes at one time point. In the dorsal region, the slope value of *Pax6* expression gradient moves from positive towards zero and then to the negative side over time. The change in the *Cdca7* expression gradient over time follows an opposite pattern, which shifts towards positive slope values from E12.5-E14.5, however the value at E15.5 is negative.

In the ventral region, no significant difference can be seen between the slope values of the *Cdca7* expression gradient (i.e. Y-axis) at all four stages, although it is worth noting that all slope values are significantly positive, meaning that the mRNA expression of *Cdca7* is increased from the lateral to medial ventral telencephalon. In contrast all *Pax6* slopes are significantly negative, this further suggests that the expression of the two genes are mutually exclusive.

Since it is clear that the expression patterns of *Pax6* and *Cdca7* are different in *Pax6^{Sey/Sey}* compared to those in *WT* and *PAX77*, next I will discuss data from different genotypes separately.

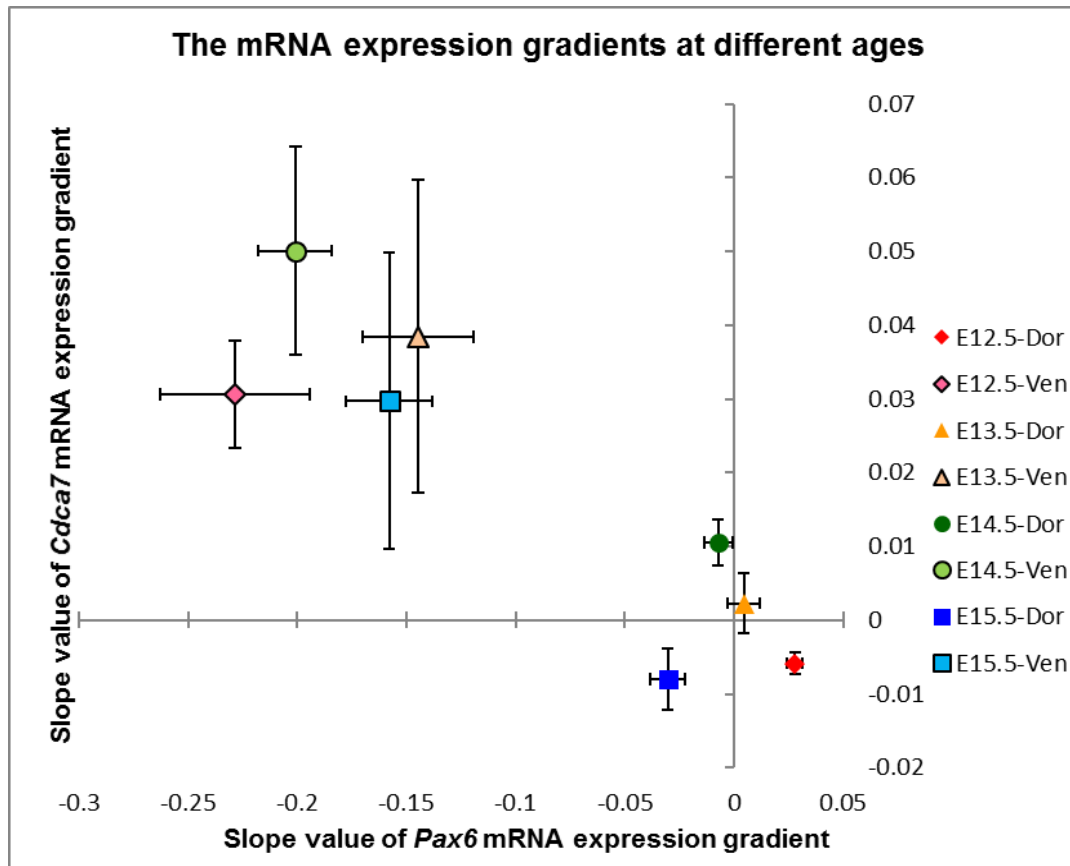


Figure 3.16 A general trend of Pax6 and Cdc7 mRNA expression gradient at different developmental stages

All data were gathered together and then separated by their positions (dorsal or ventral parts) and developmental stages. The X-axis and Y-axis represent the mRNA expression slope of *Pax6* and *Cdc7*, respectively. Each point depicts the average slope values of all three genotypes. Error bars represent the standard errors.

If Pax6 protein has multiple effects on *Cdca7* expression, in order to distinguish these effects, the slope value of *Pax6* mRNA expression was plotted against that of *Cdca7* mRNA in each sample in all three genotypes (Figure 3.17). Data collected from both dorsal and ventral regions across all examined embryonic stages were pooled in this analysis and data from dorsal and ventral were distinguished by colours. The patterns in *WT* and *PAX77* are similar to each other (Figure 3.17A and 3.17C) but the dots are much dispersed (Standard deviation or SD= 0.13 in *WT* and 0.20 in *PAX77*) in *PAX77*. The correlation between *Pax6* and *Cdca7* is distinctive in *Pax6*^{Sey/Sey} mutants compared to *WT* and *PAX77* samples (Figure 3.17B). In summary, dorsal and ventral data from *WT* and *PAX77* were located near zero point and the up-left quadrant, respectively and data from dorsal and ventral were separated clearly. Dorsal and ventral data from *Pax6*^{Sey/Sey} mutant showed higher degree of mixture compared to those from *WT* and *PAX77*, suggesting a less-defined dorsal-ventral separation of the telencephalon.

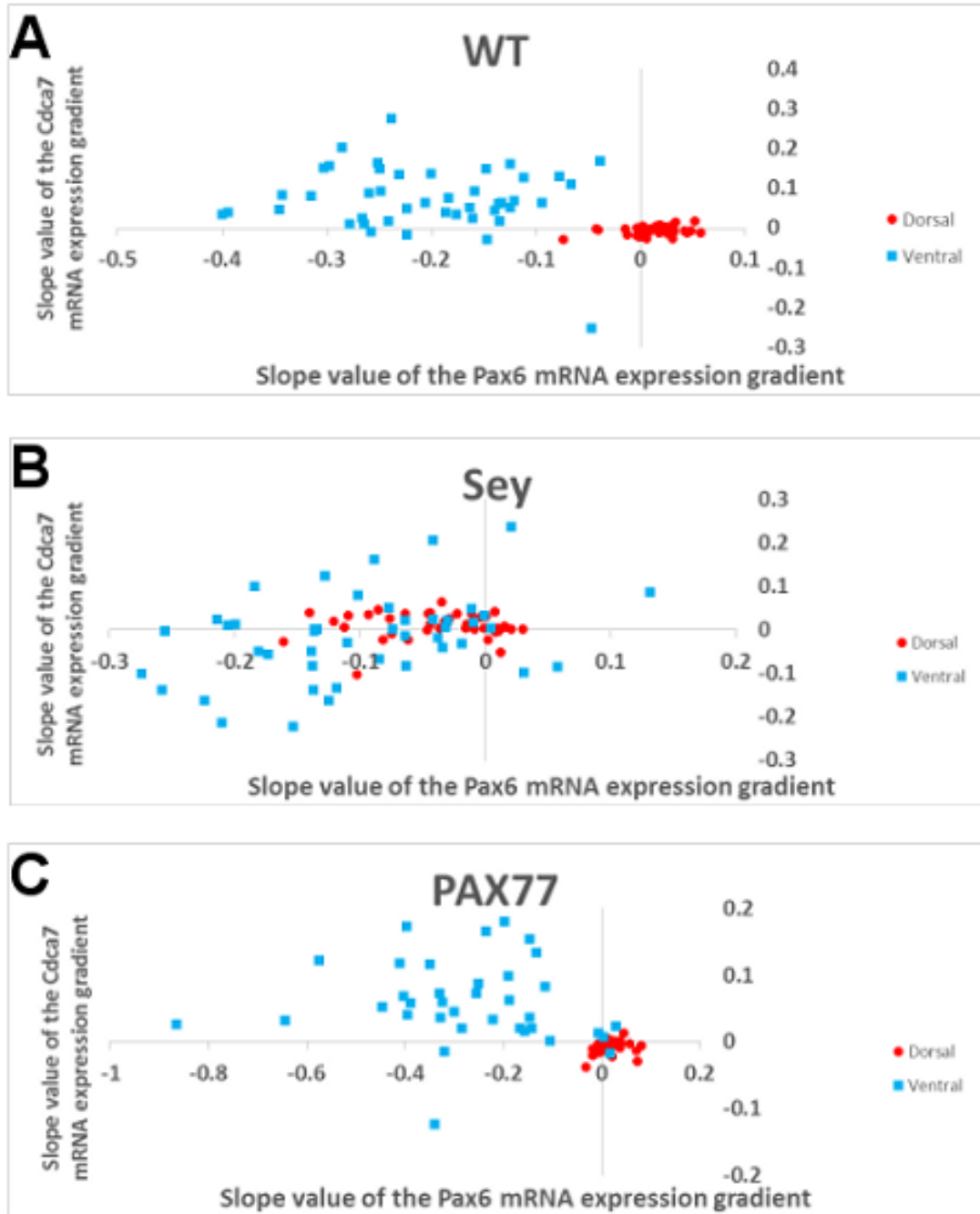


Figure 3.17 The mRNA expression gradients of different ages

Figure 3.17 The mRNA expression gradients of different ages

(A-C) Data points include all developmental stages in (A) *WT*, (B) *Pax6^{Sey/Sey}* and (C) *PAX77*, plotted separately for dorsal (red) and ventral (blue) telecephalon. The X-axis and Y-axis represent the mRNA expression slopes of *Pax6* and *Cdca7*, respectively. Dorsal slopes in *WT* and *PAX77* were located near zero point, while ventral slopes in these two genotypes were in the up-left quadrant. Dorsal and ventral data in *Pax6^{Sey/Sey}* mutant showed a high degree of overlap compared to those in *WT* and *PAX77*, suggesting a less-defined dorsal-ventral separation of the telencephalon.

In order to focus on the change of *Cdca7* mRNA expression in the presence of Pax6/PAX6 protein, similar scatter plot analysis was performed but all data from *Pax6*^{Sev/Sev} mutants were eliminated (Figure 3.18). The four panels in the figure represent four different embryonic stages from E12.5 to E15.5 (Figure 3.18A-D). Data points from the dorsal region, indicated by the red dots, located near zero in the lower-right quadrant while those from the ventral region, indicated by the blue dots, located in the up-left quadrant, suggesting a negative correlation of two genes in all ages. The slope values of *Pax6* mRNA (X-axis) were mainly positive at early stages, diffusing towards negative values over time. The slope values of *Cdca7* mRNA (Y-axis) in the dorsal region did not vary significantly over time, while variation in the ventral region increased as development progressed, suggesting a diminishing effect of Pax6 on *Cdca7* over time, especially in the vTel, where Pax6 is lowly expressed. In summary, the expression level of *Pax6* mRNA negatively correlates with the level of *Cdca7* mRNA in both *WT* and the *PAX77* over-expression model throughout the examined ages from E12.5 to E15.5, and this correlation is abolished in the loss-of-function *Pax6*^{Sev/Sev} mutants (Figure 3.17B), in agreement with the hypothesis that Pax6 protein inhibits the production of *Cdca7* mRNA.

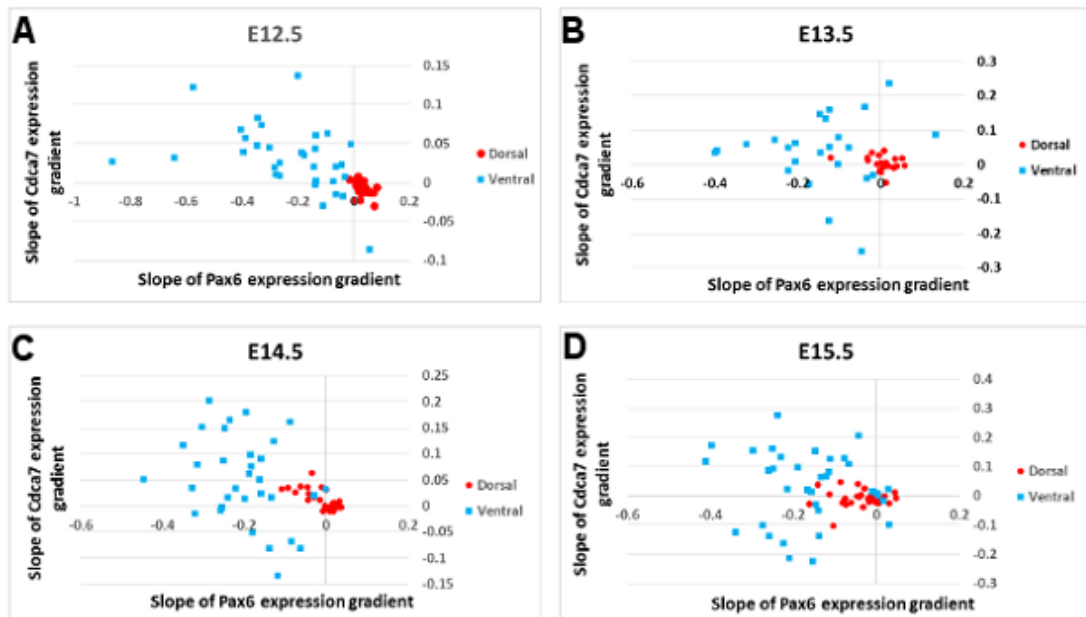


Figure 3.18 The mRNA expression gradients of *Pax6* and *Cdca7* in different ages from *WT* and *PAX77* samples

To evaluate the effect on *Cdca7* mRNA expression by the presence of PAX6/Pax6 protein, data were only collected from *WT* and *PAX77* samples from E12.5-E15.5, and plotted into panel A-D according to the stages. Data from dorsal and ventral regions were indicated by red and blue colours, respectively. Slope values of *Pax6* mRNA (X-axis) in the dorsal region were mainly positive at E12.5 and spreaded wider toward negative through time. Slope values of *Pax6* mRNA in the ventral region scattered the widest range at E12.5 and become more limited at later stages. *Cdca7* slope values (X-axis) in the dorsal region were mainly negative at E12.5 and scattered wider across zero point at later ages. *Cdca7* slope values (X-axis) in the ventral region also showed a more constrained location at E12.5 and distributed broader at later ages.

3.2.6 Cluster analysis

In order to further understand the effects of PAX6/Pax6 proteins on the expression of *Cdca7* mRNA, I performed a two-step cluster analysis using SPSS software to separate the gradient slope data into clusters and to observe factors contributing towards each cluster. Data points from all genotypes, anatomical positions and developmental stages were gathered together and both *Pax6* and *Cdca7* expression slopes were used as continuous variables. The analysis was set up to automatically divide all points into clusters (up to 15) (Figure 3.19A). The result shows that the gradient slopes can be separated into two groups according mainly to their sourcing positions (either dorsal or ventral), and the *Pax6* and *Cdca7* slope values between the two groups are significantly different (analysis of variance or ANOVA, $P < 0.001$). Figure 3.19B and 3.19C illustrate the compositions of each group. In Group 1 (Figure 3.19B), 82% of this group consist of dorsal data and the rest of them are contributed by ventral data obtained from *PAX77* and *Pax6^{Sey/Sey}* samples. The composition of Group 2 (Figure 3.19C) is even more uniform, almost 97% of this group consist of data obtained from the ventral region and only 2.9 % of the group derive from dorsal data from *Pax6^{Sey/Sey}*.

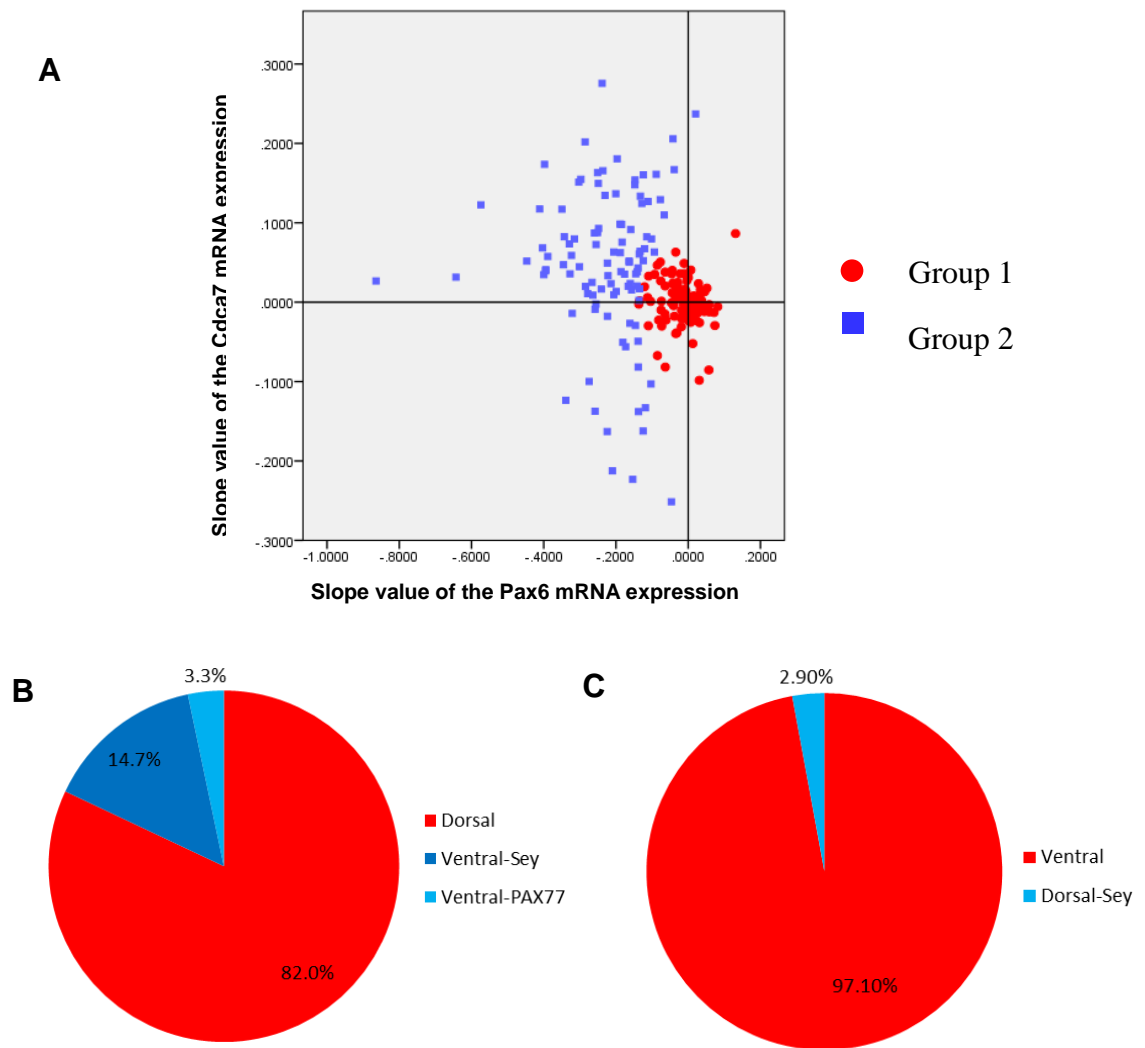


Figure 3.19 The comparison of mRNA expression slopes across time from WT, *Pax6*^{Sey/Sey} and PAX77 samples.

(A) Scatter plot showing all collected data and the X-axis and Y-axis represent the slope values of the mRNA expression gradients of *Pax6* and *Cdca7*, respectively. Two step cluster analysis by SPSS was set up to automatically divide all points into groups (up to 15). All data were clustered into two groups which mainly reflect their anatomical positions. The slope values of *Pax6* and *Cdca7* gradients between the two groups are significantly different (ANOVA, $P < 0.001$). (B) Pie chart indicating the composition of Group 1. 82% of data in this group are of dorsal origin, and the remaining derives from ventral areas from *Pax6*^{Sey/Sey} and PAX77 samples. (C) Pie chart indicating the composition of the Group 2. The majority (97%) of data in this group derive from the ventral data and 2.9 % are from the dorsal area of *Pax6*^{Sey/Sey}.

The analysis indicates that anatomical regions have a predominant influence on the cluster segregation. To discover other factors contributing to the expression pattern, all collected data were further divided into dorsal and ventral groups and were analysed separately. Figure 3.20 shows the analysis for the dorsal data using the same clustering parameters as the previous analysis. These data were clustered into two groups and the slope values of *Pax6* and *Cdca7* between the two groups are significantly different (ANOVA, $P < 0.001$). Data obtained from *WT* and *PAX77* make up 83% of Group 1, while 87.9% of Group 2 data are obtained from *Pax6^{Sey/Sey}*, indicating the clustering is mainly influenced by the presence of Pax6/PAX6 proteins (Figure 3.20B-C).

Figure 3.21A illustrates clustering result using data from the ventral region which is similar to the clustering using dorsal data, however the influence by the genotype is not as obvious. 50% of the data in Group 1 are contributed by the *Pax6^{Sey/Sey}* mutant (Figure 3.21B), while Group 2 (Figure 3.21C) are made up primarily by data obtained from *WT* and *PAX77* samples.

In summary, clustering analyses reveal that the predominant factor affecting the relative expression patterns of *Pax6* and *Cdca7* is the anatomical region in telencephalon, whereas within a specific anatomical region the most influential factor for this relative pattern is the presence or absence of PAX6/Pax6 protein.

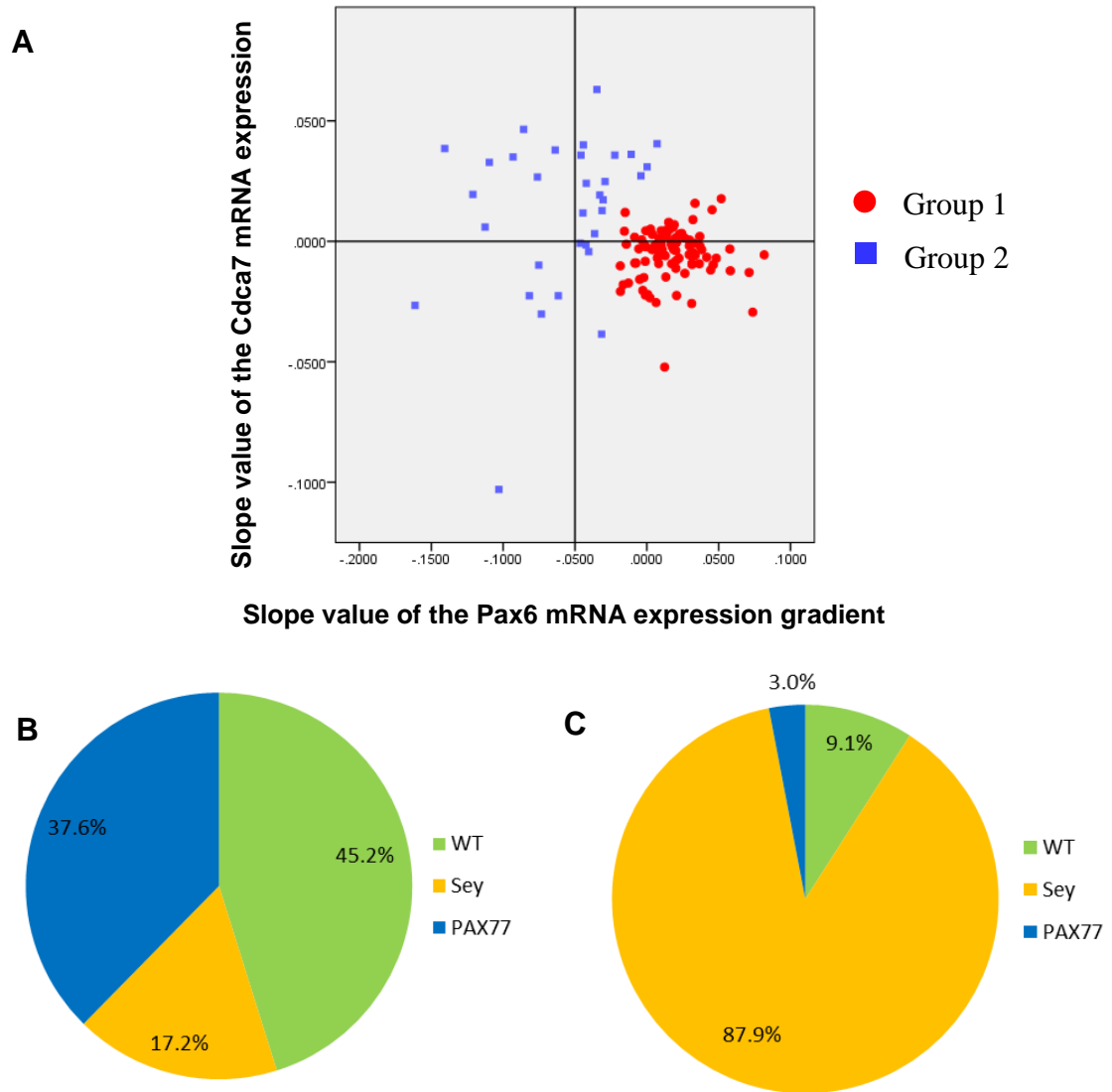


Figure 3.20 The comparison of mRNA expression slope across time from *wild-type*, *Pax6^{Sey/Sey}* and *PAX77* samples in the dorsal area.

(A) Scatter plot showing all collected data from the dorsal area. The X-axis and Y-axis represent the slope values of the mRNA expression gradients of *Pax6* and *Cdca7*, respectively. The software automatically divided the data into two groups, mainly depending on the presence of PAX6/Pax6 protein and the slope values of *Pax6* and *Cdca7* between the two groups are significantly different (ANOVA, $P < 0.001$). (B) Almost 83% of data in Group 1 are of *WT* and *PAX77* origin, the remaining 17.2% are contributed by *Pax6^{Sey/Sey}* samples. (C) The majority (88%) of Group 2 data are of *Pax6^{Sey/Sey}* origin.

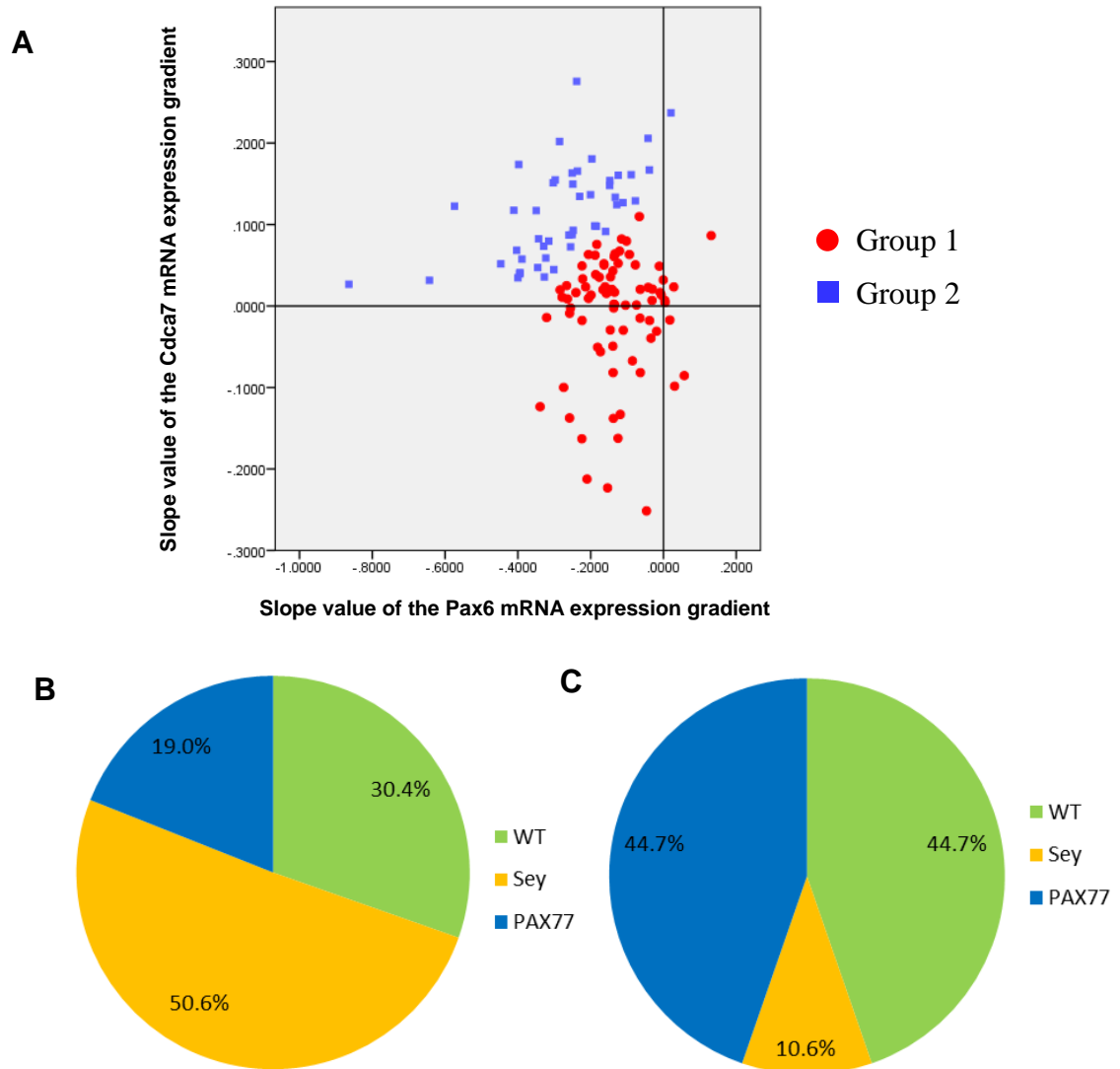


Figure 3.21 The comparison of mRNA expression slopes across time from *wild-type*, *Pax6*^{Sey/Sey} and *PAX77* samples in the ventral area

(A) Scatter plot showing all data obtained from the ventral area. The X-axis and Y-axis represent the slope values of the mRNA expression gradients of *Pax6* and *Cdca7*, respectively. The two clusters were separated largely by the presence of PAX6/Pax6 protein and the slope values of *Pax6* and *Cdca7* between two groups are significantly different (ANOVA, $P < 0.001$). (B) Pie chart showing the composition of Group 1, in which approximately 50% of the data are contributed by WT and *PAX77* samples and the rest by *Pax6*^{Sey/Sey}. (C) Pie chart showing the composition of Group 2, in which almost 90% of the data originate from WT and *PAX77* samples, proving that the presence of PAX6/Pax6 is the main determinant for the clustering.

3.2.7 The relative gene expression of *Pax6* and *Cdca7*

It is difficult to compare absolute mRNA level between samples using colorimetric ISH. To make comparisons, I performed ISH on anatomically matched sections of E14.5 embryos of all three genotypes placed on the same slide, to minimise staining variations between sections and experiment batches (Figure 3.22). The result shows that the expression level of *Cdca7* mRNA is similar in *WT* and *PAX77*, especially in the medial and rostral sections. The high-medial to low-lateral gradients can also be seen in these two genotypes. In agreement with the previous RT-qPCR-based experiment, in *Pax6^{Sev/Sev}* mutants, *Cdca7* mRNA expression is enhanced compared to the corresponding sections of *WT* and *PAX77*, and the gradient pattern is either lost or in some batches, opposite to those in *WT* and *PAX77*. These results further support that Pax6 protein negatively regulates the expression of *Cdca7* mRNA, and this repression requires functional Pax6 protein.

Finally I investigated whether the graded expression of *Pax6* and *Cdca7* is also observed at the protein level. Here I applied double immunofluorescence staining on *WT* tissue at E12.5 to visualise the protein expression of these two genes (Figure 3.23). The staining shows that Pax6 protein is indeed expressed in a medial-low to lateral-high gradient in the cortex, in agreement with the pattern of the mRNA expression. Likewise, *Cdca7* protein is expressed in a gradient opposite to Pax6 (Figure 23A-C). Higher magnification pictures reveal more details around lateral telencephalon and the PSPB region (Figure 23A'-C'). Around this region, the expression of Pax6 protein is very strong while *Cdca7* level is very low. Moving towards LGE, Pax6 protein expression suddenly reduces while *Cdca7* increases, especially in the SVZ. Together the negative correlation between the expression of Pax6 and *Cdca7* can be seen at both the transcript and the protein levels.

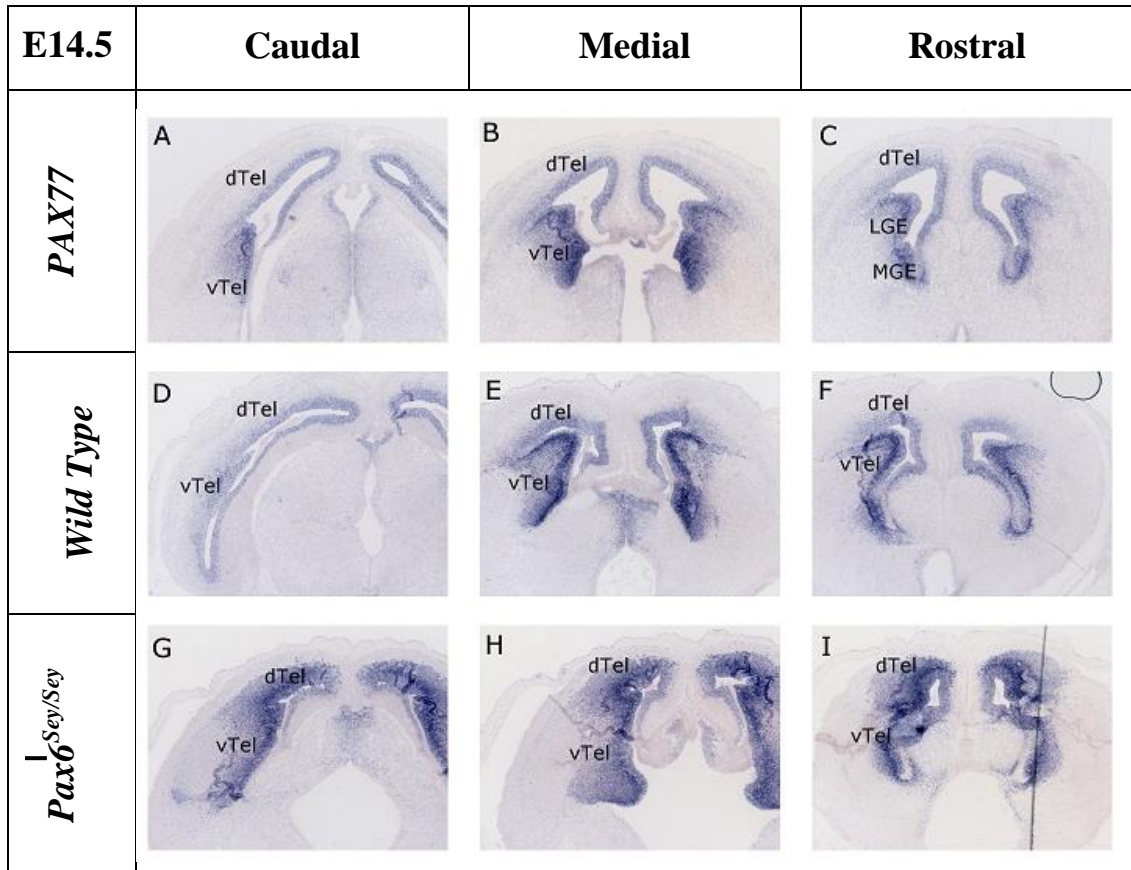
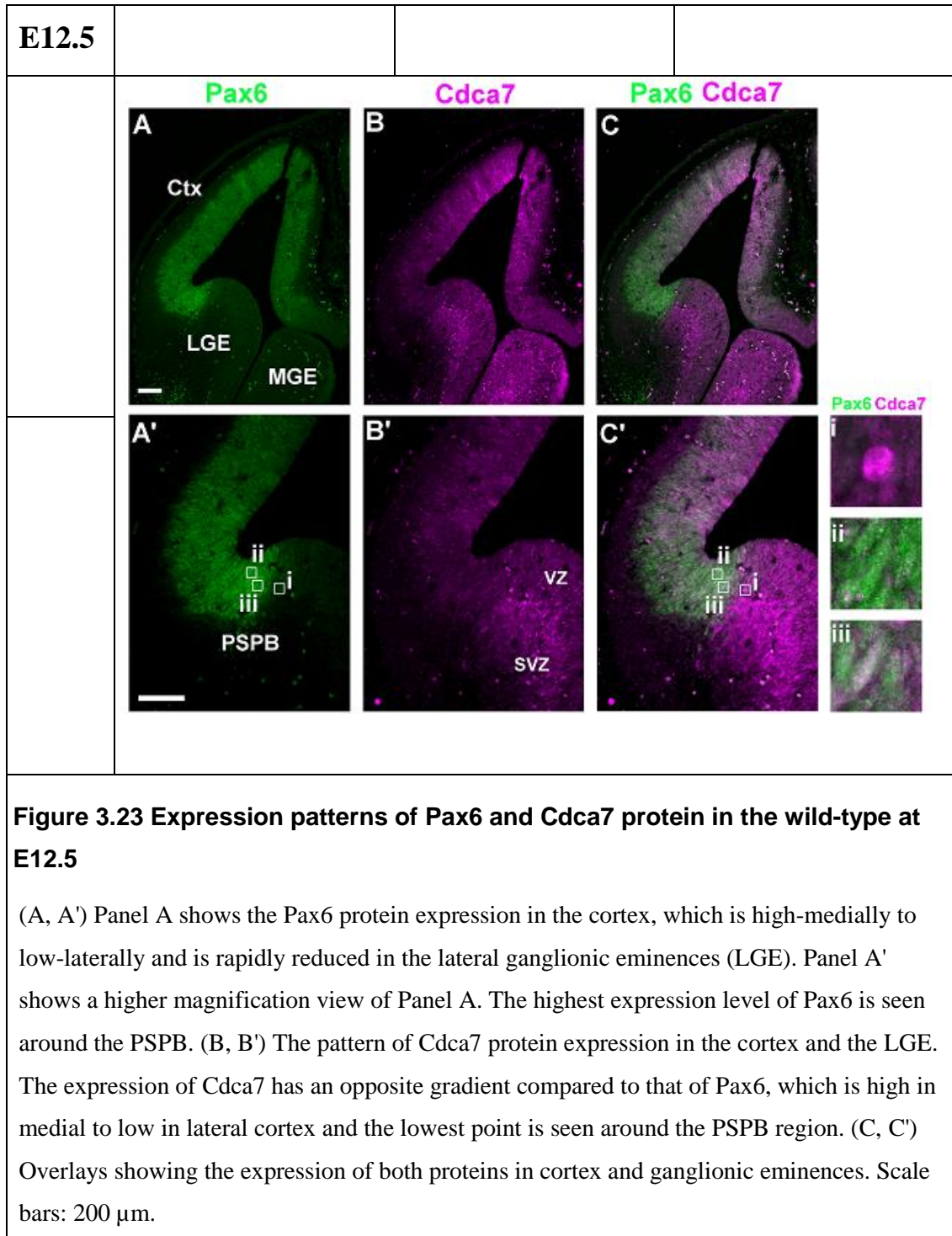


Figure 3.22 The comparison of *Cdca7* mRNA expression from *PAX77*, *wild-type* and *Pax6^{Sey/Sey}*

Sections with similar anatomical position from three genotypes were arrayed and stained on the same slides and at the same time in order to compare the relative expression level of *Cdca7* mRNA between the genotypes. (A, D, G) *Cdca7* mRNA expression at the caudal position in the three genotypes, with the highest level in the *Pax6^{Sey/Sey}* group. A high-medial to low-lateral gradient in the dTel is visible in both *PAX77* and *WT* images. (B, E, H) *Cdca7* mRNA expression at the medial position, with the highest level in the *Pax6^{Sey/Sey}* group and no obvious difference between *PAX77* and *WT*. (C, F, I) *Cdca7* mRNA expression at the rostral position. The patterns are very similar to those at the medial position. The expression level is high in the SVZ in the vTel in all three genotypes. Scale bar: 200 μ m.



3.3 Discussion

3.3.1 The spatial and temporal expression dynamics of *Pax6* and *Cdca7*

During forebrain development, combinatorial effects of various morphogens and transcription factors are required to precisely define the sub-regions along the dorso-ventral and the antero-posterior axis. Pax6 is one of the transcription factors showing differential expression both spatially and temporally in this region. The gene is expressed in a rostro-lateral^{high} to caudo-medial^{low} gradient in the dTel during early neurogenesis around E12.5 to E13.5 in rodent. This gradient is lost at later stages of neurogenesis (Bishop et al., 2000; Georgala et al., 2011; Sansom and Livesey, 2009; Walther and Gruss, 1991). The expression gradient of *Pax6* and *Cdca7* in the pallium and the dorsal-most part of subpallium are complementary to each other during early neurogenesis in *WT* and *PAX77* embryos. At E15.5, the expression gradients of the two genes become milder in the neocortex but the gradient of *Cdca7* in the subcortex is maintained. This may indicate that the expression of *Cdca7* is influenced by other factors in the subcortical area, where the influence of Pax6 becomes weaker. In *Pax6^{Sey/Sey}*, a clear difference in the direction of Pax6 expression gradient in the dTel can be seen. This is accompanied by a loss of *Cdca7* gradient at E12.5, and an opposite pattern of *Cdca7* gradient at E14.5 compared to *WT* and *PAX77*, suggesting the regional specificity of *Cdca7* expression requires functional Pax6 protein. Generally the complementary patterns of the two genes in the vTel are not as clear as those in the dTel, suggesting that *Cdca7* is regulated by other factors in the vTel.

3.3.2 The expression territory of the *Cdca7* mRNA throughout the developmental stages

In *WT* and *PAX77* tissues, *Cdca7* mRNA is expressed in the VZ of the telencephalon at E12.5. As neurogenesis proceeds from E13.5 to E15.5, the expression pattern spreads out to cover the SVZ and is highly enriched in the SVZ of the vTel. In *Pax6^{Sey/Sey}*, in addition to the vTel, *Cdca7* expression is also enhanced in the lateral and the most ventral part of dTel from E12.5 to E15.5, indicating a possible disruption of regional identity.

The regulatory role of Pax6 on Cell Division Cycle Associated 7 and cortical progenitor cell proliferation. It is known that in *Pax6^{Sey/Sey}* embryos, the boundary between pallium and subpallium is disrupted (Carney et al., 2009). In addition, dorsalisation of sub-pallial markers is also observed (Kroll and O'Leary, 2005; Stoykova et al., 2000; Toresson et al., 2000). Therefore it is worth finding out unknown factors which may influence the expression of *Cdca7* in the vTel as well as the change of expression territory of *Cdca7* in *Pax6^{Sey/Sey}* mutants.

The homeobox transcription factor *Vax1* is expressed in the subpallium, where its expression pattern is similar to *Gsx* and *Dlx*, (Anderson et al., 1999) and also in the anterior entopeduncular, preoptic area, hypothalamus and the septum (Tagliatela et al., 2004). The expression pattern of *Vax1* is also very similar to that of *Cdca7* in the subpallium. It is known that loss of *Vax1* results in decreased tangential migration of GABAergic interneurons into the neocortical VZ and also differentiation defects in LGE and MGE, while having no effect on the pallium-subpallium border and the expression pattern of the pallium marker *Pax6* (Tagliatela et al., 2004). *Cdca7* is a putative downstream target of *Mash1* (*Ascl1*) (Castro et al., 2011) and *Mash1* is known to modulate Notch signalling and is essential for proliferation of progenitors in the subcortical telencephalon (Yun et al., 2002). Although there is no clear relationship between *Vax1* and *Mash1*, *Cdca7* may be their downstream co-mediator which modulates their physiological functions in the ganglionic eminences.

In *Pax6^{Sey/Sey}* mutant mice, the ventral-most part of the dTel is largely ventralised, with ectopic expression of vTel markers and the presence of GABAergic interneurons, possibly due to dorsal cells acquiring ventral identity (Georgala et al., 2011; Kroll and O'Leary, 2005). In my ISH results, the mutant is also characterised by an enhancement of *Cdca7* expression in the SVZ in the lateral telencephalon from E13.5, while in *WT* such enhancement is not observed. Whether the dysregulation of *Cdca7* is causative of the regional misspecification in the mutant is still unknown.

3.3.3 More accurate methods needed to assess the relationship of Pax6 and Cdca7

Previous studies have used ISH to visualise the pattern of gene expression. The visualisation relies on signals produced by oligonucleotides or antisense RNA probes labelled with radioactive substances such as ³²P, or non-radioactive molecules such

The regulatory role of Pax6 on Cell Division Cycle Associated 7 and cortical progenitor cell proliferation as biotin. Both radioactive and colorimetric ISH can only provide a semi-quantitative readout of RNA expression levels (Ip et al. 2011; Sariñana et al. 2014). Limitations imposed by the detection method, such as autoradiography and photography, often result in a restricted linear range of signal detection, in which the signal intensity proportionally reflects the amount of gene expression. The readout is also relative and cannot provide absolute quantitation of the transcripts (Lazic, 2009), making comparison between experiments and/or staining batches difficult. Various steps during data processing may also introduce bias such as background correction, which eliminates pixels with intensity below a certain value and thereby making quantitation of gradients inaccurate, and the non-linear conversion between greyscale values and optical density (OD). In my ISH experiments, since my goal is to measure changes in the gradient of gene expression in the telencephalon, I did not set the background cut-off and have converted all pixels to grayscale, which are 8-bit values ranging from 0-255, with 0 being the least expressed and 255 being the most. I used a scatter plot which includes all pixel readings from the starting point in the medial dTel to the end point in the vTel, plotted against the distance from the starting point, and then I used the slope of the fitted linear regression line as the readout for the gradient of gene expression in the examined regions. Data generated with this method can be compared between samples and batches, however this does not give absolute quantitation of gene expression.

There are other methods which can be used to measure the levels of transcripts more accurately such as fluorescent ISH or quantitative RT-PCR. The latter is commonly applied as it reflects the actual amount of transcripts. In a previous study, my colleague has shown by quantitative RT-PCR that *Cdca7* mRNA expression increases in *Pax6*^{-/-} embryos at E12.5 and in *Pax6* conditional mutant cortex three days after Pax6 elimination (Mi et al., 2013). However quantitative RT-PCR requires precise regional tissue dissection and cannot visualise the overall pattern of gene expression, therefore I decided to use colorimetric ISH to study the interactive dynamics of Pax6 and *Cdca7* patterns by comparing between genotypes with differential Pax6 expression across developmental stages. My results have indeed shown that functional Pax6 protein reduces of level of *Cdca7* transcripts, this suppression may not be direct and varies between anatomical regions and

The regulatory role of Pax6 on Cell Division Cycle Associated 7 and cortical progenitor cell proliferation developmental stages, suggesting a more complex molecular network may involve in *Cdca7* regulation.

3.3.4 Effects of overexpression of human PAX6 on the expression of *Cdca7*

PAX77⁺ (*PAX77*) mouse carries 5-7 copies of Yeast Artificial Chromosome 593 (Y593), which contains 420kb of human genomic *PAX6* region, covering the *PAX6* gene and 200 kb flanking sequence on each side (Schedl et al., 1996). Overexpression of human PAX6 protein has been demonstrated to cause defects in eye development (Manuel et al., 2007; Schedl et al., 1996). In the cortex, PAX6 overexpression causes proliferation defects in radial glia cells in the rostral and central cortex but not in the caudal cortex and has little effect on cortical arealisation. Endogenous PAX6/Pax6 expression in *PAX77* is elevated by two-fold compared to that in *wild-type*, indicating a negative autoregulation in protein expression (Manuel et al., 2007). This autoregulation may be important for maintaining a stable level of protein in the environment. Autoregulation is also seen at the mRNA level, where *Pax6* mRNA is upregulated in the *Pax6*^{Sey/Sey} mutant and downregulated in *PAX77* mice (Manuel et al., 2007; Muzio et al., 2002). Although quantitation of *Pax6* transcript level cannot be reliably achieved with colorimetric *in situ* hybridization in my experiment, the opposing expression patterns between *Pax6* and *Cdca7* suggest a possible role of Pax6 in negatively regulating *Cdca7* transcription. This opposing pattern was consistent between *wild-type* and *PAX77* mice, suggesting this negative regulation was not affected by PAX6 overexpression. Figure 3.22 provides a semi-quantitative readout of *Cdca7* transcript level in wild-type, *Pax6*^{Sey/Sey} and *PAX77*. The relatively high abundance of *Cdca7* was apparent in *Pax6*^{Sey/Sey}, further supporting the function of Pax6 as a negative regulator of *Cdca7* expression. The difference in *Cdca7* transcript level between *wild-type* and *PAX77* was very little and may require fluorescent *in situ* hybridization and qRT-PCR for more valid results. In the next chapter, I have further investigated whether *Cdca7* is a direct target of Pax6 by identifying potential Pax6 binding motifs in the *Cdca7* genomic locus followed by validation of potential binding sites by chromatin immunoprecipitation.

The regulatory role of Pax6 on Cell Division Cycle Associated 7 and cortical progenitor cell proliferation
In addition, the effect of Pax6 on *Cdca7* expression has also been examined by the promoter assay.

Chapter 4 : Identification of Pax6 binding sites in the *Cdca7* locus

4.1 Introduction

4.1.1 Importance of regulation through direct binding and binding site prediction

Complex biological processes during development and organogenesis require tight regulation of signalling molecules and transcription factors, both temporally and spatially. Through direct binding to their target genomic locus, transcription factors can effectively control target protein expressions as well as the related physiological processes. Traditionally it is hard and time-consuming to identify factors that bind to chromosomes or to locate the exact position where those proteins interact with chromosomes (Bulyk, 2003). In recent years with advances in sequencing technologies and increasing availability of database platforms, scientists can predict potential binding sites by computational or *in silico* analysis to narrow down the target range (Qiu, 2003).

PAX6/Pax6 is one of the key regulators during development of tissues such as eyes, forebrain, and pancreas (Grindley et al., 1995; St-Onge et al., 1997; Walther and Gruss, 1991). It is important to understand the mechanisms behind how Pax6 regulates those developmental processes. As a transcription factor, Pax6 can directly bind to its genomic target sequences and then recruit either activators or inhibitors to affect target gene expressions (Walcher et al., 2013). There are two DNA binding domains, a paired domain (PD) and a homeodomain (HD), in the Pax6 protein. The PD can be divided into PAI and RED subdomains and each subdomain forms a helix-turn-helix structure which recognises different DNA sequences and binds to DNA individually or cooperatively between the two subdomains and the HD (Czerny et al., 1993; Jun and Desplan, 1996).

A previous study had looked into Pax6 binding sites and collectively identified an “optimal sequence”, or P6CON motif, for Pax6 PD recognition (Epstein et al., 1994). In the literature, several consensus sequences, including the P6CON motif, have been proposed to possess high Pax6-binding affinity. It has also been found that in those putative binding motifs, DNA sequences are often highly degenerate (Dermizakis

The regulatory role of Pax6 on Cell Division Cycle Associated 7 and cortical progenitor cell proliferation and Clark, 2002; Zhang, 2006). Therefore in order to identify motif sequence patterns in a precise manner, the position weight matrix (PWM) was introduced to provide a predictive model. The PWM for a particular binding motif is generated by aligning several DNA sequences known to be bound by a particular protein or a transcription factor and by calculating the likelihood of each nucleotide being located at a specific position within that particular binding motif. Results are presented as scores for each nucleotide at each DNA position. Higher scores indicate that the particular nucleotide is more likely to occur at the specific position within the motif. Using PWMs, algorithms can be generated for any transcription factors of interest to screen for novel binding regions at a genome-wide scale (Stormo, 2000). A number of previous studies have taken a genome-wide approach to find undiscovered Pax6 direct targets in human, mouse and zebrafish (Coutinho et al., 2011; Sansom et al., 2009; Xie et al., 2013)

4.1.2 How may Pax6 affect Cdca7 expression?

In previous studies, *Cdca7* was shown to be upregulated in *Pax6*^{Sey/Sey} E12.5 cortex by microarray and quantitative RT-PCR analyses (Mi et al., 2013). This implies that Pax6 may negatively regulate the expression of *Cdca7* RNA. Since *CDCA7* is a known direct target of E2F1 and is positively regulated by E2F1 (Goto et al., 2006), one possible mechanism by which Pax6 regulates the expression of *Cdca7* is through the inhibition of Cdk6 expression, which further reduces the phosphorylation of pRb protein. It has been demonstrated that the phosphorylation of pRb is increased in *Pax6*^{Sey/Sey} E12.5 cortex, which promotes the dissociation of the pRb/E2f complex (Mi et al., 2013). Hypophosphorylated pRb interacts with E2f1 and constrains the factor in the cytoplasm. Upon pRb phosphorylation, dissociated E2f factors can enter into the nucleus and upregulate its downstream targets, including *Cdca7*, thereby accelerating cell cycle transition from G1 to S phase (Bartek and Lukas, 2001).

To find out whether there is direct interaction of Pax6 with *Cdca7* genomic regions and the regulating role of Pax6 on *Cdca7* expression, in this chapter I adopted the computational approach to screen for putative Pax6 binding sites in the *Cdca7* locus. *Cdca7* genomic fragments containing putative Pax6 binding sites were used as enhancer regions for luciferase expression assays to test if Pax6 affects *Cdca7*

The regulatory role of Pax6 on Cell Division Cycle Associated 7 and cortical progenitor cell proliferation expression. Since it has previously proved that the expression of *Cdca7* is downregulated at E12.5 in *Pax6*-null mutant (Mi et al., 2013), the putative binding sites were verified by chromatin immunoprecipitation (ChIP) to reveal actual interaction between Pax6 and *Cdca7* genomic loci in E12.5 forebrain tissue.

4.2 Results

4.2.1 Identification of putative Pax6 binding sites in the regulatory elements of *Cdca7*

Cdca7 is located on Chromosome 2q31.1 in human and Chromosome 2 in mouse. The genomic region spans approximately 10,000 bp on the forward strand of Chromosome 2. The mouse gene homolog contains 9 exons and encodes a protein consisting of 392 amino acids with a predicted size of 43 kDa (Figure 4.1). *Cdca7* produces five different splicing variants, *Cdca7_001-005*; only two of which, *Cdca7_001* and *Cdca7_005*, encode proteins. The *Cdca7_005* transcript encodes a much shorter protein with 192 amino acids and only contains exons 1-5 and with no known function (Ensembl).

In order to understand whether Pax6 has direct regulatory effects on *Cdca7* gene expression, the first approach I used was to identify potential Pax6 binding sites in the *Cdca7* genomic region. Here I collaborated with Dr Ian Simpson at The University of Edinburgh. He generated a customised track which used three different Pax6 binding motifs, Pax6CON (Epstein et al., 1994), M00979 (Transfac) (Duncan et al., 1998; Zhou et al., 2000) and PC0010 (Coutinho et al., 2011) (Figure 4.2), to look for putative binding sites in the *Cdca7* genomic locus and the 5 kb region surrounding it. These motifs were represented in the form of PWMs which were created by mathematical scoring of optimal Pax6 binding patterns. I also used Transfac, which utilises a well-established transcription factor PWM database, to collectively predict putative sites. In the Transfac programme, the match and matrix score was set at 0.8 to reduce false positive hits. The output from the two algorithms (the customise track and Transfac database) showed there were 8, 12 and 10 hits in the region upstream, within and downstream of the *Cdca7* gene, respectively. After excluding hits with lower scores of possibility of matrix similarity, I settled on six

The regulatory role of Pax6 on Cell Division Cycle Associated 7 and cortical progenitor cell proliferation putative sites located in the 5 kb region upstream of the transcriptional start site (TSS) of *Cdca7* as targets for further studies. The sequences of the six putative sites are listed in Table 4.1.

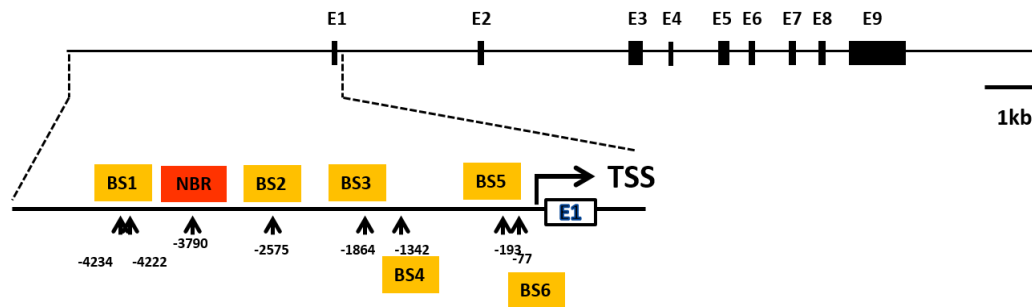


Figure 4.1 *Cdca7* genomic region and computationally predicted Pax6 binding sites relative to its TSS.

Cdca7 is located on Chromosome 2 (Ensembl, ENSMUSG00000055612) in mouse. It contains 9 exons and encodes a protein of 392 amino acids with predicted molecular weight of 43 kDa in mouse. The highlighted region presented 6 putative Pax6 binding sites (BS1-6) predicted by computational analysis and a NBR was defined as non-binding control region (NBR). The number underneath each putative binding site and the NBR represents its genomic position relative to the *Cdca7* transcriptional start site (TSS). The motifs used for prediction are shown in figure 4.2.

Table 4.1 The sequences were predicted by multiple Pax6 binding motifs within *Cdca7* genomic region

Predicted BS	Recognised by	Predicted binding site sequences
BS1	M00979	CCTGTACTGGAGCTG
BS2	P6CON	CTGCTTTCTGTTTGATTTCC
BS3	M00979	CTGTTCTGGAACCA
BS4	PC0010	GTTCCAAGAAGAGTAAA
BS5	M00979	CCAGAGCTGGGACGC
BS6	M00979	CTGTCCCGGAGCTC

The six potential Pax6 binding sites in the *Cdca7* genomic locus 5 kb upstream to the *Cdca7* transcriptional start site (TSS).

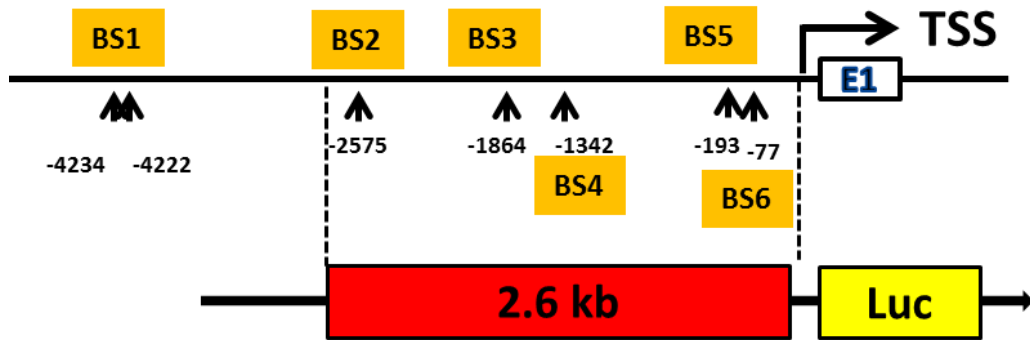
4.2.2 Functional characterisation of Pax6 binding regions in the regulatory element of *Cdca7*

Luciferase assays were performed to understand the biological consequences upon Pax6 binding onto its putative targets in the genome. Using PCR with a BAC clone (RP23-121B8) template, I amplified a genomic region spanning 2.6 kb upstream of the *Cdca7* TSS site, which contains putative binding sites 2-6 (BS2-BS6). The 2.6 kb genomic region was cloned into a pGEM-T-easy plasmid and then subcloned into firefly luciferase expression plasmid pGL4.10. The final plasmid is named “pGL4.10_2.6 kb up *Cdca7*”. A schematic view of this region and the final plasmid map are shown in figure 4.3A-B. The pGL4.10 plasmid does not contain a promoter region upstream of the firefly luciferase coding region, therefore the enzyme production requires an insertion of an upstream sequence which can act as a transcription enhancer. A SV40 late poly(A) sequence was placed downstream of the luciferase reporter gene to increase the stability of the transcribed RNA and thereby increasing the translation of the reporter (Proudfoot, 1991). A synthetic poly(A) signal/transcriptional pause site was inserted immediately before the 2.6 kb genomic region to provide a termination signal to any spurious luciferase transcription and thereby reducing background signals (Enriquez-Harris et al., 1991; Levitt et al., 1989). For luciferase experiments, this plasmid construct, together with the Renilla luciferase expression vector pRL-SV40 and different doses of Pax6 expression construct were transiently transfected into HEK293 cells. 48 hours after transfection, cells were harvested and total lysates were extracted. The luciferase activities in the lysates were quantitated using the Promega Glomax Luminometer. The luciferase readouts of Renilla luciferase served as an internal control for transfection efficiency in each sample. Normally, for consistency between data, the firefly luciferase activity in cells transfected with empty pGL4.10 plasmid is used as a baseline to which the genomic region-containing experimental group is normalised. However in this experiment the activity readings in these control cells were 1-2% of those in the experimental group. As a consequence minute variations in the absolute readings within the control group would cause significant variations in the experimental group after normalisation. Therefore all samples were instead normalised to the activity in

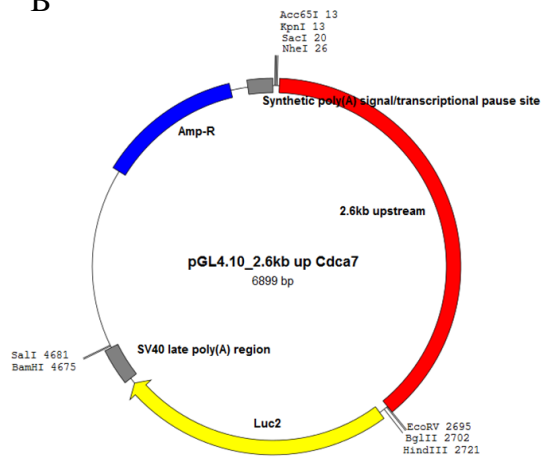
The regulatory role of Pax6 on Cell Division Cycle Associated 7 and cortical progenitor cell proliferation cells transfected with the “pGL4.10_2.6 kb up Cdca7” plasmid in the absence of the Pax6 expression construct.

Based on the RNA expression pattern visualised by *in situ* hybridisation in the previous chapter, Pax6 may act as a negative regulator of *Cdca7* transcription. Figure 4.3C shows Pax6 protein at low levels negatively regulates the promoter activity of *Cdca7*, with a reduction of approximately 10% in samples transfected with 200ng of the Pax6 expression vector compared to the no-Pax6 group however this is not statistically significant. This inhibition is absent in the group with the highest dose of Pax6, which instead enhances the promoter activity by 10% as shown in cells transfected with 500ng of the Pax6 vector, compared to the no-Pax6 control. Cells transfected with the highest dose of the Pax6 expression construct produced significantly higher *Cdca7* promoter activity compared to cells receiving other doses apart from the no-Pax6 group (Tukey, $P < 0.05$, $n = 3$). Taken together, the Pax6 expression construct has a dosage-dependent effect on the luciferase expression, suggesting that Pax6 protein affects the promoter/enhancer activity of the 2.6 kb fragment (one-way ANOVA, $P = 0.003$).

A



B



C

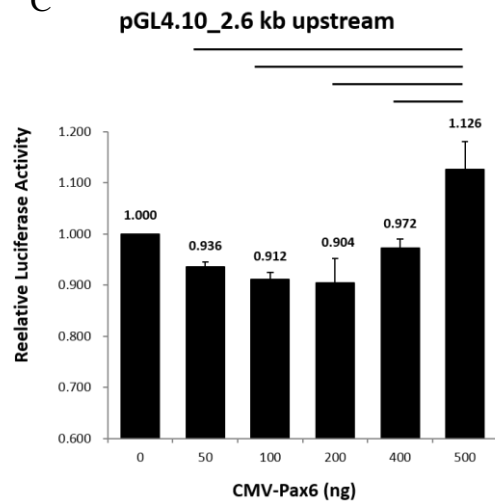


Figure 4.3 Schematic representation of the firefly luciferase construct and Pax6 mediated regulation via 2.6 kb upstream region.

Figure 4.3 Schematic representation of the firefly luciferase construct and Pax6 mediated regulation via 2.6 kb upstream region.

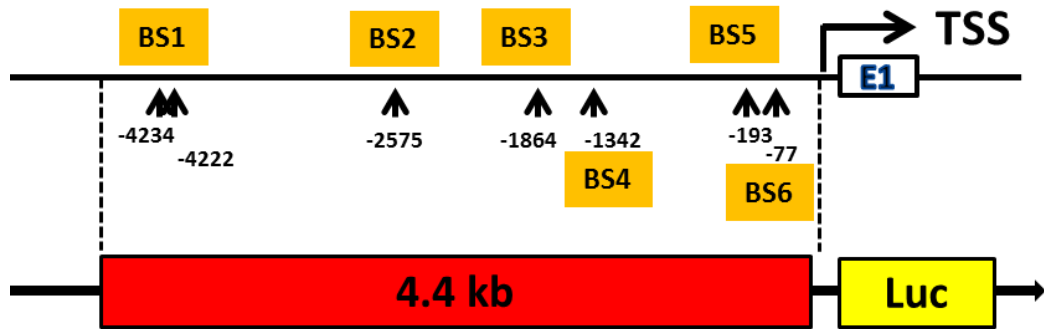
(A) 2.6 kb region upstream to the *Cdca7* TSS which contained the potential Pax6 binding sites 2-6 was inserted into a promoter-less luciferase backbone pGL4.10. (B) 2.6 kb insertion is upstream to the firefly luciferase coding sequence followed by a SV40 late poly (A) region to increase the stability of the transcribed mRNA. The final construct is almost 7 kb including an ampicillin resistance gene for selection and a synthetic poly(A) signal/transcriptional pause site before the 2.6 kb fragment to provide a termination signal to prevent background signals produced by spurious luciferase transcriptions (Enriquez-Harris et al., 1991; Levitt et al., 1989). (C) To assess the Pax6-mediated inhibition of *Cdca7* expression, firefly luciferase construct together with the transfection efficiency control Renilla luciferase vector were transiently transfected into HEK293 cells and lysates were extracted 48 hours after transfection for analysis. Bar chart showing different doses of the Pax6 expression construct, and thus the level of Pax6 protein, have differential effects on the promoter/enhancer activity of the 2.6 kb fragment (one-way ANOVA, $P=0.003$). Individual lines above the bars mark statistically significant differences between the indicated groups (Tukey, $P<0.05$, $n=3$).

A construct similar to “pGL4.10_2.6 kb up *Cdca7*” containing a larger genomic region upstream of *Cdca7* which includes all six putative Pax6 binding sites was then made. The construct is named “pGL4.10_4.4 kb up *Cdca7*”. The schematic view of this region and the plasmid map are shown in Figure 4.4A-B.

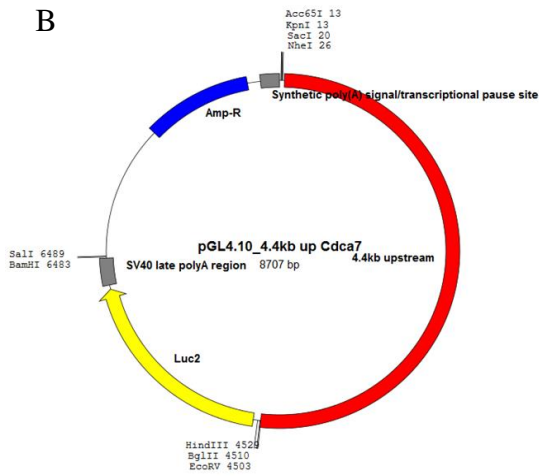
Unexpectedly, the promoter assay using the “pGL4.10_4.4 kb up *Cdca7*” construct revealed a dynamic different from the previous experiment using the 2.6 kb fragment as the enhancer element (Figure 4.4C). Instead of the opposite effects between samples with low and high level of Pax6, a steady dosage-dependent increase in the promoter activity was observed (one-way ANOVA, $P=0.012$, $n=3$). With 500ng of the Pax6 expression construct, the maximum amount in this experiment, promoter activity was enhanced by 30% compared to the no-Pax6 control (Tukey, $P<0.05$). This suggests that the effect of Pax6 protein on *Cdca7* transcription is dependent on the context of the enhancer elements.

To ensure the transfection of Pax6-expressing vector had in fact produced Pax6 protein, a western blot was performed using the same lysates extracted for the luciferase assay (Figure 4.5). The CMV promoter-driven expression of Pax6 protein was detected by a Pax6-specific antibody in cells transfected with the expression vector, in a dosage dependent manner which appeared to plateau at 400ng of the transfected plasmid. GAPDH was used as the western blot loading control. The Pax6 antibody used for this experiment recognises two isoforms, Pax6 and Pax6 (+5a) with different molecular weights 46 and 48kDa, respectively (Figure 4.5).

A



B



C

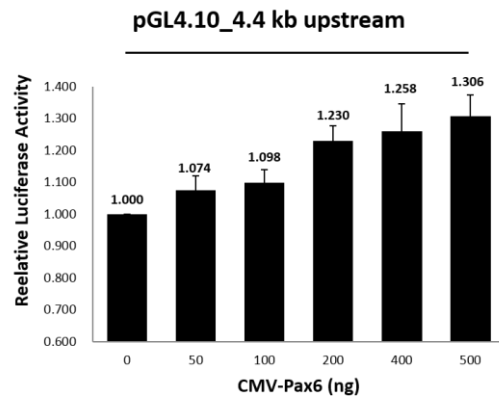


Figure 4.4 Schematic representation of the firefly luciferase construct and Pax6 mediated regulation via 4.4 kb upstream region.

Figure 4.4 Schematic representation of the firefly luciferase construct and Pax6 mediated regulation via 4.4 kb upstream region.

(A) 4.4 kb region upstream to the *Cdca7* TSS which contained all six potential Pax6 binding sites was inserted into a promoter-less firefly luciferase backbone pGL4.10. (B) 4.4 kb insertion is upstream to the firefly luciferase coding sequence followed by a SV40 late poly (A) region to increase the stability of the transcribed mRNA. The final construct is 8.7 kb in size, including an ampicillin resistance gene for selection and a synthetic poly(A) signal/transcriptional pause site before the 4.4 kb fragment to provide a termination signal for any spurious luciferase transcription (Enriquez-Harris et al., 1991; Levitt et al., 1989). (C) To assess the Pax6-mediated inhibition of *Cdca7* expression, firefly luciferase construct together with the transfection efficiency control Renilla luciferase vector were transiently transfected into HEK293 cells and lysates were extracted 48 hours after transfection for analysis. Bar chart showing the effect of different doses of the Pax6 expression construct on the promoter/enhancer activity of the 4.4 kb fragment (one-way ANOVA, $P=0.012$). With 500ng of the Pax6 expression construct, promoter activity is enhanced by 30% compared to the no-Pax6 control. The line between the 500ng and the 0ng group marks the statistically significant difference between the two groups (Tukey, $P<0.05$, $n=3$). The data showed that instead of being a transcriptional inhibitor, the presence of Pax6 leads to increased *Cdca7* promoter activity.

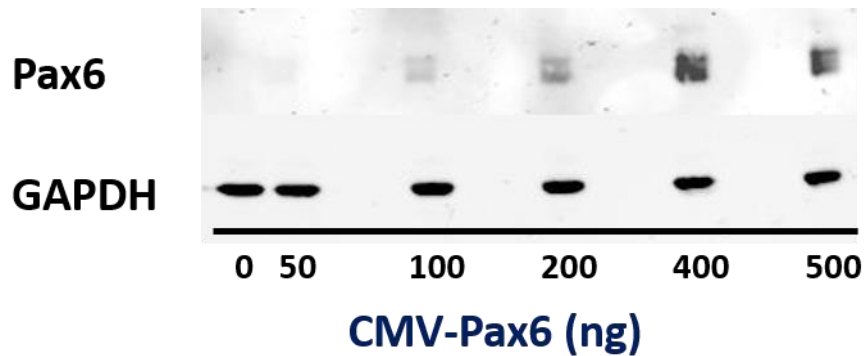


Figure 4.5 Overexpression of Pax6 protein in HEK293 cells.

HEK293 cells were transiently transfected with different doses of the CMV promoter-driven Pax6 expression vector. The resulting protein levels of Pax6 were revealed with an antibody against Pax6 by western blot, with the level of GAPDH protein as the loading control for each lysate. The transfection of the Pax6 expression construct resulted in increased cellular level of Pax6 protein in a dosage dependent manner, which appeared to plateau at 400ng of the transfected plasmid. The specific Pax6 antibody also detected two different isoforms of Pax6, Pax6+5a and Pax6-5a (Pax6) with molecular weight at 48kDa and 46kDa, respectively.

In summary, the result of the luciferase assay with the 2.6 kb fragment as the enhancer region indicates that the expression of *Cdca7* is inhibited only when Pax6 is present at a low level, while overexpressed Pax6 protein has an activation effect on *Cdca7* expression. Therefore a correct amount of Pax6 protein is important for its physiological role (Quinn et al., 2007). The discrepancy between the two *Cdca7* constructs suggests a context-dependent regulation in the *Cdca7* genomic region, as well as possible involvement of other activators such as E2f1 within the extra 1.8 kb region in the pGL4.10_4.4 kb up *Cdca7* construct which may influence *Cdca7* expression (See discussion 4.3.1 for more details).

4.2.3 Does Pax6 bind the *Cdca7* regulatory region in vivo?

In order to understand whether the regulation of *Cdca7* expression by Pax6 is dependent on the direct binding of the transcription factor to the *Cdca7* regulatory elements, ChIP was performed using an antibody against Pax6, followed by quantitative PCR (qPCR) measurement of the precipitated samples with primer pairs specific for each of the six putative Pax6 binding sites in the *Cdca7* genomic region. ChIP is a powerful tool for identifying protein-DNA interaction, which is useful for discovering specific binding regions of transcription factors. Conventional ChIP protocols normally start by crosslinking proteins with chromosomes in the cell or tissue samples using formaldehyde, followed by extraction of the crosslinked chromatin complex. The extracted chromatins are then incubated with either the antibody against the protein of interest or the IgG isotype control. Antibody-bound chromatins are then precipitated and genomic DNA is isolated from the precipitated complex. Purified genomic DNA is then used as the template for qPCR using primers detecting the regions of interest. The binding preference of a transcription factor to specific genomic sites is examined by dividing the qPCR outcomes from samples incubated with the gene-specific antibody with that from the isotype control (Kuras, 2004). In order to avoid skewing of experimental results by the low level of random background noise of the control IgG, I conducted ChIP with tissues from *Pax6*^{+/+} and *Pax6*^{Sey/Sey} E12.5 cortex and precipitated chromatin complex using only antibody against Pax6. The truncated form of Pax6 protein in *Pax6*^{Sey/Sey} mice cannot

The regulatory role of Pax6 on Cell Division Cycle Associated 7 and cortical progenitor cell proliferation be recognised by the Pax6 antibody and therefore the sample can act as a control for non-specific binding by the antibody.

Cellular extracts from the two sample groups were prepared and sonicated, which produced sheared DNA fragments ranging from 100 to 700 bp (Figure 4.6A). The sonicated samples were incubated with the Pax6 antibody, followed by precipitation and DNA purification.

Abundance of the six putative Pax6 binding regions and one putative non-bound region within the examined *Cdca7* genomic region in the precipitated samples was measured by qPCR. All data were normalised by dividing the quantity of the amplicon in *Pax6*^{+/+} samples by that in *Pax6*^{Sey/Sey} counterparts (formula A). Binding enrichment of each site was further calculated by dividing the results from formula A by that of the *Syt8* negative control (formula B), which was previously reported as a non-Pax6 binding region (Mi et al., 2013; Sansom et al., 2009). Primers for *Pou3f4* (Ninkovic et al., 2013) fragments were used as a positive binding control for Pax6.

$$\frac{\text{qPCR output for each primer from } Pax6^{+/+} \text{ samples}}{\text{qPCR output for each primer from } Pax6^{-/-} \text{ samples}} = X \text{ ----- (Formula A)}$$

$$\frac{X \text{ for each primer set}}{X \text{ for } Syt8 \text{ negative control}} = \text{fold enrichment ----- (Formula B)}$$

Results in Figure 4.6B show no significant enrichment of Pax6 binding to any examined sites, including the positive control, in relation to the negative control. All predicted binding sites and the putative non-bound region possess similar binding affinity to Pax6 protein compared the *Syt8* control. The enrichment is also absent in the *Pou3f4* positive control. This may indicate that there is no actual binding of Pax6 on the *Cdca7* genomic region but the reason behind the lack of enrichment in the positive control is unknown. Possible reasons will be discussed later in the 4.3.2

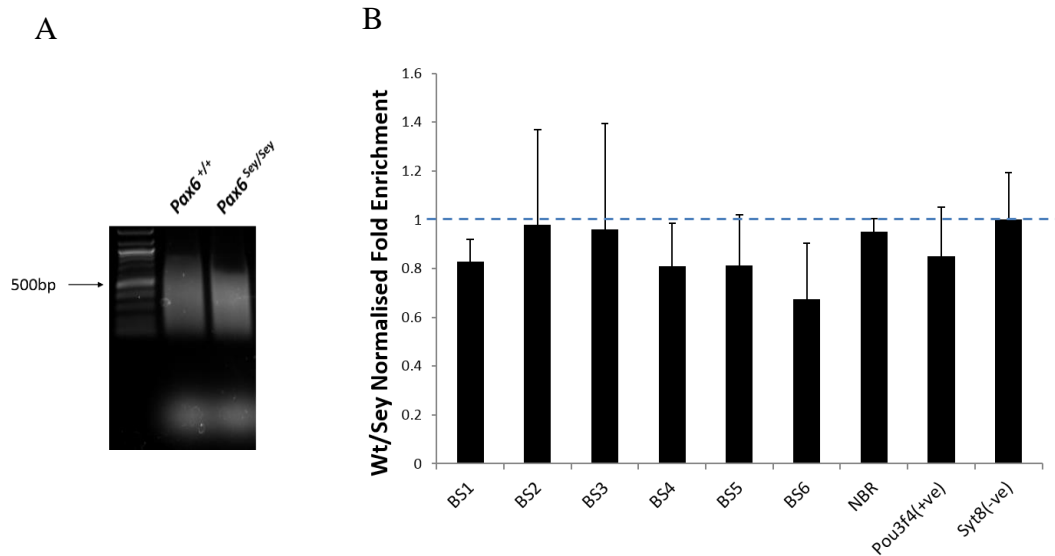


Figure 4.6 Validation of direct *in vivo* Pax6 binding to the *Cdca7* upstream regulatory elements by quantitative chromatin precipitation (qChIP).

Positions of the six putative Pax6 binding sites (BS1-6) and one chosen non-binding control region (NBR) were shown in figure 4.1. (A) Samples used in ChIP experiments were extracted from either *Pax6*^{+/+} or *Pax6*^{Sey/Sey} E12.5 cortex. Sonication of isolated chromatin resulted in sheared DNA fragments ranging from 100-700 bp. (B) The sonicated chromatin samples from *Pax6*^{+/+} or *Pax6*^{Sey/Sey} tissues (n=3) were precipitated separately with the antibody against Pax6. The precipitated DNA was purified and the abundance of BS1-6, NBR, *Pou3f4* (positive control for Pax6 binding) and *Syt8* (negative control for Pax6 binding) were measured by quantitative PCR. NBR is located 3790 bp upstream to the *Cdca7* TSS with no putative Pax6 binding site within its 450bp flanking regions. All data were normalised by dividing the average abundance in *Pax6*^{+/+} samples by that in the *Pax6*^{Sey/Sey} counterpart for each site. The enrichment of each binding site is defined as the fold-change from the *Syt8* result (Formula A and B, see text for details). The results show no apparent enrichment among all examined sites, including the positive control *Pou3f4* which is a known Pax6-binding region. The lack of enrichment suggests that technical or normalisation issues needed to be solved.

4.3 Discussion

4.3.1 The regulatory function of Pax6 on *Cdca7* expression

In the previous chapter, Pax6 was thought to negatively regulate *Cdca7* expression due to the mRNA expression patterns of the two genes as well as previous microarray and qPCR results (Mi et al., 2013). However in this chapter a more complex regulation has been revealed by the luciferase assay. Using the 2.6 kb *Cdca7* genomic fragment as the luciferase expression enhancer, Pax6 at low level causes approximately 10% reduction in *Cdca7* expression, whereas at high level the effect of Pax6 becomes activating. When the 4.4 kb genomic fragment was used, there was no reduction of luciferase expression with any dosage of Pax6. Instead, overexpression of Pax6 resulted in an enhanced output from the *Cdca7* upstream regulatory element which led to a 30% increase in *Cdca7* expression in samples with the highest dosage compared to the non-Pax6 control.

One possible mechanism by which Pax6 could inhibit *Cdca7* expression is by negatively regulating the phosphorylation of pRb through downregulating expression of the direct Pax6 target gene *Cdk6*, thereby preventing the separation of the E2f/pRb complex and downregulating expression of E2f downstream targets in the normal physiological environment (Mi et al., 2013). The luciferase assay results in this chapter correlate with such theory, with Pax6 at a low level inhibiting the promoter output of the 2.6 kb region upstream of the *Cdca7* TSS. The fact that the inhibitory effect of Pax6 was absent when a longer 4.4 kb region was used suggests this regulation is dependent on the genomic context. One possible explanation is the extra 1.8 kb region between the 2.6 kb and the 4.4 kb fragments may recruit unknown activators which mask the inhibitory effects of Pax6. This theory requires future validation by mutating the putative Pax6 binding site BS1 which is contained in this 1.8kb region, and by searching for binding sites for other transcription factors such as E2f1 and c-Myc. It should also be noted that the luciferase assay was carried out in Human Embryonic Kidney (HEK) 293 cells and the functions of Pax6 may be different in neural progenitors and in embryonic kidney cells. Although some neuronal features such as neurofilament subunits are expressed in HEK293 cells, this

The regulatory role of Pax6 on Cell Division Cycle Associated 7 and cortical progenitor cell proliferation cell line has been identified derive from the embryonic adrenal cells in a recent study (Lin et al., 2014; Shaw et al., 2002) and therefore may possess a very different set of transcription factors which may affect Pax6 functions in the cell.

It is known that *Cdca7* is a direct target of E2F1 transcription factor in HeLa cells (Goto et al., 2006). Other E2F family members E2F2 and E2F4 also bind to *CDCA7* genomic region (Goto et al., 2006). A computational prediction using JASPAR CORE 2014 database performed by Mr Zrinko Kozic has identified new putative binding sites in the region from 4.5 kb to 2.6 kb upstream to the *Cdca7* TSS (Zrinko Kozic unpublished). PWMs were obtained from JASPAR CORE 2014 database and non-redundant vertebrate matrices were selected. The 4.5 kb upstream region was scanned for putative binding sites using R language with Biostrings package and both sense and antisense sequences were aligned to the motifs in the database. Only the motif hits with alignment score equal or higher than 90% of the maximum score were chosen (Mathelier et al., 2014). From the alignment, several putative binding sites were found to locate in the region spanning 4.5 kb to 2.6 kb upstream to the *Cdca7* TSS, these include one E2f1 site, one E2f4 site, one Sox2 site and three Sox10 sites. Although the expression level and the function of E2F1 are not fully understood in HEK 293 cells, a previous study using this cell line has found an inhibitory effect of Pax6 on the *Cdk6* promoter which could consequentially reduce the activity of E2F1 (Mi et al., 2013). Given the direct role of E2F1 in *CDCA7* upregulation in HeLa cells and the possible down-regulating effect of Pax6 on E2F1 function in HEK 293 cells, whether the enhanced *Cdca7* promoter activity caused by Pax6 overexpression is mediated by E2F1 requires further validation.

Online database BioGrid which collects physical protein-protein interaction results indicates that Pax6 is physically bound to Sox2 in mouse and Sox10 in rat (Appendix 2) (Ravasi et al., 2010; Wissmüller et al., 2006). Whether Sox2 and Sox10 proteins are endogenously expressed in HEK 293 cells is currently not known, however if they are present, the overexpression of Pax6 may increase their recruitment to the *Cdca7* regulatory element and thereby influence the expression of *Cdca7*.

4.3.2 Current ChIP procedures and possible experimental errors

Chromatin immunoprecipitation is a great tool for investigating chromatin modifications and protein: DNA interactions. As described in the results section, ChIP normally uses a common cell lysate as the starting material and compares the DNA precipitated by the antibody against the protein of interest with that precipitated by a IgG isotype control raised in the same species (Kuras, 2004). DNA precipitated by the isotype control is regarded as random or background signal, which is used to normalise the signal produced by the antibody against the protein of interest.

A conventional ChIP experiment requires a minimum of four days to perform. Recently various improvements in the experimental procedures have been applied to simplify and shorten sample preparation processes and to accelerate antibody precipitation (Haring et al., 2007; Nelson et al., 2006; Schoppee Bortz and Wamhoff, 2011).

In my experiments, I adopted the procedures from previous publications and used *Syt8*, a negative control region previously shown to contain no Pax6 binding site (Mi et al., 2013; Sansom et al., 2009). I also used a Pax6 antibody manufactured by Millipore that is widely used in ChIP experiments (Díaz-Alonso et al., 2014; Xie et al., 2013). The antibody only recognises the amino-terminal of Pax6 protein, which is absent in *Pax6^{Sey/Sey}* tissues. However, the results shown in Section 4.2.5 suggest no difference in Pax6-binding affinity between all putative binding sites and the *Syt8* negative controls. There is also no affinity difference between the *Pou3f4* positive control and *Syt8*.

One technical error may have occurred during the sonication step. The sonicated fragments have a length distribution between 100 bp and 700 bp. Long DNA fragments are more likely to produce background noises due to the higher possibility of containing both *Syt8* and Pax6-binding motifs, and therefore may produce *Syt8* signals in Pax6 antibody precipitated samples.

Another possible error is that Pax6 antibody may have failed to specifically precipitate chromatin complex in this experiment. To verify the differential binding

The regulatory role of Pax6 on Cell Division Cycle Associated 7 and cortical progenitor cell proliferation affinity of the antibody to *wild-type* Pax6 and the mutant form, immunofluorescent staining was performed on *wild-type* and *Pax6^{Sey/Sey}* sections. The Pax6 antibody used in this ChIP experiment produced a specific staining pattern in *wild-type* tissues but not in *Pax6^{Sey/Sey}*, suggesting a specific binding to the *wild-type* protein (data not shown). To assess the specificity of the chromatin precipitation, western blot analysis can be done to confirm whether Pax6 protein is present at different levels in the precipitated samples between *wild-type* and *Pax6^{Sey/Sey}* before the DNA purification step.

Other issues that may affect the signal-to-noise ratio in the qPCR results are non-specific binding of chromatin to the protein A/G agarose or magnetic beads and/or to the plastic tubes used in the experiments. To prevent the former problem, beads can be blocked with non-specific serum or BSA to reduce background binding (Haring et al., 2007). In my experiments a blocking buffer containing 0.5% BSA was used to minimise non-specific binding. For the latter issue, siliconized tubes or plastic tubes pre-incubated with BSA or non-related DNA can be used to reduce non-specific binding of chromatins to the tubes.

Normalisation of qPCR results can also create unnecessary skews that may mask the true differences between samples. Conventionally, signals from the experimental ChIP group (using antibody against the protein of interest) are divided by signals from the non-specific antibody such as an isotype IgG to reveal the experimental ChIP signal as “fold change or fold enrichment” from the background levels (Haring et al., 2007; Mathieu et al., 2005; Mi et al., 2013). Because random binding signals from the control IgG antibody are very low, DNA fragments precipitated by the control IgG may produce nearly undetectable readouts in the qPCR. Any variation between these low values will falsely amplify the results in the experimental group if they were used as references for normalisation. Also because the binding affinity of non-specific control antibody to all DNA-binding proteins is low and the chromatin it precipitates should be random, using non-specific IgG control is to assume that the background noise level for each qPCR primer target region is similar, if this assumption is erroneous then the noise level produced by the IgG control may also skew the experimental results. To avoid those possibilities, a previous study used a single antibody against the protein of interest to pull down the chromatin complex

The regulatory role of Pax6 on Cell Division Cycle Associated 7 and cortical progenitor cell proliferation (Kaeser and Iggo, 2002). In my ChIP procedures, a single antibody against Pax6 protein was applied to precipitate *wild-type* (experimental) and *Pax6^{Sey/Sey}* (control) tissues, and the qPCR result of each primer set in the *wild-type* sample is normalised against that in the control sample, thereby avoiding the skewing effects of the IgG antibody.

Another normalisation method is called the “percentage of input”. This method uses un-precipitated chromatin complex as the “input DNA”. The qPCR results from the input DNA are used to normalise the ChIP results, therefore the signals produced by protein-specific and control antibodies are expressed as the percentage of the input DNA (Haring et al., 2007; Nagaki et al., 2003). To apply this method to my results, a possible way to improve my current experiment is to obtain the qPCR results before and after the precipitation process within *wild-type* and *Pax6^{Sey/Sey}* group. For each putative binding site as well as the *Pou3f4* positive and the *Syt8* negative controls, DNA purified from the *WT* and *Pax6^{Sey/Sey}* tissue lysates before antibody precipitation can be used to obtain the level of input DNAs, which can be used to normalise the qPCR results from the precipitated samples. For each examined primer set, ratios of the precipitated vs. input DNA from the two genotypes can be created separately. Therefore by comparing the ratios, it is possible to identify differential binding affinities between genomic regions and genotypes.

In summary, it is currently difficult to confirm the binding of Pax6 in the tested regions. To improve the experiment, measures need to be taken to minimise the background noises caused by the experimental conditions, the presence of Pax6 protein in precipitate samples needs to be confirmed by western blot, additional negative control primer sets should be tested, and new normalisation methods should be implemented in the future.

4.3.3 Re-exploring potential Pax6 target sites in the *Cdca7* genomic region

In this project, the original target region for putative Pax6 binding site discovery was the *Cdca7* genomic locus and the 5 kb region flanking the area. Computational predictions showed region upstream to the *Cdca7* genomic region contained several highly potential hits from the customised track. A 4.2kb upstream genomic fragment,

The regulatory role of Pax6 on Cell Division Cycle Associated 7 and cortical progenitor cell proliferation containing putative Pax6 binding sites without *Cdca7* coding region, was selected and cloned. Given the result that all identified putative binding sites within this region did not show preferential binding affinity to Pax6, an expansion in the genomic region to be analysed, as well as new identification strategies, are required to uncover potential Pax6 binding motifs. A number of highly scored putative sites within the *Cdca7* genomic region, as well as sites located downstream the region, are listed in Table 4.2. The position weight matrices for optimal Pax6 binding sequence are shown in Figure 4.7.

Table 4.2 In silico prediction of Pax6 binding sites near and within the *Cdca7* genomic region

Genomic locus		Recognised by	Predicted binding site sequences
72477524	72477538	M00979	ATCTTCACACATAAA
72478073	72478090	PC:C0000010	TCATGAAAATGAAGCCCA
72482079	72482096	PC:C0000010	ATTGTTTGGAAAATGGAG
72483980	72484001	P6CON	GATTTTGGAGTTTTGCATCAAC
72484246	72484257	M00808	CTGAGGAGATGG
72486489	72486500	M00808	GCCATTTCCCAG
72489460	72489471	M00808	CAAAAATGACAT
72489484	72489495	M00808	GTAACCACGGAG
72489486	72489500	M00979	AACCACGGAGAATGA
72490349	72490360	M00808	GACACACAGACA

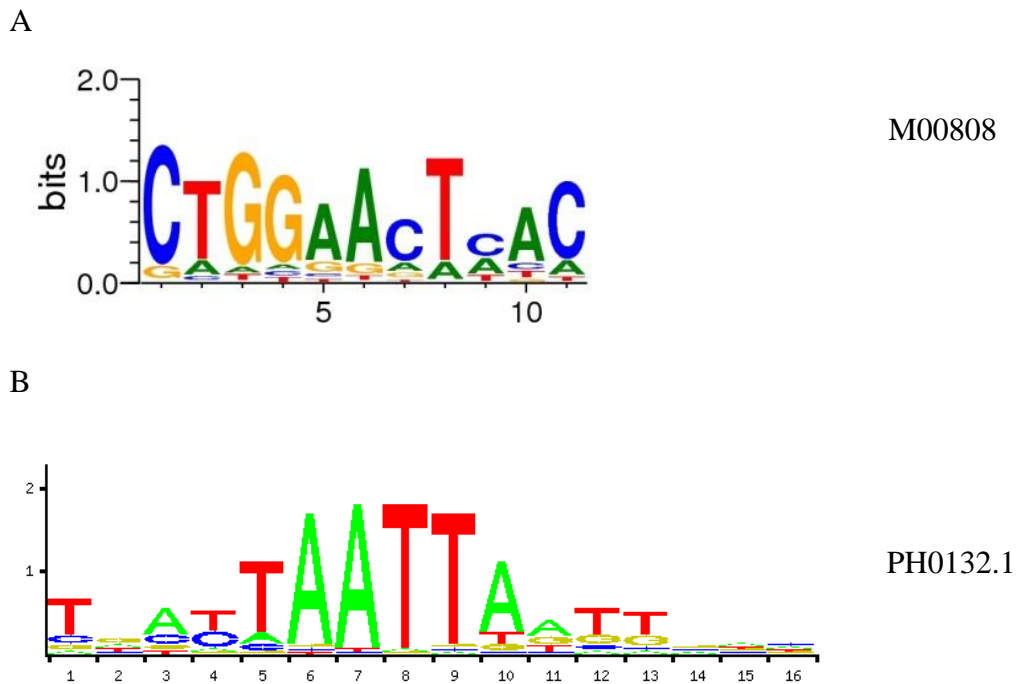


Figure 4.7 Optimal Pax6 binding motifs for *in silico* predictions.

In addition to the motifs in Figure 4.2, two alternative optimal Pax6 binding motifs are represented in position weight matrix (PWM) form. (A) M00808 recognises Pax family proteins in human and mouse (Transfac). (B) PH0132.1 binding motif is generated by Homeo domain recognition sequence (JASPAR).

New strategies regarding to look for promising Pax6 binding motifs were related to DNA structure and chromosome folding/unfolding during gene expression. DNA in mammalian cells is packed into chromatin complex, with various folding mechanisms creating tissue-specific interactions between genomic regions. In recent years, three-dimensional chromatin organisation within cells can be visualised by chromosome conformation capture (3C). The fundamental concept of 3C is to crosslink chromatin structure with formaldehyde, followed by chromatin digestion with restriction enzymes. Genomic regions sharing close physical interactions are ligated so their linkage is preserved. These interacting DNA motifs can be identified by standard PCR or high-throughput sequencing (Dekker et al., 2013).

Recently with advance in high-resolution chromosome conformation capture (Hi-C), chromosomes are believed to be segmented into topological associated domains (TADs). Based on the same principle of 3C, Hi-C can further sequence whole genomic region in a non-biased method. After Hi-C analysis, chromosome regions that interact with other can be identified. Scientists have found that the interaction frequency is higher within individual chromosome than between chromosomes. Furthermore, within individual chromosome, there are segmented units which firstly separated by the interaction frequencies. The interaction frequency is higher within each unit than between units. Later the unit is called TAD and further investigation has suggested individual TAD is possibly separated by enriched CTCF binding (Dekker et al., 2013; Dixon et al., 2012). The size of TADs in average is 880kb in mouse ES cells, where all identified TADs cover 91% of the genome (Dixon et al., 2012). Distal rearrangement of chromosome may result from interactions between promoter and enhancer elements, and Hi-C can provide genome-wide unbiased detection of protein-binding regions, which can be used to predict long-range regulatory elements, or even to predict co-expression of genes within the genome (Babaei et al., 2015; Lajoie et al., 2015; Pope et al., 2014).

Hi-C has been used in embryonic mouse forebrain to provide potential promoter-enhancer binding information (GEO no. GSE60838) (Reilly et al., 2015; Shen et al., 2012). I have combined those information, together with Pax6 ChIP-seq results in embryonic E12.5 mouse cortex (GEO no. GSE66961 Sun et al., 2015), to predict the

The regulatory role of Pax6 on Cell Division Cycle Associated 7 and cortical progenitor cell proliferation regulatory elements of *Cdca7* as well as potential Pax6 binding sites in these elements.

Figure 4.8 shows TADs in vicinity to the *Cdca7* genomic locus (chromosome 2:72314276-72324947; mouse mm9) on mouse chromosome 2. The Pax6 ChIP-seq data was also added to illustrate Pax6 binding sites within this region (Sun et al., 2015). The TAD covering the *Cdca7* genomic region spans chr2:72040001 to 73280000 and contains two Pax6 binding sites according to the ChIP-seq result. The two sites locate downstream to the *Cdca7* genomic locus, they are 600kb and 800kb away from the *Cdca7* transcription start site and might serve as distal regulatory elements for *Cdca7* expression.

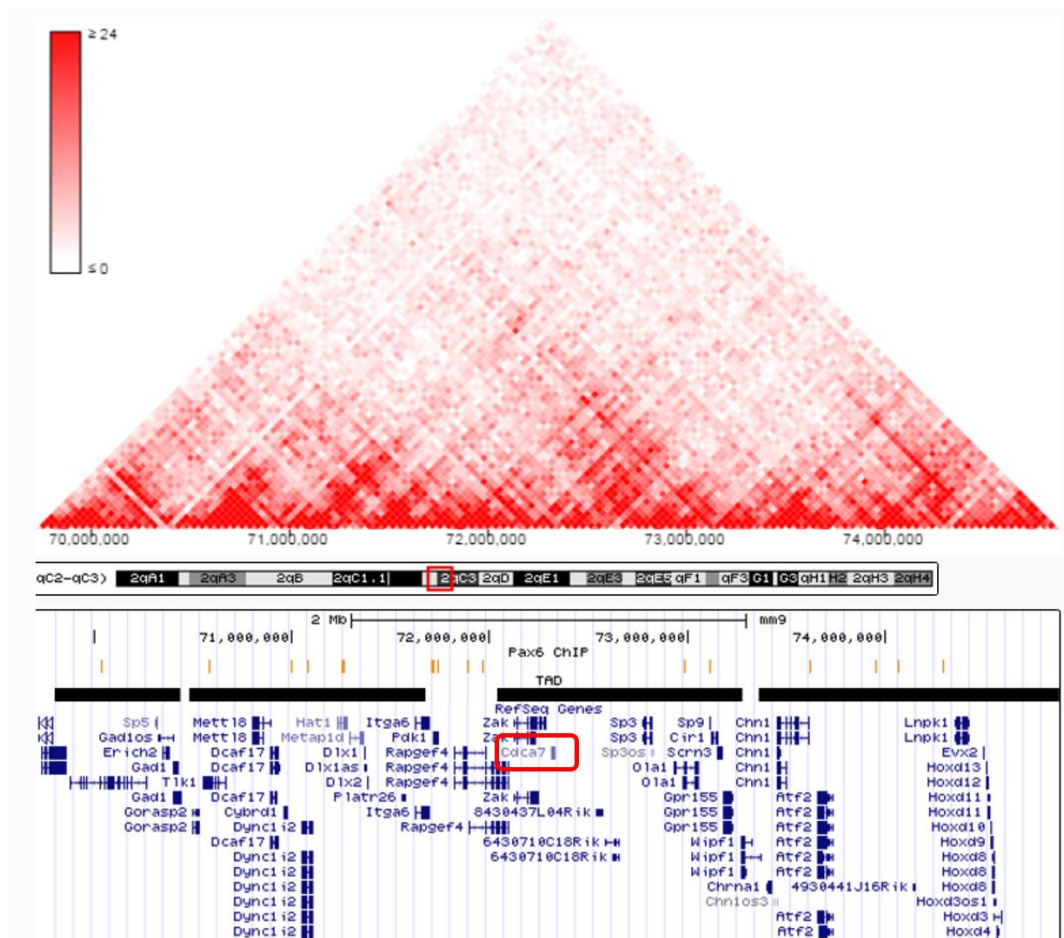


Figure 4.8 The topological associated domain and Pax6 binding sites near the *Cdca7* genomic region.

Figure showing the topological associated domain (TAD, black bar) that covers the *Cdca7* genomic region (red square). Pax6 binding sites from ChIP-seq data were overlaid as orange lines. Two Pax6 binding sites could be seen downstream of the *Cdca7* genomic region.

(Hi-C browser <http://promoter.bx.psu.edu/hi-c/download.html>, (Dixon et al., 2012)).

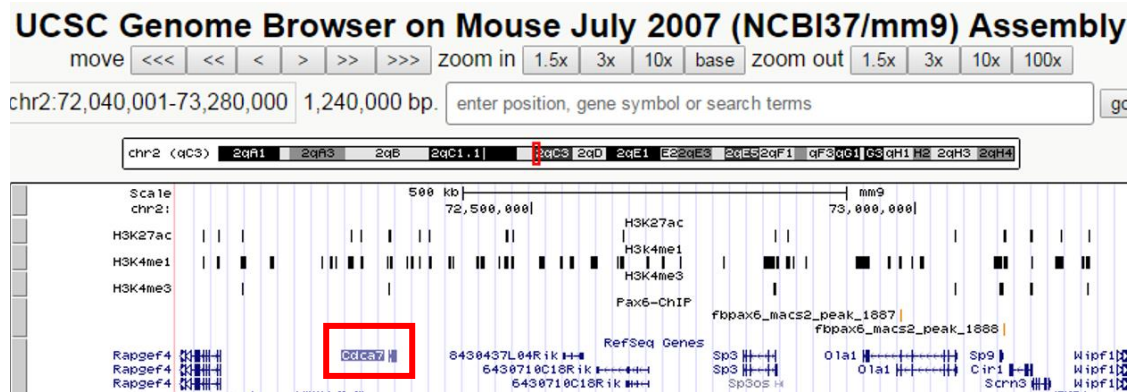


Figure 4.9 Epigenetic marks in the TAD covering the *Cdca7* genomic region.

Figure showing three different epigenetic marks in the TAD that covers the *Cdca7* genomic region (marked in red square). H3K27ac and H3K4me1 are the enhancer marks and H3K4me3 is the promoter region mark.

Figure 4.9 shows epigenetic marks within the TAD containing the *Cdca7* genomic region (Barski et al., 2007; Wang et al., 2008). Overlaying of the putative Pax6 binding regions with both promoter marker H3K4me3 and enhancer markers H3K4me1 and H3K27ac (GEO no. GSE60838) (Reilly et al., 2015) showed that one putative region at ch2: 72981193 co-localised with the enhancer marker H3K4me1. This region was further analysed for Pax6 binding motifs using JASPAR database (jaspar.genereg.net/). The score threshold was set at 80 % and a putative binding motif was identified within this region. The sequence of this motif was aligned with equivalent loci in multiple species using UCSC genome browser, and homologous sequences of this motif were found between human, mouse, rat and many other model organisms (Figure 4.10), increasing the likelihood that this motif is a genuine Pax6 binding site in the physiological environment. Further validations using luciferase assay and ChIP are required to confirm this finding.

Similar strategy was performed to screen for putative Pax6 binding sites around and within the *Cdca7* genomic locus containing the promoter marker H3K4me3. A region close to the *Cdca7* transcription start site is enriched with H3K4me3 (Figure 4.11A). Further analysis of this region by JASPAR revealed two potential Pax6 binding sites, one of which is conserved between species (summary in Table 4.3). Same analysis was also applied to the regions enriched with enhancer marks H3K4me1 and H3K27ac. Although all enhancer-enriched regions within the same TAD as *Cdca7* locus should be screened for Pax6 interaction, in this case there were no other Pax6 binding sites suggested by Pax6 ChIP-seq within this region, therefore only the 15kb region flanking *Cdca7* genomic locus was included in the analysis to maximise the possibility of getting genuine hits. Screening of Pax6 binding motifs in the entire TAD region that covers the *Cdca7* genomic locus could not be achieved by JASPAR website due to the size of fragment, therefore the analysis was done via MEME suite (meme-suite.org). Figure 4.11B shows 3 putative Pax6 binding sites in vicinity to the *Cdca7* locus were found in regions enriched with H3K27ac, and 2 sites were found in regions enriched with H3K4me1. Amongst the predicted sites, 2 of which were conserved across multiple species. All predicted sites are summarised in Table 4.3.

The regulatory role of Pax6 on Cell Division Cycle Associated 7 and cortical progenitor cell proliferation. In summary, combining data from Hi-C, Pax6 ChIP-seq, epigenetic marks screening and conservation analysis, I have found 3 potential Pax6 binding sites which may regulate the expression of *Cdca7*. These motifs require further experimental validations for Pax6 binding and their regulatory role in *Cdca7* transcription. These validations will provide direct evidence for the role of Pax6 in controlling *Cdca7* expression, and whether the regulatory function is achieved by direct or indirect binding.

Earlier in this chapter, six putative Pax6 binding sites were found by *in silico* prediction, none of which possess binding affinity to Pax6 in the experimental validation. Luciferase assays suggested possible inhibitory effect of Pax6 on *Cdca7* expression, however this effect was only present when the environmental Pax6 protein level was limited. This result revealed a complex role of Pax6 in *Cdca7* regulation, possibly involving additional regulatory factors such as the E2f and Sox family members, in agreement with previous studies on the effect of Pax6 on genes downstream of E2f. The *in vivo* function of *Cdca7* during neural development remains elusive. In the next chapter, I will be investigating the biological role of *Cdca7* during neurogenesis in the mouse cortex.

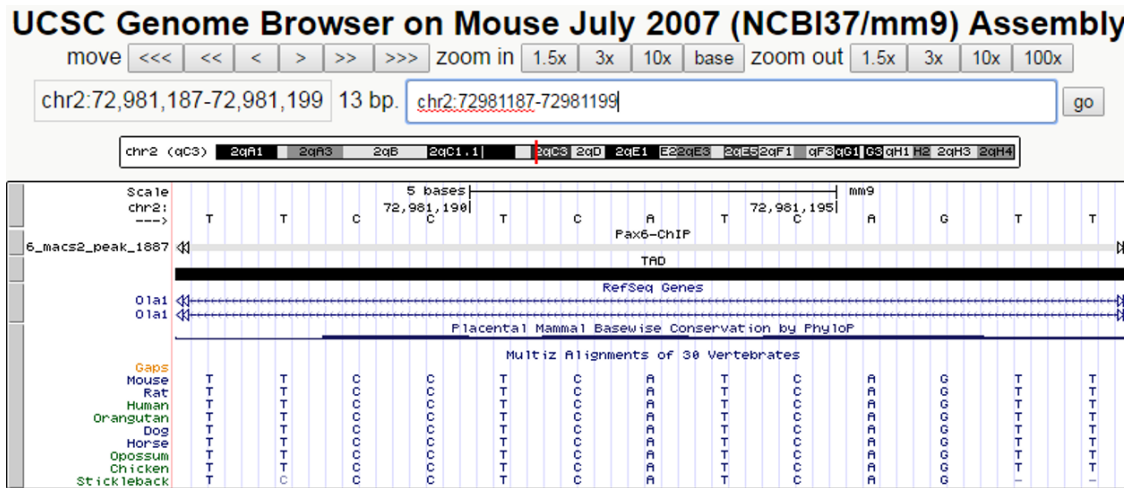
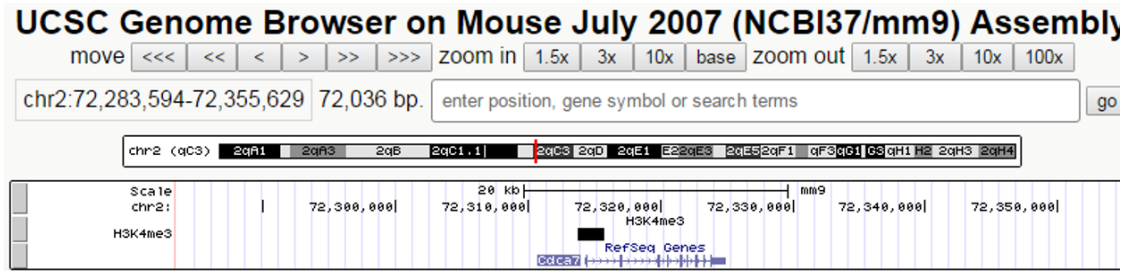


Figure 4.10 Evolutionary conservation test on one of the predicted binding sites.

One of the Pax6 binding sites predicted by ChIP-seq in the mouse embryonic cortex was shown to overlap with the enhancer mark H3K4me1. Multi-species alignment of the motif found that the sequence was evolutionary conserved, suggesting the motif was of physiological importance.

A.



B.

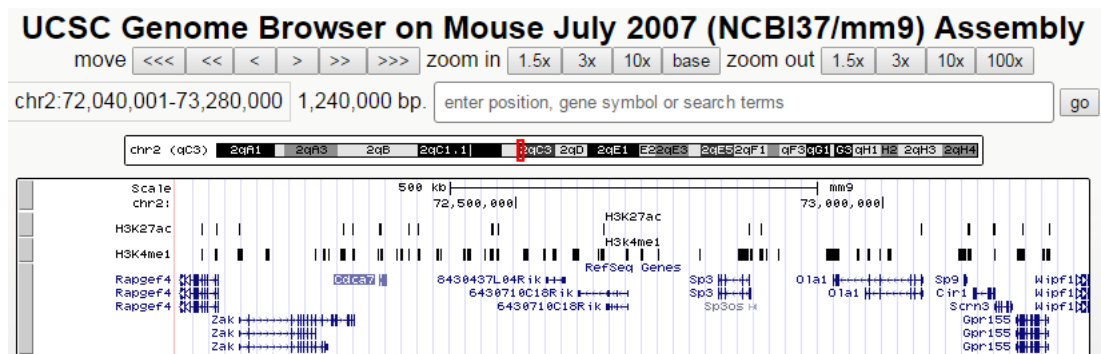


Figure 4.11 Epigenetic marks found within and close to the Cdca7 genomic region.

Figures showing regions enriched with the promoter mark H3K4me3 (A) and enhancer mark H3K27ac and H3K4me1 (B). All enriched peaks are shown in black bars.

Table 4.3 Summary of predicted binding sites

Binding sites	Recognised by	Start	End	Predicted Site Sequence	Homologous sequences found between species
1	PH0132.1	72315312	72315327	TACTTATTTAAGTGAT	N
2	PH0132.1	72315593	72315608	CTACTAATCAATTTAA	Y
3	P6CON	72981187	72981199	TTTCCTCATCAGTT	Y
4	P6CON	72317349	72317362	TTTACAAATGATTT	Y
5	PH0132.1	72318432	72318447	TGATAAAATAGTTCTA	N
6	PH0132.1	72319004	82319019	TTACTAATTGAGACAG	N
7	P6CON	72319437	72319450	TTTATGGATGAACT	N

Conservation test was carried out by pairwise comparison and for example the sequence similarity between mouse and human of binding 2 is 75%.

Chapter 5 : Understanding functions of Cdca7 in cortical progenitor cells

5.1 Introduction

5.1.1 Pax6 regulates the proliferation and differentiation of neural progenitors

Radial glia cells (RGC) or apical progenitors (APs) reside and divide in the ventricular zone (VZ) of the dorsal telencephalon and give rise to glutamatergic neurons in the cerebral cortex (Heins et al., 2002; Malatesta et al., 2000; Miyata et al., 2001; Noctor et al., 2001). Another type of progenitor cells are named intermediate progenitor cells (IPCs) or basal progenitors (BPs): they are derived from asymmetric division of RGC located in the subventricular zone (SVZ) and also give rise to glutamatergic neurons (Haubensak et al., 2004; Miyata et al., 2001; Noctor et al., 2001). RGCs either undergo symmetric division to produce two RGCs and maintain the progenitor pool or asymmetric divisions to produce one RGC and one IPC or one neuron (Haubensak et al., 2004; Huttner and Kosodo, 2005; Kawaguchi et al., 2004; Noctor et al., 2004). IPCs form a large inner SVZ and outer SVZ and undergo several rounds of division in primates, while in rodents IPCs reside in the SVZ and can only divide once to produce two neurons per cell (Fietz and Huttner, 2011; Götz and Huttner, 2005). Identification of the two distinct progenitor populations as well as the post-mitotic neurons depends on their morphologies, anatomical positions as well as their expression of molecular markers. During the differentiation process in the neocortex, transcription factors Pax6, Tbr2 and Tbr1 are expressed in the RGC, IPC and post-mitotic neurons, respectively (Englund et al., 2005), therefore these proteins are widely used as cell type-specific molecular markers. Unlike the Tbr2-expressing IPCs in the cerebral cortex, IPCs in the thalamus specifically express Olig2 and Olig3; they also express Neurogenin1 (Ngn1) and Neurogenin2 (Ngn2), which are also detected in the cortex (Wang et al., 2011).

A previous experiment has found that loss of Pax6 in Pax6^{+/+}↔Pax6^{-/-} chimeras produced a reduced number of neurons. The decreased neurogenesis is due to an early depletion of progenitor pools and also a population of immaturely derived IPCs

The regulatory role of Pax6 on Cell Division Cycle Associated 7 and cortical progenitor cell proliferation which fail to express the Tbr2 marker. These defects indicate that Pax6 is essential for neurogenesis and Tbr2 expression in a cell-autonomous fashion (Quinn et al., 2007).

Apart from regulating neurogenesis in the neocortex, Pax6 also controls the balance between proliferation and differentiation of progenitors in the spinal cord. High levels of Pax6 can drive progenitors to exit the cell cycle and differentiate by upregulating Ngn2, which reduces the expression of Pax6 by negative feedback in cells that have committed to differentiation (Bel-Vialar et al., 2007).

Pax6 is also found to regulate cell fate in mitral cells, a type of glutamatergic neuron in the olfactory bulb (OB). Mitral cells derive from Pax6⁺ cells. Pax6 levels are down-regulated in this type of cells while Tbr1 and Tbr2 levels are increased. Overexpression of Pax6 in the embryonic OB causes a reduced proportion of Tbr1⁺ Tbr2⁺ mitral progenitor cells and fewer progenitors commit to being mitral cells, indicating that Pax6 also affects cell fate in the OB (Imamura and Greer, 2013).

5.1.2 Cell cycle kinetics change during neural differentiation

During neurogenesis in mice, the total duration of a cell cycle is elongated from 8.1 hours at E11 to 18.4 hours at E16, during which the length of G1 phase is correspondingly increased from 3 hours to 12 hours (Takahashi et al., 1995). This correlation indicates that the length of G1 phase is a good representation of the total duration of a cell cycle. An early model has proposed a cell-cycle length hypothesis in which a lengthened G1 can ultimately affect cell fates. The hypothesis assumes that the determinants of cell fate are unequally distributed between the two daughter cells. When the length of G1 reaches a critical threshold allowing enough environmental as well as intrinsic signals to be involved, the daughter cell which inherits more cell fate determinants will commit to differentiative division while the other daughter remains proliferative (See also Ch1.1.4 and Figure 1.4) (Calegari and Huttner, 2003; Götz and Huttner, 2005).

Whether the prolonged G1 phase, and therefore the total cell cycle, is the cause or the consequence of neural differentiation remains elusive, but the theory described above couples G1 lengthening with fate decisions in stem cells (Lange and Calegari, 2010;

The regulatory role of Pax6 on Cell Division Cycle Associated 7 and cortical progenitor cell proliferation (Orford and Scadden, 2008; Singh and Dalton, 2009). Various previous studies have manipulated the length of G1 by targeting CDKs and cyclins in cortical neural progenitors and have shown that the lengthened G1 triggers differentiation and inhibits proliferation (Calegari and Huttner, 2003; Glickstein et al., 2009; Lange et al., 2009; Pilaz et al., 2009). However this observation was only done in a broad view of the whole cortex regardless of different regions. A recent study at the single cell scale provides further support for this theory (Roccio et al., 2013). Using fluorescent ubiquitylation-based cell-cycle indicator (Fucci) probes to track the fluorescent intensity of single cells, new categorical markers were applied to separate proliferative neural stem cells (NSCs) from differentiative NSCs as they emit different fluorescent intensities in G1. The study further concluded that in more primitive stem cells, the length of G1, as well as the ratio of G1 to total cell cycle, is shorter compared to differentiated cells (Roccio et al., 2013).

Manipulation of G1 period normally involves regulation of Cdks and cyclins (Lange and Calegari, 2010). Retinoblastoma protein (Rb) is one of the downstream targets of Cdk4 and Cdk6 (Khleif et al., 1996). Hypophosphorylated Rb forms a complex with E2f factors in the cytoplasm, which prevents E2fs from activating their downstream targets involved in cell cycle progression (Chittenden et al., 1991; Lees et al., 1993). Through direct inhibition of Cdk6 production, Pax6 regulates cell cycle progression by reducing Rb phosphorylation (Mi et al., 2013). Previous studies have observed a shortening of the cell cycle in the cortex at E12.5 in *Pax6^{Sey/Sey}* embryos (Estivill-Torres et al., 2002; Mi et al., 2013), however the downstream mechanisms behind the shortening are still unclear. Given *Cdca7* is one of the direct targets of E2f1 (Goto et al., 2006) and the activity of E2f1 is influenced by the phosphorylation of Rb, understanding the biological functions of *Cdca7* in the development of cortex and whether *Cdca7* is one of the Pax6-downstream facilitators causing the shortened cell cycle in *Pax6^{Sey/Sey}* mutants will provide a molecular paradigm of how Pax6 regulates cell differentiation. Therefore, in this chapter, I manipulated the protein level of *Cdca7* *in vivo* by *in utero* electroporation in the developing cortex of mouse embryos at E12.5 and E14.5, and observed the alterations of neurogenesis. Overexpression of *Cdca7* *in vivo* may mimic the physiological situation in *Pax6^{Sey/Sey}*

The regulatory role of Pax6 on Cell Division Cycle Associated 7 and cortical progenitor cell proliferation cortex where the protein level is up-regulated. Therefore a shortening of the duration of the cell cycle as well as fewer neurons are expected to be observed.

5.2 Results

5.2.1 Overexpression of Cdca7 *in vitro*

It is known that *Cdca7* is up-regulated in *Pax6*^{Sey/Sey} cortex but the exact functions of the protein are still unclear. To investigate its role in brain development, I adopted an *in utero* electroporation approach to overexpress *Cdca7* in mouse embryonic cortex. *Cdca7* expression clone MG205975 containing *Cdca7* cDNA open reading frame (ORF, accession number NM_025866) sequence was ordered from Origene Technologies. This clone was used as the template DNA for PCR amplification to generate *Cdca7* ORF with an influenza hemagglutinin (HA) epitope sequence, tagged at the N-terminal or the C-terminal of the *Cdca7* cDNA sequence in order to distinguish this ectopically expressed protein from the endogenous form and to allow the protein to be detected *in vivo*. The HA-tagged *Cdca7* ORF was cloned into an pCAGGS_IRES-NLS-GFP (Figure 5.1A) (Persson et al., 2002) plasmid for *in utero* electroporation, the vector expressing the N-terminal HA tag was named p_CAGGS-IRES-NLS-GFP_N-HA-Cdca7 (Figure 5.1B), while the vector expressing the C-terminal tag was named pCAGGS_IRES-NLS-GFP_C-HA-Cdca7 (referred to as N-Cdca7 and C-Cdca7 respectively in the following text).

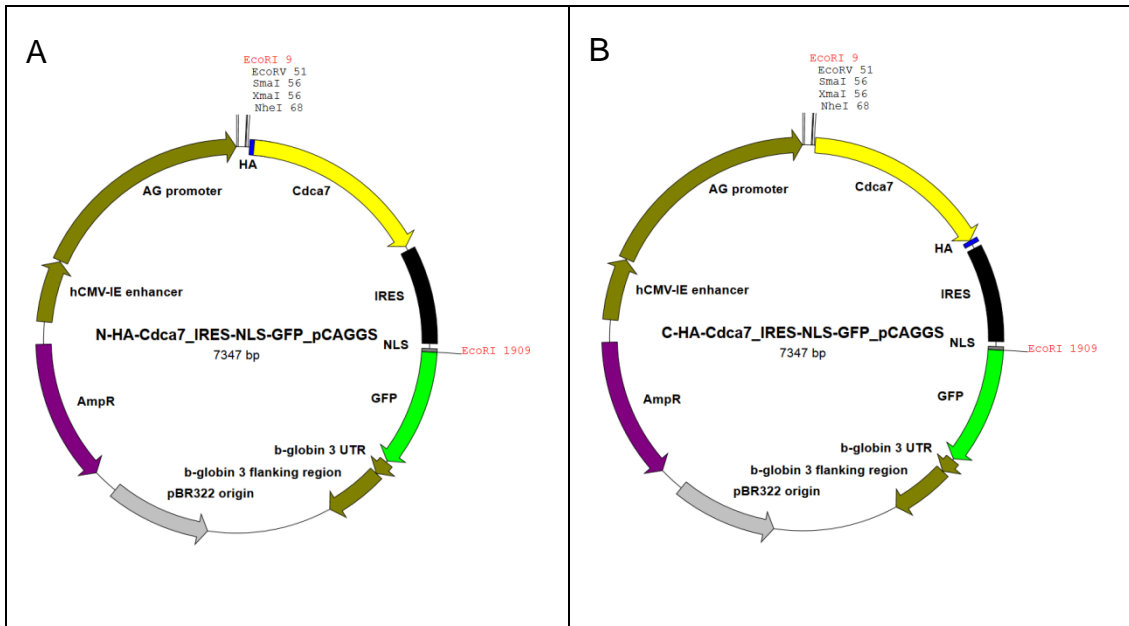


Figure 5.1 Cdca7 expression clones for *in utero* electroporation.

(A) pCAGGS_IRES-NLS-GFP plasmid was previously used for *in utero* electroporation (Persson et al., 2002). GFP transcript is translated by an internal ribosome entry site (IRES) sequence and the protein is transported into nucleus by its NLS signal peptide. There is also an ampicillin resistance gene for colony selection. (B-C) *Cdca7* expression sequence (cDNA ORF, NM_025866) was amplified from Clone MG205975 (OriGene Technologies) and then inserted into pCAGGS_IRES-NLS-GFP plasmid at the NheI restriction enzyme site. *Cdca7* gene expression is driven by the CAG promoter. *Cdca7* cDNA sequence is followed by the stop codon sequences for all three reading frames. An influenza hemagglutinin (HA) epitope sequence was added at the N-terminal (B) or C-terminal (C) of the *Cdca7* ORF for protein detection by immunofluorescence and the plasmid is called p_CAGGS-IRES-NLS-GFP_N-HA-Cdca7 (N-Cdca7) or p_CAGGS-IRES-NLS-GFP_C-HA-Cdca7 (C-Cdca7), respectively.

The regulatory role of Pax6 on Cell Division Cycle Associated 7 and cortical progenitor cell proliferation
To validate the expression of the HA-tagged Cdca7 protein by the C-Cdca7 plasmid, the vector was transiently transfected into HEK293 cells. At 48 hours post transfection, cell lysates were collected for a western blotting analysis using an antibody against the HA epitope (Figure 5.2A). An antibody against GAPDH was used as a loading control. The expression of Cdca7 was found to correlate with the level of transfected vector, suggesting that Cdca7 was produced by the plasmid and this protein can be recognised by the anti-HA antibody.

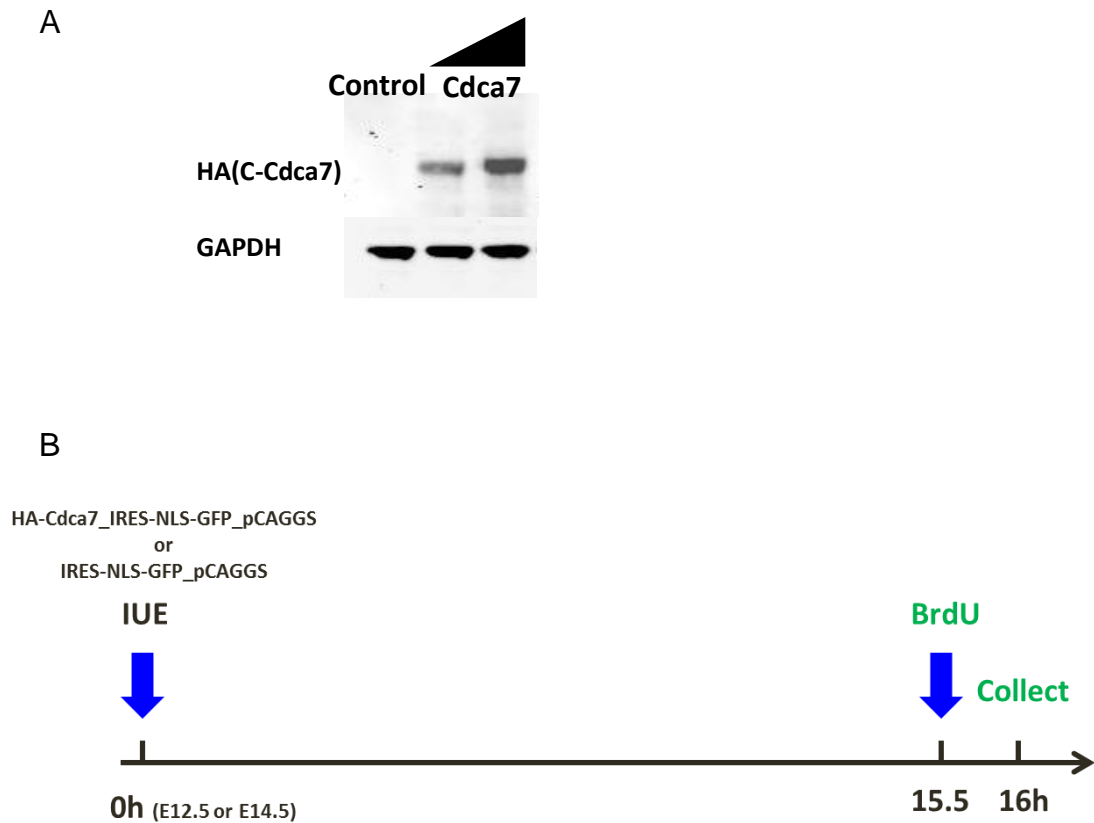


Figure 5.2 *In vitro* expression of Cdca7 and *in utero* electroporation paradigm.

(A) IRES-NLS-GFP_pCAGGS (Control) or C-Cdca7 plasmid was transiently transfected into HEK293 cells. Cell lysates were collected 48 hours post transfection and Cdca7 expression was verified using an antibody against the HA epitope. The molecular weight of Cdca7 was approximately 43 kDa. GAPDH was used as loading control. (B) After confirming the protein expression from the transfected Cdca7 clone, IRES-NLS-GFP_pCAGGS, N-Cdca7 or C-Cdca7 plasmid was used for *in utero* electroporation. 1-2 μ g of plasmids were injected into the first ventricle of embryos at E12.5 or E14.5 and plasmids were forced to enter the cortex region by electrical voltage. Plasmids were left *in vivo* for 16 hours to allow protein expression and 5-Bromo-2'-deoxyuridine (BrdU) was injected intraperitoneally into pregnant females 30 minutes before animal termination.

5.2.2 Overexpression of Cdca7 *in vivo*

Wild-type CD1 pregnant females carrying E12.5 or E14.5 embryos were used for *in utero* electroporation. Electroporations were normally performed between 1-4 pm and either control or the Cdca7 expression vector was left for 16 hours before the embryos were terminated. Single doses of the thymidine analog, 5-bromo-2'-deoxyuridine (BrdU), were given to pregnant females via intraperitoneal injection 30 minutes before the animals were culled (Figure 5.2B).

To assess the efficiency of the transfected Cdca7 expression vector, embryos were collected at 16 hours post electroporation, they were fixed and cryo-sectioned for immunofluorescence staining. In the original experiment design, antibody against the HA epitope was expected to identify Cdca7 expressed by the plasmids *in vivo*. However the immunofluorescence staining using HA antibody did not produce a specific staining pattern (data not shown). Alternatively, in this experiment, a polyclonal antibody against Cdca7 which detects both endogenous and exogenous forms of the protein was used instead. Figure 5.3 shows the expression of Cdca7 and GFP by N- Cdca7 and C- Cdca7 plasmids. It was found that the Cdca7 antibody can recognise the overexpressed Cdca7 protein regardless of the HA-tag position. GFP expression signal was detected in the nucleus with the help of its nuclear localization sequence (NLS). In the overlaid channel, co-localisation of Cdca7 and GFP proteins was observed in samples overexpressing either the N-terminal or C-terminal HA tag construct. Contralateral sections representing the opposite hemisphere of the same embryos demonstrated there was no expression leaking to the other hemisphere after the *in utero* electroporation.

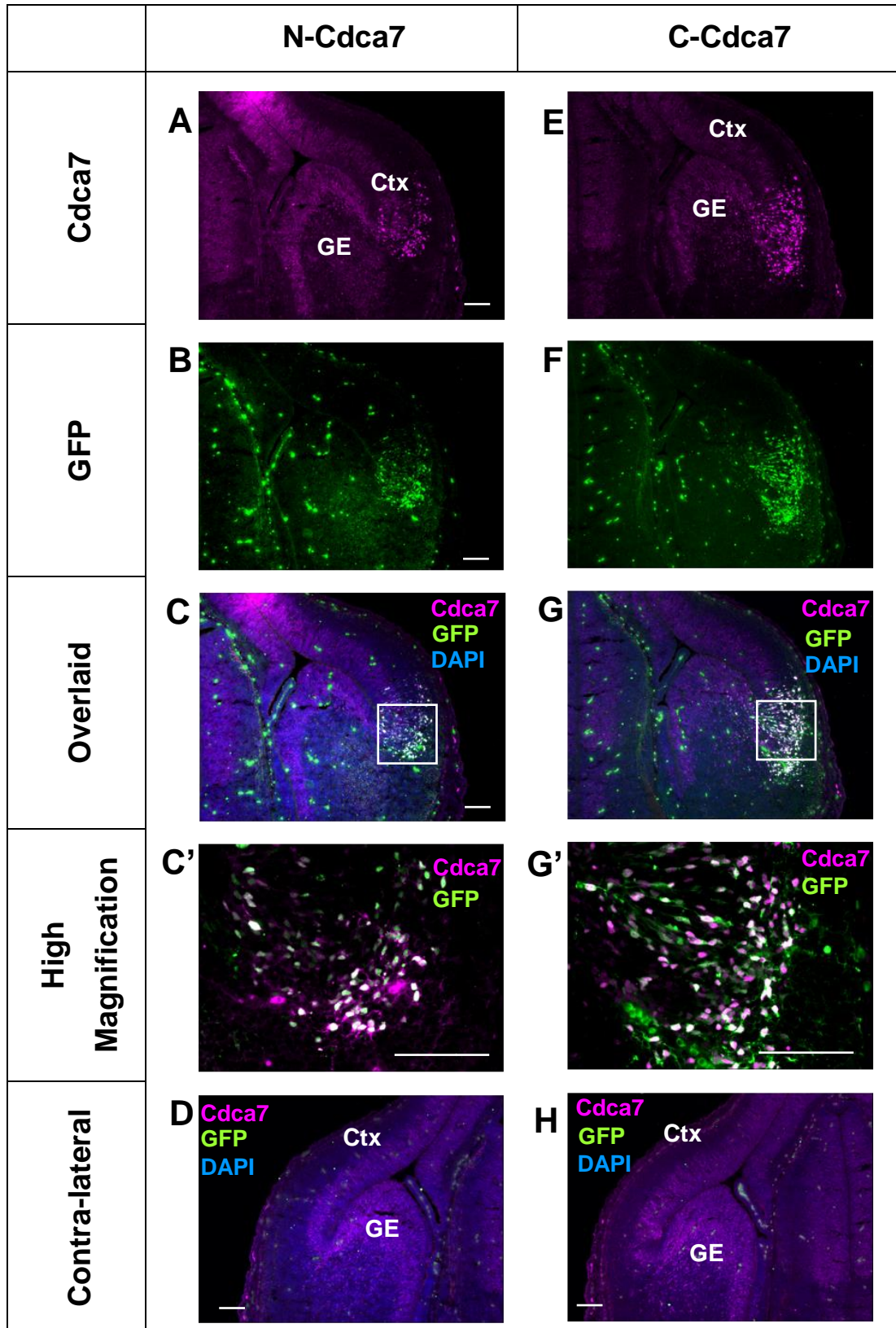


Figure 5.3 Validation of *in utero* expression of Cdca7 after electroporation.

Figure 5.3 Validation of *in utero* expression of Cdca7 after electroporation.

1-2 µg of N-Cdca7 or C-Cdca7 plasmid was used for *in utero* electroporation at E12.5. 16 hours post electroporation, embryos were harvested, PFA-fixed, cryo-protected and sectioned and immunofluorescence stained. Antibody against Cdca7 was able to detect both endogenous and exogenous (overexpressed by the plasmid) Cdca7. GFP positive cells represent electroporated cells. (A-C') Sections from N-Cdca7-electroporated embryos were stained to detect co-expression of Cdca7 and GFP. The electroporation target area was close to the ventral-most area of the dorsal telencephalon and the PSPB. Most cells with intensive Cdca7 staining, which indicates the plasmid-driven overexpressed protein, overlap with GFP staining, suggesting the Cdca7 overexpression couples with the expression of GFP in the nucleus of the same cells. (D) Contralateral photo of the same section in 5.3A-C showing the specificity of the electroporation with no GFP expression in the other hemisphere. (E-G') Sections from C-Cdca7-electroporated embryos were stained to detect co-expression of Cdca7 and GFP. The electroporation target area was also close to the ventral-most region of the dorsal telencephalon and the PSPB. Cdca7 was highly expressed in cells with GFP protein expression, indicating that the exogenous plasmid-driven Cdca7 was co-expressed with GFP in the same cells. (H) Contralateral photo of the same section in 5.3E-G showing the specificity of the electroporation with no GFP expression in the other hemisphere. (Scale bars =100µm)

5.2.3 Understanding biological functions of Cdca7 in the developing cortex

The target area of the plasmid delivery during the *in utero* electroporation spanned from the ventral-most part of the dorsal telencephalon (dTel) to the PSPB, where the expression of Pax6 and Cdca7 is the strongest and weakest, respectively. At 16 hours post electroporation, embryos were collected and their GFP expression was observed under a fluorescence microscope. The GFP⁺ embryos then underwent fixation, cryosection and immunofluorescence staining to assess the expression of a number of marker proteins.

To understand whether the overexpressed Cdca7 affects the production of IPCs, sections from the control, N-Cdca7 or C-Cdca7 plasmid-electroporated group were stained with antibodies against GFP and Tbr2. By counting the percentage of Tbr2⁺ cells in the total electroporated cells (ie. GFP⁺ cells), it was found that at E13.5 the percentage of the Tbr2⁺ population was much lower in the C-Cdca7-transfected group (36%, n=3) than that in the control (47%, n=4) and the N-Cdca7 group (45%, n=4, P<0.05, Student's t-test) (Figure 5.4). This indicates that the overexpressed C-terminal HA-tagged Cdca7 had an impact on the generation of IPCs. The overexpressed N-Cdca7 plasmids did not cause the same effect as the C-Cdca7 but produced a similar result as the control construct. The function of N-terminal HA-tagged Cdca7 protein *in vivo* is yet to be elucidated but it was eliminated at the later time point, E15.5, in this experiment.

At E15.5, the population size of IPCs seemed unrelated to the level of Cdca7 protein, as a similar proportion of Tbr2⁺ cells was observed between the control (39.9%, n=3) and the C-Cdca7 group (38.3%, n=4, P= 0.8, Student's t-test) (Figure 5.5). Therefore in terms of IPC production, the overexpressed Cdca7 may only be effective at E13.5 but not at a later stage, namely E15.5.

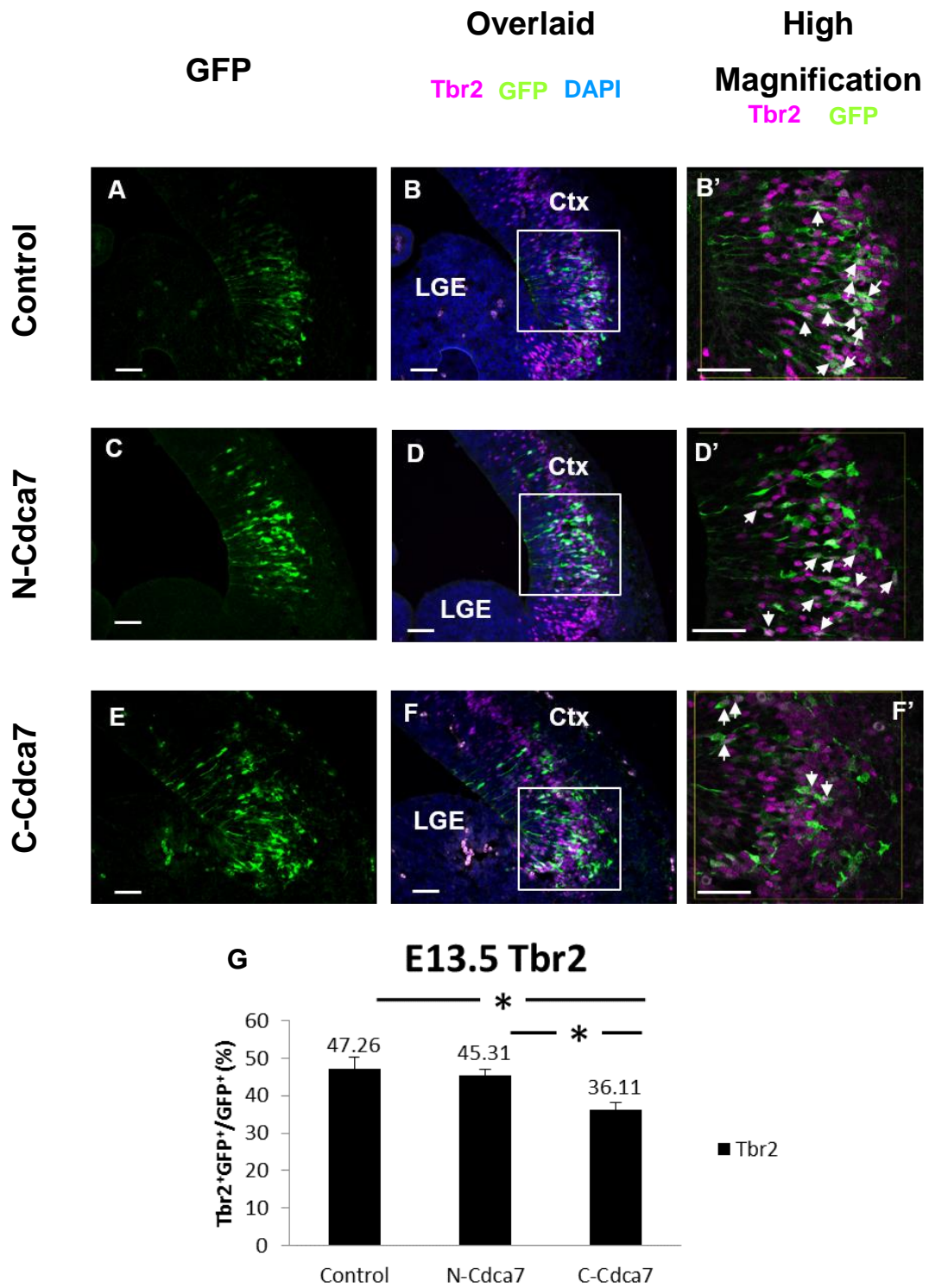


Figure 5.4 Overexpression of Cdca7 at E12.5 prevents the production of intermediate progenitor cells.

Figure 5.4 Overexpression of Cdca7 at E12.5 prevents the production of intermediate progenitor cells.

Embryos collected from the control, N-Cdca7 and C-Cdca7 treatment groups at E12.5 were processed as described in Figure 5.2B. Fixed and cryo-protected embryos were sectioned and stained using antibodies against Tbr2 and GFP. Tbr2⁺ cells represent the intermediate progenitor cells (IPCs). (A,C,E) All the three plasmids were expressed close to the ventral-most part of the dorsal telencephalon. High magnification views in Panel B', D' and F' representing the indicated 200µm² areas enlarged from Panel B, D and E, respectively. (A-B') Photos showing the expression of Tbr2 and GFP *in vivo* in an embryo electroporated with the control plasmid. High magnification image in Panel B' indicates the expression of Tbr2 in the electroporated cells (arrows). (C-D') A representative section from an N-Cdca7-electroporated embryo stained for Tbr2 and GFP. High magnification image in Panel D' indicating the expression of Tbr2 in the electroporated cells (arrows). (E-F') A representative section showing the expressions of Tbr2 and GFP in the C-Cdca7 group. High magnification image in Panel F' showing the overlapped expressions of Tbr2 and GFP (arrows; all scale bars: 50µm). (G) Bar chart showing the proportion of Tbr2⁺ cells in the total electroporated cells in each plasmid group. IPCs make up 47% of all electroporated cells in the control group (n=4) and 45% in the N-Cdca7 (n=4) group, the difference between the two groups is not statistically significant; The C-Cdca7 group has 36% of all electroporated cells being IPCs (n=3), this proportion is significantly lower than those in the control and the N-Cdca7 groups (P<0.05, Student's t-test).

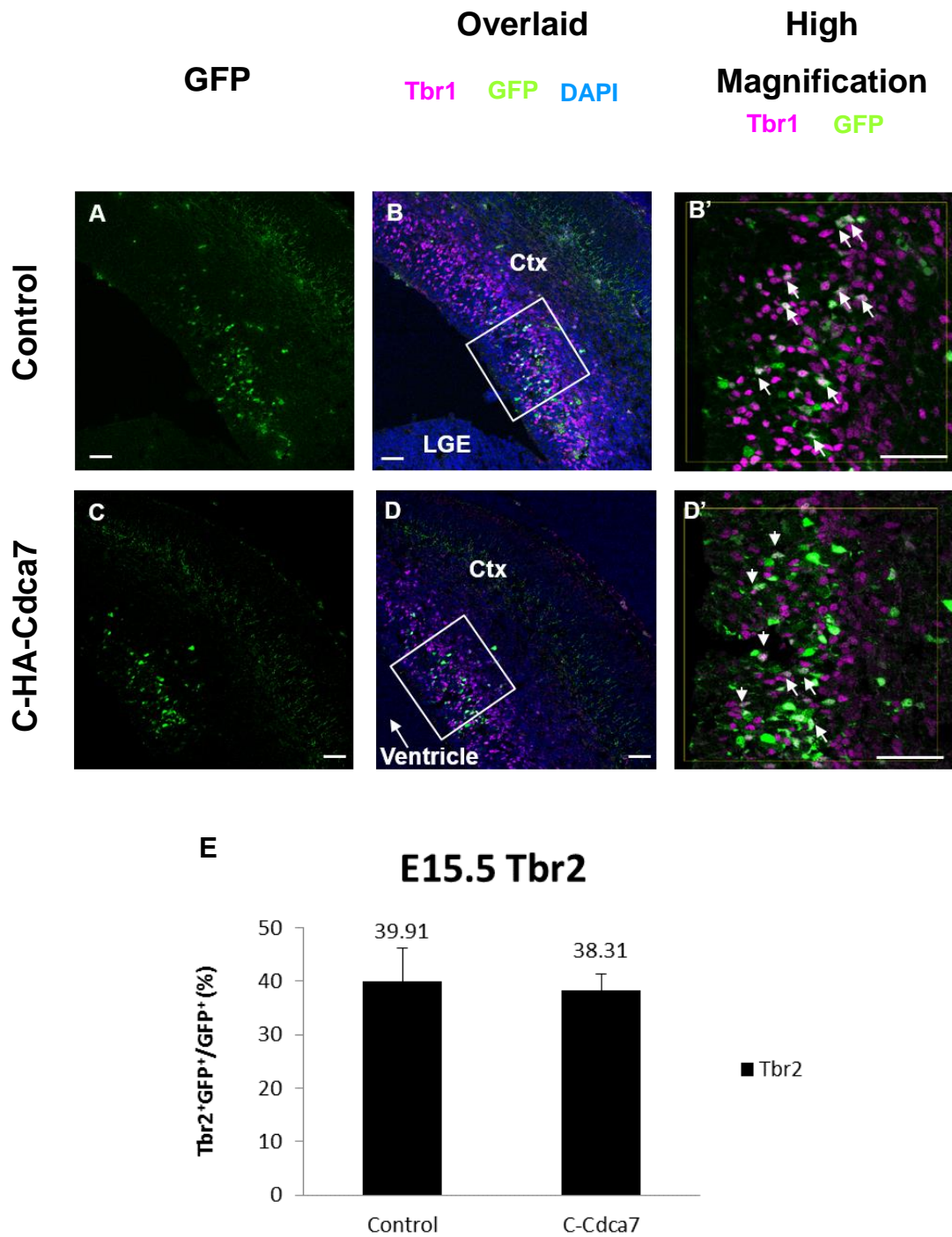


Figure 5.5 Overexpression of Cdca7 at E14.5 does not alter the production of intermediate progenitor cells.

Figure 5.5 Overexpression of Cdca7 at E14.5 does not alter the production of intermediate progenitor cells.

Embryos receiving either control or C-Cdca7 plasmid at E14.5 were collected as previously described in Figure 5.2B. All sections were fixed and stained for Tbr2 and GFP expressions. High magnification views in Panel B' and D' represent the 200 μm^2 areas enlarged from Panel B, and D, respectively. (A-B') Electroporated cells (GFP⁺) from the control group locate at the ventral-most part of the dTel and the high magnification view in Panel B' showing cells co-expressing GFP and the IPC marker Tbr2 (indicated by arrows). (C-D') Electroporated cells from C-Cdca7 group locate at the dTel similarly to the cells in the control group. High magnification image in Panel D' showing IPCs (Tbr2⁺) co-expressing marker for electroporated cells (GFP) (arrows, all scale bars: 50 μm). (E) Bar chart representing the abundance of IPCs (Tbr2⁺) in the total electroporated cells (GFP⁺) in the two plasmid groups. IPCs in the control (n=3) and the C-Cdca7 (n=4) groups are 39.9 % and 38.3% of all electroporated cells, respectively, and there is no significant difference between the groups (P=0.8, Student's t-test). The results indicate that at middle stage of neurogenesis, overexpression of Cdca7 does not affect the production of IPCs.

The regulatory role of Pax6 on Cell Division Cycle Associated 7 and cortical progenitor cell proliferation To characterise the role of Cdca7 in terminal differentiation from RGCs into neurons, the same experiment was performed to monitor neuron production and Tbr1 was used to mark the post-mitotic neurons (Englund et al., 2005). In Figure 5.6 it was observed that the overexpression of C-Cdca7 *in utero* caused a reduced production of neurons at E13.5. The mean percentage of Tbr1⁺ cells in the total population of GFP⁺ cells was 13% in the C-Cdca7 group (n=3) compared to 20% in the control (n=4, P<0.05) and 22% in the N-Cdca7 group (n=3, P<0.05, Student's t-test). No difference was observed in the neuron population size between the control and the N-Cdca7 group (P=0.5, Student's t-test).

At E15.5, the GFP⁺ cells expressing the electroporated plasmids does not overlap with the Tbr1⁺ cells in both the control (n=4) and the C-Cdca7 group (n=4) (Figure 5.7). This suggests that at 16 hours post electroporation, the electroporated cells did not have sufficient time to differentiate into neurons. It may also mean that the electroporated cells were not able migrate to the Tbr1⁺ territory as the cortex has grown much bigger at E15.5 than at E13.5.

The results from the two experiments indicate that overexpression of Cdca7 in the ventral-most part of the dTel close to the PSPB area affects regional IPC as well as neuron production especially in the early stage of the neurogenesis. To estimate the proportion of cells undergoing cell cycle progression, embryos from pregnant female mice receiving the control, N-Cdca7, or the C-Cdca7 plasmid via *in utero* electroporation at E12.5 or E14.5 were given a single dose of BrdU injected 30 minutes before the animals were culled. BrdU, as a thymidine analog, incorporates into newly synthesised DNA during S-phase of the cell cycle. The embryos were fixed and cryo-protected and the spatial distribution of BrdU⁺ and GFP⁺ cells on the sections were revealed by double immunofluorescent staining.

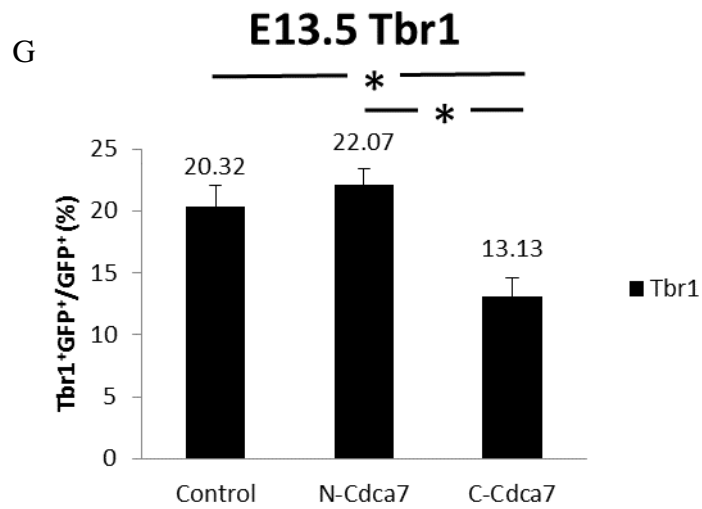
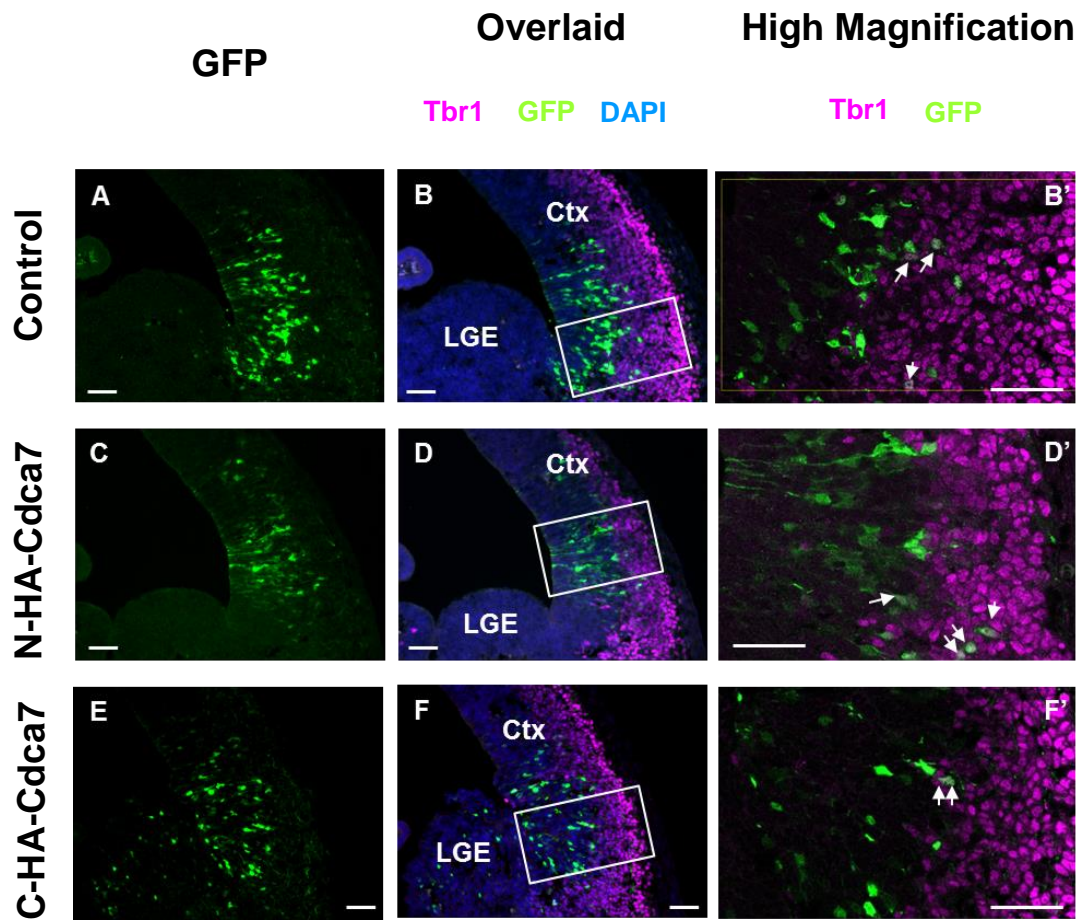


Figure 5.6 Overexpression of Cdca7 at E12.5 prevents the production of post-mitotic neurons.

Figure 5.6 Overexpression of Cdca7 at E12.5 prevents the production of post-mitotic neurons.

Embryos receiving either the control, N-Cdca7 or C-Cdca7 plasmid at E12.5 were collected as previously described in Figure 5.2B. All sections were fixed and stained for GFP (marker for electroporated cells) and the neuronal marker Tbr1. (A,C, E) GFP⁺ cells locate at the ventral-most part of the dorsal telencephalon in all groups. High magnification views in Panel B', D' and F' are enlarged from the 150µm-wide rectangles in Panel B, D and F, respectively. (A-B') A representative section in the control group. High magnification image in Panel B' showing cells co-expressing Tbr1 and GFP (indicated by arrows). (C-D') A representative section in the N-Cdca7 group. High magnification image in Panel D' showing cells co-expressing Tbr1 and GFP (indicated by arrows). GFP staining also labels cellular process. (E-F') A representative section in the C-Cdca7 group. Cells with overlapping expressions of Tbr1 and GFP are shown in F and F' (indicated by arrows, all scale bars: 50µm.) (G) The abundance of neurons in all electroporated cells is 20.3%, 22% and 13.1% in the control (n=4), the N-Cdca7 (n=3) and the C-Cdca7 (n=3) group, respectively. The difference between the C-Cdca7 group and the control or the N-Cdca7 group is statistically significant ($P < 0.05$, Student's t-test) while the difference between the control and the N-Cdca7 group is not statistically significant ($P = 0.5$, Student's t-test.). These results suggest that overexpression of Cdca7 can reduce the production of post-mitotic neurons.

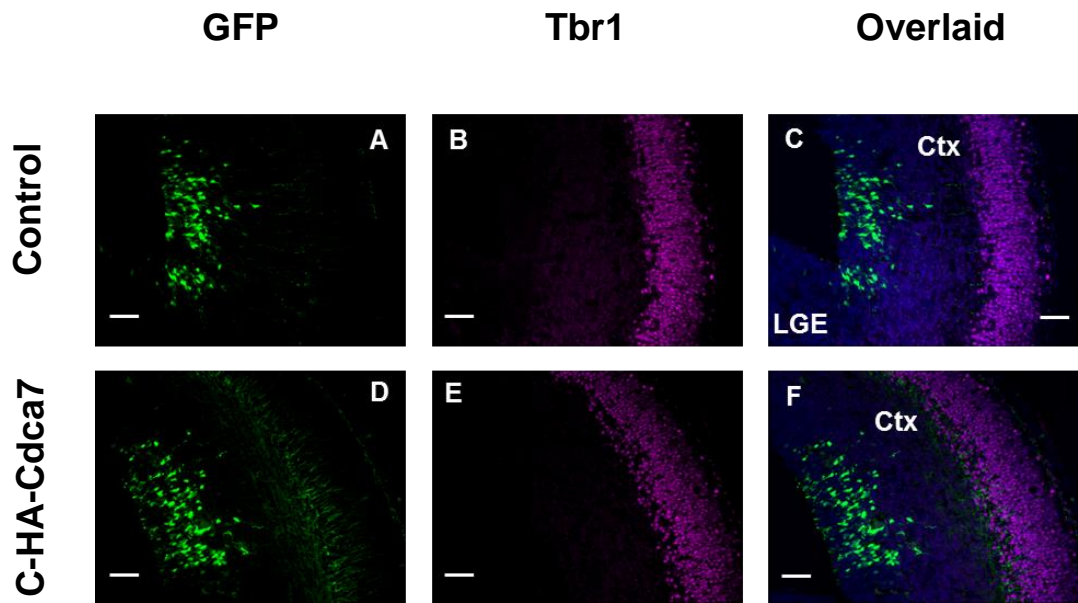


Figure 5.7 Overexpression of Cdca7 at E14.5 does not affect the production of post-mitotic neurons.

Embryos electroporated with the control or the C-Cdca7 plasmid at E14.5 were collected as described in Figure 5.2B. All sections were fixed and stained for GFP (marker for electroporated cells) and the neuronal marker Tbr1. The electroporated cells locate close to the ventral-most part of the cerebral cortex (Ctx). (A-C) A representative section in the control vector group showing the location of the electroporated cells (GFP⁺) and the neurons. The two cell populations do not appear to overlap. (D-F) A representative section in the C-Cdca7 group showing the location of the electroporated cells and the neurons. Similar to the control group, the two cell populations do not overlap (all scale bars: 50µm). These results may suggest that within 16 hours, the electroporated cells have not had enough time to differentiate into post-mitotic neurons at E15.5.

Figure 5.8 shows the abundance of BrdU⁺ cells in the total electroporated GFP⁺ cells at E13.5. The target area for the plasmid delivery was close to the ventral-most part of the dTel, where the expression of Cdca7 is the lowest across the telencephalon. High-magnification images shown in panel B', D' and F' of Figure 5.8 displayed overlapping expressions of BrdU and GFP in the control, N-Cdca7 and the C-Cdca7 groups, respectively. At E13.5, the mean percentage of BrdU incorporation in total GFP⁺ cells was 32% in the control (n=4), 27.7% in the N-Cdca7 (n=3) and 28.6% in the C-Cdca7 groups (n=3) and there were no significant differences between the groups.

At E15.5, the abundance of BrdU⁺ cells in the total population of electroporated GFP⁺ cells is shown in Figure 5.9. Panel A-B and C-D represent embryos receiving the control and the C-Cdca7 plasmid, respectively. A co-expressing pattern of BrdU and GFP can be observed in the high-magnification images in Panel B' and D'. 21.8% and 27.5% of the total electroporated GFP⁺ cells in the control (n=3) and the C-Cdca7 (n=4) group, respectively, were BrdU⁺, there was no significant difference between the groups (P=0.39, Student's t-test). The results of the BrdU incorporation experiment suggest that there is no difference in DNA synthesis nor cell division rate between the control and the Cdca7-overexpressing samples at both E13.5 and E15.5. However, whether there is a difference in the type of cells that undergo DNA synthesis between the two groups remains unclear. It is also unknown if cell cycling duration varies when Cdca7 level is manipulated.

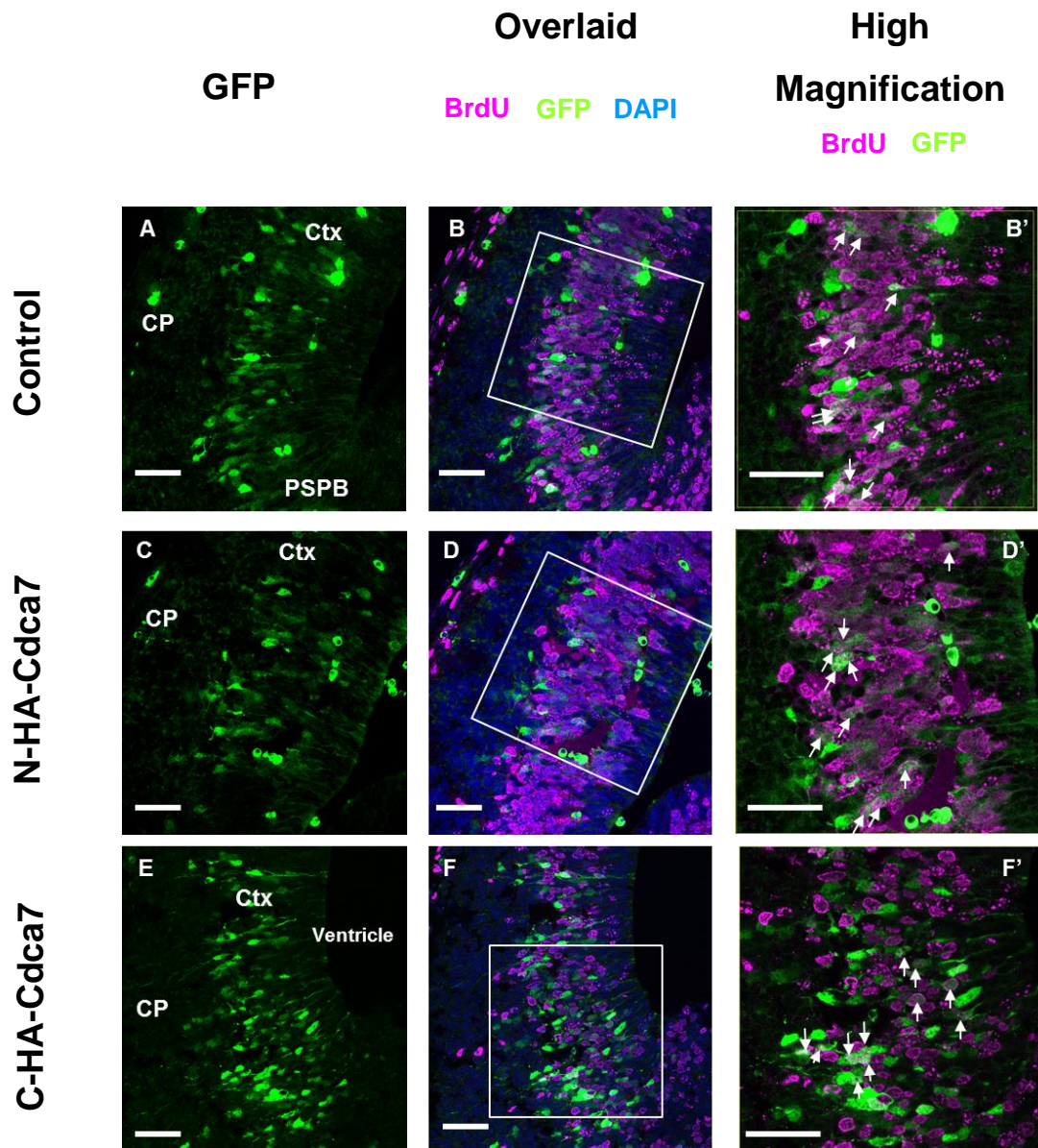


Figure 5.8 Overexpression of Cdca7 at E12.5 does not affect the cell division rate in the cortex.

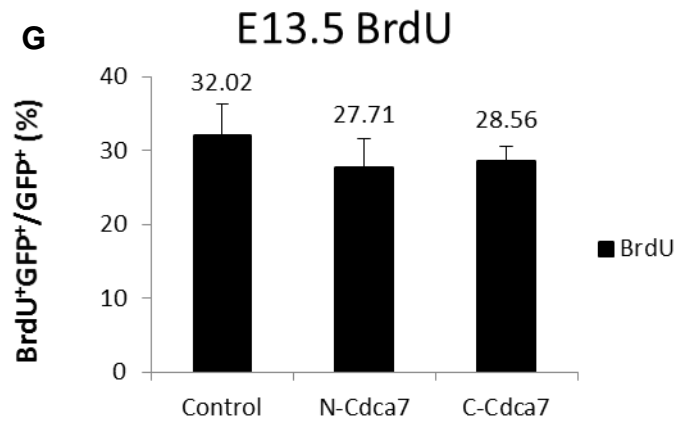


Figure 5.8 Overexpression of Cdca7 at E12.5 does not affect the cell division rate in the cortex.

Embryos electroporated with the control, N-Cdca7 or C-Cdca7 plasmid at E12.5 were collected and processed as described in Figure 5.2B. Fixed and cryo-protected embryos were sectioned and stained using antibodies against BrdU and GFP. BrdU incorporation identifies cells in the DNA synthesis phase or S phase of the cell cycle, while GFP marks the cells receiving the electroporated plasmid. (A,C,E) The electroporated cells locate close to the ventral-most part of the dTel in all three groups. High magnification views in Panel B', D' and F' are enlarged from the 200 μm^2 square area in Panel B, D and F, respectively. (A-B') A representative section in the control group showing the locations of BrdU⁺ and GFP⁺ cells. High magnification image in Panel B' showing cells possessing both BrdU incorporation and GFP expression (indicated by arrows). (C-D') A representative section in the N-Cdca7 group showing the locations of BrdU⁺ and GFP⁺ cells. High magnification image in Panel D' showing cells co-labelled with BrdU and GFP (indicated by arrows). (E-F') A representative section in the C-Cdca7 group showing the locations of BrdU⁺ and GFP⁺ cells. High magnification image in Panel F' showing cells co-labelled with BrdU and GFP (indicated by arrows, all scale bars: 50 μm). (G) Bar chart showing the frequencies of BrdU⁺ cells in the total electroporated cells (GFP⁺) in all three groups, which are 32%, 27.7% and 28.6% in the control (n=4), N-Cdca7 (n=3) and C-Cdca7 (n=3) group, respectively. There is no significant difference between the groups.

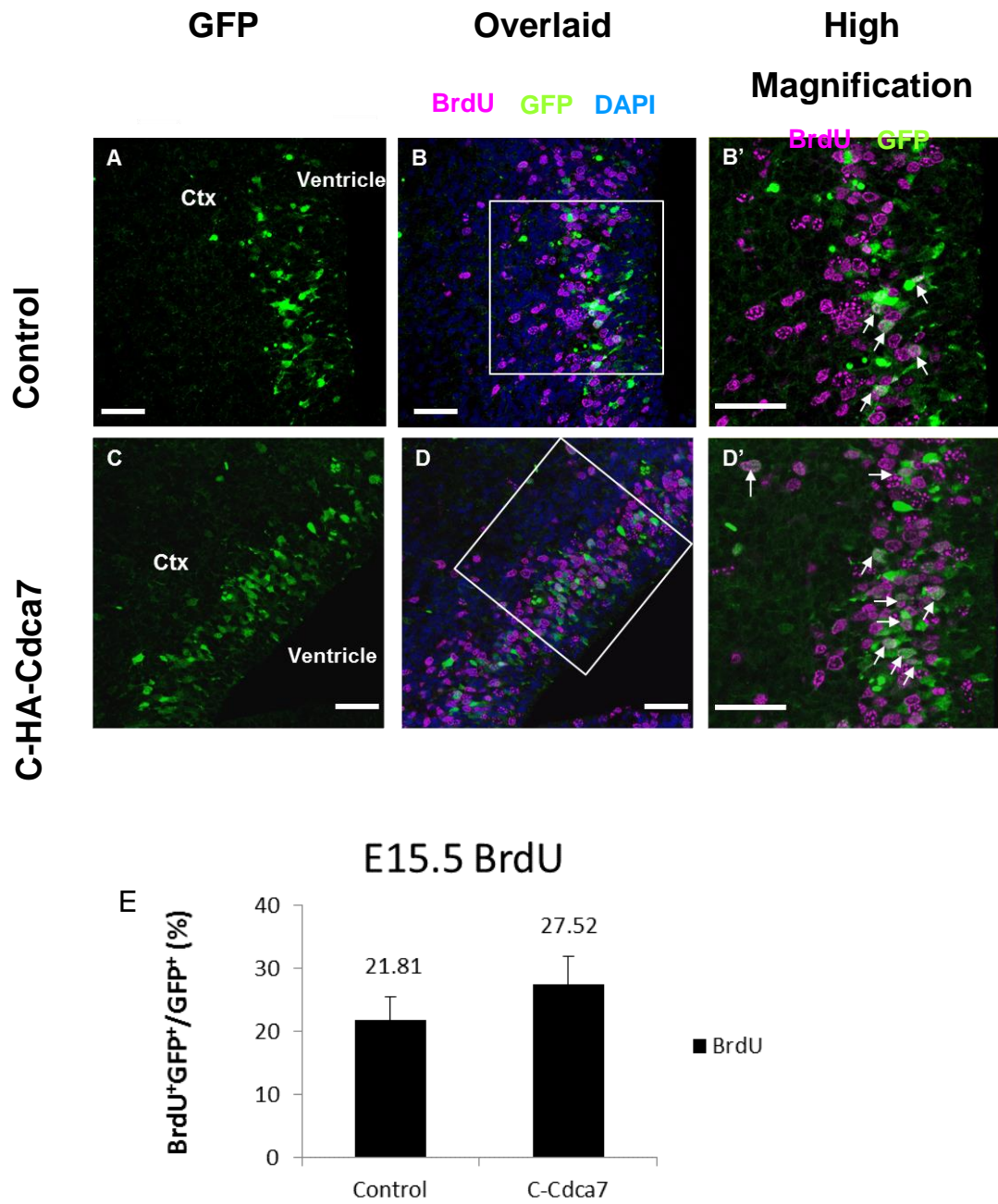


Figure 5.9 Overexpression of Cdca7 at E14.5 does not affect the cell division rate in the cortex.

Figure 5.9 Overexpression of Cdca7 at E14.5 does not affect the cell division rate in the cortex.

Embryos receiving the control or C-Cdca7 plasmid at E12.5 were collected and processed as described in Figure 5.2B. Fixed and cryo-protected embryos were sectioned and stained using antibodies against BrdU and GFP. BrdU incorporation identifies cells in the DNA synthesis phase or S phase of the cell cycle, while GFP marks the cells receiving the electroporated plasmid. (A and C) The GFP⁺ cells locate in the middle part of the cerebral cortex in both groups. High magnification views in Panel B' and D' are enlarged from the 200µm² square in Panel B and D, respectively. (A-B') A representative section in the control group showing the locations of BrdU⁺ and GFP⁺ cells. High magnification image in Panel B' showing cells possessing both BrdU incorporation and GFP expression (indicated by arrows). (C-D') A representative section in the N-Cdca7 group showing the locations of BrdU⁺ and GFP⁺ cells. High magnification image in Panel D' showing cells co-labelled with BrdU and GFP (indicated by arrows, all scale bars: 50µm). (E) Bar chart showing the frequencies of BrdU⁺ cells in the total electroporated cells (GFP⁺) in both groups, which are 21.8% and 27.5% in the control (n=3) and the C-Cdca7 (n=4) group, respectively. There is no significant difference between the groups (P=0.39, Student's t-test.) These results suggest that overexpression of Cdca7 at E14.5 has no effect on the cell division rate.

5.3 Discussion

5.3.1 Tag fusion protein: pros and cons

Recombinant proteins containing a fusion polypeptide or an affinity tag are widely recognised to have several advantages (Terpe, 2003; Waugh, 2005). Common benefits include improved solubility of proteins (Costa et al., 2014; Kapust and Waugh, 1999), ease of protein purification (Einhauer and Jungbauer, 2001; Lichty et al., 2005), increased yield of the recombinant protein (Lee et al., 2008), targeting of the protein to specific cellular locations (Pang et al., 2009) as well as enhanced detection of the protein *in vitro* and *in vivo* (Debeljak et al., 2006; Park et al., 2008). As the main application of this technique is to produce recombinant proteins such as enzymes and drugs in an economic way and at an industrial scale, the fusion tag must not interfere with the structure, function as well as the epitopic recognition of the target protein (Waugh, 2005). Additionally, the tag should also be easily removed by enzymatic cleavage to produce untagged proteins (Walker et al., 1994). There is no single tag sequence that possesses all the advantages, therefore the choice of which tag to use mainly depends on the ultimate purpose of the experiment.

In my experiments, adding a HA tag to the *Cdca7*-expressing cDNA construct was to differentiate the exogenous plasmid-expressed *Cdca7* proteins from the endogenous form and to visualise the co-expression of *Cdca7* and GFP, which are driven by the same vector. The *in vitro* transfection experiment was able to detect the expression of the *Cdca7* fusion protein using an antibody (Sigma) against the HA epitope (Figure 5.2). However the HA-antibody produced by Sigma is pre-conjugated with horseradish peroxidase (HRP) which did not produce specific staining pattern on sections. Therefore another antibody manufactured by Abcam against the HA peptide was used for immunofluorescence staining for samples following the *in utero* electroporation. Unfortunately this new antibody did not detect specific HA expression from either the N-*Cdca7* or the C-*Cdca7* groups (data not shown). This may be a result of the variations between the manufacturers of the antibodies. A previous study has shown that variance in the immunodetection of hexa-His tagged proteins arises from different usage of anti-His antibodies and creates false detection results (Debeljak et al., 2006).

The regulatory role of Pax6 on Cell Division Cycle Associated 7 and cortical progenitor cell proliferation

The main problem raised in my experiment was the different effect on neurogenesis by the two different HA-tagged Cdca7 fusion proteins. It was observed that both N-terminal and C-terminal tagged Cdca7 located in the nucleus and was detected by the Cdca7 polyclonal antibody (Proteintech) (Figure 5.3). This indicates that the addition of the tag sequence does not interfere with the cellular location of Cdca7 protein, as well as the epitope recognition of the anti-Cdca7 antibody. Different tagging positions, such as the N-terminal, C-terminal or within the ORF, have been used widely in other proteins and some tagging-related issues have been identified. A previous study has reported that an N-terminal tag affected the expression as well as the subcellular localisation of the fusion protein while the C-terminal tagged fusion protein appeared to be normal (Palmer and Freeman, 2004). Another report has also shown that C-terminal His tag sequence has influences on the folding property of β -lactamase in the thermophilic *Bacillus licheniformis* (Ledent et al., 1997). Although many studies have claimed that the HA-tag sequence does not interfere with the function of the fusion protein (Indraccolo et al., 2002; Lu et al., 2009; Surdej and Jacobs-Lorena, 1994), there are also evidences showing that adding a short HA peptide to the fusion protein has impacts on its cellular localisation (Houle et al., 2006), protein folding as well as its functions (Brothers et al., 2003; Seamon et al., 2000; Young et al., 2012). A possible explanation for the discrepancy between the two tagged forms of Cdca7 in my experiment is that the N-terminal HA tag may cause a folding problem which prevents the normal functions of Cdca7 to be exerted. Further studies using protein folding prediction and crystallography are required to fully understand the differences between the two forms.

5.3.2 Comparison of progenitor behaviours in *Pax6*^{Sey/Sey} and *wild-type* with Cdca7 overexpression

Pax6 was thought to negatively regulate *Cdca7* expression based on the mRNA expression patterns of two genes (Chapter 3) as well as the up-regulated *Cdca7* expression in *Pax6*^{Sey/Sey} mice and Pax6 conditional knock-out mice (Manuel, unpublished). It is known that Pax6 regulates the length of the cell cycle in a dose-dependent fashion in the cortex, therefore the shortening of total cycle duration of the progenitors in areas with high or moderate levels of Pax6 expression should be

The regulatory role of Pax6 on Cell Division Cycle Associated 7 and cortical progenitor cell proliferation affected by the absence of Pax6 (Mi et al., 2013). It has also been observed that the production of neurons from E12.5 to E15.5 is insufficient in *Pax6^{Sey/Sey}* mice (Estivill-Torrus et al., 2002).

The dynamics of *Cdca7* and *Pax6* expression have been described in Chapter 3 and the PSPB is the location where the highest *Pax6* expression and the weakest *Cdca7* expression are found in the telencephalon. Therefore in this chapter the target region for *Cdca7* overexpression is close to the ventral-most part of the dTel, close to the PSPB. *Cdca7* overexpression in the *wild-type* cortex, which mimics the upregulation of *Cdca7* in *Pax6^{Sey/Sey}*, was able to reduce the production of IPCs and post-mitotic neurons at E12.5-E13.5 in mice. These results suggest that *Cdca7* is one of the Pax6 downstream factors which facilitate cell cycle progression. Although the BrdU incorporation experiments demonstrated that there was no difference in the rate of cell division between the control and the *Cdca7*-overexpressing groups, the exact cell populations which undergo cell division in different groups may be different as it is known that cell cycle durations are diverse between cell types (Roccio et al., 2013). It is not clear if the length and progression through the cell cycle in neural progenitors change between the control and the *Cdca7*-overexpressed groups. There is no direct evidence showing how *Cdca7* may modulate the length of G1 phase as well as total cell cycle. One study claims that the elongated G1 is not sufficient to facilitate differentiation in murine embryonic stem cells (ESCs) (Li et al., 2012). As discussed previously, regulation of G1 length is well recognised as a key factor for progenitors to select between proliferation and differentiation (Calegari andHuttner, 2003; Götz andHuttner, 2005). In the future, manipulation of *Cdca7* levels in the progenitors, followed by identification of changes in the cell cycle kinetics by cumulative BrdU injection or with the Fucci method may provide further mechanistic details of how *Cdca7* affects neural development.

5.3.3 Effects of *Cdca7* overexpression in the mid-neurogenesis

Cdca7 overexpression early in corticogenesis reduced not only the production of Tbr2⁺ intermediate progenitors but also the production of Tbr1⁺ cells. Division of Tbr2⁺ cells generate Tbr1⁺ neuronal precursors early in corticogenesis. The average length of cell cycle in the cerebral cortex is around 10h at E12.5, which is a few

The regulatory role of Pax6 on Cell Division Cycle Associated 7 and cortical progenitor cell proliferation hours shorter than the 16h between electroporation and sacrifice in our experiments (Caviness et al., 1995; Takahashi et al., 1995). It seems likely, therefore, that the expression plasmid entered some cells that had already started to move to the subventricular zone, where they underwent a further division to produce Tbr1⁺ neuronal precursors. At later time point in this experiment, all observed electroporated cells (GFP⁺) were scattered in the VZ or SVZ but none of them have migrated to the mentle zone, where Tbr1⁺ resided. The average length of cell cycle in the cerebral cortex at E15.5 is approximately 16 hours, same as the duration from electroporation to the end point sacrifice (Takahashi et al., 1995). Since the expression of the plasmids commences approximately 6 hours following the electroporation (data not shown), ending the experiment too early may prevent the overexpressed Cdca7 from affecting the production of neurons, since progenitors would have no time to complete a single cell cycle. Pilot study has demonstrated at E14.5 that many electroporated cells migrated into the mentle zone 48 hours after electroporation, and at E15.5 the majority of electroporated cells were still located in the VZ/SVZ (data not shown) 36 hours after electroporation. In order to understand the function of Cdca7 in the production of post-mitotic neurons, a longer time frame, between 36 to 48 hours, should be used for the experiment. It should be noted that Cdca7 may also influence direct neurogenesis in early and mid-neurogenesis. Mixture of neuron production from both direct and indirect neurogenesis may be observed by leaving the Cdca7 expression plasmid *in vivo* longer than the duration for two or more cycling time, which could mask the effect of Cdca7 on direct neurogenesis.

In summary, the data suggest that overexpressed Cdca7 downregulated the production of intermediate progenitors and post-mitotic neurons at early neurogenesis (E12.5) but not at mid-neurogenesis (E14.5). This effect is not achieved by an overall alteration in proliferation. More likely it is caused by a change in the fates of the cells exposed to elevated Cdca7 levels.

Chapter 6 : General Discussion

6.1 Summary

Cdca7 has been thought to be a Pax6 downstream target which may be involved in Pax6-related cell cycle regulation in cortical progenitors. The mRNA expression pattern of *Cdca7* forms a gradient which is high medio-caudally and low latero-rostrally, opposite to the pattern of *Pax6* in both *wild-type* and *PAX77* dTel during early corticogenesis (E12.5-E13.5) in mice. However the *Cdca7* gradient is lost in the *Pax6^{Sey/Sey}* mutants. The medial^{high} to lateral^{low} gradient of *Cdca7* is also seen at the protein level and the expression of *Cdca7* is very weak at the PSPB, where the highest protein level of Pax6 is present.

Figure 6.1 summarises how Pax6 regulates the proliferation of cortical progenitors through control of cell cycle kinetics. In *wild-type*, Pax6 inhibits Cdk6 expression by directly binding to the *Cdk6* promoter. This inhibition reduces the phosphorylation level of Rb and therefore restrains E2f1 from promoting G1/S checkpoint transition. In *Pax6^{Sey/Sey}* mutants where no functional Pax6 protein is present, inhibition of Cdk6 by Pax6 is lost and the phosphorylation level of Rb is upregulated. The consequential loss of binding affinity between hyperphosphorylated Rb and E2f1 enables freed E2f1 to enter the nucleus and trigger transcription of its downstream targets. It has been observed that the duration of G1 phase as well as total cell cycle length are shorter in *Pax6* null mutants than in *wild-type* (Mi et al., 2013). It is also known that both the mRNA and protein levels of *Cdca7* are upregulated in *Pax6*-null mutants (Mi et al. 2013; Chapter 3; Martine Manuel unpublished). My ChIP validation experiment in Chapter 4 has demonstrated that the *Cdca7* proximal promoter is unlikely to be bound by Pax6, suggesting no direct control of *Cdca7* production by Pax6, at least through this promoter region. However my experiments have not ruled out the possibility of Pax6 binding motifs located within or downstream the *Cdca7* genomic locus or in the distal regulatory elements far upstream to the *Cdca7* TSS site. Further validations of potential Pax6 binding motifs in these regions are required to fully understand the regulatory role of Pax6 on *Cdca7* gene expression.

As shown by the luciferase assays described in Chapter 4, Pax6 is capable of inhibiting the activity of the *Cdca7* promoter, indicating an effect of Pax6 on *Cdca7*

The regulatory role of Pax6 on Cell Division Cycle Associated 7 and cortical progenitor cell proliferation transcription. Together these results point to a possibility that Pax6 indirectly controls Cdca7 via the Cdk6-Rb/E2f1 pathway, which eventually results in alteration of the cell cycle in neural progenitors. Overexpression of Cdca7 by *in utero* electroporation in mouse embryos leads to a decrease of IPCs and post-mitotic neurons during early neurogenesis, implying that the function of Cdca7 *in vivo* is to inhibit differentiation or to maintain the proliferative status of RGCs. However it remains elusive whether the downregulation of neuron differentiation is directly caused by the increased Cdca7 in RGCs and IPCs, or indirectly by the reduced production of IPCs in the overexpression model.

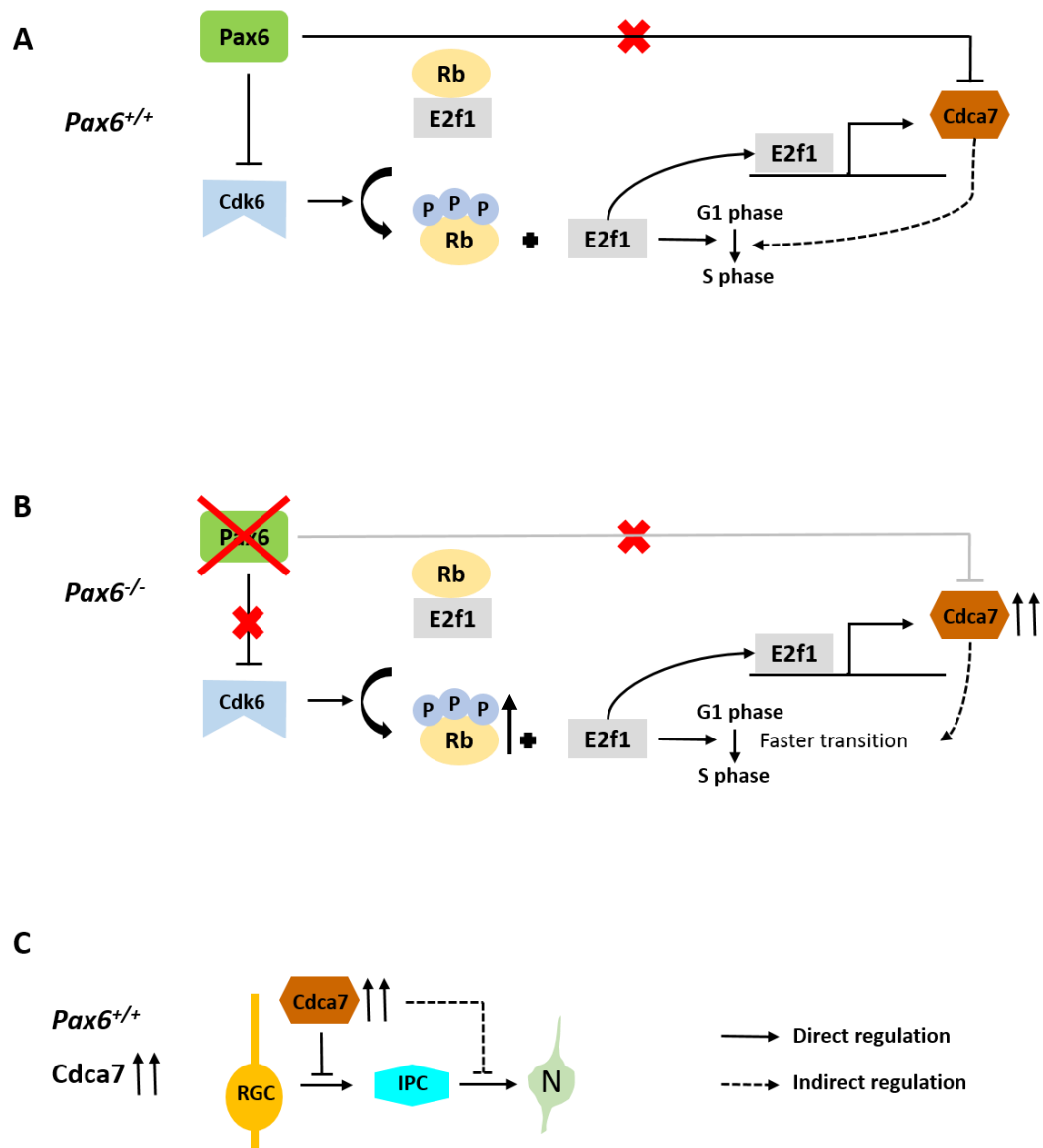


Figure 6.1 The function of *Cdca7* in the Pax6-mediated regulation of cell cycle progression.

Figure 6.1 The function of Cdca7 in the Pax6-mediated regulation of cell cycle progression.

Schematic diagrams showing the progression of cell cycle under three different physiological conditions. (A) In *wild-type*, through inhibition of the Cdk6 production, Pax6 controls the phosphorylation level of Rb, which further modulates the activity of E2f1 and G1/S checkpoint transition (Mi et al., 2013). It was hypothesised that Pax6 directly regulates Cdca7, but the ChIP validation in Chapter 4 suggests that direct regulation is less likely; instead the regulatory role of Pax6 may be mainly through the Cdk6-Rb/E2f1 pathway. Cdca7 is a known direct target of E2f1, suggesting it may facilitate G1/S transition. (B) In *Pax6^{Sev/Sev}* where no functional Pax6 protein is produced, the dysregulation of Cdk6 results in an increased level of Rb phosphorylation, which correlates with the increased free E2f1 as well as activation of E2f1-downstream targets such as *Cdca7*. It is also noted that the duration of G1 phase and total cell cycle length is shortened at E12.5 in *Pax6^{Sev/Sev}* embryos (Mi et al., 2013). (C) Overexpression of Cdca7 by *in utero* electroporation in mouse embryos results in decreased IPCs and post-mitotic neurons. However it is not clear whether the downregulation of neuron production is directly due to the role of Cdca7 on neuron differentiation, or indirectly caused by the reduced number of IPCs (Chapter 5).

6.2 The role of *Cdca7* in relation to proliferation and differentiation of progenitors remains unclear

CDCA7/*Cdca7* has been identified as a direct target of several transcription factors including c-MYC, E2f1 and Ascl1, as well as a downstream modulator of Notch signalling (Castro et al., 2011; Goto et al., 2006; Guiu et al., 2014; Osthus et al., 2005), suggesting that the regulation of *Cdca7* is complicated and interactions between factors/pathways are likely to occur.

To understand the importance of E2f factors during mouse development, various knockout (KO) strains have been developed (Chen et al., 2009; Ciemerych and Sicinski, 2005). *E2f1*-deficient mice are viable and fertile but suffer with testicular atrophy and increased incidence of tumours (Yamasaki et al., 1996). Mice with double KO in *E2f1/E2f2* can also progress into viable adulthood but develop insulin-deficient diabetes (Iglesias et al., 2004; Li et al., 2003). Moreover, the double mutant possesses an accumulated population of haematopoietic progenitors in S phase, suggesting a defective cell cycle when cells lack E2f1 and E2f2 (Iglesias et al., 2004; Li et al., 2003). Additionally, *in vitro* evidence has proved that triple KO of *E2f1-3* results in cell cycle arrest in embryonic fibroblasts through activation of the p53-p21 pathway (D.Chen et al., 2009; Chong et al., 2009). Specific triple KO of *E2f1-3* in retinal progenitors causes no developmental defects in lens during embryonic stages but the mice experience massive apoptosis and collapse of lens at P16 (Wenzel et al., 2011). It is therefore suggested that E2f1-3 are not necessary for proliferation of progenitors but are instead important for the survival of post-mitotic cells. However a contradictory study shows the level of E2f1 is downregulated in differentiated oligodendrocytes compared to that in oligodendrocyte progenitor cells in murine white matter tracts (Magri et al., 2014). It is well accepted that the activation of E2f1 facilitates G1/S transition, which links the gene to cell cycle progression. However the function of E2f1 in cortical progenitors has not been fully elucidated.

MYC is a known oncoprotein and is often upregulated in several tumours. c-Myc and N-Myc (*Mycn*) are expressed in the neural progenitors in a mutually exclusive pattern, with N-Myc in progenitors and c-Myc in differentiating neurons in mouse

The regulatory role of Pax6 on Cell Division Cycle Associated 7 and cortical progenitor cell proliferation cortex (Zinin et al. 2014; www.genepaint.org). In relation to neuronal proliferation and differentiation, both c-Myc and N-Myc possess mitogenic roles as *c-Myc/N-Myc* double KO in mouse results in a smaller brain, especially the cerebellum (Wey et al., 2010). The double KO mice are also characterised by reduced cerebellar granule neural progenitors and granule neurons, while other neuron types including astroglia, oligodendrocytes, and Purkinje neurons are increased. This finding indicates that the role of Myc proteins is more specific to the maintenance of the proliferative state of cerebellar granule neural progenitors (Wey et al., 2010). Other evidence has also proven that c-Myc co-operatively regulates neural stem cell progression with the tumour suppressor p19^{ARF}. In the early embryonic stage, around E13.5, neural stem cells (NSCs) are highly self-proliferative and low in p19^{ARF} expression; while at later stages, around E18.5, NSCs exhibit less self-proliferation and favour gliogenesis (Nagao et al., 2008). Overexpressed c-Myc protein or reduced p19^{ARF} activity in the late embryonic stage causes NSCs to retain their self-renewal and high neurogenic capacity, while *wild-type* NSCs normally prefer gliogenesis. In contrast, forced expression of p19^{ARF} and inactivation of c-Myc in the early stage leads to premature gliogenesis in the NSC population (Nagao et al., 2008). These studies support the role of c-Myc as mitogenic and promoting proliferation in stem cells. However, a recent study performed in chick embryos has demonstrated that MYC protein can promote neural differentiation by controlling the mode of cell division or cleavage plane and inhibiting Notch signalling. This neurogenic effect was further discovered to be dependent on the integrity of tissues as MYC has mitogenic function in dissociating RGCs (Zinin et al., 2014). Therefore, it should be noted that Myc protein exerts different functions *in vivo* and *in vitro*, likely due to its engagement with different downstream signalling pathways.

Taken together, since *Ascl1* is not expressed in the dTel and none of *E2f1*, *c-Myc* and *N-Myc* mRNA are expressed in a gradient pattern (Guillemot and Joyner, 1993; Lo et al., 1991 ; www.genepaint.org), the cause of *Cdca7* graded expression remains unknown. Besides, the function of *Cdca7* during neural development may be stage-dependent since overexpression of *Cdca7* at E14.5-15.5 did not alter the differentiation of progenitors (Chapter 5). It is still believed that *Cdca7* is negatively regulated by Pax6, as their expression patterns are mutually exclusive at both mRNA

The regulatory role of Pax6 on Cell Division Cycle Associated 7 and cortical progenitor cell proliferation and protein levels, but the mechanism behind the inhibition may be indirect. Whether the regional effects exerted by Pax6 on progenitor progression involves Cdca7 is still poorly understood.

Figure 6.2 illustrates the current understanding of factors that influence Cdca7 expression. The role of c-Myc is controversial as it may drive differentiation by downregulating Notch signalling or promote proliferation. Notch signalling has been found to maintain the stemness of haematopoietic cells in the presence of Cdca7 (Guiu et al., 2014). In the dTel at E12.5-E13.5, Pax6 inhibits the production of Cdk6 and thereby inactivates the function of E2f1, which accelerates cell cycle progression (Mi et al., 2013), and its downstream target Cdca7, which inhibits differentiation. It should be noted that the regulation of progenitor behaviour is both context and stage-dependent. Therefore based on the results from current and previous studies, Cdca7 is an indirect target of Pax6 and both accelerates cell cycle progression in RGCs and inhibits differentiation of RGCs into IPCs in the dTel during E12.5-E13.5.

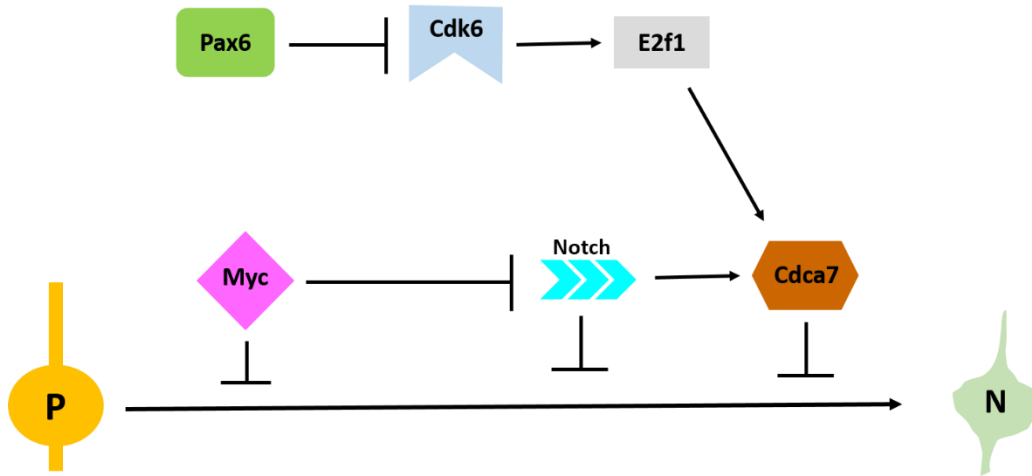


Figure 6.2 Current understanding of Cdca7 during the differentiation process from progenitors to neurons.

This summary diagram is based on findings in mouse cortex from E12.5 to E13.5, during which Pax6 negatively regulates Cdca7 through directly inhibiting Cdk6 expression. Cdca7 has been found to prevent the production of IPCs and neurons. Furthermore, Cdca7 is also controlled by Notch signalling which is essential for the maintenance of haematopoietic stem cells in the presence of Cdca7. Myc can promote both proliferation and neurogenesis and its functions needs to be precisely dissected in a spatial, temporal, and context-specific manner.

6.3 The relationship between Pax6 expression levels and neurogenesis

Pax6 is highly expressed in RGCs and downregulated in IPCs in developing cortex (Englund et al., 2005). The sequential expression of Pax6 → Ngn2 → Tbr2 markers from RGCs to IPCs has also been identified during corticogenesis (Englund et al., 2005; Scardigli et al., 2003). The sequence of development of the cortex, which commences rostromedially and ends caudomedially, correlates with the gradients of Pax6 and Tbr2 expression (Bulfone et al., 1999; Mutch et al., 2010). This further supports the finding that the regional effects exerted by Pax6 are essential for regional identity (Mi et al., 2013). The dynamic pattern of Pax6 expression during neurogenesis has been found to correlate with proliferation and cell fate decisions of retinal progenitors (Hsieh and Yang, 2009), in which Pax6 is highly expressed during preneurogenic proliferation. During neurogenic division in retinal progenitors, Pax6 is downregulated from G1 to S phase, cells then either regain Pax6 expression upon entry into G2/M phase and differentiate into retinal ganglion cells or amacrine cells, or lose their Pax6 expression and differentiate into cone photoreceptors (Hsieh and Yang, 2009). Additionally, Pax6 activates the expression of Ngn2, whose level oscillates during cell cycle progression (Shimojo et al., 2008). Several important questions remain to be addressed by future studies: 1) whether the level of Pax6 affects cell fate decision in the cortex as seen in the retina; 2) whether the level of Pax6 also oscillates during cell cycle progression; 3) is the graded expression of Pax6 in the dTel involved in the fate decisions; 4) does Cdca7, being a direct target of Notch signalling, also oscillate and facilitate the process of progenitor differentiation?

To answer whether Pax6 and Cdca7 oscillate during cell cycle progression, developing cortex from *wild-type* embryos can be dissected and separated into rostral and caudal parts followed by single cell dissociation. Isolated cortical cells can be co-labelled with a DNA marker, Hoechst, and sent for Fluorescence-activated cell sorting (FACS) analysis to look for correlations between the expression level of Pax6, Cdca7 and DNA content. After analysis, cells with differential levels of Pax6 or Cdca7 can be sorted and further maintained in an *in vitro* culture system to observe the neural differentiation process.

The regulatory role of Pax6 on Cell Division Cycle Associated 7 and cortical progenitor cell proliferation. To understand whether Pax6 is important for cell fate decisions in cortical progenitor cells, the *Tis21-GFP* transgenic mouse can be a suitable model (Haubensak et al., 2004). *Tis21* has been identified as an anti-proliferative marker expressed in progenitors that have committed to the neurogenic fate and also in progenitor-derived neurons (Iacopetti et al., 1999). In addition, all early-born neurons derive from *Tis21-GFP* cells and the majority of *Tis21*⁺ IPC-derived cells in developing cortex express neuronal features (Attardo et al., 2008; Haubensak et al., 2004). To utilise this model I would first cross the *Tis21-GFP* line with the *Pax6*^{Sey/+} line. *Pax6*^{+/+} *Tis21-GFP*⁺ cortex tissues can be dissected into rostral and caudal parts and dissociated as previous described. It is expected that cells with high levels of Pax6 should be low in *Tis21*, but it is unknown whether this correlation differs between cortex regions (Kowalczyk et al., 2009; Wong et al., 2015). In addition, overexpression of Pax6 by *in utero* electroporation in the lateral cortex in *Pax6*^{Sey/Sey} *Tis21-GFP*⁺ embryos can also provide insights into Pax6 function during neurogenic process. Tissue samples can be processed as previously described after the electroporation to validate if overexpression of Pax6 can rescue the phenotypes of the *Pax6*^{Sey/Sey} mutant.

Another transgenic model, the Fucci mouse, is a convenient tool for studying cell cycle progression. Cells from Fucci mice contain red fluorescence (RFP protein) in G1 phase and green fluorescence (GFP protein) in other phases of the cell cycle (Sakaue-Sawano et al., 2008). When coupled with siRNA-mediated regional knockdown of Pax6 by *in utero* electroporation, the Fucci model would allow us to detect differences in the length of G1 between *Pax6*^{+/+} and Pax6-inhibited cells through time-lapse imaging.

The experiments planned above will allow us to visualise the expression level of Pax6 during different phases of the cell cycle, and also to understand whether Pax6 possesses regulatory roles in G1 duration. By bridging these findings, it is hoped that the molecular mechanisms linking cell cycle regulation and the decision between proliferative and differentiative division in neural progenitor cells can be further deciphered.

References

- Anderson, S., Mione, M., Yun, K., Rubenstein, J.L., 1999. Differential origins of neocortical projection and local circuit neurons: role of Dlx genes in neocortical interneuronogenesis. *Cereb. Cortex* 9, 646–54.
- Attardo, A., Calegari, F., Haubensak, W., Wilsch-Bräuninger, M., Huttner, W.B., 2008. Live imaging at the onset of cortical neurogenesis reveals differential appearance of the neuronal phenotype in apical versus basal progenitor progeny. *PLoS One* 3, e2388. doi:10.1371/journal.pone.0002388
- Babaei, S., Mahfouz, A., Hulsman, M., Lelieveldt, B.P.F., deRidder, J., Reinders, M., Gerstein, M., Kundaje, A., Hariharan, M., Dong, X., Li, C., Chen, Y., Ding, G., Li, Y., Homouz, D., Kudlicki, A., Lan, X., Witt, H., Katsumura, K., Ye, Z., Wang, Q., Jin, F., Li, Y., Dixon, J., Selvaraj, S., Ye, Z., Botta, M., Haider, S., Leung, I., Lio, P., Mozziconacci, J., Rieder, D., Trajanoski, Z., McNally, J., Shen, Y., Yue, F., McCleary, D., Ye, Z., Edsall, L., Schoenfelder, S., Sexton, T., Chakalova, L., Cope, N., Horton, A., Papantonis, A., Cook, P., Dekker, J., Marti-Renom, M., Mirny, L., Lieberman-Aiden, E., Berkum, N.van, Williams, L., Imakaev, M., Kalhor, R., Tjong, H., Jayathilaka, N., Alber, F., Chen, L., Chen, D., Fu, L., Zhang, Z., Li, G., Zhang, H., Sandhu, K., Li, G., Poh, H., Quek, Y., Sia, Y., Boulos, R., Arneodo, A., Jensen, P., Audit, B., Winterbach, W., Mieghem, P.Van, Reinders, M., Wang, H., Ridder, D.de, Estrada, E., Bass, J.F., Diallo, A., Nelson, J., Soto, J., Myers, C., Ma, H., Zhao, X., Yuan, Y., Zeng, A., Hulsman, M., Dimitrakopoulos, C., Ridder, J.de, Liu, Z., Yan, S., Walker, J., Jiang, T., Menashe, I., Grange, P., Larsen, E., Banerjee-Basu, S., Mitra, P., Lein, E., Hawrylycz, M., Ao, N., Ayres, M., Yaffe, E., Tanay, A., Wit, E.de, Laat, W.de, Dixon, J., Selvaraj, S., Yue, F., Kim, A., Li, Y., Paulsen, J., Lien, T., Sandve, G., Holden, L., Borgan, O., Duan, Z., Andronescu, M., Schutz, K., McIlwain, S., Kim, Y., Babaei, S., Hulsman, M., Reinders, M., Ridder, J.de, Babaei, S., Akhtar, W., Jong, J.de, Reinders, M., Ridder, J.de, Maaten, L., Hinton, G., Heintzman, N., Ren, B., Imakaev, M., Fudenberg, G., McCord, R., Naumova, N., Goloborodko, A., Dong, H., Swanson, L., Chen, L., Fanselow, M., Toga, A., Grange, P., Bohland, J., Okaty, B., Sugino, K., Bokil,

The regulatory role of Pax6 on Cell Division Cycle Associated 7 and cortical progenitor cell proliferation
H., French, L., Pavlidis, P., Wolf, L., Goldberg, C., Manor, N., Sharan, R.,
Ruppin, E., Ji, S., Fakhry, A., Deng, H., Fakhry, A., Ji, S., Ronan, J., Wu, W.,
Crabtree, G., 2015. Hi-C Chromatin Interaction Networks Predict Co-
expression in the Mouse Cortex. *PLOS Comput. Biol.* 11, e1004221.
doi:10.1371/journal.pcbi.1004221

Bachler, M., Neubüser, A., 2001. Expression of members of the Fgf family and their
receptors during midfacial development. *Mech. Dev.* 100, 313–316.
doi:10.1016/S0925-4773(00)00518-9

Barski, A., Cuddapah, S., Cui, K., Roh, T.-Y., Schones, D.E., Wang, Z., Wei, G.,
Chepelev, I., Zhao, K., 2007. High-Resolution Profiling of Histone
Methylations in the Human Genome. *Cell* 129, 823–837.
doi:10.1016/j.cell.2007.05.009

Bartek, J., Lukas, J., 2001. Pathways governing G1/S transition and their response to
DNA damage. *FEBS Lett.* 490, 117–122. doi:10.1016/S0014-5793(01)02114-7

Bel-Vialar, S., Medevielle, F., Pituello, F., 2007. The on/off of Pax6 controls the
tempo of neuronal differentiation in the developing spinal cord. *Dev. Biol.* 305,
659–73. doi:10.1016/j.ydbio.2007.02.012

Bishop, K.M., Goudreau, G., O’Leary, D.D., 2000. Regulation of area identity in the
mammalian neocortex by Emx2 and Pax6. *Science* 288, 344–9.

Blais, A., Dynlacht, B.D., 2007. E2F-associated chromatin modifiers and cell cycle
control. *Curr. Opin. Cell Biol.* 19, 658–62. doi:10.1016/j.ceb.2007.10.003

Brothers, S.P., Janovick, J.A., Conn, P.M., 2003. Unexpected effects of epitope and
chimeric tags on gonadotropin-releasing hormone receptors: implications for
understanding the molecular etiology of hypogonadotropic hypogonadism. *J.*
Clin. Endocrinol. Metab. 88, 6107–12. doi:10.1210/jc.2003-031047

Bulfone, A., Martinez, S., Marigo, V., Campanella, M., Basile, A., Quaderi, N.,
Gattuso, C., Rubenstein, J.L.R., Ballabio, A., 1999. Expression pattern of the
Tbr2 (Eomesodermin) gene during mouse and chick brain development. *Mech.*
Dev. 84, 133–138. doi:10.1016/S0925-4773(99)00053-2

Bulyk, M.L., 2003. Computational prediction of transcription-factor binding site

The regulatory role of Pax6 on Cell Division Cycle Associated 7 and cortical progenitor cell proliferation locations. *Genome Biol.* 5, 201. doi:10.1186/gb-2003-5-1-201

- Calegari, F., Huttner, W.B., 2003. An inhibition of cyclin-dependent kinases that lengthens, but does not arrest, neuroepithelial cell cycle induces premature neurogenesis. *J Cell Sci* 116, 4947–4955. doi:10.1242/jcs.00825116/24/4947 [pii]
- Carney, R.S.E., Cocas, L.A., Hirata, T., Mansfield, K., Corbin, J.G., 2009. Differential regulation of telencephalic pallial-subpallial boundary patterning by Pax6 and Gsh2. *Cereb. Cortex* 19, 745–59. doi:10.1093/cercor/bhn123
- Castro, D.S., Martynoga, B., Parras, C., Ramesh, V., Pacary, E., Johnston, C., Drechsel, D., Lebel-Potter, M., Garcia, L.G., Hunt, C., Dolle, D., Bithell, A., Ettwiller, L., Buckley, N., Guillemot, F., 2011. A novel function of the proneural factor *Ascl1* in progenitor proliferation identified by genome-wide characterization of its targets. *Genes Dev* 25, 930–945. doi:10.1101/gad.62781125/9/930 [pii]
- Caviness, V.S., Takahashi, T., Nowakowski, R.S., 1995. Numbers, time and neocortical neuronogenesis: a general developmental and evolutionary model. *Trends Neurosci.* 18, 379–83.
- Chen, D., Pacal, M., Wenzel, P., Knoepfler, P.S., Leone, G., Bremner, R., 2009. Division and apoptosis of E2f-deficient retinal progenitors. *Nature* 462, 925–9. doi:10.1038/nature08544
- Chen, H.-Z., Tsai, S.-Y., Leone, G., 2009. Emerging roles of E2Fs in cancer: an exit from cell cycle control. *Nat. Rev. Cancer* 9, 785–97. doi:10.1038/nrc2696
- Chittenden, T., Livingston, D.M., Kaelin, W.G., 1991. The T/E1A-binding domain of the retinoblastoma product can interact selectively with a sequence-specific DNA-binding protein. *Cell* 65, 1073–1082. doi:10.1016/0092-8674(91)90559-H
- Chong, J.-L., Wenzel, P.L., Sáenz-Robles, M.T., Nair, V., Ferrey, A., Hagan, J.P., Gomez, Y.M., Sharma, N., Chen, H.-Z., Ouseph, M., Wang, S.-H., Trikha, P., Culp, B., Mezache, L., Winton, D.J., Sansom, O.J., Chen, D., Bremner, R., Cantalupo, P.G., Robinson, M.L., Pipas, J.M., Leone, G., 2009. E2f1-3 switch from activators in progenitor cells to repressors in differentiating cells. *Nature*

- Ciemerych, M.A., Sicinski, P., 2005. Cell cycle in mouse development. *Oncogene* 24, 2877–2898. doi:1208608 [pii]10.1038/sj.onc.1208608
- Costa, S., Almeida, A., Castro, A., Domingues, L., 2014. Fusion tags for protein solubility, purification and immunogenicity in *Escherichia coli*: the novel Fh8 system. *Front. Microbiol.* 5, 63. doi:10.3389/fmicb.2014.00063
- Coutinho, P., Pavlou, S., Bhatia, S., Chalmers, K.J., Kleinjan, D.A., vanHeyningen, V., 2011. Discovery and assessment of conserved Pax6 target genes and enhancers. *Genome Res.* 21, 1349–59. doi:10.1101/gr.124115.111
- Czerny, T., Schaffner, G., Busslinger, M., 1993. DNA sequence recognition by Pax proteins: bipartite structure of the paired domain and its binding site. *Genes Dev.* 7, 2048–61.
- Debeljak, N., Feldman, L., Davis, K.L., Komel, R., Sytkowski, A.J., 2006. Variability in the immunodetection of His-tagged recombinant proteins. *Anal. Biochem.* 359, 216–23. doi:10.1016/j.ab.2006.09.017
- Dekker, J., Marti-Renom, M.A., Mirny, L.A., 2013. Exploring the three-dimensional organization of genomes: interpreting chromatin interaction data. *Nat. Rev. Genet.* 14, 390–403. doi:10.1038/nrg3454
- Dermitzakis, E.T., Clark, A.G., 2002. Evolution of Transcription Factor Binding Sites in Mammalian Gene Regulatory Regions: Conservation and Turnover. *Mol. Biol. Evol.* 19, 1114–1121. doi:10.1093/oxfordjournals.molbev.a004169
- Díaz-Alonso, J., Aguado, T., deSalas-Quiroga, A., Ortega, Z., Guzmán, M., Galve-Roperh, I., 2014. CB1 Cannabinoid Receptor-Dependent Activation of mTORC1/Pax6 Signaling Drives Tbr2 Expression and Basal Progenitor Expansion in the Developing Mouse Cortex. *Cereb. Cortex* 25, 2395–408. doi:10.1093/cercor/bhu039
- Dixon, J.R., Selvaraj, S., Yue, F., Kim, A., Li, Y., Shen, Y., Hu, M., Liu, J.S., Ren, B., 2012. Topological domains in mammalian genomes identified by analysis of chromatin interactions. *Nature* 485, 376–380. doi:10.1038/nature11082

- The regulatory role of Pax6 on Cell Division Cycle Associated 7 and cortical progenitor cell proliferation
Duncan, M.K., Haynes, J.I., Cvekl, A., Piatigorsky, J., 1998. Dual roles for Pax-6: a transcriptional repressor of lens fiber cell-specific beta-crystallin genes. *Mol. Cell. Biol.* 18, 5579–86.
- Einhauer, A., Jungbauer, A., 2001. The FLAGTM peptide, a versatile fusion tag for the purification of recombinant proteins. *J. Biochem. Biophys. Methods* 49, 455–465. doi:10.1016/S0165-022X(01)00213-5
- Englund, C., Fink, A., Lau, C., Pham, D., Daza, R.A.M., Bulfone, A., Kowalczyk, T., Hevner, R.F., 2005. Pax6, Tbr2, and Tbr1 are expressed sequentially by radial glia, intermediate progenitor cells, and postmitotic neurons in developing neocortex. *J. Neurosci.* 25, 247–51. doi:10.1523/JNEUROSCI.2899-04.2005
- Enriquez-Harris, P., Levitt, N., Briggs, D., Proudfoot, N.J., 1991. A pause site for RNA polymerase II is associated with termination of transcription. *EMBO J.* 10, 1833–42.
- Epstein, J., Cai, J., Glaser, T., Jepeal, L., Maas, R., 1994. Identification of a Pax paired domain recognition sequence and evidence for DNA-dependent conformational changes. *J. Biol. Chem.* 269, 8355–61.
- Estivill-Torres, G., Pearson, H., vanHeyningen, V., Price, D.J., Rashbass, P., 2002. Pax6 is required to regulate the cell cycle and the rate of progression from symmetrical to asymmetrical division in mammalian cortical progenitors. *Development* 129, 455–466.
- Fietz, S.A., Huttner, W.B., 2011. Cortical progenitor expansion, self-renewal and neurogenesis—a polarized perspective. *Curr. Opin. Neurobiol.* 21, 23–35. doi:10.1016/j.conb.2010.10.002
- Fukuchi-Shimogori, T., Grove, E.A., 2003. Emx2 patterns the neocortex by regulating FGF positional signaling. *Nat. Neurosci.* 6, 825–31. doi:10.1038/nn1093
- Fukuchi-Shimogori, T., Grove, E.A., 2001. Neocortex patterning by the secreted signaling molecule FGF8. *Science* 294, 1071–4. doi:10.1126/science.1064252
- Garel, S., 2003. Molecular regionalization of the neocortex is disrupted in Fgf8 hypomorphic mutants. *Development* 130, 1903–1914. doi:10.1242/dev.00416

- The regulatory role of Pax6 on Cell Division Cycle Associated 7 and cortical progenitor cell proliferation
Georgala, P.A., Carr, C.B., Price, D.J., 2011. The role of Pax6 in forebrain development. *Dev. Neurobiol.* 71, 690–709. doi:10.1002/dneu.20895
- Glickstein, S.B., Monaghan, J.A., Koeller, H.B., Jones, T.K., Ross, M.E., 2009. Cyclin D2 is critical for intermediate progenitor cell proliferation in the embryonic cortex. *J. Neurosci.* 29, 9614–9624. doi:10.1523/JNEUROSCI.2284-09.200929/30/9614 [pii]
- Goto, Y., Hayashi, R., Muramatsu, T., Ogawa, H., Eguchi, I., Oshida, Y., Ohtani, K., Yoshida, K., 2006. JPO1/CDCA7, a novel transcription factor E2F1-induced protein, possesses intrinsic transcriptional regulator activity. *Biochim Biophys Acta* 1759, 60–68. doi:S0167-4781(06)00034-0 [pii]10.1016/j.bbaexp.2006.02.004
- Götz, M., Huttner, W.B., 2005. The cell biology of neurogenesis. *Nat. Rev. Mol. Cell Biol.* 6, 777–88. doi:10.1038/nrm1739
- Grindley, J.C., Davidson, D.R., Hill, R.E., 1995. The role of Pax-6 in eye and nasal development. *Development* 121, 1433–1442.
- Guillemot, F., Joyner, A.L., 1993. Dynamic expression of the murine Achaete-Scute homologue Mash-1 in the developing nervous system. *Mech. Dev.* 42, 171–85.
- Guiu, J., Bergen, D.J.M., DePater, E., Islam, A.B.M.M.K., Ayllón, V., Gama-Norton, L., Ruiz-Herguido, C., González, J., López-Bigas, N., Menendez, P., Dzierzak, E., Espinosa, L., Bigas, A., 2014. Identification of Cdca7 as a novel Notch transcriptional target involved in hematopoietic stem cell emergence. *J. Exp. Med.* 211, 2411–23. doi:10.1084/jem.20131857
- Haring, M., Offermann, S., Danker, T., Horst, I., Peterhansel, C., Stam, M., 2007. Chromatin immunoprecipitation: optimization, quantitative analysis and data normalization. *Plant Methods* 3, 11. doi:10.1186/1746-4811-3-11
- Haubensak, W., Attardo, A., Denk, W., Huttner, W.B., 2004. From The Cover: Neurons arise in the basal neuroepithelium of the early mammalian telencephalon: A major site of neurogenesis. *Proc. Natl. Acad. Sci.* 101, 3196–3201. doi:10.1073/pnas.0308600100
- Heins, N., Malatesta, P., Cecconi, F., Nakafuku, M., Tucker, K.L., Hack, M.A.,

The regulatory role of Pax6 on Cell Division Cycle Associated 7 and cortical progenitor cell proliferation
Chapouton, P., Barde, Y.-A., Götz, M., 2002. Glial cells generate neurons: the role of the transcription factor Pax6. *Nat. Neurosci.* 5, 308–15.
doi:10.1038/nn828

Helin, K., Harlow, E., Fattaey, A., 1993. Inhibition of E2F-1 transactivation by direct binding of the retinoblastoma protein. *Mol. Cell. Biol.* 13, 6501–8.

Houle, T.D., Ram, M.L., McMurray, W.J., Cala, S.E., 2006. Different endoplasmic reticulum trafficking and processing pathways for calsequestrin (CSQ) and epitope-tagged CSQ. *Exp. Cell Res.* 312, 4150–61.
doi:10.1016/j.yexcr.2006.09.010

Hsieh, Y.W., Yang, X.J., 2009. Dynamic Pax6 expression during the neurogenic cell cycle influences proliferation and cell fate choices of retinal progenitors. *Neural Dev* 4, 32. doi:10.1186/1749-8104-4-321749-8104-4-32 [pii]

Huttner, W.B., Kosodo, Y., 2005. Symmetric versus asymmetric cell division during neurogenesis in the developing vertebrate central nervous system. *Curr. Opin. Cell Biol.* 17, 648–57. doi:10.1016/j.ceb.2005.10.005

Iacopetti, P., Michelini, M., Stuckmann, I., Oback, B., Aaku-Saraste, E., Huttner, W.B., 1999. Expression of the antiproliferative gene TIS21 at the onset of neurogenesis identifies single neuroepithelial cells that switch from proliferative to neuron-generating division. *Proc. Natl. Acad. Sci.* 96, 4639–4644.
doi:10.1073/pnas.96.8.4639

Iglesias, A., Murga, M., Laresgoiti, U., Skoudy, A., Bernales, I., Fullaondo, A., Moreno, B., Lloreta, J., Field, S.J., Real, F.X., Zubiaga, A.M., 2004. Diabetes and exocrine pancreatic insufficiency in E2F1/E2F2 double-mutant mice. *J. Clin. Invest.* 113, 1398–407. doi:10.1172/JCI18879

Imamura, F., Greer, C.A., 2013. Pax6 regulates Tbr1 and Tbr2 expressions in olfactory bulb mitral cells. *Mol. Cell. Neurosci.* 54, 58–70.
doi:10.1016/j.mcn.2013.01.002

Indraccolo, S., Gola, E., Rosato, A., Minuzzo, S., Habeler, W., Tisato, V., Roni, V., Esposito, G., Morini, M., Albini, A., Noonan, D.M., Ferrantini, M., Amadori, A., Chieco-Bianchi, L., 2002. Differential effects of angiostatin, endostatin and

The regulatory role of Pax6 on Cell Division Cycle Associated 7 and cortical progenitor cell proliferation
interferon-alpha(1) gene transfer on in vivo growth of human breast cancer
cells. *Gene Ther.* 9, 867–78. doi:10.1038/sj.gt.3301703

Ip, B.K., Bayatti, N., Howard, N.J., Lindsay, S., Clowry, G.J., 2011. The corticofugal
neuron-associated genes ROBO1, SRGAP1, and CTIP2 exhibit an anterior to
posterior gradient of expression in early fetal human neocortex development.
Cereb. Cortex 21, 1395–407. doi:10.1093/cercor/bhq219

Ip, B.K., Wappler, I., Peters, H., Lindsay, S., Clowry, G.J., Bayatti, N., 2010.
Investigating gradients of gene expression involved in early human cortical
development. *J. Anat.* 217, 300–11. doi:10.1111/j.1469-7580.2010.01259.x

Jun, S., Desplan, C., 1996. Cooperative interactions between paired domain and
homeodomain. *Development* 122, 2639–50.

Kaesler, M.D., Iggo, R.D., 2002. Chromatin immunoprecipitation analysis fails to
support the latency model for regulation of p53 DNA binding activity in vivo.
Proc. Natl. Acad. Sci. U. S. A. 99, 95–100. doi:10.1073/pnas.012283399

Kapust, R.B., Waugh, D.S., 1999. Escherichia coli maltose-binding protein is
uncommonly effective at promoting the solubility of polypeptides to which it is
fused. *Protein Sci.* 8, 1668–1674.

Kawaguchi, A., Ogawa, M., Saito, K., Matsuzaki, F., Okano, H., Miyata, T., 2004.
Differential expression of Pax6 and Ngn2 between pair-generated cortical
neurons. *J. Neurosci. Res.* 78, 784–95. doi:10.1002/jnr.20347

Khleif, S.N., DeGregori, J., Yee, C.L., Otterson, G.A., Kaye, F.J., Nevins, J.R.,
Howley, P.M., 1996. Inhibition of cyclin D-CDK4/CDK6 activity is associated
with an E2F-mediated induction of cyclin kinase inhibitor activity. *Proc. Natl.
Acad. Sci. U. S. A.* 93, 4350–4.

Kowalczyk, T., Pontious, A., Englund, C., Daza, R.A.M., Bedogni, F., Hodge, R.,
Attardo, A., Bell, C., Huttner, W.B., Hevner, R.F., 2009. Intermediate neuronal
progenitors (basal progenitors) produce pyramidal-projection neurons for all
layers of cerebral cortex. *Cereb. Cortex* 19, 2439–50.
doi:10.1093/cercor/bhn260

Kroll, T.T., O’Leary, D.D.M., 2005. Ventralized dorsal telencephalic progenitors in

The regulatory role of Pax6 on Cell Division Cycle Associated 7 and cortical progenitor cell proliferation
Pax6 mutant mice generate GABA interneurons of a lateral ganglionic
eminence fate. *Proc. Natl. Acad. Sci. U. S. A.* 102, 7374–9.
doi:10.1073/pnas.0500819102

- Kuras, L., 2004. Characterization of protein-DNA association in vivo by chromatin immunoprecipitation. *Methods Mol. Biol.* 284, 147–62. doi:10.1385/1-59259-816-1:147
- Lajoie, B.R., Dekker, J., Kaplan, N., 2015. The Hitchhiker’s guide to Hi-C analysis: practical guidelines. *Methods* 72, 65–75. doi:10.1016/j.ymeth.2014.10.031
- Lange, C., Calegari, F., 2010. Cdks and cyclins link G1 length and differentiation of embryonic, neural and hematopoietic stem cells. *Cell Cycle* 9, 1893–1900. doi:11598 [pii]
- Lange, C., Huttner, W.B., Calegari, F., 2009. Cdk4/cyclinD1 overexpression in neural stem cells shortens G1, delays neurogenesis, and promotes the generation and expansion of basal progenitors. *Cell Stem Cell* 5, 320–331. doi:10.1016/j.stem.2009.05.026S1934-5909(09)00284-7 [pii]
- Lazic, S.E., 2009. Statistical evaluation of methods for quantifying gene expression by autoradiography in histological sections. *BMC Neurosci.* 10, 5. doi:10.1186/1471-2202-10-5
- Ledent, P., Duez, C., Vanhove, M., Lejeune, A., Fonzé, E., Charlier, P., Rhazi-Filali, F., Thamm, I., Guillaume, G., Samyn, B., Devreese, B., VanBeeumen, J., Lamotte-Brasseur, J., Frère, J.-M., 1997. Unexpected influence of a C-terminal-fused His-tag on the processing of an enzyme and on the kinetic and folding parameters. *FEBS Lett.* 413, 194–196. doi:10.1016/S0014-5793(97)00908-3
- Lee, C.-D., Sun, H.-C., Hu, S.-M., Chiu, C.-F., Homhuan, A., Liang, S.-M., Leng, C.-H., Wang, T.-F., 2008. An improved SUMO fusion protein system for effective production of native proteins. *Protein Sci.* 17, 1241–8. doi:10.1110/ps.035188.108
- Lees, J.A., Saito, M., Vidal, M., Valentine, M., Look, T., Harlow, E., Dyson, N., Helin, K., 1993. The retinoblastoma protein binds to a family of E2F transcription factors. *Mol. Cell. Biol.* 13, 7813–25.

- The regulatory role of Pax6 on Cell Division Cycle Associated 7 and cortical progenitor cell proliferation
Levitt, N., Briggs, D., Gil, A., Proudfoot, N.J., 1989. Definition of an efficient synthetic poly(A) site. *Genes Dev.* 3, 1019–25.
- Li, F.X., Zhu, J.W., Hogan, C.J., DeGregori, J., 2003. Defective Gene Expression, S Phase Progression, and Maturation during Hematopoiesis in E2F1/E2F2 Mutant Mice. *Mol. Cell. Biol.* 23, 3607–3622. doi:10.1128/MCB.23.10.3607-3622.2003
- Li, V.C., Ballabeni, A., Kirschner, M.W., 2012. Gap 1 phase length and mouse embryonic stem cell self-renewal. *Proc. Natl. Acad. Sci. U. S. A.* 109, 12550–5. doi:10.1073/pnas.1206740109
- Lichty, J.J., Malecki, J.L., Agnew, H.D., Michelson-Horowitz, D.J., Tan, S., 2005. Comparison of affinity tags for protein purification. *Protein Expr. Purif.* 41, 98–105. doi:10.1016/j.pep.2005.01.019
- Lin, Y.-C., Boone, M., Meuris, L., Lemmens, I., VanRoy, N., Soete, A., Reumers, J., Moisse, M., Plaisance, S., Drmanac, R., Chen, J., Speleman, F., Lambrechts, D., Van dePeer, Y., Tavernier, J., Callewaert, N., 2014. Genome dynamics of the human embryonic kidney 293 lineage in response to cell biology manipulations. *Nat. Commun.* 5, 4767. doi:10.1038/ncomms5767
- Lo, L.C., Johnson, J.E., Wuenschell, C.W., Saito, T., Anderson, D.J., 1991. Mammalian achaete-scute homolog 1 is transiently expressed by spatially restricted subsets of early neuroepithelial and neural crest cells. *Genes Dev.* 5, 1524–37.
- Lu, R., Li, Y., Zhang, Y., Chen, Y., Shields, A.D., Winder, D.G., Angelotti, T., Jiao, K., Limbird, L.E., Zhou, Y., Wang, Q., 2009. Epitope-tagged receptor knock-in mice reveal that differential desensitization of alpha2-adrenergic responses is because of ligand-selective internalization. *J. Biol. Chem.* 284, 13233–43. doi:10.1074/jbc.M807535200
- Magri, L., Swiss, V.A., Jablonska, B., Lei, L., Pedre, X., Walsh, M., Zhang, W., Gallo, V., Canoll, P., Casaccia, P., 2014. E2F1 coregulates cell cycle genes and chromatin components during the transition of oligodendrocyte progenitors from proliferation to differentiation. *J. Neurosci.* 34, 1481–93.

- Malatesta, P., Hartfuss, E., Götz, M., 2000. Isolation of radial glial cells by fluorescent-activated cell sorting reveals a neuronal lineage. *Development* 127, 5253–63.
- Manuel, M., Georgala, P.A., Carr, C.B., Chanas, S., Kleinjan, D.A., Martynoga, B., Mason, J.O., Molinek, M., Pinson, J., Pratt, T., Quinn, J.C., Simpson, T.I., Tyas, D.A., vanHeyningen, V., West, J.D., Price, D.J., 2007. Controlled overexpression of Pax6 in vivo negatively autoregulates the Pax6 locus, causing cell-autonomous defects of late cortical progenitor proliferation with little effect on cortical arealization. *Development* 134, 545–55. doi:10.1242/dev.02764
- Mathelier, A., Zhao, X., Zhang, A.W., Parcy, F., Worsley-Hunt, R., Arenillas, D.J., Buchman, S., Chen, C., Chou, A., Ienasescu, H., Lim, J., Shyr, C., Tan, G., Zhou, M., Lenhard, B., Sandelin, A., Wasserman, W.W., 2014. JASPAR 2014: an extensively expanded and updated open-access database of transcription factor binding profiles. *Nucleic Acids Res.* 42, D142-7. doi:10.1093/nar/gkt997
- Mathieu, O., Probst, A.V, Paszkowski, J., 2005. Distinct regulation of histone H3 methylation at lysines 27 and 9 by CpG methylation in Arabidopsis. *EMBO J.* 24, 2783–91. doi:10.1038/sj.emboj.7600743
- Mi, D., Carr, C.B., Georgala, P. a, Huang, Y.-T., Manuel, M.N., Jeanes, E., Niisato, E., Sansom, S.N., Livesey, F.J., Theil, T., Hasenpusch-Theil, K., Simpson, T.I., Mason, J.O., Price, D.J., 2013. Pax6 exerts regional control of cortical progenitor proliferation via direct repression of Cdk6 and hypophosphorylation of pRb. *Neuron* 78, 269–84. doi:10.1016/j.neuron.2013.02.012
- Miyata, T., Kawaguchi, A., Okano, H., Ogawa, M., 2001. Asymmetric Inheritance of Radial Glial Fibers by Cortical Neurons. *Neuron* 31, 727–741. doi:10.1016/S0896-6273(01)00420-2
- Mutch, C.A., Schulte, J.D., Olson, E., Chenn, A., 2010. Beta-catenin signaling negatively regulates intermediate progenitor population numbers in the developing cortex. *PLoS One* 5, e12376. doi:10.1371/journal.pone.0012376
- Muzio, L., DiBenedetto, B., DiBenedetto, B., Stoykova, A., Boncinelli, E., Gruss, P.,

The regulatory role of Pax6 on Cell Division Cycle Associated 7 and cortical progenitor cell proliferation
Mallamaci, A., 2002. Emx2 and Pax6 control regionalization of the pre-neuronogenic cortical primordium. *Cereb. Cortex* 12, 129–39.

Nagaki, K., Talbert, P.B., Zhong, C.X., Dawe, R.K., Henikoff, S., Jiang, J., 2003. Chromatin immunoprecipitation reveals that the 180-bp satellite repeat is the key functional DNA element of *Arabidopsis thaliana* centromeres. *Genetics* 163, 1221–5.

Nagao, M., Campbell, K., Burns, K., Kuan, C.-Y., Trumpp, A., Nakafuku, M., 2008. Coordinated control of self-renewal and differentiation of neural stem cells by Myc and the p19ARF-p53 pathway. *J. Cell Biol.* 183, 1243–57.
doi:10.1083/jcb.200807130

Nelson, J.D., Denisenko, O., Bomsztyk, K., 2006. Protocol for the fast chromatin immunoprecipitation (ChIP) method. *Nat. Protoc.* 1, 179–85.
doi:10.1038/nprot.2006.27

Ninkovic, J., Steiner-Mezzadri, A., Jawerka, M., Akinci, U., Masserdotti, G., Petricca, S., Fischer, J., vonHolst, A., Beckers, J., Lie, C.D., Petrik, D., Miller, E., Tang, J., Wu, J., Lefebvre, V., Demmers, J., Eisch, A., Metzger, D., Crabtree, G., Irmeler, M., Poot, R., Götz, M., 2013. The BAF complex interacts with Pax6 in adult neural progenitors to establish a neurogenic cross-regulatory transcriptional network. *Cell Stem Cell* 13, 403–18.
doi:10.1016/j.stem.2013.07.002

Noctor, S.C., Flint, A.C., Weissman, T.A., Dammerman, R.S., Kriegstein, A.R., 2001. Neurons derived from radial glial cells establish radial units in neocortex. *Nature* 409, 714–20. doi:10.1038/35055553

Noctor, S.C., Martínez-Cerdeño, V., Ivic, L., Kriegstein, A.R., 2004. Cortical neurons arise in symmetric and asymmetric division zones and migrate through specific phases. *Nat. Neurosci.* 7, 136–44. doi:10.1038/nn1172

O’Leary, D.D.M., Chou, S.-J., Sahara, S., 2007. Area patterning of the mammalian cortex. *Neuron* 56, 252–69. doi:10.1016/j.neuron.2007.10.010

Orford, K.W., Scadden, D.T., 2008. Deconstructing stem cell self-renewal: genetic insights into cell-cycle regulation. *Nat. Rev. Genet.* 9, 115–28.

- Osthus, R.C., Karim, B., Prescott, J.E., Smith, B.D., McDevitt, M., Huso, D.L., Dang, C.V, 2005. The Myc target gene JPO1/CDCA7 is frequently overexpressed in human tumors and has limited transforming activity in vivo. *Cancer Res.* doi:65/13/5620 [pii]10.1158/0008-5472.CAN-05-0536
- Palmer, E., Freeman, T., 2004. Investigation into the use of C- and N-terminal GFP fusion proteins for subcellular localization studies using reverse transfection microarrays. *Comp. Funct. Genomics* 5, 342–53. doi:10.1002/cfg.405
- Pang, J., Zeng, X., Xiao, R., Lakatta, E.G., Lin, L., 2009. Design, generation, and testing of mammalian expression modules that tag membrane proteins. *Protein Sci.* 18, 1261–71. doi:10.1002/pro.136
- Park, S.H., Cheong, C., Idoyaga, J., Kim, J.Y., Choi, J.-H., Do, Y., Lee, H., Jo, J.H., Oh, Y.-S., Im, W., Steinman, R.M., Park, C.G., 2008. Generation and application of new rat monoclonal antibodies against synthetic FLAG and OLLAS tags for improved immunodetection. *J. Immunol. Methods* 331, 27–38. doi:10.1016/j.jim.2007.10.012
- Persson, M., Stamatakis, D., teWelscher, P., Andersson, E., Böse, J., Rütter, U., Ericson, J., Briscoe, J., 2002. Dorsal-ventral patterning of the spinal cord requires Gli3 transcriptional repressor activity. *Genes Dev.* 16, 2865–78. doi:10.1101/gad.243402
- Pilaz, L.-J., Patti, D., Marcy, G., Ollier, E., Pfister, S., Douglas, R.J., Betizeau, M., Gautier, E., Cortay, V., Doerflinger, N., Kennedy, H., Dehay, C., 2009. Forced G1-phase reduction alters mode of division, neuron number, and laminar phenotype in the cerebral cortex. *Proc. Natl. Acad. Sci. U. S. A.* 106, 21924–9. doi:10.1073/pnas.0909894106
- Pope, B.D., Ryba, T., Dileep, V., Yue, F., Wu, W., Denas, O., Vera, D.L., Wang, Y., Hansen, R.S., Canfield, T.K., Thurman, R.E., Cheng, Y., Gülsoy, G., Dennis, J.H., Snyder, M.P., Stamatoyannopoulos, J.A., Taylor, J., Hardison, R.C., Kahveci, T., Ren, B., Gilbert, D.M., 2014. Topologically associating domains are stable units of replication-timing regulation. *Nature* 515, 402–405.

- Proudfoot, N., 1991. Poly(A) signals. *Cell* 64, 671–674. doi:10.1016/0092-8674(91)90495-K
- Puelles, L., Rubenstein, J.L., 1993. Expression patterns of homeobox and other putative regulatory genes in the embryonic mouse forebrain suggest a neuromeric organization. *Trends Neurosci.* 16, 472–9.
- Qiu, P., 2003. Recent advances in computational promoter analysis in understanding the transcriptional regulatory network. *Biochem. Biophys. Res. Commun.* 309, 495–501. doi:10.1016/j.bbrc.2003.08.052
- Quinn, J.C., Molinek, M., Martynoga, B.S., Zaki, P.A., Faedo, A., Bulfone, A., Hevner, R.F., West, J.D., Price, D.J., 2007. Pax6 controls cerebral cortical cell number by regulating exit from the cell cycle and specifies cortical cell identity by a cell autonomous mechanism. *Dev. Biol.* 302, 50–65.
doi:10.1016/j.ydbio.2006.08.035
- Rakic, P., Ayoub, A.E., Breunig, J.J., Dominguez, M.H., 2009. Decision by division: making cortical maps. *Trends Neurosci.* 32, 291–301.
doi:10.1016/j.tins.2009.01.007
- Ravasi, T., Suzuki, H., Cannistraci, C.V., Katayama, S., Bajic, V.B., Tan, K., Akalin, A., Schmeier, S., Kanamori-Katayama, M., Bertin, N., Carninci, P., Daub, C.O., Forrest, A.R.R., Gough, J., Grimmond, S., Han, J.-H., Hashimoto, T., Hide, W., Hofmann, O., Kamburov, A., Kaur, M., Kawaji, H., Kubosaki, A., Lassmann, T., vanNimwegen, E., MacPherson, C.R., Ogawa, C., Radovanovic, A., Schwartz, A., Teasdale, R.D., Tegnér, J., Lenhard, B., Teichmann, S.A., Arakawa, T., Ninomiya, N., Murakami, K., Tagami, M., Fukuda, S., Imamura, K., Kai, C., Ishihara, R., Kitazume, Y., Kawai, J., Hume, D.A., Ideker, T., Hayashizaki, Y., 2010. An atlas of combinatorial transcriptional regulation in mouse and man. *Cell* 140, 744–52. doi:10.1016/j.cell.2010.01.044
- Reilly, S.K., Yin, J., Ayoub, A.E., Emera, D., Leng, J., Cotney, J., Sarro, R., Rakic, P., Noonan, J.P., 2015. Evolutionary changes in promoter and enhancer activity during human corticogenesis. *Science* (80-.). 347, 1155–1159.

The regulatory role of Pax6 on Cell Division Cycle Associated 7 and cortical progenitor cell proliferation
doi:10.1126/science.1260943

- Roccio, M., Schmitter, D., Knobloch, M., Okawa, Y., Sage, D., Lutolf, M.P., 2013. Predicting stem cell fate changes by differential cell cycle progression patterns. *Development* 140, 459–70. doi:10.1242/dev.086215
- Sakaue-Sawano, A., Kurokawa, H., Morimura, T., Hanyu, A., Hama, H., Osawa, H., Kashiwagi, S., Fukami, K., Miyata, T., Miyoshi, H., Imamura, T., Ogawa, M., Masai, H., Miyawaki, A., 2008. Visualizing spatiotemporal dynamics of multicellular cell-cycle progression. *Cell* 132, 487–98.
doi:10.1016/j.cell.2007.12.033
- Sansom, S.N., Griffiths, D.S., Faedo, A., Kleinjan, D.-J., Ruan, Y., Smith, J., vanHeyningen, V., Rubenstein, J.L., Livesey, F.J., 2009. The level of the transcription factor Pax6 is essential for controlling the balance between neural stem cell self-renewal and neurogenesis. *PLoS Genet.* 5, e1000511.
doi:10.1371/journal.pgen.1000511
- Sansom, S.N., Livesey, F.J., 2009. Gradients in the brain: the control of the development of form and function in the cerebral cortex. *Cold Spring Harb. Perspect. Biol.* 1, a002519. doi:10.1101/cshperspect.a002519
- Sariñana, J., Kitamura, T., Künzler, P., Sultzman, L., Tonegawa, S., 2014. Differential roles of the dopamine 1-class receptors, D1R and D5R, in hippocampal dependent memory. *Proc. Natl. Acad. Sci. U. S. A.* 111, 8245–50.
doi:10.1073/pnas.1407395111
- Scardigli, R., Bäumer, N., Gruss, P., Guillemot, F., LeRoux, I., 2003. Direct and concentration-dependent regulation of the proneural gene Neurogenin2 by Pax6. *Development* 130, 3269–81.
- Schedl, A., Ross, A., Lee, M., Engelkamp, D., Rashbass, P., vanHeyningen, V., Hastie, N.D., 1996. Influence of PAX6 Gene Dosage on Development: Overexpression Causes Severe Eye Abnormalities. *Cell* 86, 71–82.
doi:10.1016/S0092-8674(00)80078-1
- Schoppee Bortz, P.D., Wamhoff, B.R., 2011. Chromatin immunoprecipitation (ChIP): revisiting the efficacy of sample preparation, sonication, quantification

The regulatory role of Pax6 on Cell Division Cycle Associated 7 and cortical progenitor cell proliferation of sheared DNA, and analysis via PCR. *PLoS One* 6, e26015.

doi:10.1371/journal.pone.0026015

- Seamon, J.A., Adams, M., Sengupta, S., Roth, M.J., 2000. Differential effects of C-terminal molecular tagged integrase on replication competent moloney murine leukemia virus. *Virology* 274, 412–9. doi:10.1006/viro.2000.0481
- Shaw, G., Morse, S., Ararat, M., Graham, F.L., 2002. Preferential transformation of human neuronal cells by human adenoviruses and the origin of HEK 293 cells. *FASEB J.* 16, 869–71. doi:10.1096/fj.01-0995fje
- Shen, Y., Yue, F., McCleary, D.F., Ye, Z., Edsall, L., Kuan, S., Wagner, U., Dixon, J., Lee, L., Lobanenko, V.V., Ren, B., 2012. A map of the cis-regulatory sequences in the mouse genome. *Nature* 488, 116–120. doi:10.1038/nature11243
- Shimojo, H., Ohtsuka, T., Kageyama, R., 2008. Oscillations in Notch Signaling Regulate Maintenance of Neural Progenitors. *Neuron* 58, 52–64. doi:10.1016/j.neuron.2008.02.014
- Singh, A.M., Dalton, S., 2009. The cell cycle and Myc intersect with mechanisms that regulate pluripotency and reprogramming. *Cell Stem Cell* 5, 141–9. doi:10.1016/j.stem.2009.07.003
- St-Onge, L., Sosa-Pineda, B., Chowdhury, K., Mansouri, A., Gruss, P., 1997. Pax6 is required for differentiation of glucagon-producing alpha-cells in mouse pancreas. *Nature* 387, 406–9. doi:10.1038/387406a0
- Stormo, G.D., 2000. DNA binding sites: representation and discovery. *Bioinformatics* 16, 16–23.
- Stoykova, A., Treichel, D., Hallonet, M., Gruss, P., 2000. Pax6 modulates the dorsoventral patterning of the mammalian telencephalon. *J. Neurosci.* 20, 8042–50.
- Sun, J., Rockowitz, S., Xie, Q., Ashery-Padan, R., Zheng, D., Cvekl, A., 2015. Identification of in vivo DNA-binding mechanisms of Pax6 and reconstruction of Pax6-dependent gene regulatory networks during forebrain and lens development. *Nucleic Acids Res.* 43, 6827–46. doi:10.1093/nar/gkv589

- The regulatory role of Pax6 on Cell Division Cycle Associated 7 and cortical progenitor cell proliferation
Surdej, P., Jacobs-Lorena, M., 1994. Strategy for epitope tagging the protein-coding region of any gene. *Biotechniques* 17, 560–5.
- Tagliatela, P., Soria, J.M., Caironi, V., Moiana, A., Bertuzzi, S., 2004. Compromised generation of GABAergic interneurons in the brains of *Vax1*^{-/-} mice. *Development* 131, 4239–49. doi:10.1242/dev.01299
- Takahashi, T., Nowakowski, R.S., Caviness, V.S., 1995. The cell cycle of the pseudostratified ventricular epithelium of the embryonic murine cerebral wall. *J. Neurosci.* 15, 6046–57.
- Terpe, K., 2003. Overview of tag protein fusions: from molecular and biochemical fundamentals to commercial systems. *Appl. Microbiol. Biotechnol.* 60, 523–33. doi:10.1007/s00253-002-1158-6
- Toresson, H., Potter, S.S., Campbell, K., 2000. Genetic control of dorsal-ventral identity in the telencephalon: opposing roles for Pax6 and Gsh2. *Development* 127, 4361–71.
- Tucker, J.A., Mintzer, K.A., Mullins, M.C., 2008. The BMP signaling gradient patterns dorsoventral tissues in a temporally progressive manner along the anteroposterior axis. *Dev. Cell* 14, 108–19. doi:10.1016/j.devcel.2007.11.004
- Walcher, T., Xie, Q., Sun, J., Irmeler, M., Beckers, J., Öztürk, T., Niessing, D., Stoykova, A., Cvekl, A., Ninkovic, J., Götz, M., 2013. Functional dissection of the paired domain of Pax6 reveals molecular mechanisms of coordinating neurogenesis and proliferation. *Development* 140, 1123–36. doi:10.1242/dev.082875
- Walker, P.A., Leong, L.E.C., Ng, P.W.P., Tan, S.M., Waller, S., Murphy, D., Porter, A.G., 1994. Efficient and rapid affinity purification of proteins using recombinant fusion proteases. *Nat. Biotechnol.* 12, 601–605.
- Walther, C., Gruss, P., 1991. Pax-6, a murine paired box gene, is expressed in the developing CNS. *Development* 113, 1435–49.
- Wang, L., Bluske, K.K., Dickel, L.K., Nakagawa, Y., 2011. Basal progenitor cells in the embryonic mouse thalamus - their molecular characterization and the role of neurogenins and Pax6. *Neural Dev.* 6, 35. doi:10.1186/1749-8104-6-35

- The regulatory role of Pax6 on Cell Division Cycle Associated 7 and cortical progenitor cell proliferation
- Wang, Z., Zang, C., Rosenfeld, J.A., Schones, D.E., Barski, A., Cuddapah, S., Cui, K., Roh, T.-Y., Peng, W., Zhang, M.Q., Zhao, K., 2008. Combinatorial patterns of histone acetylations and methylations in the human genome. *Nat. Genet.* 40, 897–903. doi:10.1038/ng.154
- Waugh, D.S., 2005. Making the most of affinity tags. *Trends Biotechnol.* 23, 316–20. doi:10.1016/j.tibtech.2005.03.012
- Wenzel, P.L., Chong, J.-L., Sáenz-Robles, M.T., Ferrey, A., Hagan, J.P., Gomez, Y.M., Rajmohan, R., Sharma, N., Chen, H.-Z., Pipas, J.M., Robinson, M.L., Leone, G., 2011. Cell proliferation in the absence of E2F1-3. *Dev. Biol.* 351, 35–45. doi:10.1016/j.ydbio.2010.12.025
- Wey, A., Martinez Cerdeno, V., Pleasure, D., Knoepfler, P.S., 2010. c- and N-myc regulate neural precursor cell fate, cell cycle, and metabolism to direct cerebellar development. *Cerebellum* 9, 537–47. doi:10.1007/s12311-010-0190-9
- Wissmüller, S., Kosian, T., Wolf, M., Finzsch, M., Wegner, M., 2006. The high-mobility-group domain of Sox proteins interacts with DNA-binding domains of many transcription factors. *Nucleic Acids Res.* 34, 1735–44. doi:10.1093/nar/gkl105
- Wong, F.K., Fei, J.-F., Mora-Bermúdez, F., Taverna, E., Haffner, C., Fu, J., Anastassiadis, K., Stewart, A.F., Huttner, W.B., 2015. Sustained Pax6 Expression Generates Primate-like Basal Radial Glia in Developing Mouse Neocortex. *PLoS Biol.* 13, e1002217. doi:10.1371/journal.pbio.1002217
- Xie, Q., Yang, Y., Huang, J., Ninkovic, J., Walcher, T., Wolf, L., Vitenzon, A., Zheng, D., Götz, M., Beebe, D.C., Zavadil, J., Cvekl, A., 2013. Pax6 interactions with chromatin and identification of its novel direct target genes in lens and forebrain. *PLoS One* 8, e54507. doi:10.1371/journal.pone.0054507
- Yamasaki, L., Jacks, T., Bronson, R., Goillot, E., Harlow, E., Dyson, N.J., 1996. Tumor induction and tissue atrophy in mice lacking E2F-1. *Cell* 85, 537–48.
- Young, C.L., Britton, Z.T., Robinson, A.S., 2012. Recombinant protein expression and purification: A comprehensive review of affinity tags and microbial applications. *Biotechnol. J.* 7, 620–634. doi:10.1002/biot.201100155

- The regulatory role of Pax6 on Cell Division Cycle Associated 7 and cortical progenitor cell proliferation
Yun, K., Fischman, S., Johnson, J., deAngelis, M.H., Weinmaster, G., Rubenstein, J.L.R., 2002. Modulation of the notch signaling by Mash1 and Dlx1/2 regulates sequential specification and differentiation of progenitor cell types in the subcortical telencephalon. *Development* 129, 5029–5040.
- Zhang, C., 2006. A clustering property of highly-degenerate transcription factor binding sites in the mammalian genome. *Nucleic Acids Res.* 34, 2238–2246.
doi:10.1093/nar/gkl248
- Zhou, Y., Zheng, J.B., Gu, X., Li, W., Saunders, G.F., 2000. A novel Pax-6 binding site in rodent B1 repetitive elements: coevolution between developmental regulation and repeated elements? *Gene* 245, 319–28.
- Zinin, N., Adameyko, I., Wilhelm, M., Fritz, N., Uhlén, P., Ernfors, P., Henriksson, M.A., 2014. MYC proteins promote neuronal differentiation by controlling the mode of progenitor cell division. *EMBO Rep.* 15, 383–91.
doi:10.1002/embr.201337424

Appendix 1 Quantitative Chromatin Immunoprecipitation (qChIP)

Reagents

11% Formaldehyde solution	Freshly made before usage	
Reagents	Weight or Volume	Final concentration
1M HEPES-KOH pH=7.5	50 μ L	50 mM
5M NaCl	20 μ L	100 mM
0.5M EDTA	1 μ L	1 mM
0.5M EGTA	2 μ L	0.5 mM
37% Formaldehyde (Sigma F8875)	298 μ L	11%
ddH ₂ O	To 1 mL	
0.5% BSA Blocking solution	Stored at 4°C and use in one week	
Reagents	Weight or Volume	Final concentration
BSA	250 mg	0.5%
1x PBS	50 mL	
Lysis buffer 1 (LB1)	0.2 μ m filtered and stored at 4°C	
Reagents	Weight or Volume	Final concentration
1M HEPES-KOH pH=7.5	5 mL	50 mM

The regulatory role of Pax6 on Cell Division Cycle Associated 7 and cortical progenitor cell proliferation

5M NaCl	2.8 mL	140 mM
0.5M EDTA	0.2 mL	1 mM
50% Glycerol	20 mL	10%
10% NP-40	5 mL	0.5%
10% Triton X-100	2.5 mL	0.25%
ddH ₂ O	To 100 mL	Filtered and

Lysis buffer 2 (LB2) 0.2 µm filtered and stored at 4°C

Reagents	Weight or Volume	Final concentration
1M Tris-HCl pH=8.0	1 mL	10 mM
5M NaCl	4 mL	200 mM
0.5M EDTA	0.2 mL	1 mM
0.5M EGTA	0.1 mL	0.5 mM
ddH ₂ O	To 100 mL	

Lysis buffer 3 (LB3) 0.2 µm filtered and stored at 4°C

Reagents	Weight or Volume	Final concentration
1M Tris-HCl pH=8.0	1 mL	10 mM
5M NaCl	2 mL	100 mM
0.5M EDTA	0.2 mL	1 mM
0.5M EGTA	0.1 mL	0.1 mM
10% NA-Deoxycholate	1 mL	0.1%
20% N-lauroylsarcosine	2.5 mL	0.5%

ddH₂O To 100 mL

RIPA Stored at 4°C

Reagents	Weight or Volume	Final concentration
1M HEPES-KOH pH=7.5	2.5 mL	50 mM
0.5M EDTA	0.1 mL	1 mM
10% NA-Deoxycholate	3.5 mL	0.7%
10% NP-40	5 mL	1%
8M LiCl	3.125 mL	0.5M
ddH ₂ O	To 50 mL	

Protocol

1. First Day

- 1.1 Add 1 mL of cold 1x PBS was added to cortex tissues to resuspend cells to single ones
- 1.2 Add 1x cold PBS to final 4.5 mL volume and then add one-tenth (1/10, 450 µL) of 11% Formaldehyde solution to cell pellets and leave at RT for 15 minutes.
- 1.3 Quench formaldehyde by adding one-twentieth (1/20, 250 µL) of 2.5 M glycine.
- 1.4 Cells are collected by centrifuge, 1350 g for 5 minutes at 4°C.
- 1.5 Add 1x cold PBS and repeat Step 1.4 twice.
- 1.6 Immediately freeze the cell pellets in dry ice and store at -80°C.

The regulatory role of Pax6 on Cell Division Cycle Associated 7 and cortical progenitor cell proliferation

- 1.7 For magnetic beads preparation (Dynabeads Thermo Cat no.11203D), beads are washed by blocking buffer on the rotation platform at 4°C.
- 1.8 Collect beads by desktop centrifuge, 3000 rpm for 5 minutes at 4°C.
- 1.9 Repeat step 1.7 and collect the beads by magnetic stand.
- 1.10 Add anti-Pax6 antibody (Millipore), 10 µg for each reaction and place on the rotation platform at 4°C.

2. Second Day

- 2.1 Add protease inhibitors (PI, Roche Cat no.11697498001) to LB1, 2 and 3.
- 2.2 Resuspend cell pellets in 5 mL LB1-PI and then collect cells by centrifuge at 1350 g for 5 minutes at 4°C.
- 2.3 Resuspend cells pellets in in 5 mL LB2-PI and gently mix for 10 minutes at RT.
- 2.4 Collect cells by centrifuge at 1350 g for 5 minutes at 4°C.
- 2.5 Resuspend cell pellets in 3 mL LB3-PI and transfer cells to sonication tube (polypropylene Corning tube).
- 2.6 Sonicate the cells solution for 30 seconds for 8-12 times with 30 second interval on ice. The sonicator machine is set at 30% amplitude.

*Sonication repeats are depending on the cell numbers. Normally it aims to shear the genomic DNA to 100-600 base pair in length.

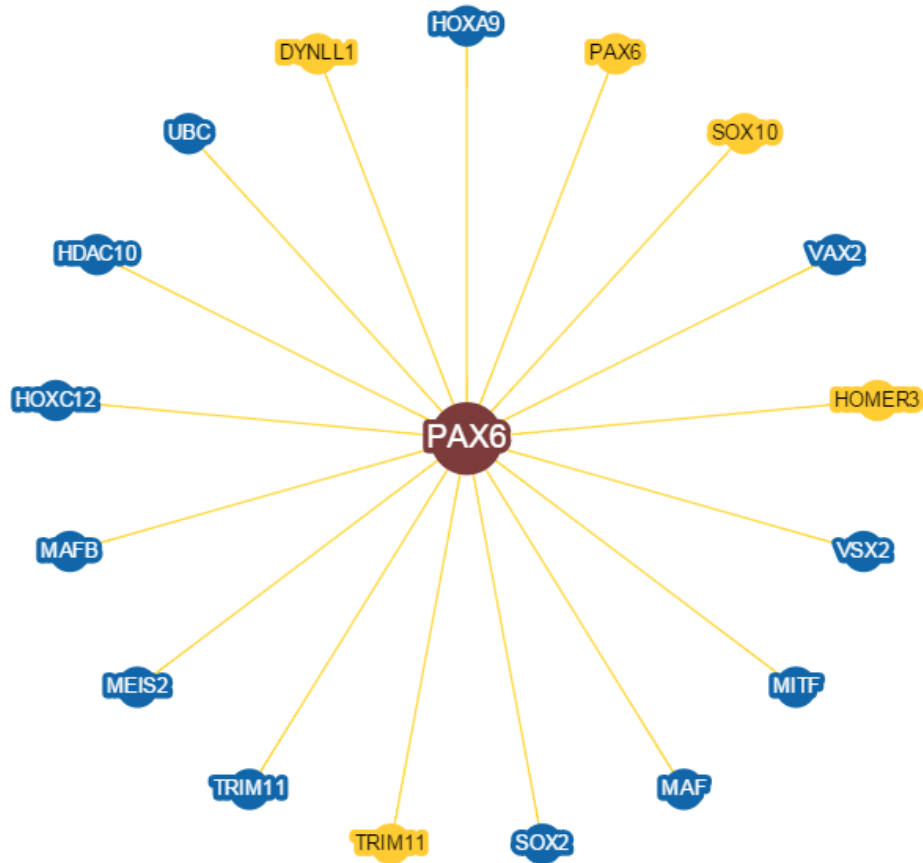
- 2.7 Add 300 µL of 10% Triton X-100 to sonicated lysate and discard the debris by spinning at 20,000g for 10 minutes at 4°C.
- 2.8 Aliquot 100 µL for whole cell extract DNA and store at -20°C.
- 2.9 Collect magnetic beads from Step 1.10 by the magnetic stand.
- 2.10 Wash beads with 1 mL blocking buffer and place on the rotation platform for 5 minutes at 4°C.

The regulatory role of Pax6 on Cell Division Cycle Associated 7 and cortical progenitor cell proliferation

- 2.11 Collect beads by magnetic stand and resuspend beads in 100 μ L of blocking buffer
- 2.12 Add sonicated lysate to beads.

3. Third Day
 - 3.1 Wash beads using 1 mL RIPA buffer and place on the rotation platform for 5 minutes at 4°C.
 - 3.2 Collect beads by magnetic stand.
 - 3.3 Repeat the wash step (2.10-2.11) for total 6 times.
 - 3.4 Wash beads with 1 mL 50 mM NaCl-TE buffer.
 - 3.5 Also add equal amount of 50 mM NaCl-TE buffer (100 μ L) to whole cell extract DNA from Step 2.8.
 - 3.6 Discard 50 mM NaCl-TE buffer from both beads (IP sample) and whole cell extract DNA by spinning at 3000 rpm for 5 minute at 4°C. From this point, IP and whole cell extract samples are treated the same.
 - 3.7 Add 100 μ L of 10% Chelex/beads (Sigma Cat no C7901) to each sample and boil for 10 minutes.
 - 3.8 Allow to cool down at RT.
 - 3.9 Add 100 μ g/mL of Proteinase K and incubate the mixture for 30 minutes at 55°C.
 - 3.10 Boil for 10 minutes and collect the supernatant by spinning at 13000 rpm for 1 minute.
 - 3.11 Add 100 μ L of ddH₂O to the beads from Step 3.10, vortex for 1 minute and collect the supernatant as step 3.10
 - 3.12 Combine the supernatants from Step 3.10 and 3.11
 - 3.13 Purify DNA by phenol/chloroform and Phase-lock gel tube (5 prime Cat no. 2302800) according to the manual instructions.

Appendix 2 The physical interactions between Pax6 and other proteins



Source: <http://thebiogrid.org/202033/summary/mus-musculus/pax6.html>